# Instrumental and Methodological Developments for Two-dimensional Capillary-Coupled Isotachophoresis/Electrophoresis-Mass Spectrometry

**Dissertation**

der Mathematisch-Naturwissenschaftlichen Fakultät
der Eberhard Karls Universität Tübingen
zur Erlangung des Grades eines
Doktors der Naturwissenschaften
(Dr. rer. nat.)

vorgelegt von
Hannes Georg Graf
aus Tübingen

Tübingen
2022

Gedruckt mit Genehmigung der Mathematisch-Naturwissenschaftlichen Fakultät der Eberhard Karls Universität Tübingen.

| | |
|---|---|
| Tag der mündlichen Qualifikation: | 21.12.2022 |
| Dekan: | Prof. Dr. Thilo Stehle |
| 1. Berichterstatterin: | Prof. Dr. Carolin Huhn |
| 2. Berichterstatter: | Prof. Dr. Udo Weimar |

*Meinen Eltern*

# Table of Contents

# List of Abbreviations

| | |
|---|---|
| $\mu_{lim}$ | limiting electrophoretic mobilities |
| 2D | two-dimensional |
| AMPA | aminomethylphosphonic acid |
| AUX | auxiliary vial housing |
| BGE | background electrolyte |
| BGE-S-BGE | BGE-Sample-BGE |
| $C^4D$ | capacitively coupled contactless conductivity detection |
| CD | conductivity detection |
| CDC | capacitance-to-digital converter |
| CDCD | CDC-based $C^4D$ detectors |
| CE | capillary electrophoresis |
| CE-$C^4D$ | capillary electrophoresis-capacitively coupled to $C^4D$ |
| CE-LIF | capillary electrophoresis-laser induced fluorescence |
| CE-MS | capillary electrophoresis-mass spectrometry |
| EDTA | ethylenediaminetetraacetic acid |
| EME | electro membrane extraction |
| EOF | electroosmotic flow |
| ESI | electrospray ionization |
| FASI | field-amplified sample injection |
| FASS | field-amplified sample stacking |
| FLD | fluorescence detection |
| FMOC-Cl | fluorenylmethyloxycarbonyl chloride |
| GC | gas chromatography |
| GLA | glyoxylic acid |
| GLP | glyphosate |
| GLU or GLUF | glufosinate |
| GLY | glycine |
| HILIC | hydrophilic interaction liquid chromatography |
| HLB | hydrophilic-lipophilic balance |
| HMPA | hydroxymethyl phosphonic acid |
| IEC | ion exchange chromatography |
| IN | intlet position of the CE instument |
| ITP | isotachophoresis |
| ITP/CE | ITP combind with CE |
| ITP/CE-MS | isotachophoresis capillary electrophoresis-mass spectrometry |
| ITP-$C^4D$/CE-MS | isotachophoresis-$C^4D$/capillary electrophoresis-MS |
| ITP-MS | isotachophoresis-mass spectrometry |
| LC | liquid chromatography |

| | |
|---|---|
| LE | leading electrolyte |
| LIF | laser induced fluorescence spectrophotometry |
| LOD | limits of detection |
| LOQ | limit of quantification |
| L-S-L | leading electrolyte-sample-leading electrolyte |
| LVSS | large volume sample stacking |
| MCPA | 2-methyl-4-chlorophenoxyacetic acid |
| MES | 2-(*N*-morpholino)ethanesulfonic acid |
| MIP | molecularly imprinted polymer |
| MMLC | mixed-mode liquid chromatography |
| MS | mass spectrometry |
| MS/MS | tandem mass spectrometry |
| MWCNT | multiwalled carbon nanotube |
| NAMPA | *N*-acetyl AMPA |
| NGLP | *N*-acetyl glyphosate |
| OUT | outlet position of the CE instument |
| OXA | oxamic acid |
| PGC | porous graphitic carbon |
| $P_i$ | inorganic phosphate |
| p$K_a$ | negative decadic logarithmic acidity dissociation constant |
| p$K_a^\circ$ | negative decadic logarithmic thermodynamic acidity dissociation constant |
| Pro | proline |
| RPLC-MS | reversed phase liquid chromatography-mass spectrometry |
| SAR | sarcosine |
| SAX | strong anion exchange |
| SFC | supercritical fluid chromatography |
| SLM | supported liquid membrane |
| SPE | solid phase extraction |
| SPE-CE | SPE coupled to CE |
| TE | terminating electrolyte |
| tITP | transient isotachophoresis |
| T-S-BGE | terminating electrolyte-sample-BGE |
| T-S-T | terminating electrolyte-sample-terminating electrolyte |
| UV/Vis | UV/visible |

# Acknowledgements

An erster Stelle bedanke ich mich bei meiner Doktormutter, Prof. Carolin Huhn, welche mir ein interdisziplinäres Themengebiet anvertraute, dass neben meinem chemisch-physikalischen Wissen auch die Entwicklungen von mechanischen Bauteilen, elektronischen Schaltungen und Software umfasste. Vielen Dank für die fachlichen Diskussionen an kniffligen Stellen, deine Unterstützung, dein großes Vertrauen und die Freiheiten Neues zu probieren.

Ich möchte auch Ihnen, Prof. Udo Weimar, herzlich dafür danken, dass Sie sich bereit erklärt haben, zweiter Betreuer und auch zweiter Berichterstatter für diese Arbeit zu sein. Ebenso gilt mein Dank Prof. Reinhold Fink und Prof. Michael Lämmerhofer, die sich bereit erklärt haben, als Prüfer an der Disputationsprüfung teilzunehmen.

Die gute Atmosphäre im Arbeitskreis hat die Zeit der Promotion sehr schnell vergehen lassen und kleinerer oder größere Hürden mit guter Laune überwinden lassen. Hierfür bedanke ich mich bei allen Mitgliedern des Arbeitskreises die ich in meiner Zeit dort erleben durfte. Gerne erinnere ich mich an fruchtbare Diskussionen und Gespräche sowie gemeinsame Tagungen und Aktionen. Vielen Dank Benjamin Rudisch für exzellente Einarbeitung in neue, komplexe Themengebiete zu denen ich zuvor keinen Zugang hatte, die zahlreichen Diskussionen und die gute Zusammenarbeit bei den Publikationen. Für eine Vielzahl an Diskussionen insbesondere in Bezug auf die Glyphosatanalytik und sein immer offenes Ohr bedanke ich mich bei Benedikt Wimmer. Für die Einarbeitung in die Geräte des Arbeitskreises und Einführung in Arbeitstechniken bedanke ich mich bei Michel Banet, Sarah Knoll, Dr. Martin Meixner, Dr. Tanja Melzer und Dr. Tobias Rösch. Ein großer Dank gilt auch Stephie Bock, Lisa Engelbart, Nadja Kalinke, und Viola Wurster für die guten fachlichen als auch privaten Gespräche.

Ohne die großartige Unterstützung meiner Praktikantinnen und Praktikanten wären die in dieser Arbeit gezeigten Ergebnisse nicht so schnell erreicht worden, da unzählige

Mess- und Auswertungsarbeiten von Ihnen übernommen wurden. Ich danke hierfür Sonja Biebl, Rinor Kelmendi, Johanna Manegold, Linda Müller, Lukas Ude und Benjamin Weber sowie Christina Breitenstein.

Besonderer Dank gilt auch den Werkstätten des chemischen Zentralinstituts. Insbesondere bedanke ich mich bei Alexander Schnapper für seine fachliche Beratung, die zügige Fertigung der vielen Präzisionsteile und den 3D-Druck von Bauteilen. Weiterhin bedanke ich mich bei Christof Binder und Cornelia Halder, Walter Schaal und Gerd Vollmer. Darüber hinaus bedanke mich auch bei der Firma LightFab für die Beratung hinsichtlich einer optimierten Geometrie des Chip-Interfaces für die Fertigung mittels selective laser etching. Dank dem Projekt DEAL konnten alle Publikationen, die im Rahmen dieser Dissertation entstanden sind, open-source gemacht werden.

Abschließend möchte ich mich bei meinen Eltern für ihre Unterstützung und die Ermöglichung meines Studiums bedanken.

# List of Research Papers

1. Graf, H. G., Rudisch, B. M., Manegold, J., Huhn, C., Advancements in capacitance-to-digital converter-based $C^4D$ technology for detection in capillary electrophoresis using amplified excitation voltages and comparison to classical and open-source $C^4Ds$. *Electrophoresis* 2021, *42*, 1306-1316, DOI: 10.1002/elps.202000394 cited as [1]

Conceptualization: Hannes Graf, and Benjamin Rudisch; Development: Hannes Graf; Experiments and evaluation: Hannes Graf and Johanna Manegold (under supervision by Hannes Graf); Writing original draft preparation: Hannes Graf; Writing review & editing: Hannes Graf and Carolin Huhn; Supervision: Carolin Huhn.



2. Graf, H. G., Biebl, S. M., Müller, L., Breitenstein, C., Huhn, C., Capillary electrophoresis applied for the determination of acidity constants and limiting electrophoretic mobilities of ionizable herbicides including glyphosate and its metabolites and for their simultaneous separation. *Journal of Separation Science* 2022; *45*, 1128-1139, DOI: 10.1002/jssc.202100952 cited as [2]

Conceptualization: Hannes Graf; Experiments and evaluation: Hannes Graf and Sonja Biebl, Linda Müller, Christina Breitenstein (all under supervision by Hannes Graf); Writing original draft preparation: Hannes Graf; Writing review & editing: Hannes Graf and Carolin Huhn; Supervision: Carolin Huhn.



3. Graf, H. G., Rudisch, B. M., Ude, L., Müller, L., Huhn, C., Picomolar detection limits for glyphosate by two-dimensional column-coupled isotachophoresis/capillary electrophoresis mass spectrometry. *Journal of Separation Science* 2022; *45*, 3887-3899, DOI: 10.1002/jssc.202200519 cited as [3]

Conceptualization: Hannes Graf and Benjamin Rudisch; Experiments and evaluation: Hannes Graf and Lukas Ude, Linda Müller (both under supervision by Hannes Graf); Writing original draft preparation: Hannes Graf; Writing review & editing: Hannes Graf and Carolin Huhn; Supervision: Carolin Huhn.

# Abstract English

The very low sample loadability of a few nanoliters precludes the application of capillary electrophoresis-mass spectrometry (CE-MS) in environmental trace analysis. Therefore, analyte enrichment is required to achieve the desired limits of detection. This can be achieved using the inherent preconcentration abilities of isotachophoresis (ITP), when coupled online to CE-MS.

In this study, a compact 2D setup for column-coupled isotachophoresis capillary electrophoresis-mass spectrometry (ITP/CE-MS) based on a modified commercial CE-MS setup for the sensitive analysis of anionic analytes is presented. Beside instrumental inventions, methodological aspects are a major focus of this thesis. The selected model compounds, glyphosate and its metabolites, are inherently difficult to analyze by chromatographic methods due to their high charge and polarity, necessitating derivatization. In contrast, electrophoretic methods are ideal, because their separation mechanism requires charged analytes and allow to analyze very sample volumes

The ITP/CE-MS setup was developed as a hybrid solution based on standard capillaries and a microfluidic glass chip as interface with integrated conductivity detection. This intermediate detector enabled to reliably transfer the stack of analytes between the separation dimensions. Thanks to the hybrid design, it was possible to use a single commercial CE-MS device with a modified injection system, a third vial holder (pressurizable, connectable to high voltage) and a high voltage switching box for ITP/CE-MS measurements. All modifications were flexibly installed in the commercial CE instrument and did not require any disassembly of the CE instrument. This allowed fast switching between 2D and 1D applications on the same device.

To optimize the separation conditions for both dimensions, the p$K_a$ values and limiting electrophoretic mobilities for glyphosate and its metabolites were determined between pH 1.2 and 12.0 by CE coupled to conductivity detection (CE-$C^4D$) at a very high

resolution using suitable buffer systems and the free AnglerFish software developed by Malý et al. (Malý et al., *Electrophoresis*. 2020, 41, 493-501). Thanks to the software-based correction of ionic strength effects on the analytes' effective electrophoretic mobility, the very low p$K_a$ values of the analytes were precisely determined for the first time.

With these data, optimal separation conditions for CE at different pH values were simulated and confirmed in experiments. CE-MS was successfully applied to real samples. The results revealed that phosphate is the most critical matrix component. In parallel, ITP-MS was optimized to ensure preconcentration of analytes as well as an effective separation from phosphate, not included in the ITP stack.

Finally, ITP-$C^4D$/CE-MS measurements were conducted to analyze glyphosate in aqueous samples achieving impressive limits of detection in the picomolar range.

# Zusammenfassung Deutsch

Die Nachweisgrenzen in der Kapillarelektrophorese-Massenspektrometrie (CE-MS) sind aufgrund der sehr geringen Probenbeladbarkeit für einige Anwendungen, wie z. B. die Analyse von Spurenstoffen in der Umwelt, nicht ausreichend. Daher ist eine Anreicherung des Analyten erforderlich. Zur Verbesserung der Nachweisgrenzen kann die Isotachophorese, welche Analyte effektive anreichern kann, als zusätzliche Trenndimension mit der CE-MS gekoppelt werden.

In dieser Studie wird ein kompakter 2D-Aufbau für die säulengekoppelte Isotachophorese/Kapillarelektrophorese-Massenspektrometrie (ITP/CE-MS) basierend auf einem modifizierten kommerziellen CE-MS-Aufbau für die nachweisstarke Analyse von anionischen Analyten vorgestellt. Neben instrumentellen Arbeiten sind auch methodische Aspekte ein Schwerpunkt dieser Dissertation. Die ausgewählten Verbindungen, Glyphosat und seine Metaboliten, sind aufgrund ihrer hohen Ladung und Polarität von Natur aus schwierig durch chromatographische Verfahren zu analysieren. In der Regel müssen sie vor der Analyse derivatisiert werden. Dagegen eignen sich elektrophoretische Methoden ideal für geladene Analyten, da dies die Grundlage des Trennmechanismus darstellt und zudem geringe Probenvolumen analysiert werden können.

Der ITP/CE-MS-Aufbau wurde in einem Hybridformat basierend auf Standardkapillaren und einem mikrofluidischen Glaschip als Schnittstelle mit integrierter Leitfähigkeitsdetektion entwickelt. Der intermediäre Detektor ermöglichte einen zuverlässigen Transfer der mittels ITP aufkonzentrierten Analyte zwischen den Trenndimensionen. Dank des Hybriddesigns war es möglich, ein einziges kommerzielles CE-MS-Gerät mit einem modifizierten Injektionssystem, einem dritten Vial-Halter (mit Druck beaufschlagbar, an Hochspannung anschließbar) und einer Hochspannungs-Schaltbox für ITP/CE-MS-Messungen zu verwenden. Alle Modifikationen konnten flexibel in das CE-Gerät selbst eingebaut werden und

erforderten keine Demontage des CE-Geräts. Dies ermöglichte ein schnelles Wechseln zwischen 2D- und 1D-Anwendung auf demselben Gerät.

Um die Trennbedingungen für beide Dimensionen zu optimieren, wurden die p*K*s-Werte und die elektrophoretischen Grenzmobilitäten für Glyphosat und seine Metabolite zwischen pH 1,2 und 12,0 durch Kapillarelektrophorese-Leitfähigkeitsdetektion (CE-$C^4D$) mit sehr hoher Auflösung unter Verwendung geeigneter Puffersysteme und der kostenlosen AnglerFish-Software von Malý et al. bestimmt (Malý et al., *Electrophoresis*. 2020, 41, 493-501). Durch die softwarebasierte Korrektur der Ionenstärkeeffekte auf die effektive elektrophoretische Mobilität der Analyte konnten erstmals die sehr niedrigen p*K*s -Werte der Analyten präzise bestimmt werden.

Mit diesen Daten wurden optimale Trennbedingungen für die CE bei unterschiedlichen pH-Werten simuliert und experimentell bestätigt. CE-MS wurde erfolgreich auf reale Proben angewendet. Die Ergebnisse zeigten, dass Phosphat die kritischste Matrixkomponente ist. Parallel dazu wurde die ITP-MS Trennung optimiert, um neben der Anreicherung der Analyte auch die effektive Abtrennung von Phosphat sicherzustellen, sodass es nicht im ITP-Stack enthalten ist.

Schließlich wurden ITP-$C^4D$/CE-MS-Messungen durchgeführt, um Glyphosat in wässrigen Proben zu analysieren, wobei hervorragende Nachweisgrenzen im pikomolaren Bereich erreicht wurden.

# 1 Motivation

The analysis of a wide range of non-polar to medium polar substances is well established, while the analysis of very polar and ionic compounds is still challenging. This analytical gap was mentioned by Reemtsma et al. and discussed as a threat to the quality of our water resources since these compounds are highly water soluble and can escape wastewater treatment, are mobile also in subsurface environments and may potentially contaminate drinking water [4, 5]. To close this gap, several derivatization approaches were published, and chromatographic and electromigrative separation methods were developed. Since these separation methods rely on orthogonal separation mechanisms, it is beneficial to establish both, especially with regard to possible matrix effects [5].

A drawback of electromigrative separation techniques, like capillary electrophoresis (CE), are their comparatively poor limits of detection (LOD) which are not sufficient for trace analysis due to their inherently low sample loadability. To improve LODs, different off-line and on-line sample preconcentration techniques were described in literature. Among all on-line preconcentration methods, isotachophoresis (ITP) proved to be the most robust, powerful, and universal one. Hence, in this thesis, a new approach was investigated for the sensitive analysis of very polar ionizable analytes by column-coupled isotachophoresis with intermediate capacitively coupled contactless conductivity detection/capillary electrophoresis-mass spectrometry (ITP-$C^4D$/CE-MS).

# 2 Introduction

## 2.1 Challenges in analyzing polar analytes

Persistent and mobile water micropollutants stem from diverse chemical classes and application fields. At the same time, they are problematic in analytics since they are not well addressed by common and well-established methods, like reversed phase liquid chromatography interfaced with mass spectrometry (RPLC-MS). This limitation is due to their polar character and makes it difficult to include them in multi-analyte methods and thus in routine analysis [6]. The need to monitor these compounds becomes also evident by the fact, that biotic transformation processes usually produce degradation products that are more polar and more water-soluble than the parent compounds [7]. Gas chromatography (GC) is not applicable to polar compounds since they have a very low vapor pressure preventing evaporation. Further, their high polarity strongly prevents interaction with the stationary phase in RPLC so many of them elute in or close to the void volume so that quenching effects are likely in the ionization process of the mass spectrometric detection. Time consuming and laborious derivatization steps can be implemented in sample preparation to reduce the polarity of analytes and to increase their volatility, however, at the cost of reduced accuracy and throughput. In addition, appropriate derivatization methods are not available for all target analytes [8]. A derivatization free analysis by chromatographic methods is possible when using hydrophilic interaction liquid chromatography (HILIC) [9], supercritical fluid chromatography (SFC) [10], mixed-mode liquid chromatography (MMLC) [11] or ion exchange chromatography (IEC) [12] but none of them is yet established in routine analysis. Electrophoretic separation methods can be used as an alternative for charged and ionizable analytes [6].

## 2.2 State of the art in the analysis of glyphosate and its metabolites

As a challenging model analyte for a mobile water contaminant glyphosate was selected in this thesis. Its polar character and its three ionizable functional groups make its separation difficult. In addition, direct detection by spectrophotometric techniques is hardly possible due to the absence of a chromophore. As glyphosate is the herbicide most heavily applied worldwide, also its transformation products from its major microbial degradation pathways are of interest [13-16]. Glyphosate is either transformed into aminomethylphosphonic acid (AMPA) and glyoxylic acid by glyphosate oxidoreductase or into sarcosine and phosphate by carbon-phosphorus lyase. Further, glyphosate can be acetylated to *N*-acetyl glyphosate by glyphosate *N*-acetyltransferase in genetically modified plants which further degrades to *N*-acetyl AMPA. Sarcosine further degrades to glycine by sarcosine oxidase, whereas AMPA further reacts to phosphate and methylamine by C-P lysase [16-22]. Another metabolite, rarely detected, is hydroxymethyl phosphonic acid (HMPA), which was observed in surface water [20]. A scheme of the degradation pathways is given in Figure 1. In order to show all methods' broader applicability, further acidic model analytes were included like the herbicides glufosinate and 2-methyl-4-chlorophenoxyacetic acid (MCPA) as well as oxamic acid, formed during ozonation from the herbicide chloridazon [23], their structural formulas are shown in Figure 1.

The need for glyphosate analysis is comprehensible by its ubiquitous occurrence in the environment [24-26]. Residues can also be found in food samples like cereals, vegetables, fruits and nuts, animal-derived products, baby food, alcoholic beverages, water samples, and urine samples, etc. [15, 27-29]. The LOD required for a glyphosate determination method can be derived from the maximum contaminant level specified by directives. The maximum contaminant level for pesticides (includes glyphosate) is 0.1 μg/L according to the council directive 98/83/EC on the quality of water intended for human consumption in the European Union, whereas according to the United States National primary drinking water regulations a concentration of 0.7 mg/L in

water is permitted. Maximum residue levels in food range from 0.1 mg/kg up to 30 mg/kg depending on the matrix and the directive [26].

The main metabolite of glyphosate, AMPA, can also originate from degradation of phosphonates like nitrilotris-methylenephosphonic acid, diethylenetriaminepenta-methylenephosphonic acid, ethylene diamine-tetra-methylenephosphonic acid, hexaethylenediamine-tetramethylenephosphonic acid and 1-hydroxyethane 1,1-diphosphonic acid. They are used as detergents, fire retardants, anticorrosives and anti-scaling agents etc. [30].

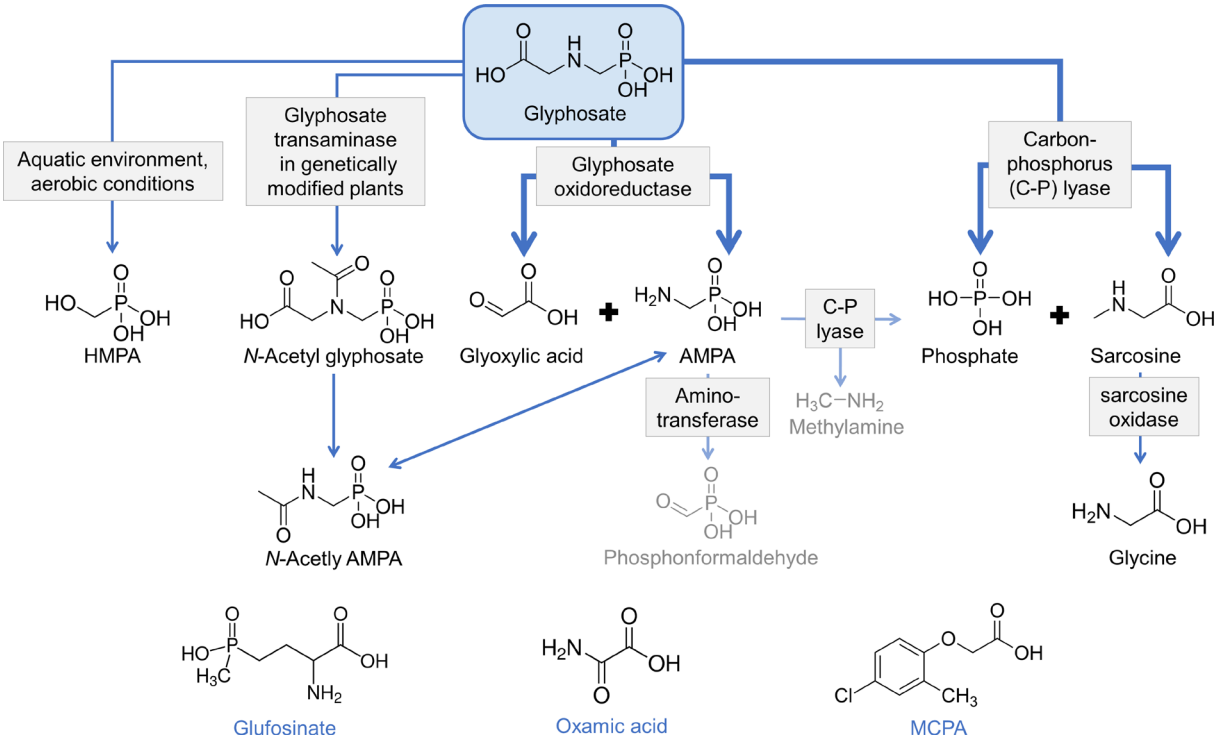


Figure 1. Degradation pathways of glyphosate adapted from [16]. Substances greyed were not included in this study. The bottom row (blue font) shows the structural formulas of further acidic model analytes that were part of this study.

A large variety of separation and detection methods were applied to samples containing glyphosate and its metabolites. Screening the literature from 2016 to early 2022, about 200 papers were published on the topic of glyphosate analysis using a separation technique. Ranked by the number of reports, the following separation methods were used: liquid chromatography, ion chromatography, capillary electrophoresis, and gas chromatography. Most often, mass spectrometry (MS) was used for detection, followed by UV/Vis spectrophotometry, fluorescence

detection (FLD) and conductivity detection (CD). Several reviews regarding glyphosate analysis were published [14, 15, 31-37]. An extensive summary on publications (2016-early 2022) using liquid or ion chromatographic separation methods of glyphosate and its metabolites can be found in the Appendix I in Table A1 including analyzed matrix and LOD data. A summary of CE methods until 2018 was published by Gauglitz et al. [38] and a continuation of it was compiled in Appendix I, Table A2.

In the following sections, selected separation methods are discussed in more detail to demonstrate the advantages and limitations of the electromigrative separation techniques developed in this thesis. The focus here lies on the separation rather than LODs, which strongly depend also on sample pretreatment including enrichment strategies.

### 2.2.1 Chromatographic separation methods

#### 2.2.1.1 Reversed phase liquid chromatography

Despite the need for derivatization to reduce the analytes' polarity, reversed phase liquid chromatography on $C_{18}$ columns coupled to tandem mass spectrometry (MS/MS) is currently the first choice for glyphosate analysis. Fluorenylmethyloxycarbonyl chloride (FMOC-Cl) was nearly exclusively used in precolumn derivatization [39-42], which is also described in the DIN ISO 16308:2017-09 for the determination of glyphosate and AMPA in water [43]. Since glyphosate tends to form complexes with metal ions or organic matter, derivatization can be impaired and therefore also reliable quantification. Acidification [40] and addition of ethylenediaminetetraacetic acid (EDTA) [44] reduce the problem. The *N*-acetylated metabolites of glyphosate and AMPA are difficult to be included in the screening and the derivatization step itself is time consuming [45]. Reversed phase liquid chromatography was applied to water samples [40-42, 46], soil samples [39, 47], food samples [48-50] and urine samples [51], etc. Mostly, MS/MS detection was chosen for analysis of FMOC derivatives. A broader variety of derivatization strategies was described when using

fluorescence [52] or UV/Vis detection [53-56]. Depending on the sample preparation and the sample volume used, the detection limits can vary greatly. For example, Surapong et al. reported a twentyfold lower LOD after introduction of a solid phase extraction (SPE) step in the sample preparation [57]. An exceptional low LOD below 1 ng/L for RPLC-MS/MS was reported by Hanke et al. using SPE and evaporation to enrich the samples by a factor >300 [42].

#### 2.2.1.2 Liquid chromatography using porous graphitic carbon columns

In combination with mass spectrometry, porous graphitic carbon (PGC) columns were employed to directly separate underivatized glyphosate and AMPA [58], including also their *N*-acetylated counterparts [59]. Successful applications in different matrices included beer [60], food [61], serum [62], and soils [63].

#### 2.2.1.3 Hydrophilic interaction liquid chromatography

Hydrophilic interaction liquid chromatography (HILIC) coupled to tandem mass spectrometry was used for a derivatization-free separation of glyphosate. Common HILIC columns applied were the Obelisc N (Sielc) [45, 64-66], the anionic polar pesticide [49, 67, 68] and Torus DEA (Waters) [69-71]. Advantageously, HILIC-MS is well suited for the analysis of the *N*-acetylated forms of AMPA and glyphosate as shown by Dias et al. [67], Lopez et al. [45, 65] and Manzano-Sánchez et al. [69]. However, Botero-Coy et al. reported that the robustness of HILIC columns suffers from rapid degradation over time and extreme care and continuous testing of retention times and peak shapes was required for a reliable analysis [64].

#### 2.2.1.4 Ion exchange chromatography

Strong anion exchange (SAX) chromatography coupled to tandem mass spectrometry was also applied for glyphosate analysis. Alternatively, conductivity detection or fluorescence detection enabled by post-column derivatizations with o-phthalaldehyde [72-74] were used. Applications include analyses of food [75-77], water [78], human urine [79], and serum [80], etc.

### 2.2.2 Gas chromatography

For the separation of glyphosate by gas chromatography a derivatization step is required to increase volatility. Most often, a reaction to yield the trifluoroacetic acid derivate was performed, but many other approaches were also described [81-83]. The major detection method was mass spectrometry with electron impact ionization [81, 82, 84, 85], but also detection by electron capture [86] or flame photometry was implemented [87]. In case of tandem mass spectrometric detection limits of quantification (LOQ) in the 10-100 ng/L range were reported [84].

### 2.2.3 Electrophoretic methods

In about 50 publications, the analysis of glyphosate by electrophoretic methods was described. For detection, nonspecific methods like capacitively coupled contactless conductivity detection ($C^4D$) and indirect UV/Vis spectrophotometry were often chosen. After derivatization of the analytes also laser induced fluorescence or UV/Vis spectrophotometry were used. The most specific detection was provided by CE-MS. A wide range of separation conditions were used with the pH of the background electrolyte (BGE) ranging from 2 to 10. An overview on pesticide/herbicide analysis by CE in general is covered in [88-92].

#### 2.2.3.1 Capillary electrophoresis-capacitively coupled contactless conductivity detection

Separations of glyphosate, AMPA and glufosinate at a pH of 6.3 and with cetrimonium bromide as electroosmotic flow (EOF) modifier were reported by See et al. using a CE-$C^4D$ setup. Preconcentration of analytes was achieved by field-amplified sample injection (FASI), large volume sample stacking (LVSS), dynamic supported liquid membrane tip extraction, electro membrane extraction (EME) and combinations thereof providing LODs of glyphosate as low as 0.005 µg/L [93-96].

#### 2.2.3.2 Capillary electrophoresis-indirect UV/Vis spectrophotometry

An alternative universal detection method to $C^4D$ is indirect UV/Vis spectrophotometry when an absorbing probe ion is part of the BGE and displaced by the analyte ions during separation. In glyphosate analysis, the most common probe ion was phthalate using a pH of the BGE between 6.5 and 7.5. The LODs were in the range of 2 to 800 µg/L and strongly depended on the enrichment techniques used like FASI [97], supported liquid membrane extraction [98], SPE with cation or anion exchange resin or molecularly imprinted polymers [99-102].

#### 2.2.3.3 Capillary electrophoresis-UV/Vis spectrophotometry

To enable glyphosate detection by direct UV/Vis spectrophotometry, a derivatization step was required to introduce a chromophore. Most often, the amine function of glyphosate and AMPA were addressed for labeling with FMOC or phenylisothiocyanate. In contrast to derivatization procedures prior to chromatographic separation, no sample clean-up from derivatization agent residues was necessary. To yield LODs in the low µg/L range, preconcentration methods like SPE or LVSS were chosen [103-105]. Also, a FASI sweep-micellar electrokinetic chromatography was used in combination with UV/Vis detection [106].

#### 2.2.3.4 Capillary electrophoresis-laser induced fluorescence detection

Also, capillary electrophoresis-laser induced fluorescence detection (CE-LIF) requires a derivatization step of the analytes. A wide range of derivatization reagents was applied, for example, fluorescein isothiocyanate and derivatives of it [107-112]. Muñoz et al. used CdTe/CdS quantum dots for derivatization to induce fluorescence [113]. The separations were not only performed in capillaries but also on chip devices [109]. Both CE and methods of micellar electrokinetic chromatography were used for separation [110-112, 114]. A sodium borate buffer at pH 8 to 10 was used in most applications allowing LODs in the µg/L to sub-µg/L range. Sometimes, organic modifiers [108, 115] or detergents like Brij-35 [107] were added to improve resolution. An indirect CE-LIF method was reported using fluorescein as probe ion [116].

#### 2.2.3.5 Capillary electrophoresis-mass spectrometry

The most specific detection method for CE is mass spectrometry. No derivatization of glyphosate is required, and the LODs are in the μg/L range. In case of electrospray ionization (ESI) volatile buffers made of ammonium acetate or formate were used at a pH between 2.4 and 10 [117-119]. Lowest glyphosate LODs were achieved using sample-induced (50 mM phosphate from extraction media) transient isotachophoresis (tITP) in soil analysis (LOD: 5 μg/L) [120] or dispersive SPE in combination with a sheathless ESI interface for baby food analysis (LOD: 0.5 μg/L) [121]. Inductively coupled plasma mass spectrometry was also applied to detect glyphosate after separation by CE but showed LODs in the range of 50-760 μg/L due to high ionization potential of phosphorus [122, 123].

#### 2.2.3.6 Isotachophoretic methods

ITP is not only useful as a preconcentration method, but it can also be used to achieve analyte separation. Regarding glyphosate determination, ITP with conductivity detection was used by Křivanková et al. for analyzing glyphosate synthesis mixtures. Chloride was used in the leading electrolyte (LE) (pH 9.25) and beta-alanine in the terminating electrolyte (TE) (pH 11) [124]. Goodwin et al. also used ITP with conductivity detection, but used a column-coupled setup to enhance the loadability by a large inner diameter of the first capillary whereas the detection took place in a small inner diameter capillary to elongate the zones and therefore lower the detection limit to 25 μg/L. Glyphosate from an aqueous standard solution was stacked between chloride (as LE, pH 5.2) and 2-(*N*-morpholino)ethanesulfonic acid (MES) (as TE) [125]. A more sophisticated setup developed by Koukalová et al. also used ITP coupled to conductivity detection with an asymmetric neutralization reaction boundary using electrokinetic injection dosing, reaching an LOD of 6 mg/L which was subsequently improved to 153 μg/L by carrier ampholyte free isoelectric focusing requiring a three electrode setup and two different acidic leading electrolytes [126].

## 2.3 Enrichment principles for capillary electrophoresis

Based on the fact, that only very low volumes of the sample can be injected into the capillary, a wide variety of enrichment methods were implemented in CE methods to optimize LODs. They can be categorized based on their physicochemical principle, into chromatographic, electrophoretic, and isotachophoretic methods. In addition, also electric field-driven extraction can be performed. Bi-annual reviews from Breadmore et al. [127] and Gebauer et al. classified these methods in sample stacking [128] and isotachophoresis [129]. Further reviews are [5, 130-132]. Applications in glyphosate analysis are reviewed below.

### 2.3.1 Chromatographic enrichment

#### 2.3.1.1 Solid phase extraction

Solid phase extraction is based on the ability of the stationary phase to bind the target analytes at the conditions given in the (modified) sample solution while elution is achieved by using suitable conditions. By selecting an appropriate solid phase, ideally, only target analytes are retained and matrix removal as well as analyte enrichment can be achieved. A wide variety of chemistries are available for different adsorbents, for example reversed phase ($C_8$, $C_{18}$), hydrophilic-lipophilic balance (HLB), mixed mode/cation-exchange, mixed-mode/anion-exchange, weak anion exchange, multiwalled carbon nanotubes (MWCNTs), and molecularly imprinted polymers (MIPs) are commonly used for SPE [131, 133-135]. Enrichment is possible since a large amount of sample containing low concentrated analyte can be processed and analytes eluted in a much smaller volume [136]. Weaknesses of this approach are particularly evident when the focus is on very polar analytes, since the use of ion exchange resins as sorption material requires ionic eluents, which can impair separation by CE or self-elution is observed for samples of high-ionic strength [92, 136]. Several strategies were published to couple SPE with a direct stream of analytes to CE (SPE-CE) [134, 137]. When the SPE sorbent is inserted into the CE capillary itself

in-line SPE-CE is used, which can be performed with a regular CE instrument. The sorbent in the capillary leads to a high back pressure causing slow sample loading. Furthermore, it influences the separation process, and a residue-free removal of matrix components is not ensured, which can also impair the separation. These limitations can be circumvented by using an on-line SPE-CE approach where the SPE column is not part of the CE capillary itself. The desorption volume of the SPE is then transferred directly to the capillary via an interface with flow-switching capabilities. Vials, valves, and T-pieces are interfaces used most often for on-line SPE-CE [137]. Often, only a fraction of the desorbed volume is injected limited by the low loadability of the CE [127, 137].

Regarding the analysis of glyphosate by CE with an offline SPE-CE, different sorbents were examined. Given the strong acidity of glyphosate and AMPA, anion-exchange residues were often applied for the analysis of tap and surface water samples with elution by chloride ions [100, 104]. Sample enrichment by cation-exchange SPE was carried out for strongly acidified water samples using a mixture of aqueous hydrochloric acid and methanol for elution [99]. The strong affinity of phosphonic acids to aluminum and titanium ions, was utilized for SPE strategies: 1) alumina-coated iron oxide nanoparticles were applied to extract glyphosate from fruit samples. Elution was accomplished with phosphate as a strong competitor [138]. 2) $Fe_3O_4$ nanoparticles with immobilized $Ti^{4+}$ were used to enrich glyphosate and AMPA from river water. The eluate with trisodium phosphate was subjected to derivatization with FMOC-Cl and final analysis by CE-UV [105]. 3) Dispersive SPE with core-shell mesoporous silica microspheres coated by titanium dioxide were used to extract and enrich glyphosate from the supernatant of dissolved baby food followed by elution using 5 % ammonia in methanol [121]. Molecularly imprinted polymers were also used for SPE of mineral, ground, and seawaters with elution by hydrochloric acid or ammonia solutions [101, 102]. A review dedicated to SPE of glyphosate in the analyses of environmental, plant, and food samples was compiled by Rigobello-Masini et al. [139]. Neither in-line nor on-line SPE-CE was reported in glyphosate analysis.

#### 2.3.1.2 Liquid-liquid extraction

A water-immiscible organic phase is used in liquid-liquid extraction to transfer hydrophobic analytes from an aqueous sample to an organic phase. The distribution of the analyte between the two phases can be adjusted by pH, the addition of a complexing agent or salts, etc. [133]. Enrichment and compatibility to CE analysis is achieved by evaporating the organic solvent and reconstitution of the residue in an aqueous injection solution [92]. The drawbacks of this approach are a less-than-quantitative recoveries resulting for example from incomplete phase separations, the use of specialty glassware and the disposal of large quantities of organic solvents [133]. For glyphosate, the transfer to an organic phase is difficult due to its high polarity. Only after prior derivatization to a less polar compound is this method usefully applicable.

**Single-drop micro extraction**

A miniaturized liquid-liquid extraction method is single-drop micro extraction, where a large volume of sample is extracted by a drop of extraction phase which is typically supported by a microsyringe. For on-line coupling with CE the drop can also be supported by the tip of the separation capillary [140]. Given glyphosate's and AMPA's high electrophoretic mobility, this extraction method would be interesting for pesticide analysis.

**Supported liquid membrane extraction**

In supported liquid membrane (SLM) extraction, a three-phase system is used. Two aqueous phases are separated by an organic phase immobilized in a porous hydrophobic membrane. One of the aqueous phases is the donor solution containing the sample and the other aqueous phase is the acceptor solution [90]. An example application was a miniaturized SLM setup housed directly in a CE vial allowing direct injection into a capillary which was mounted in a commercial CE instrument [141]. SLMs were also applied for glyphosate analysis: Dżygiel et al. combined a classic SLM approach with CE and indirect UV/Vis absorbance detection [98]. See et al. used a dynamic supported liquid membrane tip extraction with a cationic carrier for offline enrichment prior to analysis by CE-$C^4D$ with LVSS [95].

## 2.3.2 Electrophoretic enrichment principles

### 2.3.2.1 Field-amplified sample stacking

One of the simplest methods to enhance LODs in capillary electrophoresis is the use of field-amplified sample stacking (FASS). When the conductivity of the injected sample plug is lower than the one of the BGE, a higher electric field is present in the sample plug, which enhances the migration velocity of the analyte ions in the sample plug. This causes a concentration of analyte ions at the boundary between the sample plug and the BGE [142]. If an electrokinetic sample injection is used instead of a hydrodynamic one, the method is called field-amplified sample injection (FASI) [127], which can reach impressive enrichment factors, however, normally strongly matrix-dependent. In glyphosate analysis, See et al. used FASI in combination with CE-$C^4D$ reaching an impressive LOD of 500 pM in aqueous standard solutions. To enhance enrichment and reproducibility, a water plug was injected prior to the FASI step. A tenfold higher LOD for tap water samples was determined due to the sample dilution necessary to reduce matrix effects from salts [94]. Cikalo et al. applied the same method (FASI + water plug) to aqueous standard solutions in combination with indirect UV detection yielding an LOD of 10 nM while experiments with aqueous wheat extracts failed due to their high sample conductivity [97].

### 2.3.2.2 Large-volume sample stacking

Large-volume sample stacking (LVSS) also requires samples dissolved in a low-conductivity solution. After hydrodynamic injection of the sample, the analyte ions are stacked at the boundary between the sample plug and the BGE when voltage is applied due to the higher migration velocity of the analyte ions in the sample plug caused by the higher electric field. The sample solvent is removed at the same time since the analyte ions and the EOF move in opposite directions. There are two different operational modes: 1) LVSS with polarity switching is a two-step process. First, the polarity of the inlet is set identical to the charge of the analytes and the charge of the capillary surface (for cations, a capillary coating is required) leading to an EOF directed

to the inlet. This step is stopped when the current equals about 95 % of the current of the capillary filled only with BGE. Second, the separation step is conducted by applying reversed voltage [143-145]. 2) For LVSS without polarity switching a voltage with the same sign as the analytes is applied to the inlet. The removal of the sample solvent is achieved by a high EOF towards the inlet within the sample plug and a lowered or reversed EOF in the zone filled with BGE. This spatial EOF difference can be achieved by using an EOF modifier in the BGE [146] or a lower pH in the BGE than in the sample, which leads to a lowered EOF [147]. Applications of LVSS in glyphosate analysis were reported occasionally, for example in combination with detection by MS [120], $C^4D$ (tap water sample) [94], UV/Vis absorbance [103], or flame photometric detection (aqueous standard sample) [148].

#### 2.3.2.3 pH-mediated stacking

With pH-mediated stacking it is a possible to transform a high-conductive sample plug into a low-conductivity one. This allows sample stacking like in FASS or LVSS. To lower the conductivity of a zone, a titration is performed in the capillary, for example, by an acid migrating into a zone of high pH resulting in a decreased ionic strength [149, 150]. This method is especially useful in combination with of an electrokinetic sample injection.

#### 2.3.2.4 Dynamic pH junction

In case of analytes whose mobilities and charges are a function of the pH, the dynamic pH junction can be applied. A large sample plug is hydrodynamically injected, and its pH is chosen so that the analyte has no overall charge or, in case of ampholytes as analytes, is oppositely charged in the sample plug than in the BGE. After applying voltage, ions from the BGE (especially $H^+$ and $OH^-$) of a high or low pH (depending on the analytes) migrate into the sample plug of a different pH. There, analytes are mobilized. The zone with uncharged analytes is narrowed and analytes are concentrated [149]. This method can be used regardless of the conductivity of the sample solution. An application of this method to glyphosate is not yet described, but

a possible approach is to use a very acidic sample to protonate glyphosate and therefore lower its mobility. For separation, a BGE with a higher pH can be used. To meet the requirements for this method under less harsh conditions, it would be useful to derivatize glyphosate to a less acidic compound.

### 2.3.3 Isotachophoretic enrichment

Another online enrichment technique uses isotachophoresis (ITP) with a discontinuous electrolyte system. A sample plug is injected between a terminating (TE) and a leading electrolyte (LE). The electrophoretic mobilities of analytes must be lower than the one of the leading ions but higher than the one of the terminating ions. After application of voltage, the analytes are concentrated (stacked) between the leading and terminating zones according to the Kohlrausch regulation function [151]. On the one hand, the use of ITP allows to concentrate trace substances in the presence of ionic macrocomponents and on the other to separate matrix compounds from the analytes by selecting appropriate leading/terminating ions with mobilities slower or faster than the matrix compounds. Different approaches in combining ITP and CE (ITP/CE) were described in literature, discussing also theoretical aspect [152-157] and providing illustrative model applications [127, 129]. In general, it can be distinguished between transient isotachophoresis (tITP), two-dimensional single capillary ITP/CE and column-coupled ITP/CE which in turn can be categorized according to the type of transition from ITP to CE conditions: 1) L-S-L, where the leading electrolyte (L) from the ITP step serves as the background electrolyte (BGE) during CE (S = sample), 2) T-S-T, where the terminating electrolyte (T) from the ITP step serves as the BGE during CE, 3) BGE-S-BGE, where L, T and BGE are mutually different, and 4) T-S-BGE, where the ITP is only partially dissolved for sample ions faster than the coion of the BGE [154, 157].

#### 2.3.3.1 Transient isotachophoresis

Transient ITP (tITP) is performed in a single capillary and is accomplished through a coion that temporarily serves as leading or terminating ion. This coion can originate from a macrocomponent of the sample (sample-induced tITP), from the addition of a transient leading ion to the sample or from a zone injected separately. The other coion originates from the BGE. The tITP stack dissipates to zone electrophoretic separation over time [127, 158, 159]. A sample-induced tITP of glyphosate caused by an excess of phosphate ions originating from soil extraction media was observed by Wimmer et al. in CE-MS [120, 160].

#### 2.3.3.2 Two-dimensional single capillary ITP/CE

In two-dimensional single capillary ITP/CE, ITP and CE are conducted in two steps, by performing first ITP and subsequently CE in the same capillary. This requires to remove either LE or TE prior to the CE step [161-163]. Since in most setups counterflow is used to achieve this, a coupling to mass spectrometric detection is not straightforward. Two single capillary ITP/CE-MS setups were reported but not yet applied for glyphosate analysis [160].

#### 2.3.3.3 Column-coupled ITP/CE

This section is mostly taken from my publication [3], see Appendix III, Paper 3.

A higher flexibility, for example, in the choice of different capillary inner diameters and different electrolytes can be achieved by column-coupling ITP to CE. The first applications of column-coupled ITP/CE were described by Kaniansky and Marák [164] using an adapted column-coupled ITP/ITP setup originally developed by Everaerts et al. [165, 166]. The modular, hydrodynamically closed setup with two capillaries of different inner diameters, each equipped with one conductivity detector and an additional UV/Vis detector in the second dimension [165-168], was used in its commercialized version in about forty publications, the most recent of the major contributing authors are [169-173]. This setup was mostly used with a T-S-T system [164, 174]. Column-coupled ITP/CE was also hyphenated to laser induced

fluorescence detection (LIF) in a setup developed and applied by Mikuš et al. for ultrasensitive detection of fluorescing compounds in multicomponent matrices [175]. In 2010, Foret et al. coupled the commercial ITP/CE setup with MS, hydrodynamically transferring the analytes to the MS [176]. This setup was applied by Piešťanský et al. to determine pheniramine [177, 178], varenicline [179] and serotonin [180] in urine.

Earlier attempts of combining column-coupled ITP/CE to MS used two high voltage supplies and a narrow capillary (for CE) inserted into a wider capillary (for ITP). The electrokinetic transfer between both dimensions required all ITP separation potentials to be offset by +2 kV relative to the MS. After the analyte transfer to the second dimension column, the ITP capillary was flushed with LE to provide a homogeneous BGE for the second dimension CE [181, 182]. A similar fluidic setup was used by Peterson et al., who continuously applied voltage from the TE vial to the MS while the ITP was flushed back and forth over the splitting point by injecting LE from a side channel. A UV/Vis detector mounted just before the splitting point timed the fractions [183].

In several publications, Neusüß et al. described column-coupling methods with final detection by MS. Different valves made from polyether ether ketone and a polyaryletherketone/polytetrafluoroethylene composite were used for interfacing. Depending on the separation modes coupled, at least two CE instruments were used and up to two intermediate detectors (UV/Vis and $C^4D$) were mounted in front of the valve to calculate the arrival time of analytes in the valve and to transfer them to the second dimension via valve switching [184, 185]. Several studies used ITP/CE fully integrated on microfluidic chips with conductivity detection at the end of each separation dimension [186-188]. This column-coupling ITP-$C^4D$/CE-$C^4D$ approach fully integrated in a microfluidic chip was also used by Horčičiak et al. for the analysis of glyphosate using a BGE-S-BGE electrolyte system [189]. Further column-coupling strategies applied with other combinations of separation modes are reviewed elsewhere [168, 190]. An almost complete list of ITP/CE-MS and ITP/CE setups and their application in presented in the Appendix I, Tables A3 and A4.

### 2.3.4 Electric field-driven extraction

The extraction through a membrane may be supported by electric fields to enable electro membrane extraction (EME). Here, a direct current electric potential is applied across an SLM. Charged analytes with a sufficient solubility in the immobilized organic phase are forced by the electric field to migrate from the donor solution through the SLM into the acceptor phase. Ideally, this results in an efficient elimination of matrix components, like salt ions or high molecular weight species since they are not able to pass the SLM, whose selectivity is tuned accordingly. Additionally, analytes can be enriched since the volume of the acceptor solution can be lower than the one of the donor solution [191]. Current reviews on this topic are [192-194]. As an alternative to a SLM, See et al. presented and electric field-driven extraction and preconcentration method using a cationic carrier-mediated polymer inclusion membrane. The model analytes glyphosate and AMPA were analyzed online by CE-$C^4D$ and a 26 to 95-fold enrichment was reached [93, 96].

# 3 Results and Discussion

All results and most of the discussions in this thesis were published after a peer-review process under the Creative Commons license (CC BY 4.0), compare *List of Research Papers* and references [1-3]. Some sections contain literal quotes from my publications (see indication at the section header).

With the aim to achieve sensitive analysis of glyphosate and its metabolites, a two-dimensional column-coupled ITP/CE-MS approach was developed, because ITP is the most robust, powerful, and universal preconcentration method. It allows matrix removal, does not require offline sample preparation steps, and provides a clearly higher loadability compared to CE. Ideally, the setup is user-friendly, automatized, compact and requires only minor modifications to a commercial CE-MS device. The methodological and instrumental details of this approach were described in my publications [1, 3], see Appendix III, Papers 1 and 3.

To optimize the conditions for the analysis, the $pK_a^{\circ}$ values and limiting electrophoretic mobilities for glyphosate and its metabolites were determined, compare my publication [2], see Appendix III, Paper 2. This allowed to individually optimize the conditions for the ITP and the CE step by simulations, which were then verified experimentally. For the ITP step, the focus was set on the simultaneous analyte enrichment and the removal of phosphate as the most critical matrix component in CE separations of glyphosate [120, 189].

The development of the ITP-$C^4D$/CE-MS method is divided in an instrumental part and a methodological part.

## 3.1 Instrumental developments

First, the strategy for column-coupling ITP with CE-MS and the required modifications of a commercial CE-MS instrument are presented. To facilitate the analyte transfer between the separation dimensions, intermediate $C^4D$ was integrated and all necessary electronics were developed. The results with the new detector were compared for on-capillary detection to other $C^4Ds$ and finally adapted for in-chip application.

### 3.1.1 Strategy of column-coupled ITP/CE-MS

This section contains text excerpts that were part of my publication [3].

The basis for the new setup was an earlier ITP-$C^4D$/CE-MS setups which was develop by Kler et al. and who also used an adapted CE-MS instrument [168]. It was applied to cationic analytes (mostly peptides) using the LE as BGE in the second dimension CE-MS forming an L-S-L system which is less common in ITP/CE compared to T-S-T systems [168]. In a further development of Kler et al., a hybrid capillary-chip setup with a common section between the ITP and CE dimension were presented and included intermediate $C^4D$ detection directly in front of or on the common section enabling reliable analyte transfer in a non-aqueous ITP-$C^4D$/CE-MS [195]. A commercial CE-MS instrument was extended by an external multivial holder and a custom-made multiport high voltage source to allow a free choice of the BGE in the CE dimension (BGE-S-BGE format) [195]. Both setups had a straight separation path in the chip avoiding bends for analyte migration inevitably leading to band broadening. Using microfluidic chips made from glass, a homogeneous surface was present over the whole migration path. Kler et al. showed also that similar dimensions of the entire separation path are beneficial [168].

In this thesis, a new user-friendly and compact ITP-$C^4D$/CE-MS setup was developed to achieve sensitive analyses of anionic analytes. It combines the previous achievements by Kler et al. with an improved interface technology suggested by Sydes et al. [168, 195, 196]. A scheme of the new setup is given in Figure 2A. A hybrid capillary microfluidic glass chip was used on a single adapted commercial CE-MS instrument.

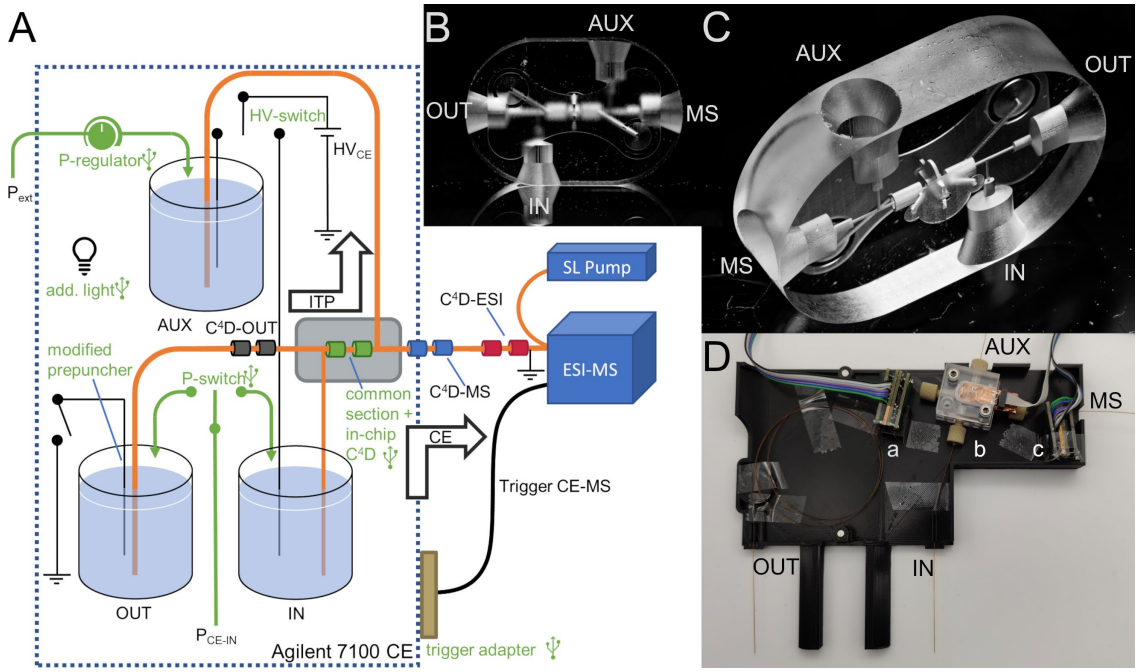


Figure 2. (A) Scheme of the ITP-C$^4$D/CE-MS setup with four C$^4$Ds (one in-chip) and ESI-MS detection; gray box: microfluidic chip, amber: capillaries, green: compressed air (P) supplied by the CE instrument ($P_{CE-IN}$) or the external laboratory pressure system ($P_{ext}$), black: electric circuit, the green text indicates adaptions to the commercial CE-MS. (B) Front and (C) back view photo of the fused silica chip including a double T-shaped microfluidic structure to transfer analytes between two dimensions (common section) and a C$^4$D geometry around it. (D) Photo of the open 3D printed CE cassette with the fluidic setup including a) C$^4$D-OUT, b) in-chip C$^4$D and c) C$^4$D-MS. The capillaries are labeled according to the capillary ends. Figure and figure caption were taken from [3], see Appendix III, Paper 3.

The core element of the setup was a microfluidic chip produced with selective laser-induced etching technology, see Figure 2B and C [197]. The chip included a double T-shaped microfluidic structure (inner diameter: 100 µm) giving rise to a common section of 4 mm with an inner volume of 31 nL. Since an intermediate in-chip C$^4$D was placed directly on this common section of the ITP and CE dimension, no calculations or preliminary evaluation steps to successfully time the transfer of the analytes were needed in this setup. This is advantageous especially for first dimension separations, where the migration speed changes over time such as ITP conducted at constant voltage. Effects on EOF velocities, changes in buffer pH, and so forth, are thus considered automatically, giving rise to higher robustness of the setup. All components including the capillary-chip connections were modular and flexibly installed. The CE cassette was replaced by a 3D printed one to allow a more flexible positioning of the chip interface in it and ensure an easy installation in the CE instrument, see Figure 2D.

### 3.1.2 Modifications of a CE-MS setup towards a 2D ITP/CE-MS setup

This section contains text excerpts that were part of my publication [3].

When modifying the commercial CE-MS instrument for 2D applications, it was desired to make as few changes as possible to the standard CE-MS setup. Thus, the four capillaries inserted into the chip interface were installed as follows: 1) The ITP (1st dimension) was performed from the CE's outlet (OUT) to the auxiliary vial housing (AUX) which was installed in a recess of the CE's insulation plate. 2) The CE-MS separation (2nd dimension) was performed from the CE's inlet position (IN) to the MS as in standard CE-MS, compare Figure 2A. Therefore, the sample injection must be accomplished from the CE's outlet. This was well possible using the autosampler with a small adaptation of the CE's pressurization system. The built-in precise compressed air system of the CE is only connected to the inlet position. To enable pressurization of the outlet vial, the compressed air supply of the inlet was split, and two software-controlled solenoid valves connected it either to IN or OUT or both. The compressed air system was connected to the vials via a prepuncher, which also ensured the access of the electrodes and capillaries to the vials. Vials were sealed to maintain the applied pressure when the vial handler was in the top position. In the load position of the vial handler, a gap between the prepuncher and the electrode was present. By the CE's software, the outlet could just be set to the load position. Therefore, an elongated prepuncher was developed to seal the outlet vial already in the load position. At the inlet, the vial was lifted some millimeters to close this gap while applying pressure.

The auxiliary vial housing was an airtight container for a vial, which was equipped with an electrode and a compressed air connector to apply of high voltage and compressed air to the housed vial. Sufficient insulation was necessary to prevent flashovers between its electrode and the CE's housing.

### 3.1.3 Capacitance-to-digital converter-based $C^4D$ technology for detection in capillary electrophoresis

The results of this section are published as part of my publication [1], see Appendix III, Paper 1. This section contains text excerpts that were part of my publication [1].

To reliably transfer the analytes from the first to the second separation dimension, it was desired to have a detection on the common section of both dimensions. Since in ITP, a discontinuous electrolyte system is used, the difference in conductivities becomes visible by a large conductivity change, when the boundary between the electrolytes passes the detector. This makes conductivity detection the most suitable detection method to follow the ITP. Using laser-induced etching, a $C^4D$ detection geometry was integrated in the microfluidic chip which was filled with conductive silver paint. The detection electronics were developed in this thesis.

In a preliminary step, an on-capillary conductivity detector based on capacitance-to-digital converter (CDC) technology was developed. The aim was to improve sensitivity, handling, and price of CDC-based $C^4D$ detectors (CDCD) and to reach LODs similar to classic $C^4Ds$ with more sophisticated electric circuits. The results are published in [1], see Appendix III, Paper 1

To obtain best LODs for an on-capillary CDCD, a systematic study was conducted regarding electrode length, the use of a differential measurement mode and different excitation voltages. A scheme of the entire CDCD assembly is shown in Figure 3A with its components. On the CE side, two detection devices, consisting of the detection head and the supply unit, were mounted. The data were transmitted wirelessly to the master device which was connected to a computer. A home-written program with real-time data plotting was used for data acquisition allowing automated and manual measurements using the CE's trigger signal.

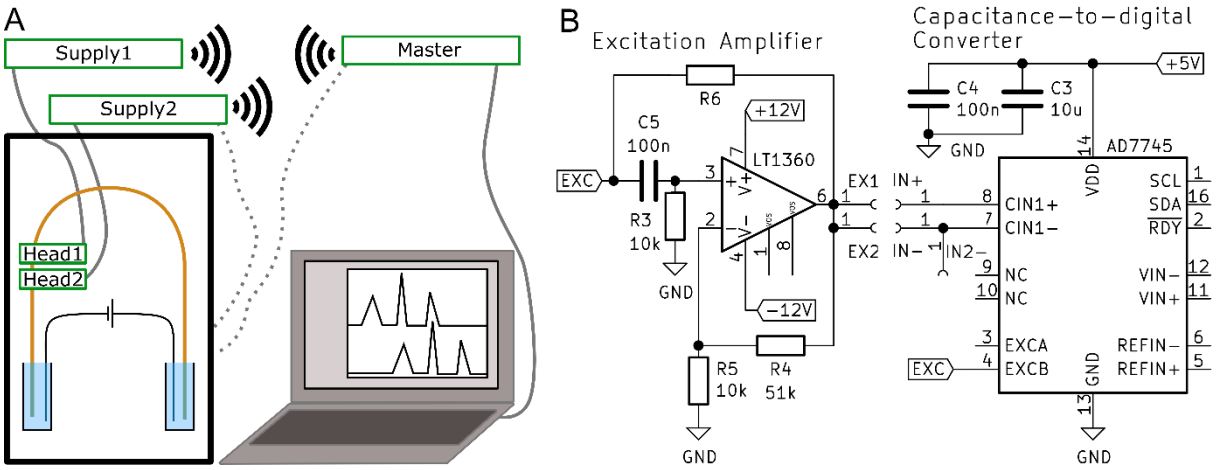


Figure 3. (A) Schematic of the of the CDCD assembly. On the CE side, two detection devices were mounted. Each consisted of the detection head (Head1, Head2) mounted on the capillary and a modular supply unit (Supply1, Supply2). The data were transmitted wirelessly from the detection device to the master device (Master) connected via USB to a computer. Additionally, the trigger from the CE can be connected either to one of the detection devices or to the master device (dotted lines). (B) Schematic diagram of the main circuit parts of the detection head. Resistors without values are jumpers. Figure and figure caption were taken from [1], see Appendix III, Paper 1.

A schematic diagram of the main part of the circuit of the detection head is depicted in Figure 3B. It was adapted from the circuitry published by Drevinskas et al. [198]: only the main component, the AD7745 (integrated circuit for capacitance to digital conversion), and its voltage supply were identical to the published circuitry. The excitation voltage (EXCB) of the AD7745 was set to a 5 V amplitude and a 32 kHz square wave signal. An operational amplifier (LT1360) was added to implement a higher excitation voltage of 24 V. The electrodes had common $C^4D$ electrode geometry. They were mounted perpendicular to the printed circuit board, and were made from hypodermic needles [199-201]. In case of differential measurements, a second electrode pair was mounted. The grounded shielding of the detection head was made from adhesive copper foil. The supply unit supplied voltages, enabled the configuration of the detector and wireless data transmission as well as handling of the trigger signals from the CE instrument.

To judge the performance of the CDCDs, a direct comparison to the Open$C^4D$ from do Lago [202] and a commercial $C^4D$ was carried out using a $C^4D$ optimized background electrolyte (20 mM MES / histidine). For the fully optimized CDCD with two electrodes

of 10 mm length and a square wave excitation voltage with a frequency of 32 kHz and an amplitude of 24 V, LODs (signal-to-noise: 3) for the inorganic cations $K^+$ and $Li^+$ were approx. 4 µM. A measurement with a concentration just above the LOD is depicted in Figure 4. Comparable results were obtained for the commercial $C^4D$. The LODs for the Open$C^4D$ were twice as high. Depending on the measurement conditions, LODs between 0.1 µM and 3.7 µM (LOQs of 0.3 µM to 12.3 µM) (mostly for $K^+$) were reported for $C^4Ds$ in literature [202-214].

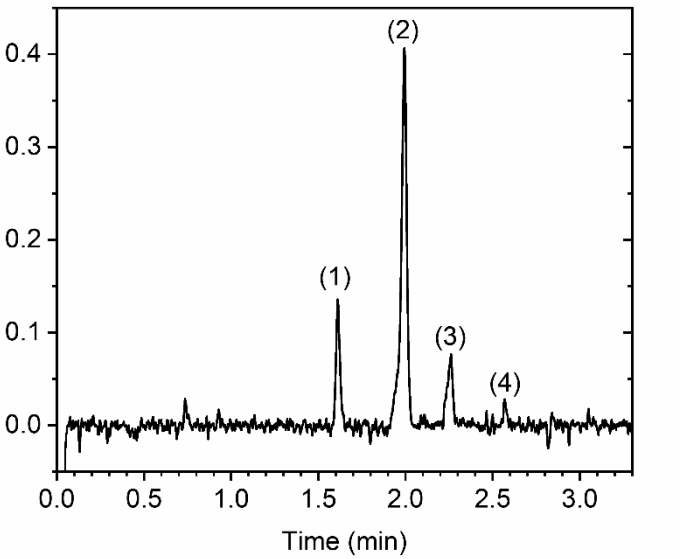


Figure 4. Baseline-subtracted electropherogram of the separation at 14 kV of 6.25 µM $K^+$ (1), $Na^+$ (2) impurity, $Li^+$ (3) and the $H^+$-cation of tris(hydroxymethyl)aminomethane (4) in a 20 mM MES / histidine BGE recorded by a CDCD with an excitation voltage of 24 V and an electrode length of 2 × 10 mm. The sample was injected for 5 s at 50 mbar in a fused silica capillary (50 cm × 50 µm inner diameter). The effective length was 31.5 cm. Figure and figure caption were taken from [1], see Appendix III, Paper 1.

A drawback of the CDCDs is their presumably broader detection window compared to the Open$C^4D$ and the commercial $C^4D$ which was visible from the lower plate numbers of the CDCD. For $C^4D$ it is known that the plate number is reduced when using longer electrodes at low excitation frequencies [200]. The CDCD had the lowest excitation frequency and the longest electrodes in the comparison.

The detection head of the CDCD was small and only a simple electric circuit was used while showing a comparable performance to other C$^4$Ds. The battery-powered CDCD setups with their wireless data transmission made it possible to use them near a high-voltage source, since avoiding a potential connection prevented flashovers to the electronics. Additionally, the CDCD was low-priced, and the simple assembly proved beneficial in production, handling, and robustness. The exceptionally low weight of the on-capillary detection head (< 3g) compared to other setups is noteworthy. This makes it possible, that the capillary itself can carry the detector head making the handling very flexible. The hardware and self-written software were optimized for real-time data plotting.

All these properties were beneficial compared to known setups, and therefore, the detection head of the CDCD setup was used and adapted to fit on the C$^4$D geometry integrated in the microfluidic chip. The tubular electrodes were replaced by spring contact pins which connected the electronics to the C$^4$D geometry filled with silver paint in the chip. Information of the adapted CDC setup can be found in the Supporting Information of [3] and in the Appendix III, Paper 3. As an alternative to the CDCD a modified version of the OpenC$^4$D was developed, but not further evaluated in this thesis. The design can be found in the Appendix II, Part A.

## 3.2 Methodological developments

The separability and stacking of compounds in CE and ITP are easily predictable by simulations. However, this requires the knowledge of the acidity constants p$K_a$ and the limiting electrophoretic mobilities $\mu_{lim}$ of the compounds. In the following sections the strategy to determine these values is summarized and finally the results are used to optimize the separations conditions for both ITP-MS and CE-MS.

### 3.2.1 Determination of acidity constants and limiting electrophoretic mobilities of ionizable herbicides

The results of this section are published as part of my publication [2], see Appendix III, Paper 2. This section contains text excerpts that were part of my publication [2].

To determine the negative decadic logarithmic thermodynamic acidity dissociation constant (p$K_a^\circ$) and limiting electrophoretic mobilities ($\mu_{lim}$) of glyphosate and its transformation products, the AnglerFish software published by Malý et al. was used [215]. Besides experimentally determined effective electrophoretic mobilities of the analytes in BGEs of different pH, it requires the BGEs' composition, and initial estimates of the p$K_a^\circ$ and $\mu_{lim}$. pH values of the BGEs in the range of pH 1.3 to 12 were selected with an increment of about 0.3 using the software PeakMaster providing all parameters of the BGEs like ionic strength, pH, and electrolyte concentrations [216]. Entering the composition of the BGE was necessary to correct the electrophoretic mobilities for ionic strength effects allowing enhanced freedom in the choice of the BGE composition [215]. The determination of the effective electrophoretic mobilities at different pH was necessary, since the speciation of glyphosate and its transformation products is complex due to several acidic and/or basic functional groups. Detection by $C^4D$ enabled their analyses despite the lack of a chromophoric system.

The pH dependence of the effective electrophoretic mobilities of all analytes including the fits by Anglerfish software are shown in Figure 5. The error bars of the effective electrophoretic mobilities determined here were too small to become visible in the

figure. Despite some challenges during the detection of peaks, excellent electrophoretic mobility data at a high resolution were acquired proven by $R^2 \geq 0.98$ of the fit for all analytes. This allowed to precisely determine $pK_a^\circ$ and $\mu_{lim}$ data by the AnglerFish software. A narrow gradation in pH helped to identify the analyte peaks and reduced possible influences by outliers and analyte peaks not detectable, for example, due to system peaks, on the results. In comparison to other p$K_a$ determination methods like potentiometric titration lower analyte consumption, the applicability to impure samples and the extended pH range are the major advancements of p$K_a$ determination by CE-C$^4$D in combination with software-supported evaluation. Compared to early studies using the AnglerFish software the pH range was extended to a pH as low as 1.3 and up to pH 12 to accurately determine the very low $pK_a^\circ$ values of *N*-acetyl AMPA and *N*-acetyl glyphosate [215]. The $\mu_{lim}$ data were determined for all analytes except for glyoxylic acid, glycine, and phosphate for the first time.

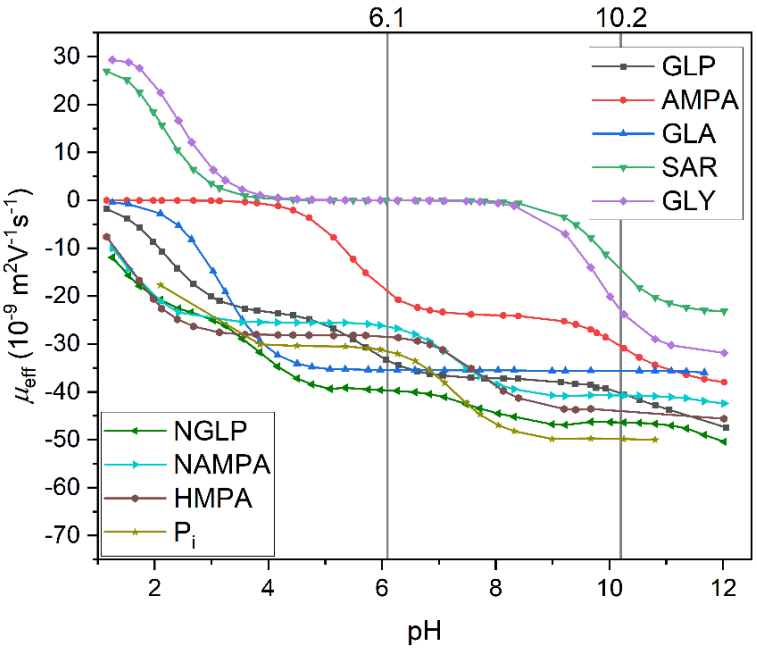


Figure 5. pH-dependent change in the effective electrophoretic mobilities (points) and fits by AngerFish (lines) of glyphosate and its transformation products (abbreviations see Table 1) at an ionic strength of 10 mM (pH > 2). Vertical lines indicate pH values suitable for separations which were used in this thesis. Analyte abbreviation, see Table 1. Figure and figure caption are adapted from [2], see Appendix III, Paper 2.

Table 1. Thermodynamic acidity constants $pK_a^\circ$ and limiting electrophoretic mobilities $\mu_{lim}$ ($10^{-9}m^2V^{-1}s^{-1}$) for different charge numbers of the analytes of +1 to -3. Only the higher amount of the charge numbers relevant for the specific $pK_a^\circ$ are indicated. Table and table caption were taken from [2], see Appendix III, Paper 2.

| **Substance** | $R^2$ | | **+1** | **-1** | **-2** | **-3** |
|---|---|---|---|---|---|---|
| *glyphosate and its transformation products* | | | | | | |
| Glyphosate (GLP) | 0.998 | $\mu_{lim}$ | - | 26.4±0.1 | 45.5±0.1 | 60.1±0.3 |
| | | $pK_a^\circ$ | - | 2.25±0.01 | 5.77±0.02 | 10.55±0.05 |
| Aminomethylphosphonic acid (AMPA) | 0.999 | $\mu_{lim}$ | - | 27.2±0.1 | 45.0±0.2 | - |
| | | $pK_a^\circ$ | - | 5.51±0.01 | 10.31±0.03 | - |
| Glyoxylic acid (GLA) | 0.979 | $\mu_{lim}$ | - | 39.1±0.5 | - | - |
| | | $pK_a^\circ$ | - | 3.22±0.06 | - | - |
| Sarcosine (SAR) | 0.997 | $\mu_{lim}$ | 36.5±0.5 | 26.3±0.3 | - | - |
| | | $pK_a^\circ$ | 2.02±0.02 | 10.00±0.02 | - | - |
| Glycine (GLY) | 0.996 | $\mu_{lim}$ | 37.3±1.0 | 35.1±0.8 | - | - |
| | | $pK_a^\circ$ | 2.35±0.05 | 9.81±0.05 | - | - |
| *N*-acetyl glyphosate (NGLP) | 0.989 | $\mu_{lim}$ | - | 26.1±1.0 | 48.4±0.6 | 62.7±0.5 |
| | | $pK_a^\circ$ | - | 1.14±0.13 | 3.97±0.11 | 7.80±0.24 |
| *N*-acetyl AMPA (NAMPA) | 0.982 | $\mu_{lim}$ | - | 28.7±0.4 | 49.4±0.4 | - |
| | | $pK_a^\circ$ | - | 1.41±0,07 | 7.40±0.08 | - |
| Hydroxymethyl phosphonic acid (HMPA) | 0.990 | $\mu_{lim}$ | - | 31.4±0.2 | 52.8±0.4 | - |
| | | $pK_a^\circ$ | - | 1.57±0.03 | 7.77±0.07 | - |
| Phosphoric acid ($P_i$) | 0.979 | $\mu_{lim}$ | - | 33.7±1.2 | 59.7±1.3 | n.d. |
| | | $pK_a^\circ$ | - | 1.98±0.16 | 7.39±0.17 | n.d. |
| *model substances* | | | | | | |
| Glufosinate (GLU or GLUF) | 0.997 | $\mu_{lim}$ | 21.1±0.9 | 23.3±0.2 | 43.3±0.4 | - |
| | | $pK_a^\circ$ | 1.88±0.07 | 2.90±0.07 | 9.87±0.05 | - |
| MCPA | 0.990 | $\mu_{lim}$ | - | 26.2±0.1 | - | - |
| | | $pK_a^\circ$ | - | 2.96±0.02 | - | - |
| Oxamic acid (OXA) | 0.990 | $\mu_{lim}$ | - | 40.8±0.3 | - | - |
| | | $pK_a^\circ$ | - | 1.90±0.02 | - | - |

### 3.2.2 Development of CE methods for ionizable herbicides

By the aid of the p$K_a$ and limiting electrophoretic mobility data determined in this thesis, it was easy to select best separation conditions: A pH of 6.1 and 10.2 for the BGE showed promising conditions for a successful baseline separation of glyphosate and its metabolites as indicated in Figure 5 and supported by the simulations with by the PeakMaster software from Malý [216]. As can be seen from Tables A1 and A2 in Appendix I, no study has reported the simultaneous separation of such many glyphosate metabolites before.

#### 3.2.2.1 Slightly acidic separation conditions

The results of this section are published as part of my publication [2], see Appendix III, Paper 2. This section contains text excerpts that were part of my publication [2].

Analysis of all metabolites of glyphosate was performed by CE-MS. To avoid the influence of $CO_2$ dissolution on the BGE's pH, acidic conditions were chosen. The simulation by PeakMaster (Figure 6A) showed a complete separation of all metabolites of glyphosate except glycine and sarcosine which are uncharged at pH 6.1 (compare Figure 5). MCPA and oxamic acid were also included in the simulation, revealing no comigration with other analytes. The simulation was successfully reproduced by CE-MS regarding the migration order for an aqueous sample but impressively also in a spiked beer sample, see Figure 6B and C. In the non-spiked beer sample, only a peak originating from phosphate was visible, compare Figure 6D, but it seemed not to impair the separation by transient ITP. Peaks from other target analytes were not detected. Slightly longer migration times for all analytes were observed when injecting spiked beer samples. These may be due to the adsorption of matrix components and thus a reduced EOF, which would necessitate optimized rinsing steps. Other reasons are field amplification phenomena or transient sample-induced isotachophoresis. Despite fragmentor voltage optimization, both *N*-acetyl AMPA and *N*-acetyl glyphosate showed in-source decay as the masses of the $[M-H]^-$ for AMPA and glyphosate were observed at the migration times of their acetylated derivates.

Differences between the electropherograms in Figure 6A and B are mainly caused by coupling CE to MS via the sheath liquid interface: ions from the sheath liquid migrate into the capillary, which influences the separation conditions upon locally changing the BGE composition [120, 217]. Baseline separation and a good migration time precision with a relative standard deviation below 1.4 % for all analytes were reached for an aqueous standard analyte mixture (2.5 µM ($n$ = 3) or 25 µM ($n$ = 6)). The peak area precision did not exceed a relative standard deviation of 16 % ($n$ = 3; $c$ = 2.5 µM) or 20 % ($n$ = 6; $c$ = 25 µM). It was possible to achieve a limit of quantification (LOQ) of 0.25 µM (~42 µg/L) for glyphosate with an injection over 15 s at 100 mbar when only glyphosate was measured in selected ion monitoring mode. See et al. described similar LOQs for CE-$C^4D$ at a pH of 6.3 for glyphosate and AMPA in spiked tap water samples at comparable separation conditions [94]. In comparison, when analyzing water samples, a non-derivatization normal phase LC-MS method with SPE pretreatment achieved LOQs in the range of 20 ng/L for glyphosate, glufosinate and AMPA [218]. HILIC-MS methods had LOQs of 20 µg/kg for glyphosate and its degradation products in peas and soya cake [67].

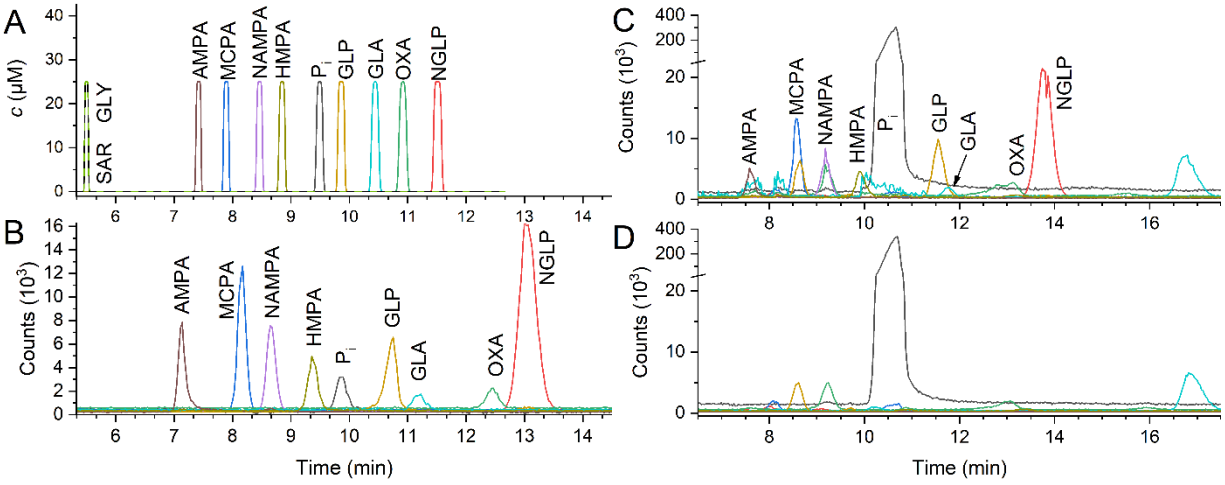


Figure 6. A) Simulated and B) experimental electropherograms by CE-MS analysis after injection of a mixture of analytes (c = 25 µM) for 10 s × 50 mbar (~7.3 mm) in water (curve of [$P_i$-H]- offset by -1524; SAR and GLY only in simulation) and C) beer as well as D) the non-spiked beer sample. All samples contained 10 mM $NH_4AcO$. Injected beer samples were diluted to 80 % (v/v) beer by the aqueous solutions added. Separations were performed at 15 kV and 70 mbar pressure in a bare fused silica capillary with a length of 60 cm and an id of 50 µm at pH 6.1 in 20 mM $NH_4AcO$ and 0.78 mM AcOH, see also Sections 2.3 and 2.6 in reference [2]. For A) the migration time of uncharged substances was set to 5.5 min. For abbreviations, see Table 1. Figure and its caption were taken from [2], see Appendix III, Paper 2.

### 3.2.2.2 Alkaline separation conditions

The results of this section are published as part of my publication [3], see Appendix III, Paper 3. This section contains text excerpts that were part of my publication [3].

As predicted by simulations, see Figure 7A, a BGE with a pH of 10.2 allowed a baseline separation of all glyphosate metabolites by CE-MS, especially of glyphosate and its two main metabolites AMPA and sarcosine, compare Figure 7B. Due to insufficient ionization efficiency in the ESI process, glyoxylic acid was not detected. Separations at lower pH values were discarded due to insufficient robustness to small pH changes especially for sarcosine and glycine, see Figure 5. The comparatively high effective electrophoretic mobility of the slowest target ion sarcosine also simplified the search for a suitable terminating ion in case of coupling ITP with CE as a preconcentration step. When monitoring only AMPA, glyphosate and sarcosine, LOQs were estimated to 5 and 2 µM for glyphosate and AMPA, respectively, while sarcosine was hardly detectable.

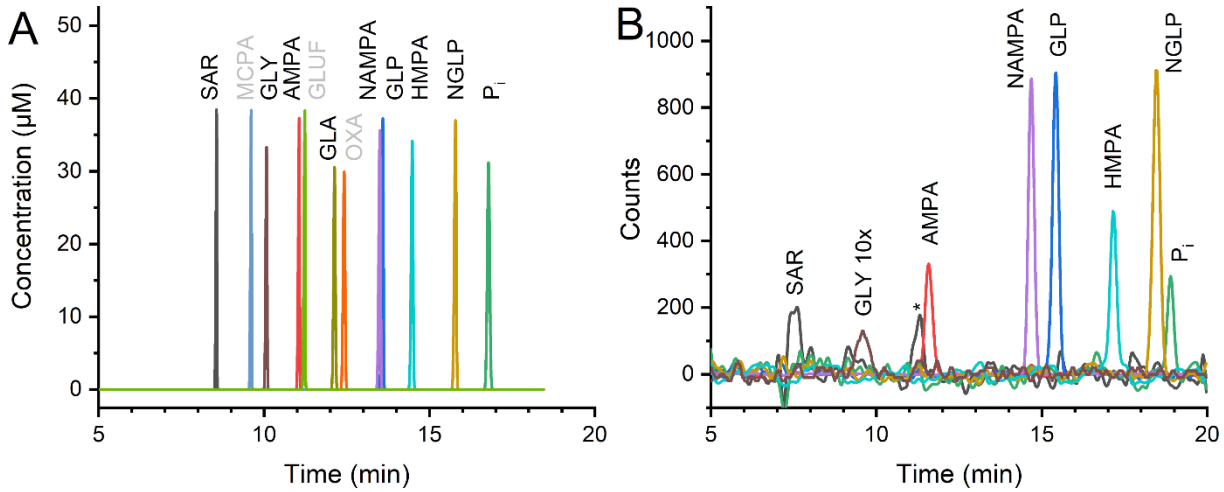


Figure 7. (A) Simulated electropherogram for the separation of a mixture of AMPA, GLA, glyphosate (GLP), GLUF, GLY, HMPA, MCPA, NAMPA, NGLP, OXA, $P_i$ and sarcosine (SAR) ($c$ = 50 µM, each) dissolved in BGE, and the corresponding (B) experimental electropherogram of a subset of analytes (highlighted in panel A). The pseudo molecular $[M\text{-}H]^-$ ions were recorded by MS in selected ion monitoring mode after injecting the sample for 5 s × 30 mbar and a separation by CE at +10 kV and -10 mbar pressure at the inlet. The aqueous BGE was made from 10 mM $(NH_4)_2CO_3$ and 115 mM $NH_4OH$, pH 10.2; The bare fused silica capillary had a length of 60 cm and an inner diameter of 75 µm. Drying gas was supplied at 11 L/min. The data curve of GLY in (B) was amplified by a factor of ten. No GLA signal was recorded. The $[SAR\text{-}H]^-$ trace showed a signal from an impurity marked with an asterisk. For abbreviations see Table 1. Figure and its caption were taken from [3]. see Appendix III, Paper 3.

### 3.2.3 Development of an ITP-MS methods for ionizable herbicides

The results of this section are published as part of my publication [3], see Appendix III, Paper 3. This section contains text excerpts that were part of my publication [3].

On the one hand, the ITP simulations focused on preconcentrating all target ions, which required a pH >9 of the electrolytes, and on the other hand on ensuring that the mobility of the leading ions was lower than that of phosphate ions to exclude them from the ITP stack. This should allow removing phosphate in the first dimension by front-cutting in ITP/CE. Phosphate is critical since it is widely present in environmental samples but also used to extract glyphosate from soils and sediments [189, 219]. Aiming at an L-S-L system for an ITP/CE setup, MS-compatible electrolyte components had to be used. All desired features could be combined at a pH of the LE of 10.2 using formate or carbonate as leading ions and proline as terminating ion, compare Figure 8A. The fast-migrating *N*-acetyl glyphosate could not be included in the ITP stack. Advantageously, both, phosphate and chloride, were removed successfully migrating zone electrophoretically in the LE.

Experiments with formate as leading ion showed that carbonate ions from atmospheric carbon dioxide, dissolved in basic solutions, impaired ITP separations. The addition of barium hydroxide to the TE successfully reduced this interference and further allowed to omit proline in the TE since hydroxide proved suitable as terminating ion. This was possible because the electrophoretic mobility of hydroxide was low using the weak base ammonia as the counterion in ITP under basic conditions, compare [220]. A detailed discussion using formate as leading ion with ITP-$C^4D$ experiments including also spiked river water experiments can be found in the Appendix II, Part B.

The use of carbonate in the LE was further advantageous as phosphate ions were better separated from the ITP stack due to a greater difference in effective electrophoretic mobilities compared to formate. The high buffer capacity was another advantage. Potassium hydroxide was sufficient as TE with hydroxide ions serving as terminating ions. This avoided barium salts precipitating in the ESI interface.

The isotachopherogram given in Figure 8B shows the successful separation of phosphate (c = 5 mM) as an interfering ionic macroconstituent from a selection of the model analytes (glyphosate, AMPA, and sarcosine ($c$ = 100 µM, each)), which cover the full mobility range of the ITP stack. All analytes migrated in the migration order predicted by simulations for this ITP electrolyte system. The detection of analytes in the low nanomolar range is shown in Figure 8C. However, at these low concentrations the length of the individual analyte zones in peak mode ITP was so small that the analyte zones were no longer detected sufficiently separated for precise quantification as quenching effects become likely [160, 165].

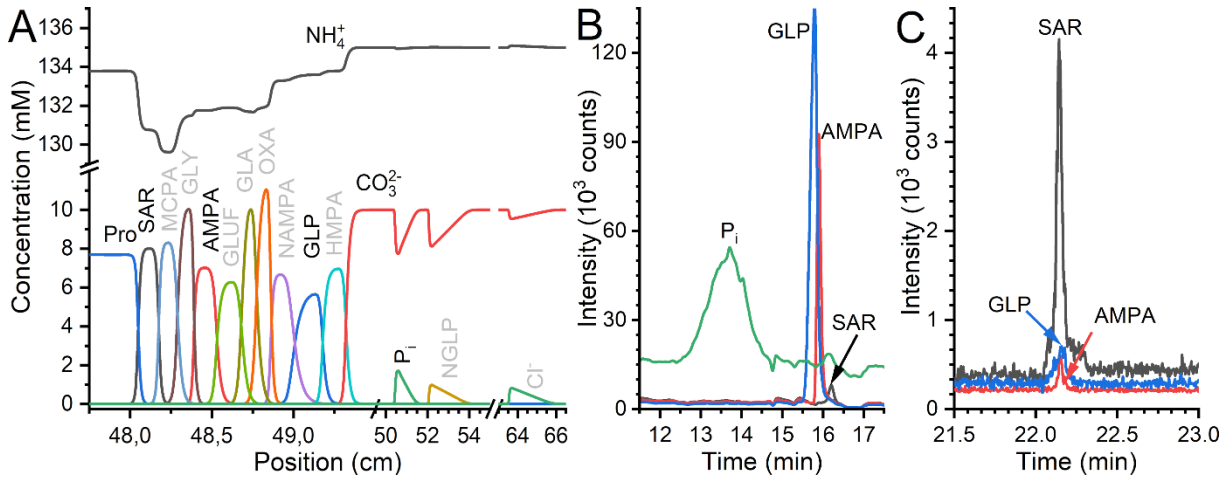


Figure 8. (A) Simulated ITP with the analytes: AMPA, GLA, GLP, GLUF, GLY, HMPA, MCPA, NAMPA, NGLP,OXA, $P_i$, SAR, and $Cl^-$ ($c$ = 1 mM, each) at a pH of 10.2 in the LE. LE: 10 mM carbonate, TE: 5 mM proline (Pro), counterion: 135 mM $NH_3$. (B) + (C) Mass traces of $[M-H]^-$ ions recorded by ESI-MS after ITP separation. A sample mixture of (B) 100 µM AMPA, glyphosate (GLP), sarcosine (SAR) and 5 mM $Na_2HPO_4$ ($P_i$) dissolved in 135 mM $NH_4OH$ or (C) 5 nM AMPA, GLP and SAR dissolved in LE was injected for (B) 10 s or (C) 20 s at 100 mbar and separated by ITP at (B) -12 or (C) -14 kV and (B) 75 or (C) 80 mbar pressure support. (B) + (C) LE: 10 mM $(NH_4)_2CO_3$, 115 mM $NH_4OH$; TE: 10 mM KOH, 135 mM $NH_4OH$. The bare fused silica capillary had a length of (B) 50 or (C) 65 cm and an inner diameter of 75 µm. The MS' capillary ESI voltage was set to (B) -3500 V or (C) -4000 V and the peak width of the MS was set to (B) 0.15 or (C) 0.05 min to achieve optimal settings for low analyte concentrations and narrow peaks in (C). For abbreviations, see Table 1. Figure and Figure caption were taken from [3], see Appendix III, Paper 3.

## 3.3 Application of ITP-C$^4$D/CE-MS

The results of this section are published as part of my publication [3], see Appendix III, Paper 3. This section contains text excerpts and figures that were part of my publication [3].

### 3.3.1 Results of ITP-C$^4$D/CE-MS

To demonstrate the applicability of the new 2D setup, the focus was set on glyphosate and AMPA as the most important analytes present in environmental and food samples. For these analytes, a good comparison with literature data is possible.

The ITP-C$^4$D/CE-MS method can be divided into four steps: A) preparation of runs, B) column-coupled ITP-C$^4$D, C) analyte transfer and D) column-coupled CE-MS. These steps are presented in the panels in Figure 9 and discussed in my publication [3] in detail. For maximum insight into the separation process three optional home-built conductivity detectors (OpenC$^4$Ds [202]) were used, which were named according to the capillary ends, compare Figure 2A. Traces of C$^4$D and MS detection as well as the current during voltage application are shown in Figure 10A and B for an injection of glyphosate and AMPA at a concentration of 50 nM. The zero point of the time scale was set to the application of voltage to the CE-MS step.

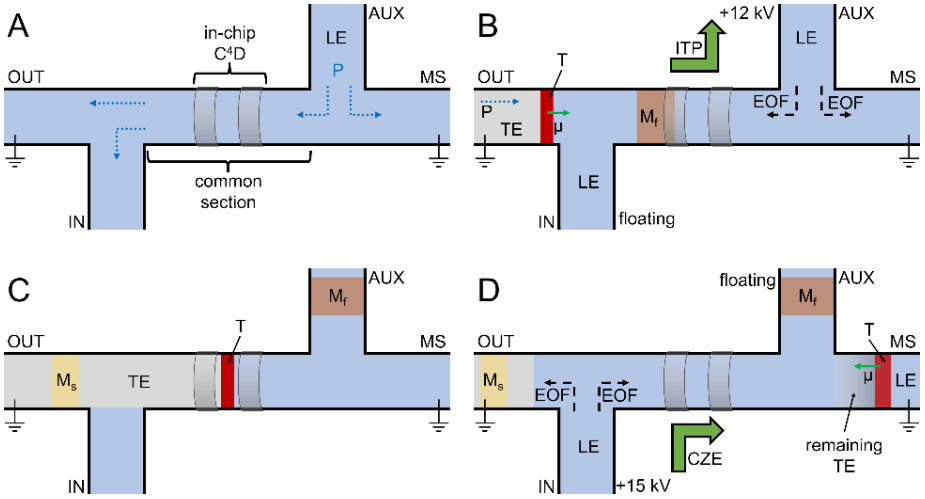


Figure 9. Schematic depiction of the steps during ITP-C⁴D/CE-MS. Step (A) Preparation of measurements: all capillaries were purged from the auxiliary vial (AUX) with LE. Step (B) Column-coupled ITP-C⁴D: The target analytes (T) stacked at the LE-TE boundary prior to entering the common section. Electrophoretic migration of analytes from AUX to OUT, but transport by EOF and pressure from OUT to AUX. Step (C) Analyte transfer: when the LE-TE boundary was detected by the in-chip C⁴D, the ITP was stopped and the high voltage supply replugged. Step (D) Column-coupled CE-MS: only the stacked target analytes reach the MS being transported by the high EOF, while migrating electrophoretically towards the chip interface. Abbreviations: T: target analytes; $M_f$, $M_s$: matrix components with an electrophoretic mobility faster than the LE ($M_f$) or slower than the TE ($M_s$); P: pressure support; μ: migration direction of anions; OUT, IN, MS: capillary to the CE's outlet, inlet position and to the CE-MS interface, respectively, see also Figure 2A. Figure and Figure caption were taken from [3].

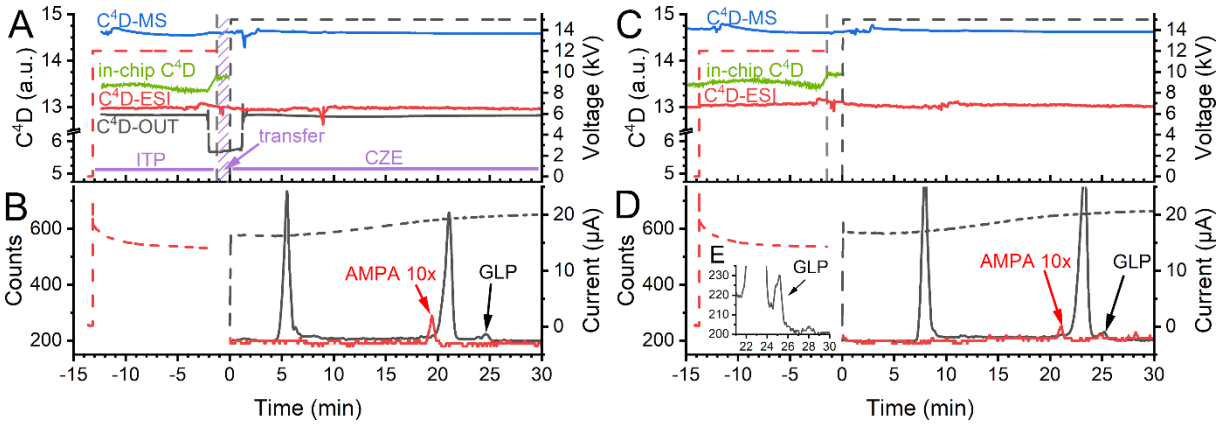


Figure 10. Data acquired during ITP-C⁴D/CE-MS. Injection at 100 mbar for 20 s of glyphosate (GLP) and aminomethylphosphonic acid (AMPA) at a concentration of (A+B) 50 nM or (C-E) 500 pM each dissolved in the LE. In panel (A) the ITP, transfer, and CE step are indicated in purple. (A, C) Solid curves: C⁴D traces of the detectors C⁴D-OUT (4.5 cm in front of first T-crossing), in-chip C⁴D (on the common section), C⁴D-MS (8.0 cm behind the second T-crossing) and C⁴D-ESI (12.7 cm in front of MS), see Figure 2A. (A,C) Dashed curves: applied voltage by the CE. (B,D) Solid curves: MS traces from selected ion monitoring for *m/z* 168.1 $[GLP-H]^-$ and 110.0 $[AMPA-H]^-$. (B,D) Dashed curves: measured driving current. (E) Enlarged section of the MS trace for *m/z* 168.1 showing the GLP peak at 500 pM (84.5 ng/L, S/N~10). For further details, see Sections 2.2.2, 2.2.4, and 3.2 in [3]. The zero point of the time scale was set to the application of voltage to the CE-MS step. Figure and Figure caption were taken from [3].

### 3.3.2 Discussion of ITP-C$^4$D/CE-MS

The new setup was well suited to perform column-coupled ITP-C$^4$D/CE-MS. The major achievements of this development compared to literature methods are summarized below, see also Table A3 in Appendix I :

#### Instrumental modifications

- The hybrid capillary microfluidic chip approach allowed to use a commercial CE-MS instruments to operate the setup. Only minor, flexibly installed modifications were necessary. The setup made use of the high precision injection system and automation in liquid handling. A 3D printed CE cassette avoided mechanical stress to the fluidic system and the compact setup allowed to use short capillaries. Switching between 2D and 1D applications was straightforward. The simplicity of the setup is obvious since neither additional external high voltage supplies (Reinhoud, Mazereeuw, Kler 2014) [181, 182, 195, 221, 222], a second CE instrument (Kohl) [181, 182, 184, 185, 223] nor pumps or syringes for liquid handling were required (Peterson, Piešťanský) [165, 176, 177, 183, 224, 225].
- It was not necessary to block migration paths, all channel ends were left open, which greatly facilitated the operation of the setup. On the other hand, restrictions regarding the choice of electrolytes were given, preventing the use of a BGE-S-BGE system as applied by Kler et al. (Kler 2014) [195]. Further, the two dimensions were not fully separated from each other as in the valve-based setup presented by the Neusüß group (Kohl) [184, 185, 223].
- No capillary coatings were required, instead, the system operated at high EOF conditions, consequently no laborious coating steps were necessary as required for the setup of Peterson et al. [183, 224, 225] and Kler et al. [168]

**Interface**

- Capillaries were just clamped but not glued as in other setups to the interface (Kler) [168, 195], which was possible due to butt-end connections after laser-induced etching of the glass chip interface. All capillaries could flexibly be exchanged. In addition, a very low dead volume avoided band broadening. This was clearly lower than in column-coupling approaches with valves with transfer volumes of 4 to 20 nL (Kohl) [184, 185, 223].
- By using an interface without moving parts and sample transfer by voltage switching only, neither current nor liquid leakages were observed since no mechanical wear compared to valve-based approaches could occur (Kohl) [184, 185, 223].
- A remarkably high migration time precision could be expected in the second dimension given the fixed transfer volume of 31 nL provided by the common section between both separation dimension. Other transfer volumes were possible by replacing the interface-chip with a chip of other dimensions of the common section, which was easily possible thanks to its manufacturing by laser-induced etching. In other setups the start and the end of the analyte transfer depended on the timing of the applied voltage/electrolyte injection (Reinhoud, Mazereeuw, Peterson, Kler 2013, Piešťanský) [165, 168, 176, 177, 181-183, 221, 222, 224, 225].
- The glass interface provided a homogeneous surface along the whole separation path and depending on the inner diameter of the capillaries a uniform shape of the cross section was given. Both measures ensured low band broadening by a uniform EOF and the absence of pressure differences.
- With the analyte transfer based on voltage switching and without flushing of fluidic network sections prior to the CE separation as in the setups of Reinhoud et al. [181, 182, 221] and Mazereeuw et al. [222], band broadening was reduced to a minimum. This was further supported omitting any hydrodynamic flow during the CE step as required by the setup of Peterson et al. [183, 224, 225] or

during the transfer step to the MS from a hydrodynamically closed ITP/CE setup as used by Piešťanský et al. [165, 176, 177].

- Easy and reliable analyte transfer was enabled using a detector directly on the common section. Therefore, effects on EOF velocities, changes in buffer pH, and so forth, are considered automatically and first dimension separations, where the migration speed changes over time, such as ITP operated at a constant voltage, can be easily coupled to CE-MS. It was not necessary to calculate the arrival time of the analytes at the transfer point as in all other setups published, except from the setup described by Kler et al. (Kler 2014) [195].
- The double T-structure enabled matrix removal by front-cutting in contrast to mono T-shaped microfluidic structures as used by Kler et al. (Kler 2013) [168].

**Electrolyte system**

- The L-S-L electrolyte system is simpler than a BGE-S-BGE system and allowed the use of a less sophisticated setup than the one introduced by Kler et al. (Kler 2014) [195] and proved ideal for environmental samples with ionic macrocomponents being mainly inorganic anions with high effective electrophoretic mobilities. These were removed by excluding them from the mobility windows of the ITP.
- To facilitate the optimization of the electrolytic system in ITP/CE-MS, individual optimization of both, the CE, and the ITP step was performed and supported by simulations.

A remarkably low LOD (signal-to-noise: 3) of 150 pM (25 ng/L) for glyphosate improving LODs of the individual method (CE-MS and ITP-MS) by a factor of 10,000 were achieved by the column-coupled setup. Glyphosate was successfully separated from AMPA as predicted by the individual CE-MS analyses, compare Figure 10D and E. The relative standard deviation of the peak area (n=3) for a sample with a concentration of 500 nM was 11 % for AMPA and 20 % for glyphosate. The precision of the migration times was very good with 1.1 and 2.8 %. For comparison, under optimized CE-$C^4D$ conditions with a field-enhanced sample injection, See et al. reached

a four times higher LOD of 100 ng/L for glyphosate [94]. For electrophoretic methods with C4D, lower LODs were only demonstrated using offline preconcentrating methods. For example, dynamic supported liquid membrane tip extraction was used by See et al. achieving a LOD of ~50 ng/L [95]. See et al. combined electromembrane extraction with large volume sample stacking to improve the LOD to 64 ng/L [96]. Horčičiak et al. presented a chip-based column-coupling ITP-C4D/CE-C4D setup and reached a LOD of 2.5 µg/L in a BGE-S-BGE electrolyte system [189]. CE-MS without derivatization and preconcentrating steps provided a LOD of 5 µg/L for glyphosate [120]. Only with chromatographic techniques, for example LC-MS/MS in combination with derivatization and solid phase extraction with an enrichment factor > 300, a LOD below 1 ng/L was reached [42]. The developed method revealed the lowest published LOD for glyphosate using electrophoretic separations without any additional offline preconcentration step and for the first time ITP/CE-MS was applied to anionic analytes.

### 3.3.3 Perspectives of the ITP-C4D/CE-MS setup

To further improve the LOD, a study to evaluate the maximum loadability of the ITP capillary and their optimal dimensions is required. In addition, the ITP-C4D/CE-MS should be applied to all degradation products of glyphosate, which should be well possible given the results of simulations and single dimension ITP-MS and CE-MS experiments. Also, the possibility to simultaneously remove phosphate as the most critical interfering matrix compound, should be investigated using for example soil or food extracts. In future, studies are required to examine, if multiple heart cuts refilling the common intersection are possible when an ionic macroconstituent has an electrophoretic mobility in between those of analytes, similar to the work of Peterson et al. [183]. In addition, also the analysis time should be shortened by using higher separation voltages and shorter capillaries. An automatized stop of the ITP step, voltage switching by a high voltage relay and the subsequent start of the CE step all triggered by the in-chip C4D will further improve the repeatability and precision of the method and would enable unattended measurements.

# 4 Summary

This thesis shows the fast development of a new two-dimensional column-coupled instrumentation and an electromigrative analytical method with very low limits of detection for the trace analysis of the challenging anionic model analytes glyphosate and its metabolites. This was enabled by the intense combination of basic analytical research, methodological and instrumental developments. Beside analytical expertise, this required interdisciplinary knowledge on physicochemical processes, as well as in designing mechanical components, electronic circuits, and software. All results were published in the research papers [1-3], see Appendix III.

Basic analytical research enabled to precisely determine $pK_a^\circ$ and limiting electrophoretic mobility data of the model analytes. Except from sufficient water solubility, no restrictions with regard to the type of analytes amenable are given, since CE-C$^4$D with software-supported evaluation allowed to determine these data even in buffers of varying ionic strength and at extreme pH values, compare Section 3.2.1. With these valuable data, it was possible to intensely model electrophoretic separations for method development, both CE-MS (Section 3.2.2) and ITP-MS (Section 3.2.3) were addressed to find suitable starting conditions for further experimental optimization. This strongly reduced the experimental workload and provided electrolyte compositions for both high resolution between all analytes of interest but also removal of phosphate as the most important ionic macroconstituent of environmental samples. The final buffer system proved well suitable for 2D coupling in an L-S-L system, which even allowed to remove phosphate by front-cutting.

On the instrumental side, the whole fluidic setup, the chip interface with integrated detection, the hard- and software for detection and automation but also modifications to a commercial CE-MS instrument were developed. With this hybrid and modular setup, a commercial CE-MS instrument can easily be modified for high-end two-dimensional separations. Especially the new in-chip C$^4$D placed directly on the

common section connecting the two separation dimensions allowed to reliably transfer analytes between the two dimensions. This eliminated the need to calculate the arrival time of the analytes at the transfer point based on their migration speed. The in-chip $C^4D$, the mostly automatized liquid handling and the fact that a slightly modified commercial CE-MS instrument was used allowed an easy operation of the whole setup. Together with the individually optimized separation conditions no further intense optimization phase for the column-coupled setup was necessary which revealed a remarkably low LOD (signal-to-noise: 3) of 150 pM (25 ng/L) for glyphosate improving LODs of the individual method by a factor of 10,000. This result demonstrates the first successful application of column-coupled ITP/CE in combination with mass spectrometric detection to anionic analytes. Furthermore, such an approach was applied for the first time to environmental samples. All in all, the developed setup will improve the environmental analysis of ionic substances providing a valuable alternative to common chromatographic techniques. An expansion of the method repertoire for ionic substances is of particular interest because metabolites are often more polar and more water-soluble than their parent substances and often contain ionizable functional groups.

The intertwined development using expertise from engineering to basic analytical research led to an ITP-$C^4D$/CE-MS setup, which can be made suitable for routine analysis after some further work on automation. The setup overcame all challenges and limitations of using mass spectrometric detection for ITP/CE analysis such as working with a hydrodynamically open channel system and a fixed ground potential at the MS inlet. The setup was applied to environmental samples. The first results were promising with a high precision in migration times also for river water samples.

# References


[1] Graf, H. G., Rudisch, B. M., Manegold, J., Huhn, C., *Electrophoresis*. 2021, *42*, 1306-1316, DOI: 10.1002/elps.202000394.

[2] Graf, H. G., Biebl, S. M., Müller, L., Breitenstein, C., Huhn, C., *J. Sep. Sci.* 2022, *45*, 1128-1139, DOI: 10.1002/jssc.202100952.

[3] Graf, H. G., Rudisch, B. M., Ude, L., Müller, L., Huhn, C., *J. Sep. Sci.* 2022, *45*, 3887-3899, DOI: 10.1002/jssc.202200519.

[4] Reemtsma, T., Berger, U., Arp, H. P., Gallard, H., Knepper, T. P., Neumann, M., Quintana, J. B., Voogt, P., *Environ. Sci. Technol.* 2016, *50*, 10308-10315, DOI: 10.1021/acs.est.6b03338.

[5] Knoll, S., Rösch, T., Huhn, C., *Anal. Bioanal. Chem.* 2020, *412*, 6149-6165, DOI: 10.1007/s00216-020-02811-5.

[6] Zahn, D., Neuwald, I. J., Knepper, T. P., *Anal. Bioanal. Chem.* 2020, *412*, 4763-4784, DOI: 10.1007/s00216-020-02520-z.

[7] Boxall, A. B., Sinclair, C. J., Fenner, K., Kolpin, D., Maund, S. J., *Environ. Sci. Technol.* 2004, *38*, 368A-375A, DOI: 10.1021/es040624v.

[8] Steinborn, A., Alder, L., Michalski, B., Zomer, P., Bendig, P., Martinez, S. A., Mol, H. G., Class, T. J., Pinheiro, N. C., *J. Agric. Food Chem.* 2016, *64*, 1414-1421, DOI: 10.1021/acs.jafc.5b05852.

[9] Guo, Y., *Biomed. Chromatogr.* 2022, e5332, DOI: 10.1002/bmc.5332.

[10] Neuwald, I., Muschket, M., Zahn, D., Berger, U., Seiwert, B., Meier, T., Kuckelkorn, J., Strobel, C., Knepper, T. P., Reemtsma, T., *Water Res.* 2021, *204*, 117645, DOI: 10.1016/j.watres.2021.117645.

[11] Zhang, K., Liu, X., *J. Pharm. Biomed. Anal.* 2016, *128*, 73-88, DOI: 10.1016/j.jpba.2016.05.007.

[12] Bigard, A., Cardinael, P., Agasse, V., *Crit. Rev. Anal. Chem.* 2022, 1-13, DOI: 10.1080/10408347.2022.2036942.

[13] Benbrook, C. M., *Environ. Sci. Eur.* 2016, *28*, 1-15, DOI: 10.1186/s12302-016-0070-0.

[14] Valle, A. L., Mello, F. C. C., Alves-Balvedi, R. P., Rodrigues, L. P., Goulart, L. R., *Environ. Chem. Lett.* 2018, *17*, 291-317, DOI: 10.1007/s10311-018-0789-5.

[15] Soares, D., Silva, L., Duarte, S., Pena, A., Pereira, A., *Foods*. 2021, *10*, 2785, DOI: 10.3390/foods10112785.

[16] Castrejón-Godínez, M. L., Tovar-Sánchez, E., Valencia-Cuevas, L., Rosas-Ramírez, M. E., Rodríguez, A., Mussali-Galante, P., *Microorganisms*. 2021, *9*, 2322, DOI: 10.3390/microorganisms9112322.

[17] Rueppel, M. L., Brightwell, B. B., Schaefer, J., Marvel, J. T., *J. Agric. Food Chem.* 1977, *25*, 517-528, DOI: 10.1021/jf60211a018.

[18] *EFSA Journal*. 2009, *7*, 1310, DOI: 10.2903/j.efsa.2009.1310.

[19] Zhan, H., Feng, Y., Fan, X., Chen, S., *Appl. Microbiol. Biotechnol.* 2018, *102*, 5033-5043, DOI: 10.1007/s00253-018-9035-0.

[20] *EFSA Journal*. 2015, *13*, 4302, DOI: 10.2903/j.efsa.2015.4302.

[21] Kaczynski, P., Lozowicka, B., Wolejko, E., Iwaniuk, P., Konecki, R., Dragowski, W., Lozowicki, J., Amanbek, N., Rusilowska, J., Pietraszko, A., *J. Hazard. Mater*. 2020, *393*, 122443, DOI: 10.1016/j.jhazmat.2020.122443.

[22] Feng, D., Soric, A., Boutin, O., *Sci. Total Environ.* 2020, *742*, 140559, DOI: 10.1016/j.scitotenv.2020.140559.

[23] Fleischer, S., Weiss, S. C., Lucke, T., Seitz, W., Schulz, W., Weber, W. H., *Ozone: Sci. Eng.* 2015, *37*, 441-449, DOI: 10.1080/01919512.2015.1040911.

[24] Silva, V., Montanarella, L., Jones, A., Fernández-Ugalde, O., Mol, H. G. J., Ritsema, C. J., Geissen, V., *Sci. Total Environ.* 2018, *621*, 1352-1359, DOI: 10.1016/j.scitotenv.2017.10.093.

[25] Vereecken, H., *Pest. Manag. Sci.* 2005, *61*, 1139-1151, DOI: 10.1002/ps.1122.

[26] Huhn, C., *Anal. Bioanal. Chem.* 2018, *410*, 3041-3045, DOI: 10.1007/s00216-018-1000-3.

[27] Vicini, J. L., Jensen, P. K., Young, B. M., Swarthout, J. T., *Compr. Rev. Food Sci. Food Saf.* 2021, *20*, 5226-5257, DOI: 10.1111/1541-4337.12822.

[28] Xu, J., Smith, S., Smith, G., Wang, W., Li, Y., *Food Control*. 2019, *106*, 106710, DOI: 10.1016/j.foodcont.2019.106710.

[29] Niemann, L., Sieke, C., Pfeil, R., Solecki, R., *J. Verbrauch. Lebensm.* 2015, *10*, 3-12, DOI: 10.1007/s00003-014-0927-3.

[30] Grandcoin, A., Piel, S., Baurès, E., *Water Res.* 2017, *117*, 187-197, DOI: 10.1016/j.watres.2017.03.055.

[31] Gill, J. P. K., Sethi, N., Mohan, A., *Environ. Chem. Lett.* 2016, *15*, 85-100, DOI: 10.1007/s10311-016-0585-z.

[32] Ding, J., Guo, H., Liu, W.-w., Zhang, W.-w., Wang, J.-w., 2015, *03*, 88-95.

[33] Arkan, T., Molnár-Perl, I., *Microchem. J.* 2015, *121*, 99-106, DOI: 10.1016/j.microc.2015.02.007.

[34] Singh, S., Kumar, V., Datta, S., Wani, A. B., Dhanjal, D. S., Romero, R., Singh, J., *Environ. Chem. Lett.* 2020, *18*, 663-702, DOI: 10.1007/s10311-020-00969-z.

[35] Koskinen, W. C., Marek, L. J., Hall, K. E., *Pest. Manag. Sci.* 2016, *72*, 423-432, DOI: 10.1002/ps.4172.

[36] Raina-Fulton, R., *J. AOAC Int.* 2014, *97*, 965-977, DOI: 10.5740/jaoacint.sgeraina-fulton.

[37] Quick Method for the Analysis of Highly Polar Pesticides in Food Involving Extraction with Acidified Methanol and LC- or ICMS/MS Measurement - I. Food of Plant Origin (QuPPe-PO-Method) – Version 12 (published on EURL-SRM website on July 23, 2021); Anastassiades, M., Wachtler, A.-K., Kolberg, D. I., Eichhorn, E., Marks, H., Benkenstein, A., Zechmann, S., Mack, D., Wildgrube, C., Barth, A., Sigalov, I., Görlich, S., Dörk, D., Cerchia, G., URL: https://www.eurl-pesticides.eu/docs/public/tmplt_article.asp?CntID=887&LabID=200&Lang=EN.

[38] Gauglitz, G., Wimmer, B., Melzer, T., Huhn, C., *Anal. Bioanal. Chem.* 2018, *410*, 725-746, DOI: 10.1007/s00216-017-0679-x.

[39] Botero-Coy, A. M., Ibáñez, M., Sancho, J. V., Hernández, F., *J. Chromatogr. A*. 2013, *1292*, 132-141, DOI: 10.1016/j.chroma.2012.12.007.

[40] Ibáñez, M., Pozo, O. J., Sancho, J. V., López, F. J., Hernández, F., *J. Chromatogr. A*. 2006, *1134*, 51-55, DOI: 10.1016/j.chroma.2006.07.093.

[41] Ibáñez, M., Pozo, O. J., Sancho, J. V., López, F. J., Hernández, F., *J. Chromatogr. A*. 2005, *1081*, 145-155, DOI: 10.1016/j.chroma.2005.05.041.

[42] Hanke, I., Singer, H., Hollender, J., *Anal. Bioanal. Chem.* 2008, *391*, 2265-2276, DOI: 10.1007/s00216-008-2134-5.

[43] DIN ISO 16308:2017-09, Wasserbeschaffenheit – Bestimmung von Glyphosat und AMPA – Verfahren mittels Hochleistungs-Flüssigkeitschromatographie (HPLC) mit tandem-massenspektrometrischer Detektion, DOI: 10.31030/2679839.

[44] Freuze, I., Jadas-Hecart, A., Royer, A., Communal, P. Y., *J. Chromatogr. A*. 2007, *1175*, 197-206, DOI: 10.1016/j.chroma.2007.10.092.

[45] López, S. H., Scholten, J., Kiedrowska, B., de Kok, A., *J. Chromatogr. A*. 2019, *1594*, 93-104, DOI: 10.1016/j.chroma.2019.02.024.

[46] Poiger, T., Buerge, I. J., Bächli, A., Müller, M. D., Balmer, M. E., *Environ. Sci. Pollut. Res. Int.* 2017, *24*, 1588-1596, DOI: 10.1007/s11356-016-7835-2.

[47] De Gerónimo, E., Lorenzón, C., Iwasita, B., Costa, J. L., *Soil Sci.* 2018, *183*, 34-40, DOI: 10.1097/ss.0000000000000225.

[48] Liao, Y., Berthion, J. M., Colet, I., Merlo, M., Nougadère, A., Hu, R., *J. Chromatogr. A*. 2018, *1549*, 31-38, DOI: 10.1016/j.chroma.2018.03.036.

[49] Jansons, M., Pugajeva, I., Bartkevics, V., Karkee, H. B., *J. Chromatogr. B*. 2021, *1177*, 122779, DOI: 10.1016/j.jchromb.2021.122779.

[50] Thompson, T. S., van den Heever, J. P., Limanowka, R. E., *Food Addit. Contam. Part A Chem. Anal. Control Expo. Risk Assess.* 2019, *36*, 434-446, DOI: 10.1080/19440049.2019.1577993.

[51] Franke, A. A., Li, X., Lai, J. F., *Anal. Bioanal. Chem.* 2020, *412*, 8313-8324, DOI: 10.1007/s00216-020-02966-1.

[52] Wang, S., Liu, B., Yuan, D., Ma, J., *Talanta*. 2016, *161*, 700-706, DOI: 10.1016/j.talanta.2016.09.023.

[53] Küsters, M., Gerhartz, M., *J. Sep. Sci.* 2010, *33*, 1139-1146, DOI: 10.1002/jssc.200900556.

[54] Gębura, K., Wieczorek, P. P., Poliwoda, A., *Membranes*. 2021, *12*, 20, DOI: 10.3390/membranes12010020.

[55] Qian, K., Tang, T., Shi, T., Wang, F., Li, J., Cao, Y., *Anal. Chim. Acta*. 2009, *635*, 222-226, DOI: 10.1016/j.aca.2009.01.022.

[56] Fontàs, C., Sanchez, J. M., *J. Sep. Sci.* 2020, *43*, 3931-3939, DOI: 10.1002/jssc.202000645.

[57] Surapong, N., Burakham, R., *ACS Omega*. 2021, *6*, 27007-27016, DOI: 10.1021/acsomega.1c03488.

[58] Goncharova, E. N., Statkus, M. A., Tsizin, G. I., Selimov, R. N., *Mosc. Univ. Chem. Bull.* 2019, *73*, 265-271, DOI: 10.3103/s0027131418060056.

[59] Nørskov, N. P., Jensen, S. K., Sørensen, M. T., *J. Chromatogr. A*. 2019, *1605*, 360343, DOI: 10.1016/j.chroma.2019.06.064.

[60] Wuethrich, A., Haddad, P. R., Quirino, J. P., *Electrophoresis*. 2016, *37*, 1122-1128, DOI: 10.1002/elps.201600050.

[61] Savini, S., Bandini, M., Sannino, A., *J. Agric. Food Chem.* 2019, *67*, 2716-2722, DOI: 10.1021/acs.jafc.8b06483.

[62] López-Ruiz, R., Romero-González, R., Garrido Frenich, A., *J. Pharm. Biomed. Anal.* 2020, *190*, 113492, DOI: 10.1016/j.jpba.2020.113492.

[63] Zhang, P., Rose, M., Van Zwieten, L., *J. AOAC Int.* 2019, *102*, 952-965, DOI: 10.5740/jaoacint.18-0287.

[64] Botero-Coy, A. M., Ibáñez, M., Sancho, J. V., Hernández, F., *J. Chromatogr. A*. 2013, *1313*, 157-165, DOI: 10.1016/j.chroma.2013.07.037.

[65] López, S. H., Dias, J., de Kok, A., *Food Control*. 2020, *115*, 107289, DOI: 10.1016/j.foodcont.2020.107289.

[66] López, S. H., Dias, J., Mol, H., de Kok, A., *J. Chromatogr. A*. 2020, *1625*, 461226, DOI: 10.1016/j.chroma.2020.461226.

[67] Dias, J., López, S. H., Mol, H., de Kok, A., *J. Sep. Sci.* 2021, *44*, 2165-2176, DOI: 10.1002/jssc.202001134.

[68] Kim, L., Baek, S., Son, K., Lee, H. D., Choi, D. S., Kim, C. J., Noh, H. H., *Sci. Rep.* 2021, *11*, 17597, DOI: 10.1038/s41598-021-96529-8.

[69] Manzano-Sánchez, L., Martínez-Martínez, J. A., Domínguez, I., Martínez Vidal, J. L., Frenich, A. G., Romero-González, R., *Foods*. 2020, *9*, 553, DOI: 10.3390/foods9050553.

[70] Giang, L. T., Thien, T. L. T., Yen, D. H., *Vietnam J. Chem.* 2020, *58*, 74-79, DOI: 10.1002/vjch.2019000132.

[71] Shinde, R., Halim, N., Banerjee, A. K., *J. AOAC Int.* 2020, *103*, 1528-1533, DOI: 10.1093/jaoacint/qsaa066.

[72] Melton, L. M., Taylor, M. J., Flynn, E. E., *Food Chem.* 2019, *298*, 125028, DOI: 10.1016/j.foodchem.2019.125028.

[73] Dovidauskas, S., Okada, I. A., dos Santos, F. R., *J. Chromatogr. A*. 2020, *1632*, 461603, DOI: 10.1016/j.chroma.2020.461603.

[74] de Souza, A. P. F., Rodrigues, N. R., Reyes, F. G. R., *Food. Addit. Contam. Part B Surveill.* 2021, *14*, 40-47, DOI: 10.1080/19393210.2020.1855676.

[75] Adams, S., Guest, J., Dickinson, M., Fussell, R. J., Beck, J., Schoutsen, F., *J. Agric. Food Chem.* 2017, *65*, 7294-7304, DOI: 10.1021/acs.jafc.7b00476.

[76] Gasparini, M., Angelone, B., Ferretti, E., *J. Mass Spectrom.* 2020, *55*, e4624, DOI: 10.1002/jms.4624.

[77] Chiesa, L. M., Nobile, M., Panseri, S., Arioli, F., *Food Addit. Contam. Part A Chem. Anal. Control Expo. Risk Assess.* 2019, *36*, 592-600, DOI: 10.1080/19440049.2019.1583380.

[78] Feltracco, M., Barbaro, E., Morabito, E., Zangrando, R., Piazza, R., Barbante, C., Gambaro, A., *Environ. Sci. Pollut. Res. Int.* 2022, *29*, 16383-16391, DOI: 10.1007/s11356-021-16957-x.

[79] Ruiz, P., Dualde, P., Coscollà, C., Fernández, S. F., Carbonell, E., Yusà, V., *Sci. Total Environ.* 2021, *801*, 149688, DOI: 10.1016/j.scitotenv.2021.149688.

[80] Zhang, H., Liu, X., Huo, Z., Sun, H., Zhang, F., Zhu, B., *Microchem. J.* 2021, *170*, 106614, DOI: 10.1016/j.microc.2021.106614.

[81] Arkan, T., Molnár-Perl, I., *Microchem. J.* 2017, *132*, 262-267, DOI: 10.1016/j.microc.2017.02.004.

[82] Motojyuku, M., Saito, T., Akieda, K., Otsuka, H., Yamamoto, I., Inokuchi, S., *J. Chromatogr. B*. 2008, *875*, 509-514, DOI: 10.1016/j.jchromb.2008.10.003.

[83] Stalikas, C. D., Pilidis, G. A., *J. Chromatogr. A*. 2000, *872*, 215-225, DOI: 10.1016/s0021-9673(99)01300-x.

[84] Conrad, A., Schröter-Kermani, C., Hoppe, H. W., Rüther, M., Pieper, S., Kolossa-Gehring, M., *Int. J. Hyg. Environ. Health*. 2017, *220*, 8-16, DOI: 10.1016/j.ijheh.2016.09.016.

[85] Hori, Y., Fujisawa, M., Shimada, K., Hirose, Y., *J. Anal. Toxicol.* 2003, *27*, 162-166, DOI: 10.1093/jat/27.3.162.

[86] Tongo, I., Onokpasa, A., Emerure, F., Balogun, P. T., Enuneku, A. A., Erhunmwunse, N., Asemota, O., Ogbomida, E., Ogbeide, O., Ezemonye, L., *Int. J. Environ. Sci. Technol.* 2021, *19*, 1467-1482, DOI: 10.1007/s13762-021-03212-6.

[87] Moye, H. A., Deyrup, C. L., *J. Agric. Food Chem.* 2002, *32*, 192-195, DOI: 10.1021/jf00122a005.

[88] Chang, P. L., Hsieh, M. M., Chiu, T. C., *Int. J. Environ. Res. Public Health*. 2016, *13*, 409, DOI: 10.3390/ijerph13040409.

[89] Bol'shakova, D. S., Amelin, V. G., *J. Anal. Chem.* 2016, *71*, 965-1013, DOI: 10.1134/s1061934816100026.

[90] Rojano-Delgado, A. M., Luque de Castro, M. D., *Electrophoresis*. 2014, *35*, 2509-2519, DOI: 10.1002/elps.201300556.

[91] Hernández-Borges, J., Frías-García, S., Cifuentes, A., Rodríguez-Delgado, M. A., *J. Sep. Sci.* 2004, *27*, 947-963, DOI: 10.1002/jssc.200401820.

[92] Picó, Y., Rodríguez, R., Mañes, J., *Trends Anal. Chem.* 2003, *22*, 133-151, DOI: 10.1016/s0165-9936(03)00302-9.

[93] See, H. H., Hauser, P. C., *Anal. Chem.* 2011, *83*, 7507-7513, DOI: 10.1021/ac201772g.

[94] See, H. H., Hauser, P. C., Ibrahim, W. A., Sanagi, M. M., *Electrophoresis*. 2010, *31*, 575-582, DOI: 10.1002/elps.200900380.

[95] See, H. H., Hauser, P. C., Sanagi, M. M., Ibrahim, W. A., *J. Chromatogr. A*. 2010, *1217*, 5832-5838, DOI: 10.1016/j.chroma.2010.07.054.

[96] See, H. H., Stratz, S., Hauser, P. C., *J. Chromatogr. A*. 2013, *1300*, 79-84, DOI: 10.1016/j.chroma.2013.01.062.

[97] Cikalo, M. G., Goodall, D. M., Matthews, W., *J. Chromatogr. A*. 1996, *745*, 189-200, DOI: 10.1016/0021-9673(96)00265-8.

[98] Dżygiel, P., Wieczorek, P., *J. Chromatogr. A*. 2000, *889*, 93-98, DOI: 10.1016/s0021-9673(00)00120-5.

[99] Khrolenko, M., Dżygiel, P., Wieczorek, P., *Ars Separatoria Acta*. 2003, 56-63.

[100] Corbera, M., Hidalgo, M., Salvadó, V., Wieczorek, P. P., *Anal. Chim. Acta*. 2005, *540*, 3-7, DOI: 10.1016/j.aca.2004.12.028.

[101] Puzio, K., Claude, B., Amalric, L., Berho, C., Grellet, E., Bayoudh, S., Nehmé, R., Morin, P., *J. Chromatogr. A*. 2014, *1361*, 1-8, DOI: 10.1016/j.chroma.2014.07.043.

[102] Claude, B., Berho, C., Bayoudh, S., Amalric, L., Coisy, E., Nehmé, R., Morin, P., *Environ. Sci. Pollut. Res. Int.* 2017, *24*, 12293-12300, DOI: 10.1007/s11356-017-8844-5.

[103] Chang, S. Y., Wei, M.-Y., *J. Chin. Chem. Soc.* 2005, *52*, 785-792, DOI: 10.1002/jccs.200500110.

[104] Amelin, V. G., Bol'shakov, D. S., Tretiakov, A. V., *J. Anal. Chem.* 2012, *67*, 386-391, DOI: 10.1134/s1061934812020037.

[105] Dong, Y.-l., Guo, D.-q., Cui, H., Li, X.-j., He, Y.-j., *Anal. Methods*. 2015, *7*, 5862-5868, DOI: 10.1039/c5ay00109a.

[106] Gotti, R., Fiori, J., Bosi, S., Dinelli, G., *J. Chromatogr. A*. 2019, *1601*, 357-364, DOI: 10.1016/j.chroma.2019.05.013.

[107] Cao, L., Deng, T., Liang, S., Tan, X., Meng, J., *Anal. Sci.* 2014, *30*, 759-766, DOI: 10.2116/analsci.30.759.

[108] Navarrete-Casas, M., Segura-Carretero, A., Cruces-Blanco, C., Fernández-Gutiérrez, A., *Pest. Manag. Sci.* 2005, *61*, 197-203, DOI: 10.1002/ps.961.

[109] Wei, X., Gao, X., Zhao, L., Peng, X., Zhou, L., Wang, J., Pu, Q., *J. Chromatogr. A*. 2013, *1281*, 148-154, DOI: 10.1016/j.chroma.2013.01.039.

[110] Molina, M., Silva, M., *Electrophoresis*. 2001, *22*, 1175-1181, DOI: 10.1002/1522-2683()22:6<1175::Aid-elps1175>3.0.Co;2-8.

[111] Molina, M., Silva, M., *Electrophoresis*. 2002, *23*, 1096-1103, DOI: 10.1002/1522-2683(200204)23:7/8<1096::Aid-elps1096>3.0.Co;2-e.

[112] Molina, M., Silva, M., *Electrophoresis*. 2002, *23*, 2333, DOI: 10.1002/1522-2683(200207)23:14<2333::Aid-elps2333>3.0.Co;2-5.

[113] Muñoz, R., Guevara-Lara, A., Santos, J. L. M., Miranda, J. M., Rodriguez, J. A., *Microchem. J.* 2019, *146*, 582-587, DOI: 10.1016/j.microc.2019.01.059.

[114] Sung, I. H., Lee, Y. W., Chung, D. S., *Anal. Chim. Acta*. 2014, *838*, 45-50, DOI: 10.1016/j.aca.2014.05.013.

[115] Orejuela, E., Silva, M., *Electrophoresis*. 2005, *26*, 4478-4485, DOI: 10.1002/elps.200500290.

[116] Chang, S. Y., Liao, C.-H., *J. Chromatogr. A*. 2002, *959*, 309-315, DOI: 10.1016/s0021-9673(02)00453-3.

[117] Safarpour, H., Asiaie, R., *Electrophoresis*. 2005, *26*, 1562-1566, DOI: 10.1002/elps.200410429.

[118] Goodwin, L., Startin, J. R., Keely, B. J., Goodall, D. M., *J. Chromatogr. A*. 2003, *1004*, 107-119, DOI: 10.1016/s0021-9673(03)00572-7.

[119] Kawai, M., Iwamuro, Y., Iio-Ishimaru, R., Chinaka, S., Takayama, N., Hayakawa, K., *Anal. Sci.* 2011, *27*, 857-860, DOI: 10.2116/analsci.27.857.

[120] Wimmer, B., Pattky, M., Zada, L. G., Meixner, M., Haderlein, S. B., Zimmermann, H. P., Huhn, C., *Anal. Bioanal. Chem.* 2020, *412*, 4967-4983, DOI: 10.1007/s00216-020-02751-0.

[121] Liu, J., Feng, W., Tian, M., Hu, L., Qu, Q., Yang, L., *J. Chromatogr. A*. 2021, *1659*, 462519, DOI: 10.1016/j.chroma.2021.462519.

[122] Wuilloud, R. G., Shah, M., Kannamkumarath, S. S., Altamirano, J. C., *Electrophoresis*. 2005, *26*, 1598-1605, DOI: 10.1002/elps.200410098.

[123] Yang, G., Xu, X., Shen, M., Wang, W., Xu, L., Chen, G., Fu, F., *Electrophoresis*. 2009, *30*, 1718-1723, DOI: 10.1002/elps.200800387.

[124] Křivánková, L., Boček, P., *Electrophoresis*. 1986, *7*, 100-103, DOI: 10.1002/elps.1150070210.

[125] Goodwin, L., Hanna, M., Startin, J. R., Keely, B. J., Goodall, D. M., *Analyst*. 2002, *127*, 204-206, DOI: 10.1039/b110665c.

[126] Koukalová, L., Glovinová, E., Ondračka, T., Pospíchal, J., *Electrophoresis*. 2022, *43*, 417-424, DOI: 10.1002/elps.202000398.

[127] Breadmore, M. C., Grochocki, W., Kalsoom, U., Alves, M. N., Phung, S. C., Rokh, M. T., Cabot, J. M., Ghiasvand, A., Li, F., Shallan, A. I., Keyon, A. S. A., Alhusban, A. A., See, H. H., Wuethrich, A., Dawod, M., Quirino, J. P., *Electrophoresis*. 2019, *40*, 17-39, DOI: 10.1002/elps.201800384.

[128] Šlampová, A., Malá, Z., Gebauer, P., *Electrophoresis*. 2019, *40*, 40-54, DOI: 10.1002/elps.201800261.

[129] Malá, Z., Gebauer, P., *Electrophoresis*. 2019, *40*, 55-64, DOI: 10.1002/elps.201800239.

[130] Simpson, S. L., Jr., Quirino, J. P., Terabe, S., *J. Chromatogr. A*. 2008, *1184*, 504-541, DOI: 10.1016/j.chroma.2007.11.001.

[131] Wen, Y., Li, J., Ma, J., Chen, L., *Electrophoresis*. 2012, *33*, 2933-2952, DOI: 10.1002/elps.201200240.

[132] Hernández-Borges, J., Borges-Miquel, T. M., Rodríguez-Delgado, M. A., Cifuentes, A., *J. Chromatogr. A*. 2007, *1153*, 214-226, DOI: 10.1016/j.chroma.2006.10.070.

[133] Kumar, A., Malik, A. K., Picó, Y., *Electrophoresis*. 2010, *31*, 2115-2125, DOI: 10.1002/elps.201000021.

[134] Patel, V. D., Shamsi, S. A., Sutherland, K., *Trends Anal. Chem.* 2021, *139*, 116240, DOI: 10.1016/j.trac.2021.116240.

[135] Płotka-Wasylka, J., Szczepańska, N., de la Guardia, M., Namieśnik, J., *Trends Anal. Chem.* 2016, *77*, 23-43, DOI: 10.1016/j.trac.2015.10.010.

[136] Breadmore, M. C., Haddad, P. R., *Electrophoresis*. 2001, *22*, 2464-2489, DOI: 10.1002/1522-2683(200107)22:12<2464::Aid-elps2464>3.0.Co;2-u.

[137] Ramautar, R., Somsen, G. W., de Jong, G. J., *Electrophoresis*. 2010, *31*, 44-54, DOI: 10.1002/elps.200900510.

[138] Hsu, C. C., Whang, C. W., *J. Chromatogr. A*. 2009, *1216*, 8575-8580, DOI: 10.1016/j.chroma.2009.10.023.

[139] Rigobello-Masini, M., Pereira, E. A. O., Abate, G., Masini, J. C., *Chromatographia*. 2019, *82*, 1121-1138, DOI: 10.1007/s10337-019-03748-3.

[140] Suntornsuk, L., Anurukvorakun, O., *Electrophoresis*. 2022, *43*, 939-954, DOI: 10.1002/elps.202100236.

[141] Pantůčková, P., Kubáň, P., *J. Chromatogr. A*. 2017, *1519*, 137-144, DOI: 10.1016/j.chroma.2017.08.084.

[142] Kartsova, L. A., Bessonova, E. A., *J. Anal. Chem.* 2009, *64*, 326-337, DOI: 10.1134/s1061934809040029.

[143] Albert, M., Debusschere, L., Demesmay, C., Rocca, J. L., *J. Chromatogr. A*. 1997, *757*, 281-289, DOI: 10.1016/s0021-9673(96)00783-2.

[144] Harland, G. B., McGrath, G., McClean, S., Smyth, W. F., *Anal. Commun.* 1997, *34*, 9-11, DOI: 10.1039/a607848f.

[145] Chen, M., Huang, Y., Xu, L., Zhang, H., Zhang, G., Chen, A., *Biomed. Chromatogr.* 2018, *32*, e4125, DOI: 10.1002/bmc.4125.

[146] Albert, M., Debusschere, L., Demesmay, C., Rocca, J. L., *J. Chromatogr. A*. 1997, *757*, 291-296, DOI: 10.1016/s0021-9673(96)00782-0.

[147] He, Y., Lee, H. K., *Anal. Chem.* 1999, *71*, 995-1001, DOI: 10.1021/ac981100e.

[148] Hooijschuur, E. W. J., Kientz, C. E., Dijksman, J., Brinkman, U. A. T., *Chromatographia*. 2001, *54*, 295-301, DOI: 10.1007/bf02492673.

[149] Malá, Z., Křivánková, L., Gebauer, P., Boček, P., *Electrophoresis*. 2007, *28*, 243-253, DOI: 10.1002/elps.200600397.

[150] Hadwiger, M. E., Torchia, S. R., Park, S., Biggin, M. E., Lunte, C. E., *J. Chromatogr. B*. 1996, *681*, 241-249, DOI: Doi 10.1016/0378-4347(95)00549-8.

[151] Kohlrausch, F., *Ann. Phys.* 1897, *298*, 209-239, DOI: 10.1002/andp.18972981002.

[152] Křivánková, L., Gebauer, P., Thormann, W., Mosher, R. A., Boček, P., *J. Chromatogr. A*. 1993, *638*, 119-135, DOI: 10.1016/0021-9673(93)83421-n.

[153] Kaniansky, D., Marák, J., Laštinec, J., Reijenga, J. C., Onuska, F. I., *J. Microcolumn Sep.* 1999, *11*, 141-153, DOI: 10.1002/(sici)1520-667x(1999)11:2<141::Aid-mcs7>3.0.Co;2-2.

[154] Křivánková, L., Gebauer, P., Boček, P., *J. Chromatogr. A*. 1995, *716*, 35-48, DOI: 10.1016/0021-9673(95)00553-y.

[155] Křivánková, L., Pantůčková, P., Boček, P., *J. Chromatogr. A*. 1999, *838*, 55-70, DOI: 10.1016/s0021-9673(99)00169-7.

[156] Kvasnička, F., Jaroš, M., Gaš, B., *J. Chromatogr. A*. 2001, *916*, 131-142, DOI: 10.1016/s0021-9673(01)00616-1.

[157] Bahga, S. S., Santiago, J. G., *Analyst*. 2013, *138*, 735-754, DOI: 10.1039/c2an36150g.

[158] Gebauer, P., Boček, P., *Electrophoresis*. 2000, *21*, 3898-3904, DOI: 10.1002/1522-2683(200012)21:18<3898::Aid-elps3898>3.0.Co;2-b.

[159] Timerbaev, A. R., Hirokawa, T., *Electrophoresis*. 2006, *27*, 323-340, DOI: 10.1002/elps.200500320.

[160] Melzer, T., Wimmer, B., Bock, S., Posch, T. N., Huhn, C., *Electrophoresis*. 2020, *41*, 1045-1059, DOI: 10.1002/elps.201900454.

[161] Reinhoud, N. J., Tjaden, U. R., van der Greef, J., *J. Chromatogr. A*. 1993, *641*, 155-162, DOI: 10.1016/0021-9673(93)83469-9.

[162] Lamoree, M. H., Reinhoud, N. J., Tjaden, U. R., Niessen, W. M., van der Greef, J., *Biol. Mass. Spectrom.* 1994, *23*, 339-345, DOI: 10.1002/bms.1200230607.

[163] van der Vlis, E., Mazereeuw, M., Tjaden, U. R., Irth, H., van der Greef, J., *J. Chromatogr. A*. 1995, *712*, 227-234, DOI: 10.1016/0021-9673(95)00366-u.

[164] Kaniansky, D., Marák, J., *J. Chromatogr. A*. 1990, *498*, 191-204, DOI: 10.1016/s0021-9673(01)84247-3.

[165] Everaerts, F. M., Beckers, J. L., Verheggen, T. P. E. M., Isotachophoresis: theory, instrumentation and applications. Elsevier, Amsterdam 1976.

[166] Everaerts, F. M., Verheggen, T. P. E. M., Mikkers, F. E. P., *J. Chromatogr. A*. 1979, *169*, 21-38, DOI: 10.1016/0021-9673(75)85030-8.

[167] Urbánek, M., Blechtová, L., Pospíšilová, M., Polášek, M., *J. Chromatogr. A*. 2002, *958*, 261-271, DOI: 10.1016/s0021-9673(02)00316-3.

[168] Kler, P. A., Posch, T. N., Pattky, M., Tiggelaar, R. M., Huhn, C., *J. Chromatogr. A*. 2013, *1297*, 204-212, DOI: 10.1016/j.chroma.2013.04.046.

[169] Procházková, A., Křivánková, L., Boček, P., *J. Chromatogr. A*. 1999, *838*, 213-221, DOI: 10.1016/s0021-9673(99)00114-4.

[170] Marák, J., Staňová, A., Vaváková, V., Hrenáková, M., Kaniansky, D., *J. Chromatogr. A*. 2012, *1267*, 252-258, DOI: 10.1016/j.chroma.2012.07.075.

[171] Pantůčková, P., Křivánková, L., *Electrophoresis*. 2010, *31*, 3391-3399, DOI: 10.1002/elps.201000193.

[172] Kvasnička, F., Čopíková, J., Ševčík, R., Václavíková, E., Synytsya, A., Vaculová, K., Voldřich, M., *Electrophoresis*. 2011, *32*, 1090-1093, DOI: 10.1002/elps.201000578.

[173] Mikuš, P., Kovaľ, M., Maráková, K., Piešťanský, J., Havránek, E., *Talanta*. 2013, *103*, 294-300, DOI: 10.1016/j.talanta.2012.10.047.

[174] Piešťanský, J., Cizmarova, I., Matuskova, M., Mikuš, P., *Electrophoresis*. 2022, *43*, 998-1009, DOI: 10.1002/elps.202100209.

[175] Mikuš, P., Veizerová, L., Piešťanský, J., Maráková, K., Havránek, E., *Electrophoresis*. 2013, *34*, 1223-1231, DOI: 10.1002/elps.201200556.

[176] Tomáš, R., Kovaľ, M., Foret, F., *J. Chromatogr. A*. 2010, *1217*, 4144-4149, DOI: 10.1016/j.chroma.2010.02.021.

[177] Piešťanský, J., Maráková, K., Kovaľ, M., Mikuš, P., *J. Chromatogr. A*. 2014, *1358*, 285-292, DOI: 10.1016/j.chroma.2014.06.083.

[178] Piešťanský, J., Maráková, K., Kovaľ, M., Havránek, E., Mikuš, P., *Electrophoresis*. 2015, *36*, 3069-3079, DOI: 10.1002/elps.201500351.

[179] Piešťanský, J., Maráková, K., Veizerová, L., Galba, J., Mikuš, P., *Anal. Chim. Acta*. 2014, *826*, 84-93, DOI: 10.1016/j.aca.2014.04.003.

[180] Piešťanský, J., Matuskova, M., Cizmarova, I., Majerova, P., Kovac, A., Mikuš, P., *J. Chromatogr. A*. 2021, *1648*, 462190, DOI: 10.1016/j.chroma.2021.462190.

[181] Reinhoud, N. J., Tinke, A. P., Tjaden, U. R., Niessen, W. M. A., van der Greef, J., *J. Chromatogr. A*. 1992, *627*, 263-271, DOI: 10.1016/0021-9673(92)87206-n.

[182] Tinke, A. P., Reinhoud, N. J., Niessen, W. M. A., Tjaden, U. R., van der Greef, J., *Rapid Commun. Mass Spectrom.* 1992, *6*, 560-563, DOI: 10.1002/rcm.1290060905.

[183] Peterson, Z. D., Bowerbank, C. R., Collins, D. C., Graves, S. W., Lee, M. L., *J. Chromatogr. A*. 2003, *992*, 169-179, DOI: 10.1016/s0021-9673(03)00235-8.

[184] Kohl, F. J., Montealegre, C., Neusüß, C., *Electrophoresis*. 2016, *37*, 954-958, DOI: 10.1002/elps.201500579.

[185] Römer, J., Kiessig, S., Moritz, B., Neusüß, C., *Electrophoresis*. 2021, *42*, 374-380, DOI: 10.1002/elps.202000180.

[186] Troška, P., Chudoba, R., Danč, L., Bodor, R., Horčičiak, M., Tesařová, E., Masár, M., *J. Chromatogr. B*. 2013, *930*, 41-47, DOI: 10.1016/j.jchromb.2013.04.042.

[187] Bodor, R., Madajová, V., Kaniansky, D., Masár, M., Jöhnck, M., Stanislawski, B., *J. Chromatogr. A*. 2001, *916*, 155-165, DOI: 10.1016/s0021-9673(00)01080-3.

[188] Graß, B., Neyer, A., Jöhnck, M., Siepe, D., Eisenbeiß, F., Weber, G., Hergenröder, R., *Sens. Actuators B Chem.* 2001, *72*, 249-258, DOI: 10.1016/s0925-4005(00)00643-2.

[189] Horčičiak, M., Masár, M., Bodor, R., Danč, L., Bel, P., *J. Sep. Sci.* 2012, *35*, 674-680, DOI: 10.1002/jssc.201100942.

[190] Kohl, F. J., Sánchez-Hernández, L., Neusüß, C., *Electrophoresis*. 2015, *36*, 144-158, DOI: 10.1002/elps.201400368.

[191] Drouin, N., Kubáň, P., Rudaz, S., Pedersen-Bjergaard, S., Schappler, J., *Trends Anal. Chem.* 2019, *113*, 357-363, DOI: 10.1016/j.trac.2018.10.024.

[192] Pedersen-Bjergaard, S., Huang, C., Gjelstad, A., *J. Pharm. Anal.* 2017, *7*, 141-147, DOI: 10.1016/j.jpha.2017.04.002.

[193] Yamini, Y., Seidi, S., Rezazadeh, M., *Anal. Chim. Acta*. 2014, *814*, 1-22, DOI: 10.1016/j.aca.2013.12.019.

[194] Eie, L. V., Pedersen-Bjergaard, S., Hansen, F. A., *J. Pharm. Biomed. Anal.* 2022, *207*, 114407, DOI: 10.1016/j.jpba.2021.114407.

[195] Kler, P. A., Huhn, C., *Anal. Bioanal. Chem.* 2014, *406*, 7163-7174, DOI: 10.1007/s00216-014-8152-6.

[196] Sydes, D., Kler, P. A., Hermans, M., Huhn, C., *Electrophoresis*. 2016, *37*, 3020-3024, DOI: 10.1002/elps.201600262.

[197] Hermans, M., Gottmann, J., Riedel, F., *J. Laser Micro Nanoeng.* 2014, *9*, 126-131, DOI: 10.2961/jlmn.2014.02.0009.

[198] Drevinskas, T., Maruška, A., Briedis, V., *Electrophoresis*. 2015, *36*, 292-297, DOI: 10.1002/elps.201400320.

[199] Zemann, A. J., Schnell, E., Volgger, D., Bonn, G. K., *Anal. Chem.* 1998, *70*, 563-567, DOI: 10.1021/ac9707592.

[200] Tůma, P., Opekar, F., Štulík, K., *Electrophoresis*. 2002, *23*, 3718-3724, DOI: 10.1002/1522-2683(200211)23:21<3718::Aid-elps3718>3.0.Co;2-u.

[201] Kubáň, P., Hauser, P. C., *Electrophoresis*. 2004, *25*, 3387-3397, DOI: 10.1002/elps.200406059.

[202] Francisco, K. J., do Lago, C. L., *Electrophoresis*. 2009, *30*, 3458-3464, DOI: 10.1002/elps.200900080.

[203] Ďurč, P., Foret, F., Pokojová, E., Homola, L., Skřičková, J., Herout, V., Dastych, M., Vinohradská, H., Kubáň, P., *Anal. Bioanal. Chem.* 2017, *409*, 3507-3514, DOI: 10.1007/s00216-017-0318-6.

[204] Greguš, M., Foret, F., Kubáň, P., *Electrophoresis*. 2015, *36*, 526-533, DOI: 10.1002/elps.201400456.

[205] Greguš, M., Foret, F., Kindlova, D., Pokojová, E., Plutinský, M., Doubková, M., Merta, Z., Binková, I., Skřičková, J., Kubáň, P., *J. Breath Res.* 2015, *9*, 027107, DOI: 10.1088/1752-7155/9/2/027107.

[206] Kubáň, P., Greguš, M., Pokojová, E., Skřičková, J., Foret, F., *J. Chromatogr. A*. 2014, *1358*, 293-298, DOI: 10.1016/j.chroma.2014.06.091.

[207] Mori, M., Ishikawara, F., Tomoda, T., Yamada, S., Okamoto, M., Itabashi, H., Seki, Y., Matsumoto, R., Shoho, Y., Martha, L., Sumino, H., Murakami, M., *J. Chromatogr. B*. 2016, *1012-1013*, 178-185, DOI: 10.1016/j.jchromb.2016.01.037.

[208] Sáiz, J., Duc, M. T., Koenka, I. J., Martín-Alberca, C., Hauser, P. C., García-Ruiz, C., *J. Chromatogr. A*. 2014, *1372C*, 245-252, DOI: 10.1016/j.chroma.2014.10.085.

[209] Kubáň, P., Kobrin, E.-G., Kaljurand, M., *J. Chromatogr. A*. 2012, *1267*, 239-245, DOI: 10.1016/j.chroma.2012.06.085.

[210] Huang, T., Kang, Q., Zhu, X., Zhang, Z., Shen, D., *Anal. Methods*. 2013, *5*, 6839-6847, DOI: 10.1039/c3ay41508b.

[211] Kobrin, E. G., Lees, H., Fomitšenko, M., Kubáň, P., Kaljurand, M., *Electrophoresis*. 2014, *35*, 1165-1172, DOI: 10.1002/elps.201300380.

[212] Nogueira, T., Lago, C. L. d., *Microchem. J.* 2011, *99*, 267-272, DOI: 10.1016/j.microc.2011.05.014.

[213] Chang Guo, C., Lei Guang, L., Yu Jun, S., Yu Ping, L., *Electrochim. Acta*. 2009, *54*, 6959-6962, DOI: 10.1016/j.electacta.2009.06.046.

[214] Kubáň, P., Evenhuis, C. J., Macka, M., Haddad, P. R., Hauser, P. C., *Electroanalysis*. 2006, *18*, 1289-1296, DOI: 10.1002/elan.200603528.

[215] Malý, M., Boublík, M., Pocrnić, M., Ansorge, M., Lorinčíková, K., Svobodová, J., Hruška, V., Dubský, P., Gaš, B., *Electrophoresis*. 2020, *41*, 493-501, DOI: 10.1002/elps.201900283.

[216] Malý, M., Dovhunová, M., Dvořák, M., Gerlero, G. S., Kler, P. A., Hruška, V., Dubský, P., *Electrophoresis*. 2019, *40*, 683-692, DOI: 10.1002/elps.201800400.

[217] Foret, F., Thompson, T. J., Vouros, P., Karger, B. L., Gebauer, P., Boček, P., *Anal. Chem.* 2002, *66*, 4450-4458, DOI: 10.1021/ac00096a010.

[218] Pan, S., Chen, X., Li, X., Jin, M., *J. Sep. Sci.* 2019, *42*, 1045-1050, DOI: 10.1002/jssc.201800957.

[219] Wimmer, B., Neidhardt, H., Schwientek, M., Haderlein, S. B., Huhn, C., *Pest. Manag. Sci.* 2022, *78*, 2550-2559, DOI: 10.1002/ps.6883.

[220] Malá, Z., Gebauer, P., *Anal. Chim. Acta*. 2018, *998*, 67-74, DOI: 10.1016/j.aca.2017.10.013.

[221] Stegehuis, D. S., Tjaden, U. R., van der Greef, J., *J. Chromatogr. A*. 1992, *591*, 341-349, DOI: 10.1016/0021-9673(92)80251-o.

[222] Mazereeuw, M., Spikmans, V., Tjaden, U. R., van der Greef, J., *J. Chromatogr. A*. 2000, *879*, 219-233, DOI: 10.1016/s0021-9673(00)00259-4.

[223] Hühner, J., Jooß, K., Neusüß, C., *Electrophoresis*. 2017, *38*, 914-921, DOI: 10.1002/elps.201600457.

[224] Bowerbank, C. R., Lee, M. L., *J. Microcolumn. Sep.* 2001, *13*, 361-370, DOI: 10.1002/mcs.10019.

[225] Chen, S., Lee, M. L., *Anal. Chem.* 2000, *72*, 816-820, DOI: 10.1021/ac990727+.

## Appendix I



## Appendix II



## Appendix III

Paper 1:

Graf, H. G., Rudisch, B. M., Manegold, J., Huhn, C., Advancements in capacitance-to-digital converter-based C$^4$D technology for detection in capillary electrophoresis using amplified excitation voltages and comparison to classical and open-source C$^4$Ds. *Electrophoresis* 2021, *42*, 1306-1316, DOI: 10.1002/elps.202000394

+ Supporting Information and Manual for CDCDs

Paper 2:

Graf, H. G., Biebl, S. M., Müller, L., Breitenstein, C., Huhn, C., Capillary electrophoresis applied for the determination of acidity constants and limiting electrophoretic mobilities of ionizable herbicides including glyphosate and its metabolites and for their simultaneous separation. *Journal of Separation Science* 2022; *45*, 1128-1139, DOI: 10.1002/jssc.202100952

+ Supporting Information

Paper 3:

Graf, H. G., Rudisch, B. M., Ude, L., Müller, L., Huhn, C., Picomolar detection limits for glyphosate by two-dimensional column-coupled isotachophoresis/capillary electrophoresis mass spectrometry. *Journal of Separation Science* 2022; *45*, 3887-3899, DOI: 10.1002/jssc.202200519

+ Supporting Information

# Appendix I

Table A1. Chromatographic methods for glyphosate and AMPA analysis published between 2016 and 2022. Only references were included where the limit of quantification (LOQ) or the limit of detection (LOD) were specified in addition to the separation column used. The LOQ and LOD value are strongly dependent on the use sample volume, pretreatment, and extraction procedure. (Separation on HILIC, normal phase and mixed mode columns)

| Author | Ref | Year | Mode[1)] | Detect.[2)] | Derivat.[3)] | Type[4)] | Glyphosate | AMPA | $t_{R,GLP}$[5)] | $t_{R,AMPA}$[5)] | Matrix |
|---|---|---|---|---|---|---|---|---|---|---|---|
| Ding | [1] | 2016 | HILIC | MS/MS | - | LOD | 5-8 µg/kg | - | 8.7 | - | food |
| Guo | [2] | 2018 | HILIC | MS/MS | - | LOD | 20 µg/L | 20 µg/L | 2.5 | 2.5 | blood |
| Guo | [3] | 2019 | HILIC | MS/MS | - | LOD | 0.15 µg/L | 0.1 µg/L | 3.9 | 3.9 | surface water |
| Franke | [4] | 2020 | HILIC | MS/MS | - | LOD | 0.5-5 µg/L | 0.5-5 µg/L | n.g. | n.g. | water /urine |
| Fritz-Wallace | [5] | 2020 | HILIC | MS/MS | - | LOD | 2 µg/L | 5 µg/L | 0.4 | 0.45 | reactor fluids |
| Cutillas [a)] | [6] | 2021 | HILIC/IX | MS/MS | - | LOD | 10-20 µg/kg | 10-50 µg/kg | 5.78 | 1.023 | vegetables |
| Sandoval-Gío | [7] | 2021 | HILIC/NP | MS/MS | - | LOD | 0.05 µg/L | - | n.g. | - | tissue |
| Shinde | [8] | 2020 | HILIC/WAX | MS/MS | - | LOQ | 0.01 mg/kg | 0.02 mg/kg | 6.54 | 3.54 | palm oil |
| Giang | [9] | 2020 | HILIC/WAX | MS/MS | - | LOD | 3 µg/kg | 3 µg/kg | 5.45 | 3.41 | water |
| Manzano-Sánchez [b)] | [10] | 2020 | HILIC/WAX | MS/MS | - | LOQ | 50-100 µg/kg | 50-100 µg/kg | 7.79 | 6.49 | vegetables, fruits |
| Kim | [11] | 2021 | HILIC/WAX | MS/MS | - | LOD | 0.5 µg/L | n.g. | 4.1 | 2,3 | mealworms |
| Dias [a)] | [12] | 2021 | HILIC/WAX | MS/MS | - | LOD | 20-50 µg/kg | 20-50 µg/kg | 3.88 | 0.72 | seed cake, peas, soya cake |
| Jansons | [13] | 2021 | HILIC/WAX | MS/MS | - | LOD | 3 µg/kg | 3 µg/kg | 15.18 | 8.71 | food, tissue, milk |
| Nielsen | [14] | 2018 | NP | MS/MS | - | LOQ | < 200 µg/kg | < 200 µg/kg | n.g. | n.g. | intestinal samples |
| Pan | [15] | 2019 | NP | MS/MS | - | LOD | 0.01-0.03 µg/L | n.g. | 3.73 | 5.79 | tap, river, well water |
| Parvez | [16] | 2018 | NP/HILIC/IX | MS/MS | - | LOD | 0.02-0.1 µg/L | - | n.g. | - | water, urine |
| López [b)] | [17] | 2019 | NP/HILIC/IX | MS/MS | - | LOQ | 20-100 µg/kg | 20-50 µg/kg | 2.5 | n.g. | fruits, vegetables, grain |
| Chen | [18] | 2019 | NP/HILIC/IX | MS/MS | - | LOD | 3 µg/L | 1 µg/L | 3.5 | 2.28 | urine |
| López | [19] | 2020 | NP/HILIC/IX | MS/MS | - | LOD | 0.2 µg/L (10 µg/kg) | - | n.g. | - | beers, plant milk, wine |
| López [b)] | [20] | 2020 | NP/HILIC/IX | MS/MS | - | LOQ | 10-200 µg/kg | 10-200 µg/kg | 2.6 | n.g. | cow milk, tissue chicken meat, eggs |
| Dias [b)] | [12] | 2021 | NP/HILIC/IX | MS/MS | - | LOD | 20 µg/kg | 50 µg/kg | 1.08 | 1.42 | seed cake; peas; soya cake |
| Ohara | [21] | 2021 | NP/IX/RP | MS/MS | acetylation | LOD | 20 µg/L | 20 µg/L | 2.05 | 1.46 | urine, plasma |
| Nomura | [22] | 2020 | NP/RP/WIX | MS/MS | - | LOD | 0.1 µg/L | - | 3.4 | - | urine |

Continuation of Table A1. (Separation on PGC and mixed mode columns)

| Author | Ref | Year | Mode[1)] | Detect.[2)] | Derivat.[3)] | Type[4)] | Glyphosate | AMPA | $t_{R,GLP}$[5)] | $t_{R,AMPA}$[5)] | Matrix |
|---|---|---|---|---|---|---|---|---|---|---|---|
| Wuethrich | [23] | 2016 | PGC | MS/MS | - | LOD | 3 µg/L | 6 µg/L | 4.6 | 1.5 | beer |
| Pupke | [24] | 2016 | PGC | MS/MS | - | LOD | 4 µg/L | 0.8 µg/L | n.g. | n.g. | saline water |
| Lee | [25] | 2017 | PGC | MS/MS | - | LOD | 0.078 - 0.156 µg/L | - | 1.86 | - | vaccines |
| Park | [26] | 2019 | PGC | MS/MS | - | LOQ | 0.05 µg/L | - | n.g. | - | surface water |
| Chiarello | [27] | 2019 | PGC | MS/MS | - | LOD | 10 µg/kg | n.g. | 1 | 0.77 | olive oils |
| Goncharova | [28] | 2019 | PGC | MS/MS | - | LOD | 13 µg/L | 12 µg/L | 7.6 | 4.38 | aqueous standards |
| Zhan | [29] | 2019 | PGC | MS/MS | - | LOD | 16 µg/kg | 16 µg/kg | 2.5 | 1.12 | soils |
| Savini | [30] | 2019 | PGC | MS/MS | - | LOD | 3 µg/kg | 3 µg/kg | 3.46 | 2.02 | vegetable, juice, fruit puree |
| López-Ruiz | [31] | 2020 | PGC | MS/MS | - | LOD | 25 µg/L | - | 3.9 | - | human blood serum |
| Gormez | [32] | 2019 | PGC | MS/MS | - | LOD | <5 µg/kg | <5 µg/kg | 8.96 | n.g. | pomegranate |
| Vera-Candioti | [33] | 2021 | PGC | MS | - | LOD | 0.2 µg/L | 0.2 µg/L | n.g. | n.g. | surface and groundwater |
| Limon | [34] | 2021 | PGC | IRMS | - | LOD | 1250 µg/L | - | n.g. | - | river water |
| Han | [35] | 2016 | RP/HILIC | MS/MS | - | LOD | 50 µg/L | 50 µg/L | 0.9 | 0.88 | blood |
| Ulrich | [36] | 2021 | RP/WAX | MS/MS | - | LOD | 0.23 µg/L | 0.30 µg/L | 4.5 | 2.7 | hard waters |
| Chamkasem | [37] | 2016 | RP/WIX | MS/MS | - | LOD | 15 µg/kg | 18 µg/kg | 2.05 | 1.1 | soybean and corn |
| Chamkasem | [38] | 2017 | RP/WIX | MS/MS | - | LOD | 6 µg/kg | - | 2.7 | - | grapes |

n.g.: not given.

1) Separation principle, abbreviations: HILIC: hydrophilic interaction liquid chromatography, IX: ion exchange, LX: ligand exchange, NP: normal phase, PEG: polyethyleneglycol phase, PGC: porous graphitic carbon, RP: reversed phase, SAX: strong anion exchange, SCX: strong cation exchange, SEC size exclusion chromatography, WAX: weak anion exchange; WIX: weak ion exchange.

2) Abbreviations: FLD: fluorescence detection, ICP: Inductively coupled plasma, IRMS: isotope-ratio mass spectrometry, MS: mass spectrometry, MS/MS: tandem mass spectrometry, UV ultraviolet absorption spectrophotometry.

3) Derivatization method, unless otherwise stated, pre-column derivatization. Abbreviations: AQC: 6-aminoquinolyl-*N*-hydroxysuccinimidyl carbamate; MERC: 2-mercaptoethanol, OPA: o-phthalaldehyde, PFBBr: 2,3,4,5,6- pentafluorobenzyl bromide; p-TsCl: p-toluenesulfonyl chloride

4) Type of data specified in the two columns to the right. Abbreviations: LOD: limit of detection; LOQ: Limit of quantification

5) retention time $t_R$ in minutes. Abbreviations: GLP: glyphosate.

a) *N*-acetyl AMPA included in study.

b) *N*-acetyl AMPA and *N*-acetyl glyphosate included in study.

s) with enrichment by solid phase extraction.

m) same separation method, but different mass spectrometer.

Continuation of Table A1. (Separation on C18 columns, years: 2016-2018)

| Author | Ref | Year | Mode[1)] | Detect.[2)] | Derivat.[3)] | Type[4)] | Glyphosate | AMPA | $t_{R,GLP}$[5)] | $t_{R,AMPA}$[5)] | Matrix |
|---|---|---|---|---|---|---|---|---|---|---|---|
| Ronco | [39] | 2016 | RP C18 | MS | FMOC-Cl | LOQ | 0.02 µg/L | 0.02 µg/L | n.g. | n.g. | surface water, bottom sediments |
| Wang | [40] | 2016 | RP C18 | FLD | FMOC-Cl | LOD | 0.6 µg/L | 0.3 µg/L | 6.4 | 7.6 | seawater |
| Tsao | [41] | 2016 | RP C18 | MS/MS | - | LOD | 100 µg/L | - | 0.87 | - | blood, serum |
| Schrübbers | [42] | 2016 | RP C18 | MS | FMOC-Cl | LOD | 12 µg/kg | 12 µg/kg | 3.9 | 8.8 | leaf |
| Gomez-Caballero | [43] | 2016 | RP C18 | FLD | FMOC-Cl | LOD | 250 µg/kg | n.g. | 4.8 | 8.9 | water and soil |
| Klátyik | [44] | 2017 | RP C18 | MS/MS | FMOC-Cl | LOD | 0.001 µg/L | - | n.g. | - | natural water |
| Poiger | [45] | 2017 | RP C18 | MS/MS | FMOC-Cl | LOQ | 0.005 µg/L | 0.005 µg/L | 5.5 | 8.7 | surface, ground water |
| Claude | [46] | 2017 | RP C18 | MS/MS | FMOC-Cl | LOD | 0.01 µg/L | 0.01 µg/L | n.g. | n.g. | environmental waters |
| Slomberg | [47] | 2017 | RP C18 | MS/MS | FMOC-Cl | LOD | 0.025 µg/L | 0.025 µg/L | n.g | n.g. | surface water |
| DIN ISO 16308:2017-09 | [48] | 2017 | RP C18 | MS/MS | FMOC-Cl | LOQ | 0.03 µg/L | 0.03 µg/L | 3.18 | 3.39 | surface water |
| Cristoni | [49] | 2017 | RP C18 | MS/MS | - | LOD | 0.06 µg/L | - | 3 | - | fruit juice |
| Toss | [50] | 2017 | RP C18 | MS/MS | FMOC-Cl | LOD | 0.2 µg/L | n.g. | 6.5 | 7.5 | surface water |
| Kongtip | [51] | 2017 | RP C18 | FLD | - | LOD | 0.4 µg/L | - | n.g | - | serum |
| Polyiem | [52] | 2017 | RP C18 | FLD | FMOC-Cl | LOD | 0.5 µg/L | - | 5.73 | - | urine |
| Oulkar | [53] | 2017 | RP C18 | MS/MS | FMOC-Cl | LOQ | 0.5-2 µg/kg | n.g. | 3.91 | 5.67 | plant matrices |
| Padilla-Alonso | [54] | 2017 | RP C18 | FLD | FMOC-Cl | LOD | 3.2 µg/L | 2.8 µg/L | 9.0 | 11.1 | water |
| Klátyik | [44] | 2017 | RP C18 | UV | FMOC-Cl | LOD | 5 µg/L | - | 6.71 | - | natural water |
| Tong | [55] | 2017 | RP C18 | MS/MS | FMOC-Cl | LOQ | 50-100 µg/kg | 50-100 µg/kg | 5.9 | 6.2 | tea plant |
| Tittlemier | [56] | 2017 | RP C18 | MS/MS | FMOC-Cl | LOQ | 50-100 µg/kg | 50-200 µg/kg | n.g. | n.g. | wheat, oats, barley, malt, lentils |
| Drzyzga | [57] | 2017 | RP C18 | UV | p-TsCl | LOD | 7.4 µg/L | 2.6 µg/L | 16.1 | 10.3 | bacterial cult. media |
| De Gerónimo | [58] | 2018 | RP C18 | MS/MS | FMOC-Cl | LOD | 0.2-0.3 µg/kg | 0.5-0.7 µg/kg | n.g. | n.g. | soil |
| Virginia | [59] | 2018 | RP C18 | MS/MS | FMOC-Cl | LOD | 0.3 µg/kg | 0.4 µg/kg | n.g. | n.g. | soil |
| Pinto | [60] | 2018 | RP C18 | MS/MS | FMOC-Cl | LOD | 0.35 µg/L | 0.1 µg/L | 3.21 | 3.37 | irrigation water |
| Alonso | [61] | 2018 | RP C18 | MS | FMOC-Cl | LOD | 0.5 µg/L; 2 µg/kg | 0.5 µg/L; 2 µg/kg | n.g. | n.g. | rainwater, soil |
| Demonte | [62] | 2018 | RP C18 | MS/MS | FMOC-Cl | LOQ | 0.6 µg/L | 0.2 µg/L | 3.3 | 3.49 | ground, surface water |
| Erban | [63] | 2018 | RP C18 | MS/MS | FMOC-Cl | LOQ | 1 µg/kg | 1 µg/kg | n.g. | n.g. | soil |
| Li | [64] | 2018 | RP C18 | UV | FMOC-Cl | LOD | 1680 µg/L | 555 µg/L | 22 | 25 | abiotic degradation |

Continuation of Table A1. (Separation on C18 columns, years: 2018-2022)

| Author | Ref | Year | Mode[1)] | Detect.[2)] | Derivat.[3)] | Type[4)] | Glyphosate | AMPA | $t_{R,GLP}$[5)] | $t_{R,AMPA}$[5)] | Matrix |
|---|---|---|---|---|---|---|---|---|---|---|---|
| Leyva-Soto | [65] | 2018 | RP C18 | FLD | FMOC-Cl | LOD | 5 µg/L | 15 µg/L | n.g. | n.g. | soil, surface water |
| Liao | [66] | 2018 | RP C18 | MS/MS | FMOC-Cl | LOQ | 5 µg/kg | - | 7 | - | food samples |
| Matozzo | [67] | 2018 | RP C18 | MS/MS | FMOC-Cl | LOD | - | 0.2 µg/L | - | n.g. | seawater samples |
| Exterkoetter | [68] | 2019 | RP C18 | FLD | FMOC-Cl | LOD | 0.06-0.18 µg/L | 0.02-0.24 µg/L | 23 | 24.5 | soil, sediment, water |
| Carretta | [69] | 2019 | RP C18 | MS/MS | AccQ•Tag | LOD | 0.2 µg/L | 0.05 µg/L | 3.64 | 3.9 | runoff water |
| Muskus | [70] | 2019 | RP C18 | MS/MS | FMOC-Cl | LOD | 1 µg/L | 10 µg/L | n.g. | n.g. | soil |
| Thompson | [71] | 2019 | RP C18 | MS/MS | FMOC-Cl | LOQ | 1 µg/k | 1 µg/k | 7.3 | 8.1 | honey |
| Sun | [72] | 2019 | RP C18 | MS | FMOC-Cl | LOQ | 1680 µg/kg | 1100 µg/kg | n.g. | n.g. | soil |
| Barker | [73] | 2019 | RP C18 | MS/MS | FMOC-Cl | LOD | 2.76 µg/L | 7.4 µg/L | 4.72 | 4.99 | sugar beet |
| Usui | [74] | 2019 | RP C18 | FLD | FMOC-Cl | LOD | 200 µg/L | - | n.g. | - | serum |
| Wumbei | [75] | 2019 | RP C18 | MS/MS | FMOC-Cl | LOD | 40 µg/kg | - | n.g. | - | yam |
| Oliveira Pereira | [76] | 2019 | RP C18 | FLD | OPA-MRCE | LOD | 5 µg/L | 1.7 µg/L | 8.9 | 6.2 | water, soil |
| de F. Sousa | [77] | 2019 | RP C18 | UV | FMOC-Cl | LOD | 90 µg/L | - | 2.97 | - | air with polyurethane foams |
| Franke | [4] | 2020 | RP C18 | MS/MS | FMOC-Cl | LOD | 0.037 µg/L | 0.020 µg/L | 5.15 | 11.04 | urine |
| Correia | [78] | 2020 | RP C18 | MS/MS | n.g. | LOD | 0.3798 µg/L | 1.0103 µg/L | 2.08 | 2.08 | water samples |
| Fontàs | [79] | 2020 | RP C18 | UV | AQC | LOD | 0.5 mg/L | 0.2 mg/L | 3.8 | 13.5 | standard solutions |
| Zhang | [80] | 2020 | RP C18 | MS/MS | FMOC-Cl | LOD | 1.5 µg/kg | - | 1.2 | - | corn |
| Umsza-Guez | [81] | 2021 | RP C18 | FLD | FMOC-Cl | LOD | <5 µg/L | - | n.g. | - | propolis |
| Ferhi | [82] | 2021 | RP C18 | FLD | FMOC-Cl | LOD | 0.00025 µg/L | - | n.g. | - | drilling water, wastewater |
| Bayebila Menanzambi | [83] | 2021 | RP C18 | MS/MS | FMOC-Cl | LOD | 0.08 µg/L | - | n.g. | - | urine |
| Bressán | [84] | 2021 | RP C18 | MS/MS | FMOC-Cl | LOD | 0.5 µg/L | - | 4.75 | - | urine |
| Martin-Reina | [85] | 2021 | RP C18 | MS/MS | FMOC-Cl | LOD | 0.5 µg/L | 0.1 µg/L | 3.88 | 4.74 | urine |
| Gębura | [86] | 2021 | RP C18 | UV | pTS-Cl | LOD | 2 µg/kg | 21 µg/kg | 13.7 | 10.4 | walnuts, soybeans, barley, lentil |
| Surapong | [87] | 2021 | RP C18 | UV | FMOC-Cl | LOD | 450-750µg/L | 450-750µg/L | n.g. | n.g. | water, soil, and vegetable samples |
| Surapong[s)] | [87] | 2021 | RP C18 | UV | FMOC-Cl | LOD | 21.0−22.5 µg/L | 21.0−22.5 µg/L | n.g. | n.g. | |
| Delhomme | [88] | 2021 | RP C18 | MS/MS | FMOC-Cl | LOQ | 30-230 µg/kg | 25-200 µg/kg | 7.57 | 8.79 | soil and earthworms |

Continuation of Table A1. (Separation on different reverse phase and size exclusion/ligand exchange columns)

| Author | Ref | Year | Mode[1)] | Detect.[2)] | Derivat.[3)] | Type[4)] | Glyphosate | AMPA | $t_{R,GLP}$[5)] | $t_{R,AMPA}$[5)] | Matrix |
|---|---|---|---|---|---|---|---|---|---|---|---|
| Jansons [m)] | [13] | 2021 | RP C18 | MS/MS | Dansyl-Cl | LOD | 3-8 µg/kg | 3 µg/kg | 12.73 | 11.33 | food, tissue, milk |
| Jansons [m)] | [13] | 2021 | RP C18 | MS/MS | Dansyl-Cl | LOD | 3-80 µg/kg | 3 µg/kg | 13.01 | 11.63 | food, tissue, milk |
| Wang | [89] | 2021 | RP C18 | MS/MS | FMOC-Cl | LOD | 40 µg/kg | 100 µg/kg | 7.5 | 8.9 | tea |
| Cruz | [90] | 2021 | RP C18 | MS/MS | FMOC-Cl | LOQ | 5 µg/kg | 5 µg/kg | n.g. | n.g. | breakfast cereals |
| Wirth | [91] | 2021 | RP C18 | MS/MS | FMOC-Cl | LOD | - | 6.2 µg/L | - | 9.7 | lysimeter soil samples |
| Pérez-Mayán | [92] | 2022 | RP C18 | MS/MS | FMOC-Cl | LOQ | 1 µg/L | 0.5 µg/L | 5.7 | n.g. | wine |
| Connolly | [93] | 2017 | RP C3 | MS/MS | | LOD | 0.5 µg/L | - | n.g. | - | urine |
| Connolly | [94] | 2018 | RP C8 | MS/MS | n.g. | LOQ | 0.5 µg/L | - | n.g. | - | urine |
| Tiago | [95] | 2020 | RP C8 | ICP-MS/MS | - | LOQ | 1.09 µg/L | 0.29 µg/L | 4.2 | 2 | water |
| Pimenta | [96] | 2020 | RP C8 | UV | FMOC-Cl | LOD | 300 µg/L | 300 µg/L | 15.1 | 16.5 | water |
| Pimenta | [96] | 2020 | RP C8 | ICP-MS/MS | - | LOD | 8.2 µg/L | 8.2 µg/L | 4.2 | 2.2 | water |
| Marín | [97] | 2020 | RP PEG | MS/MS | FMOC-Cl | LOQ | 0.5 µg/L (water), 1.6-2.5 mg/kg | n.g. | 7.76 | 13.88 | vegetables, soil, irrigation water |
| Bienvenu | [98] | 2020 | RP phenyl | MS/MS | PFBBr | LOD | 0.077 µg/L | 0.086 µg/L | 4.2 | 4.01 | urine |
| Jaikwang | [99] | 2020 | RP phenyl | MS/MS | - | LOD | 2.5 µg/L | 2.5 µg/L | 5.93 | 6.06 | urine |
| Guo | [100] | 2016 | SEC/LX | MS/MS | - | LOD | 0.02-0.05 µg/L | | 1.9 | 7.1 | water |
| Jensen | [101] | 2016 | SEC/LX | MS/MS | - | LOD | 0.02-2.8 µg/L | 0.03-1.7 µg/L | 1.6 | 4.7 | bovine + human milk, human urine |
| Zoller | [102] | 2018 | SEC/LX | MS/MS | - | LOD | 0.2-0.4 µg/kg | 0.5-1 µg/kg | n.g. | n.g. | wheat, beer, wine, meat, fish, seeds |
| Riter | [103] | 2018 | SEC/LX | MS/MS | - | LOQ | 50 µg/kg | 50 µg/kg | 2 | 13.6 | raw agricultural commodities |

Continuation of Table A1. (Separation by ion chromatography)

| Author | Ref | Year | Mode[1)] | Detect.[2)] | Derivat.[3)] | Type[4)] | Glyphosate | AMPA | $t_{R,GLP}$[5)] | $t_{R,AMPA}$[5)] | Matrix |
|---|---|---|---|---|---|---|---|---|---|---|---|
| Steinborn | [104] | 2016 | SAX | MS/MS | - | LOD | 0.5 µg/L | - | 9.7 | - | breast milk |
| Boušová[a)] | [105] | 2016 | SAX | MS/MS | - | LOD | 5-10 µg/kg | 10 µg/kg | 9.7 | 5.68 | lettuce, oranges, flour |
| Adams[a)] | [106] | 2017 | SAX | MS/MS | - | LOD | 5 µg/kg | 10 µg/kg | 15.1 | 11.6 | cereals, grapes, baby food |
| Rajski[b)] | [107] | 2018 | SAX | MS/MS | - | LOQ | 10 µg/kg | 10 µg/kg | 16 | 12.5 | fruit, vegetables |
| Rodrigues | [108] | 2018 | SAX | FLD | OPA (post) | LOQ | 20 µg/kg | 20 µg/kg | 21 | 42 | soy-based infant formula |
| Okada | [109] | 2019 | SAX | MS/MS | - | LOD | 0.25 µg/L | 0.25 µg/L | 10.9 | 5.9 | environmental water |
| Lajin | [110] | 2019 | SAX | ICP-MS | - | LOD | 0.27 µg/L | 0.14 µg/L | 4.1 | 1.4 | tap, ground, river water |
| Jansons | [111] | 2019 | SAX | MS/MS | - | LOQ | 10 µg/kg | 10 µg/kg | n.g. | n.g. | beer and oat flour |
| Santilio | [112] | 2019 | SAX | MS/MS | - | LOD | 2-4 µg/kg | - | 1.2 | - | rice, maize |
| Chiesa | [113] | 2019 | SAX | MS | - | LOD | 4.3 µg/kg | 9.3 µg/kg | 23.87 | 14.25 | honey, fish, bovine muscle |
| Melton | [114] | 2019 | SAX | MS/MS | - | LOD | 5 µg/kg | n.g. | 11.98 | 4.89 | fruits, vegetables |
| Pareja | [115] | 2019 | SAX | MS/MS | - | LOQ | 5 µg/kg | 20 µg/kg | 15.2 | 9.7 | honey |
| Geerdink | [116] | 2020 | SAX | MS/MS | - | LOQ | 0.01 µg/L | 0.01 µg/L | 11.6 | 26 | surface water |
| Pires | [117] | 2020 | SAX | FLD | OPA (post) | LOQ | 0.2 µg/L | 0.5 µg/L | 20 | 5.7 | surface, ground water |
| Gasparini [b)] | [118] | 2020 | SAX | MS/MS | - | LOQ | 10 µg/kg | 50 µg/kg | 16.6 | 13 | grapes, honey, wheat |
| Dovidauskas | [119] | 2020 | SAX | CD | - | LOD | 15 µg/L | 80 µg/L | 44.6 | n.g. | water |
| Panseri | [120] | 2020 | SAX | MS/MS | - | LOQ | 5 µg/kg | 5 µg/kg | 23.66 | 14.15 | baby food |
| Ruiz | [121] | 2021 | SAX | MS/MS | - | LOQ | 0.1 µg/L | 0.1 µg/L | n.g. | n.g. | urine |
| Schütze | [122] | 2021 | SAX | CD+MS/MS | - | LOD | 0.2 µg/L | - | 11.5 | - | human urine |
| Zhang | [123] | 2021 | SAX | MS/MS | - | LOD | 0.6 µg/L | 1.2 µg/L | 8 | 1.7 | serum |
| Pérez-Mayán | [92] | 2022 | SAX | MS/MS | - | LOQ | 1 µg/L | 0.8 µg/L | 10.05 | n.g. | wine |
| Feltracco | [124] | 2021 | SAX | MS/MS | - | LOD | 0.0054 µg/L | 0.0016 µg/L | 13.9 | 8.1 | water, sea water |
| Vu | [125] | 2021 | SCX | MS/MS | - | LOQ | 0.5 µg/L | 0.5 µg/L | n.g. | n.g. | tap, river, estuary, sea water |
| de Souza | [126] | 2021 | SCX | FLD | OPA (post) | LOD | 20 µg/kg | 20 µg/kg | 6.8 | 10.5 | honey |
| de Souza | [127] | 2021 | SCX | FLD | OPA (post) | LOD | 20 µg/kg | 20 µg/kg | n.g. | n.g. | soybean |

## References Table A1


[1] Ding, J., Jin, G., Jin, G., Shen, A., Guo, Z., Yu, B., Jiao, Y., Yan, J., Liang, X., *Food Anal. Methods*. 2016, *9*, 2856-2863, DOI: 10.1007/s12161-016-0468-8.

[2] Guo, H., Wang, H., Zheng, J., Liu, W., Zhong, J., Zhao, Q., *Forensic Sci. Int.* 2018, *283*, 111-117, DOI: 10.1016/j.forsciint.2017.12.016.

[3] Guo, H., Gao, Y., Guo, D., Liu, W., Wang, J., Zheng, J., Zhong, J., Zhao, Q., *SN Applied Sciences*. 2019, *1*, DOI: 10.1007/s42452-019-0306-x.

[4] Franke, A. A., Li, X., Lai, J. F., *Anal. Bioanal. Chem.* 2020, *412*, 8313-8324, DOI: 10.1007/s00216-020-02966-1.

[5] Fritz-Wallace, K., Engelmann, B., Krause, J. L., Schäpe, S. S., Pöppe, J., Herberth, G., Rösler, U., Jehmlich, N., von Bergen, M., Rolle-Kampczyk, U., *Rapid Commun. Mass Spectrom.* 2020, *34*, e8668, DOI: 10.1002/rcm.8668.

[6] Cutillas, V., Fernández-Alba, A. R., *MethodsX*. 2021, *8*, 101306, DOI: 10.1016/j.mex.2021.101306.

[7] Sandoval-Gío, J. J., Polanco-Rodríguez, A. G., Araujo-León, J. A., Burgos-Díaz, M. I., Yáñez-Rivera, B., Candelero-de la Cruz, J., *Bull. Environ. Contam. Toxicol.* 2021, DOI: 10.1007/s00128-021-03412-3.

[8] Shinde, R., Halim, N., Banerjee, A. K., *J. AOAC Int.* 2020, *103*, 1528-1533, DOI: 10.1093/jaoacint/qsaa066.

[9] Giang, L. T., Thien, T. L. T., Yen, D. H., *Vietnam J. Chem.* 2020, *58*, 74-79, DOI: 10.1002/vjch.2019000132.

[10] Manzano-Sánchez, L., Martínez-Martínez, J. A., Domínguez, I., Martínez Vidal, J. L., Frenich, A. G., Romero-González, R., *Foods*. 2020, *9*, 553, DOI: 10.3390/foods9050553.

[11] Kim, L., Baek, S., Son, K., Lee, H. D., Choi, D. S., Kim, C. J., Noh, H. H., *Sci. Rep.* 2021, *11*, 17597, DOI: 10.1038/s41598-021-96529-8.

[12] Dias, J., López, S. H., Mol, H., de Kok, A., *J. Sep. Sci.* 2021, *44*, 2165-2176, DOI: 10.1002/jssc.202001134.

[13] Jansons, M., Pugajeva, I., Bartkevics, V., Karkee, H. B., *J. Chromatogr. B*. 2021, *1177*, 122779, DOI: 10.1016/j.jchromb.2021.122779.

[14] Nielsen, L. N., Roager, H. M., Casas, M. E., Frandsen, H. L., Gosewinkel, U., Bester, K., Licht, T. R., Hendriksen, N. B., Bahl, M. I., *Environ. Pollut.* 2018, *233*, 364-376, DOI: 10.1016/j.envpol.2017.10.016.

[15] Pan, S., Chen, X., Li, X., Jin, M., *J. Sep. Sci.* 2019, *42*, 1045-1050, DOI: 10.1002/jssc.201800957.

[16] Parvez, S., Gerona, R. R., Proctor, C., Friesen, M., Ashby, J. L., Reiter, J. L., Lui, Z., Winchester, P. D., *Environ. Health.* 2018, *17*, 23, DOI: 10.1186/s12940-018-0367-0.

[17] López, S. H., Scholten, J., Kiedrowska, B., de Kok, A., *J. Chromatogr. A*. 2019, *1594*, 93-104, DOI: 10.1016/j.chroma.2019.02.024.

[18] Chen, D., Miao, H., Zhao, Y., Wu, Y., *J. Chromatogr. A*. 2019, *1587*, 73-78, DOI: 10.1016/j.chroma.2018.11.030.

[19] López, S. H., Dias, J., Mol, H., de Kok, A., *J. Chromatogr. A*. 2020, *1625*, 461226, DOI: 10.1016/j.chroma.2020.461226.

[20] López, S. H., Dias, J., de Kok, A., *Food Control*. 2020, *115*, 107289, DOI: 10.1016/j.foodcont.2020.107289.

[21] Ohara, T., Yoshimoto, T., Natori, Y., Ishii, A., *Nagoya J. Med. Sci.* 2021, *83*, 567-587, DOI: 10.18999/nagjms.83.3.567.

[22] Nomura, H., Hamada, R., Saito, I., Nakane, K., Sawa, R., Ukai, M., Shibata, E., Sato, M., Kamijima, M., Ueyama, J., *Environ. Health Prev. Med.* 2020, *25*, 83, DOI: 10.1186/s12199-020-00918-w.

[23] Wuethrich, A., Haddad, P. R., Quirino, J. P., *Electrophoresis*. 2016, *37*, 1122-1128, DOI: 10.1002/elps.201600050.

[24] Pupke, D., Daniel, L., Proefrock, D., *J. Chromatogr. Sep. Tech.* 2016, *7*, 1000338, DOI: 10.4172/2157-7064.1000338.

[25] Lee, J. H., Park, H. N., Park, H.-J., Heo, S., Park, S. S., Park, S.-K., Baek, S. Y., *Chromatographia*. 2017, *80*, 1741-1747, DOI: 10.1007/s10337-017-3417-9.

[26] Park, H., May, A., Portilla, L., Dietrich, H., Münch, F., Rejek, T., Sarcletti, M., Banspach, L., Zahn, D., Halik, M., *Nat. Sustain.* 2019, *3*, 129-135, DOI: 10.1038/s41893-019-0452-6.
[27] Chiarello, M., Jiménez-Medina, M. L., Marín Saéz, J., Moura, S., Garrido Frenich, A., Romero-González, R., *Food Addit. Contam. Part A Chem. Anal. Control Expo. Risk Assess.* 2019, *36*, 1376-1384, DOI: 10.1080/19440049.2019.1631493.
[28] Goncharova, E. N., Statkus, M. A., Tsizin, G. I., Selimov, R. N., *Mosc. Univ. Chem. Bull.* 2019, *73*, 265-271, DOI: 10.3103/s0027131418060056.
[29] Zhang, P., Rose, M., Van Zwieten, L., *J. AOAC Int.* 2019, *102*, 952-965, DOI: 10.5740/jaoacint.18-0287.
[30] Savini, S., Bandini, M., Sannino, A., *J. Agric. Food Chem.* 2019, *67*, 2716-2722, DOI: 10.1021/acs.jafc.8b06483.
[31] López-Ruiz, R., Romero-González, R., Garrido Frenich, A., *J. Pharm. Biomed. Anal.* 2020, *190*, 113492, DOI: 10.1016/j.jpba.2020.113492.
[32] Gormez, E., Golge, O., Kabak, B., *J. Chromatogr. A*. 2021, *1642*, 462038, DOI: 10.1016/j.chroma.2021.462038.
[33] Vera-Candioti, J., Araujo, P. I., Huerga, I. R., Rojas, D. E., Cristos, D. S., Malmantile, A. D., *Environ. Monit. Assess.* 2021, *193*, 689, DOI: 10.1007/s10661-021-09462-8.
[34] Limon, A. W., Moingt, M., Widory, D., *Rapid Commun. Mass Spectrom.* 2021, *35*, e9017, DOI: 10.1002/rcm.9017.
[35] Han, J., Moon, H., Hong, Y., Yang, S., Jeong, W. J., Lee, K. S., Chung, H., *Forensic Sci. Int.* 2016, *265*, 41-46, DOI: 10.1016/j.forsciint.2015.12.049.
[36] Ulrich, J. C., Ferguson, P. L., *Anal. Bioanal. Chem.* 2021, *413*, 3763-3774, DOI: 10.1007/s00216-021-03324-5.
[37] Chamkasem, N., Harmon, T., *Anal. Bioanal. Chem.* 2016, *408*, 4995-5004, DOI: 10.1007/s00216-016-9597-6.
[38] Chamkasem, N., *J. Agric. Food Chem.* 2017, *65*, 7535-7541, DOI: 10.1021/acs.jafc.7b02419.
[39] Ronco, A. E., Marino, D. J., Abelando, M., Almada, P., Apartin, C. D., *Environ. Monit. Assess.* 2016, *188*, 458, DOI: 10.1007/s10661-016-5467-0.
[40] Wang, S., Liu, B., Yuan, D., Ma, J., *Talanta*. 2016, *161*, 700-706, DOI: 10.1016/j.talanta.2016.09.023.
[41] Tsao, Y. C., Lai, Y. C., Liu, H. C., Liu, R. H., Lin, D. L., *J. Anal. Toxicol.* 2016, *40*, 427-436, DOI: 10.1093/jat/bkw042.
[42] Schrübbers, L. C., Masís-Mora, M., Rojas, E. C., Valverde, B. E., Christensen, J. H., Cedergreen, N., *Talanta*. 2016, *146*, 609-620, DOI: 10.1016/j.talanta.2015.07.059.
[43] Gomez-Caballero, A., Diaz-Diaz, G., Bengoetxea, O., Quintela, A., Unceta, N., Goicolea, M. A., Barrio, R. J., *J. Chromatogr. A*. 2016, *1451*, 23-32, DOI: 10.1016/j.chroma.2016.05.017.
[44] Klátyik, S., Takács, E., Mörtl, M., Földi, A., Trábert, Z., Ács, É., Darvas, B., Székács, A., *Int. J. Environ. Anal. Chem.* 2017, *97*, 901-921, DOI: 10.1080/03067319.2017.1373770.
[45] Poiger, T., Buerge, I. J., Bächli, A., Müller, M. D., Balmer, M. E., *Environ. Sci. Pollut. Res. Int.* 2017, *24*, 1588-1596, DOI: 10.1007/s11356-016-7835-2.
[46] Claude, B., Berho, C., Bayoudh, S., Amalric, L., Coisy, E., Nehmé, R., Morin, P., *Environ. Sci. Pollut. Res. Int.* 2017, *24*, 12293-12300, DOI: 10.1007/s11356-017-8844-5.
[47] Slomberg, D. L., Ollivier, P., Radakovitch, O., Baran, N., Sani-Kast, N., Bruchet, A., Scheringer, M., Labille, J., *Environ. Chem.* 2017, *14*, 64–73, DOI: 10.1071/en16038.
[48] DIN ISO 16308:2017-09, Wasserbeschaffenheit – Bestimmung von Glyphosat und AMPA – Verfahren mittels Hochleistungs-Flüssigkeitschromatographie (HPLC) mit tandem-massenspektrometrischer Detektion, DOI: 10.31030/2679839.
[49] Cristoni, S., Dusi, G., Brambilla, P., Albini, A., Conti, M., Brambilla, M., Bruno, A., Di Gaudio, F., Ferlin, L., Tazzari, V., Mengozzi, S., Barera, S., Sialer, C., Trenti, T., Cantu, M., Rossi Bernardi, L., Noonan, D. M., *J. Mass Spectrom.* 2017, *52*, 16-21, DOI: 10.1002/jms.3895.
[50] Toss, V., Leito, I., Yurchenko, S., Freiberg, R., Kruve, A., *Environ. Sci. Pollut. Res. Int.* 2017, *24*, 7880-7888, DOI: 10.1007/s11356-017-8522-7.

[51] Kongtip, P., Nankongnab, N., Phupancharoensuk, R., Palarach, C., Sujirarat, D., Sangprasert, S., Sermsuk, M., Sawattrakool, N., Woskie, S. R., *J. Agromedicine*. 2017, *22*, 282-289, DOI: 10.1080/1059924X.2017.1319315.
[52] Polyiem, W., Hongsibson, S., Chantara, S., Kerdnoi, T., Patarasiri, V., Prapamonto, T., Sapbamrer, R., *J. Pharmacol. Toxicol.* 2017, *12*, 97-102, DOI: 10.3923/jpt.2017.97.102.
[53] Oulkar, D. P., Hingmire, S., Goon, A., Jadhav, M., Ugare, B., Thekkumpurath, A. S., Banerjee, K., *J. AOAC Int.* 2017, *100*, 631-639, DOI: 10.5740/jaoacint.17-0046.
[54] Padilla-Alonso, D. J., Garza-Tapia, M., Chávez-Montes, A., González-Horta, A., Waksman de Torres, N. H., Castro-Ríos, R., *J. Liq. Chromatogr. Relat. Technol.* 2017, *40*, 147-155, DOI: 10.1080/10826076.2017.1295057.
[55] Tong, M., Gao, W., Jiao, W., Zhou, J., Li, Y., He, L., Hou, R., *J. Agric. Food Chem.* 2017, *65*, 7638-7646, DOI: 10.1021/acs.jafc.7b02474.
[56] Tittlemier, S. A., Drul, D., Lake, B., Zirdum, T., Hammond, E., Sobering, D., Lin, W. J., Tran, M., Roscoe, M., *Cereal Chem.* 2017, *94*, 1028–1036, DOI: 10.1094/cchem-01-17-0021-r.
[57] Drzyzga, D., Lipok, J., *Environ. Sci. Pollut. Res. Int.* 2017, *24*, 24364-24375, DOI: 10.1007/s11356-017-0068-1.
[58] De Gerónimo, E., Lorenzón, C., Iwasita, B., Costa, J. L., *Soil Sci.* 2018, *183*, 34-40, DOI: 10.1097/ss.0000000000000225.
[59] Virginia, A., Zamora, M., Barbera, A., Castro-Franco, M., Domenech, M., De Gerónimo, E., Costa, J. L., *Agric. Syst.* 2018, *167*, 103-112, DOI: 10.1016/j.agsy.2018.09.005.
[60] Pinto, E., Soares, A. G., Ferreira, I. M. P. L. V. O., *Anal. Methods*. 2018, *10*, 554-561, DOI: 10.1039/c7ay02722b.
[61] Alonso, L. L., Demetrio, P. M., Agustina Etchegoyen, M., Marino, D. J., *Sci. Total Environ.* 2018, *645*, 89-96, DOI: 10.1016/j.scitotenv.2018.07.134.
[62] Demonte, L. D., Michlig, N., Gaggiotti, M., Adam, C. G., Beldoménico, H. R., Repetti, M. R., *Sci. Total Environ.* 2018, *645*, 34-43, DOI: 10.1016/j.scitotenv.2018.06.340.
[63] Erban, T., Stehlik, M., Sopko, B., Markovic, M., Seifrtova, M., Halesova, T., Kovaricek, P., *Chemosphere*. 2018, *207*, 78-83, DOI: 10.1016/j.chemosphere.2018.05.004.
[64] Li, H., Wallace, A. F., Sun, M., Reardon, P., Jaisi, D. P., *Environ. Sci. Technol.* 2018, *52*, 1109-1117, DOI: 10.1021/acs.est.7b03692.
[65] Leyva-Soto, L. A., Balderrama-Carmona, A. P., Moran-Palacio, E. F., Diaz-Tenorio, L. M., Gortares-Moroyoqui, P., *Appl. Ecol. Env. Res.* 2018, *16*, 5127-5140, DOI: 10.15666/aeer/1604_51275140.
[66] Liao, Y., Berthion, J. M., Colet, I., Merlo, M., Nougadère, A., Hu, R., *J. Chromatogr. A*. 2018, *1549*, 31-38, DOI: 10.1016/j.chroma.2018.03.036.
[67] Matozzo, V., Marin, M. G., Masiero, L., Tremonti, M., Biamonte, S., Viale, S., Finos, L., Lovato, G., Pastore, P., Bogialli, S., *Fish Shellfish Immunol.* 2018, *83*, 321-329, DOI: 10.1016/j.fsi.2018.09.036.
[68] Exterkoetter, R., Rozane, D. E., da Silva, W. C., Toci, A. T., Cordeiro, G. A., Benassi, S. F., Boroski, M., *J. Soils Sediments*. 2019, *19*, 2240-2250, DOI: 10.1007/s11368-018-2210-1.
[69] Carretta, L., Cardinali, A., Marotta, E., Zanin, G., Masin, R., *J. Chromatogr. A*. 2019, *1600*, 65-72, DOI: 10.1016/j.chroma.2019.04.047.
[70] Muskus, A. M., Krauss, M., Miltner, A., Hamer, U., Nowak, K. M., *Sci. Total Environ.* 2019, *658*, 697-707, DOI: 10.1016/j.scitotenv.2018.12.195.
[71] Thompson, T. S., van den Heever, J. P., Limanowka, R. E., *Food Addit. Contam. Part A Chem. Anal. Control Expo. Risk Assess.* 2019, *36*, 434-446, DOI: 10.1080/19440049.2019.1577993.
[72] Sun, M., Li, H., Jaisi, D. P., *Water Res.* 2019, *163*, 114840, DOI: 10.1016/j.watres.2019.07.007.
[73] Barker, A. L., Dayan, F. E., *J. Agric. Food Chem.* 2019, *67*, 2061-2065, DOI: 10.1021/acs.jafc.8b05672.

[74] Usui, K., Minami, E., Fujita, Y., Kubota, E., Kobayashi, H., Hanazawa, T., Yoshizawa, T., Kamijo, Y., Funayama, M., *J. Pharm. Biomed. Anal.* 2019, *174*, 175-181, DOI: 10.1016/j.jpba.2019.05.040.
[75] Wumbei, A., Goeteyn, L., Lopez, E., Houbraken, M., Spanoghe, P., *Food. Addit. Contam. Part B Surveill.* 2019, *12*, 231-235, DOI: 10.1080/19393210.2019.1609098.
[76] Oliveira Pereira, E. A., Freitas Melo, V., Abate, G., Masini, J. C., *Anal. Bioanal. Chem.* 2019, *411*, 2317-2326, DOI: 10.1007/s00216-019-01672-x.
[77] de F. Sousa, M. G., da Silva, A. C., dos Santos Araújo, R., Rigotto, R. M., *Environ. Monit. Assess.* 2019, *191*, 604, DOI: 10.1007/s10661-019-7764-x.
[78] Correia, N. M., Carbonari, C. A., Velini, E. D., *J. Environ. Sci. Health B*. 2020, *55*, 574-582, DOI: 10.1080/03601234.2020.1742000.
[79] Fontàs, C., Sanchez, J. M., *J. Sep. Sci.* 2020, *43*, 3931-3939, DOI: 10.1002/jssc.202000645.
[80] Zhang, Y., Dang, Y., Lin, X., An, K., Li, J., Zhang, M., *J. Chromatogr. A*. 2020, *1619*, 460939, DOI: 10.1016/j.chroma.2020.460939.
[81] Umsza-Guez, M. A., Silva-Beltrán, N. P., Machado, B. A. S., Balderrama-Carmona, A. P., *Int. J. Environ. Health Res.* 2021, *31*, 507-517, DOI: 10.1080/09603123.2019.1670335.
[82] Ferhi, S., Vieillard, J., Garau, C., Poultier, O., Demey, L., Beaulieu, R., Penalva, P., Gobert, V., Portet-Koltalo, F., *J. Environ. Chem. Eng.* 2021, *9*, 106120, DOI: 10.1016/j.jece.2021.106120.
[83] Bayebila Menanzambi, T., Dufour, P., Pirard, C., Nsangu, J., Mufusama, J. P., Mbinze Kindenge, J., Marini Djang'eing'a, R., Charlier, C., *Arch. Public Health*. 2021, *79*, 197, DOI: 10.1186/s13690-021-00717-x.
[84] Bressán, I. G., Llesuy, S. F., Rodriguez, C., Ferloni, A., Dawidowski, A. R., Figar, S. B., Giménez, M. I., *J. Chromatogr. B*. 2021, *1171*, 122616, DOI: 10.1016/j.jchromb.2021.122616.
[85] Martin-Reina, J., Dahiri, B., Carbonero-Aguilar, P., Soria-Dıaz, M. E., González, A. G., Bautista, J., Moreno, I., *Microchem. J.* 2021, *170*, 106760, DOI: 10.1016/j.microc.2021.106760.
[86] Gębura, K., Wieczorek, P. P., Poliwoda, A., *Membranes*. 2021, *12*, 20, DOI: 10.3390/membranes12010020.
[87] Surapong, N., Burakham, R., *ACS Omega*. 2021, *6*, 27007-27016, DOI: 10.1021/acsomega.1c03488.
[88] Delhomme, O., Rodrigues, A., Hernandez, A., Chimjarn, S., Bertrand, C., Bourdat-Deschamps, M., Fritsch, C., Pelosi, C., Nélieu, S., Millet, M., *J. Chromatogr. A*. 2021, *1651*, 462339, DOI: 10.1016/j.chroma.2021.462339.
[89] Wang, Y., Gao, W., Li, Y., Xiao, Y., Song, W., Yao, T., Cheng, M., Wang, W., Hou, R., *J. Agric. Food Chem.* 2021, *69*, 7969-7978, DOI: 10.1021/acs.jafc.1c01757.
[90] Cruz, J. M., Murray, J. A., *Food Chem.* 2021, *342*, 128213, DOI: 10.1016/j.foodchem.2020.128213.
[91] Wirth, M. A., Longwitz, L., Kanwischer, M., Gros, P., Leinweber, P., Werner, T., *Ecotoxicol. Environ. Saf.* 2021, *225*, 112768, DOI: 10.1016/j.ecoenv.2021.112768.
[92] Pérez-Mayán, L., Castro, G., Ramil, M., Cela, R., Rodriguez, I., *Anal. Bioanal. Chem.* 2022, *414*, 1445-1455, DOI: 10.1007/s00216-021-03775-w.
[93] Connolly, A., Jones, K., Galea, K. S., Basinas, I., Kenny, L., McGowan, P., Coggins, M., *Int. J. Hyg. Environ. Health*. 2017, *220*, 1064-1073, DOI: 10.1016/j.ijheh.2017.06.008.
[94] Connolly, A., Basinas, I., Jones, K., Galea, K. S., Kenny, L., McGowan, P., Coggins, M. A., *Int. J. Hyg. Environ. Health*. 2018, *221*, 1012-1022, DOI: 10.1016/j.ijheh.2018.06.007.
[95] Tiago, J. P. F., Sicupira, L. C., Barros, R. E., de Pinho, G. P., Silvério, F. O., *J. Environ. Sci. Health B*. 2020, *55*, 558-565, DOI: 10.1080/03601234.2020.1733369.

[96] Pimenta, E., da Silva, F., Barbosa, É., Cacique, A., Cassimiro, D., de Pinho, G., Silvério, F., *J. Braz. Chem. Soc.* 2020, *31*, 298-304, DOI: 10.21577/0103-5053.20190175.
[97] Marín, J., Campillo, N., Hernández-Córdoba, M., Garrido, I., Fenoll, J., Viñas, P., *Anal. Methods*. 2020, *12*, 2039-2045, DOI: 10.1039/d0ay00120a.
[98] Bienvenu, J. F., Bélanger, P., Gaudreau, E., Provencher, G., Fleury, N., *Anal. Bioanal. Chem.* 2021, *413*, 2225-2234, DOI: 10.1007/s00216-021-03194-x.
[99] Jaikwang, P., Junkuy, A., Sapbamrer, R., Seesen, M., Khacha-ananda, S., Mueangkhiao, P., Wunnapuk, K., *Chromatographia*. 2020, *83*, 467-475, DOI: 10.1007/s10337-019-03853-3.
[100] Guo, H., Riter, L. S., Wujcik, C. E., Armstrong, D. W., *J. Chromatogr. A*. 2016, *1443*, 93-100, DOI: 10.1016/j.chroma.2016.03.020.
[101] Jensen, P. K., Wujcik, C. E., McGuire, M. K., McGuire, M. A., *J. Environ. Sci. Health B*. 2016, *51*, 254-259, DOI: 10.1080/03601234.2015.1120619.
[102] Zoller, O., Rhyn, P., Rupp, H., Zarn, J. A., Geiser, C., *Food. Addit. Contam. Part B Surveill.* 2018, *11*, 83-91, DOI: 10.1080/19393210.2017.1419509.
[103] Riter, L. S., Wujcik, C. E., *J. AOAC Int.* 2018, *101*, 867-875, DOI: 10.5740/jaoacint.17-0317.
[104] Steinborn, A., Alder, L., Michalski, B., Zomer, P., Bendig, P., Martinez, S. A., Mol, H. G., Class, T. J., Pinheiro, N. C., *J. Agric. Food Chem.* 2016, *64*, 1414-1421, DOI: 10.1021/acs.jafc.5b05852.
[105] Boušová, K., Bruggink, C., Godula, M., Center, S., *ThermoScientific Application Note*. 2016, *661*.
[106] Adams, S., Guest, J., Dickinson, M., Fussell, R. J., Beck, J., Schoutsen, F., *J. Agric. Food Chem.* 2017, *65*, 7294-7304, DOI: 10.1021/acs.jafc.7b00476.
[107] Rajski, L., Díaz Galiano, F. J., Cutillas, V., Fernández-Alba, A. R., *J. AOAC Int.* 2018, *101*, 352-359, DOI: 10.5740/jaoacint.17-0410.
[108] Rodrigues, N. R., de Souza, A. P. F., *Food Addit. Contam. Part A Chem. Anal. Control Expo. Risk Assess.* 2018, *35*, 723-730, DOI: 10.1080/19440049.2017.1419286.
[109] Okada, E., Coggan, T., Anumol, T., Clarke, B., Allinson, G., *Anal. Bioanal. Chem.* 2019, *411*, 715-724, DOI: 10.1007/s00216-018-1490-z.
[110] Lajin, B., Goessler, W., *Talanta*. 2019, *196*, 357-361, DOI: 10.1016/j.talanta.2018.12.075.
[111] Jansons, M., Pugajeva, I., Bartkevics, V., *J. Sep. Sci.* 2019, *42*, 3077-3085, DOI: 10.1002/jssc.201900308.
[112] Santilio, A., Pompili, C., Giambenedetti, A., *J. Environ. Sci. Health B*. 2019, *54*, 205-210, DOI: 10.1080/03601234.2018.1550306.
[113] Chiesa, L. M., Nobile, M., Panseri, S., Arioli, F., *Food Addit. Contam. Part A Chem. Anal. Control Expo. Risk Assess.* 2019, *36*, 592-600, DOI: 10.1080/19440049.2019.1583380.
[114] Melton, L. M., Taylor, M. J., Flynn, E. E., *Food Chem.* 2019, *298*, 125028, DOI: 10.1016/j.foodchem.2019.125028.
[115] Pareja, L., Jesús, F., Heinzen, H., Hernando, M. D., Rajski, Ł., Fernández-Alba, A. R., *Anal. Methods*. 2019, *11*, 2123-2128, DOI: 10.1039/c9ay00543a.
[116] Geerdink, R. B., Hassing, M., Ayarza, N., Bruggink, C., Wielheesen, M., Claassen, J., Epema, O. J., *Anal. Chim. Acta*. 2020, *1133*, 66-76, DOI: 10.1016/j.aca.2020.05.058.
[117] Pires, N. L., Passos, C. J. S., Morgado, M. G. A., Mello, D. C., Infante, C. M. C., Caldas, E. D., *J. Environ. Sci. Health B*. 2020, *55*, 794-802, DOI: 10.1080/03601234.2020.1784668.
[118] Gasparini, M., Angelone, B., Ferretti, E., *J. Mass Spectrom.* 2020, *55*, e4624, DOI: 10.1002/jms.4624.
[119] Dovidauskas, S., Okada, I. A., dos Santos, F. R., *J. Chromatogr. A*. 2020, *1632*, 461603, DOI: 10.1016/j.chroma.2020.461603.
[120] Panseri, S., Nobile, M., Arioli, F., Biolatti, C., Pavlovic, R., Chiesa, L. M., *Food Chem.* 2020, *330*, 127205, DOI: 10.1016/j.foodchem.2020.127205.

[121] Ruiz, P., Dualde, P., Coscollà, C., Fernández, S. F., Carbonell, E., Yusà, V., *Sci. Total Environ.* 2021, *801*, 149688, DOI: 10.1016/j.scitotenv.2021.149688.
[122] Schütze, A., Morales-Agudelo, P., Vidal, M., Calafat, A. M., Ospina, M., *Chemosphere*. 2021, *274*, 129427, DOI: 10.1016/j.chemosphere.2020.129427.
[123] Zhang, H., Liu, X., Huo, Z., Sun, H., Zhang, F., Zhu, B., *Microchem. J.* 2021, *170*, 106614, DOI: 10.1016/j.microc.2021.106614.
[124] Feltracco, M., Barbaro, E., Morabito, E., Zangrando, R., Piazza, R., Barbante, C., Gambaro, A., *Environ. Sci. Pollut. Res. Int.* 2022, *29*, 16383-16391, DOI: 10.1007/s11356-021-16957-x.
[125] Vu, C. T., Le, P. T., Chu, D. B., Bui, V. H., Phung, T. L. A., Nguyen Le, H. Y., Labanowski, J., Mondamert, L., Herrmann, M., Behra, P., *J. Chromatogr. A*. 2021, *1649*, 462188, DOI: 10.1016/j.chroma.2021.462188.
[126] de Souza, A. P. F., Rodrigues, N. R., Reyes, F. G. R., *Food. Addit. Contam. Part B Surveill.* 2021, *14*, 40-47, DOI: 10.1080/19393210.2020.1855676.
[127] de Souza, A. P. F., Ferreira, G. S., Pagliarini, F. S., Rodrigues, N. R., *J. Consum. Prot. Food Safety*. 2021, *16*, 45-50, DOI: 10.1007/s00003-021-01320-6.

Table A2. Electrophoretic methods for glyphosate analysis published between 2016 and 2022. Continuation of Gauglitz et al. [1].

| Author | Claude 2017 | Moraes 2018 | | Gotti 2019 | Muñoz 2019 | Wimmer 2020 | Liu 2021 | Koukalová 2022 | |
|---|---|---|---|---|---|---|---|---|---|
| Reference | [2] | [3] | | [4] | [5] | [6, 7] | [8] | [9] | [9] |
| Analytes | GLP, AMPA | GLP, AMPA | GLP, AMPA | GLP, AMPA derivatized with FMOC-Cl | GLP | GLP, AMPA | GLP, AMPA, GLUF, MPPA | GLP | GLP |
| Method | Indirect CE–UV (240 nm) with phthalate probe ion<br><br>adopted from [10] | Indirect CE–UV (254 nm) with 3,5-dinitrobenz-oic acid probe ion | Indirect CE–UV (234 nm) with pyridine-2,6- dicarbo-xylic acid probe ion | Field amplified sample injection sweep-MEKC-UV (210 nm) | CE-LIF (570/488 nm) | CE-ESI-MS (TOF) with sheath liquid interface | CE-ESI-MS (TOF) with sheathless interface | ITP-$C^4D$ with asymmetric neutralization reaction boundary using electrokinetic injection dosing | ITP-$C^4D$ with on-capillary pre-concentration by asymmetric neutralization boundary and carrier ampho-lyte-free iso-electric focusing |
| Capillary* | 50 µm, 60.2/50 cm | 75 µm, 58.5/50 cm | | 50 µm, 80/71.5 cm | 75 µm, 30/71.5 cm | 50 µm, 65 cm | 50 µm, 80 cm | PTFE 800 µm x 9 cm | |
| BGE | 7.5 mM phthalic acid, 51.3 mM L-histidine, 1 mM CTAB, pH 6.5 | 10 mM 3,5-dinitrobenzoi c acid, 0.2 mM CTAB, pH 8.4 | 10 mM pyridine-2,6-dicarboxylic acid, 0.2 mM CTAB, pH 8.5 | 50 mM sodium phosphate (pH 2.2) + 100 mM sodium dodecyl sulfate | 5.2 mM tetraborate solution, pH 10.0 | 175 mM formic acid adjusted to pH 2.8 with $NH_4OH$ | 10 % HOAc in 10 % methanol | LE: 10 mM HCl + 20 mM beta-alanine, pH 3.5 TE: 10 mM benzoic acid, pH 3 | LE1 [LE2]: 20 [10] mM HCl 500 [10] mM histidine, pH 1.7 [5.5],TE: 20 mM HOAc, pH 3.9 |
| Coating | Uncoated, but CTAB as EOF modifier | | | Uncoated | Uncoated | Polyvinyl alcohol or uncoated | Uncoated | PTFE, Triton X100 as EOF modifier and for bubble suppression | |
| Injection | 30 s x 35 mbar | 6 s x 50 mbar | 8 s x 50 mbar | Water plug: 10 s x 50 mbar Sample: 700 s x −10 kV | 5 s x 35 mbar | 10 s x 75 mbar | 10 s x 690 mbar | 1500 s x 250 µA | 1500 s x 250 µA |
| Separation time, condition | 10 min, -25 kV | 6.5 min, -15 kV | 6.5 min, -17 kV | 11 min, -25 kV | 4 min, 17.2 kV | 8 min, -30 kV and 30 mbar | 12 min, -25 kV and 138 mbar | n.g., 250 µA | 40 min, 250 µA |
| Rinsing between runs | 5 min BGE | 3 min BGE | 3 min BGE | 3 x 3 min: 1 M NaOH, $H_2O$, 100 mM sodium phosphate buffer (pH 2.2) | 4 x 2 min: 1 M NaOH, 0.1 M NaOH water, BGE | 5 min BGE | Hydrochloric acid, deionized water and BGE for 3, 5 and 5 min | n.g. | n.g. |
| LOD (GLP) | n.g. | 2.9 µM | 2.9 µM | 10 nM | 25.7 mg/kg | < 5µg/L | 0.5 µg/L (m) [a)] 23.1 µg/L (i) [a)] | 35 µM | 0.9 µM |

| | | | | | | | | | |
|---|---|---|---|---|---|---|---|---|---|
| Linear range (GLP) | n.g. | | | - | 77.1 to 700 mg/kg | 5–3000 µg/L | 0.002-1 mg/L | n.g. | n.g. |
| Precision (GLY), RSD | n.g. | 0.3 % (time), 2.3 % (area) | 1.3%(time), 3.7 % (area) | 1.7 % (time) 4.3 % (area, corrected) | 4.3 % (area) | 0.7 % (time) 6.1 % (area) | 3.3 % (time) 9 % (area) | n.g. | n.g. |
| Real samples | Environmental waters | Environmental waters | Environmental waters | Extracts from wheat flour | Soil samples | Beer and soil | Baby foods | Environmental waters | Environmental waters |
| Comments | GLP and AMPA enriched by molecularly imprinted polymer solid phase extraction, elution with 0.1 M HCl. 0.2 M HCl in sample | Intense experimental method optimization (pH 4.4 – 10.4, separation voltage: -13 to -21kV, injection time: 4 to 12 s | | Aqueous extracts from wheat flour were processed by a C18 and a strong anion exchange (acetate form) solid phase extraction prior to FMOC-Cl derivatization | Aqueous extracts were mixed with CdTe/CdS quantum dots (45.9 mg/L). Design of experiment for voltage, BGE and quantum dot concentration | Sample-induced transient ITP by phosphate (50 mM) containing soil extraction media | Dispersive SPE with core-shell mesoporous silica micro-spheres coated by titanium dioxide, elution with 5% ammonia. Food extraction with 2:1 MeOH: $H_2O$, 0.5 % HOAc | Performed on a specialized ITP setup<br><br>Sample in 1 M benzoic acid + 20 mM beta-alanine, pH 7.5 | Performed on a specialized ITP setup with 3 electrodes and 3 electrolyte chambers<br><br>Sample in 20 mM histidine, pH 7.5 |

AMPA: aminomethylphosphonic acid, BGE: background electrolyte, CTAB: cetyltrimethylammonium bromide, EOF: electroosmotic flow, FMOC-Cl: fluorenylmethyloxycarbonyl chloride, GLP: glyphosate, LE: leading electrolyte, LOD: limit of detection, MPPA: 3-methylphosphinicopropionic acid, RSD: relative standard deviation, TE: terminating electrolyte

[a)](i) instrumental, (m) methodic *inner dimeter; total length / length to detector

## References Table A2


[1] Gauglitz, G., Wimmer, B., Melzer, T., Huhn, C., *Anal. Bioanal. Chem.* 2018, *410*, 725-746, DOI: 10.1007/s00216-017-0679-x.

[2] Claude, B., Berho, C., Bayoudh, S., Amalric, L., Coisy, E., Nehmé, R., Morin, P., *Environ. Sci. Pollut. Res. Int.* 2017, *24*, 12293-12300, DOI: 10.1007/s11356-017-8844-5.

[3] Moraes, M. P., Gonçalves, L. M., Pereira, E. A., *Int. J. Environ. Anal. Chem.* 2018, *98*, 258-270, DOI: 10.1080/03067319.2018.1446528.

[4] Gotti, R., Fiori, J., Bosi, S., Dinelli, G., *J. Chromatogr. A*. 2019, *1601*, 357-364, DOI: 10.1016/j.chroma.2019.05.013.

[5] Muñoz, R., Guevara-Lara, A., Santos, J. L. M., Miranda, J. M., Rodriguez, J. A., *Microchem. J.* 2019, *146*, 582-587, DOI: 10.1016/j.microc.2019.01.059.

[6] Wimmer, B., Pattky, M., Zada, L. G., Meixner, M., Haderlein, S. B., Zimmermann, H. P., Huhn, C., *Anal. Bioanal. Chem.* 2020, *412*, 4967-4983, DOI: 10.1007/s00216-020-02751-0.

[7] Wimmer, B., Neidhardt, H., Schwientek, M., Haderlein, S. B., Huhn, C., *Pest. Manag. Sci.* 2022, *78*, 2550-2559, DOI: 10.1002/ps.6883.

[8] Liu, J., Feng, W., Tian, M., Hu, L., Qu, Q., Yang, L., *J. Chromatogr. A*. 2021, *1659*, 462519, DOI: 10.1016/j.chroma.2021.462519.

[9] Koukalová, L., Glovinová, E., Ondračka, T., Pospíchal, J., *Electrophoresis*. 2022, *43*, 417-424, DOI: 10.1002/elps.202000398.

[10] Cikalo, M. G., Goodall, D. M., Matthews, W., *J. Chromatogr. A*. 1996, *745*, 189-200, DOI: 10.1016/0021-9673(96)00265-8.

Table A3. Comparison of column-coupled ITP/CE-MS setups.

| | Reinhoud | Mazereeuw | Peterson | Kler | Piešťanský | Kler | Kohl | Graf / This setup |
|---|---|---|---|---|---|---|---|---|
| References | [1-3] | [4] | [5-7] | [8] | [9-11] | [12] | [13-15] | [16] |
| Group [a)] | van der Geef | van der Geef | Lee | Huhn | Mikuš | Huhn | Neusüß | Huhn |
| Year | 1992 | 2000 | 2003 | 2013 | 2014 | 2014 | 2016 | 2022 |
| Mode | ITP/CE-MS | ITP/CEC-MS | Comprehensive ITP/CE-MS | ITP/CE-MS | ITP/CE-MS | ITP/CE-MS | Heart-cutting CE/CE-MS | ITP/CE-MS |
| Interface arrangement | CE capillary inserted into the ITP capillary via septum | T-piece from polyethylene | T-piece from quartz<br>glued | T-piece from borofloat glass<br>glued | T-piece probably from PMMA<br>screwed | Double T-piece from borofloat glass, glued | fully electrically isolated mechanical valve (20 nL) | Double T-piece from BFS<br>screwed |
| High voltage setup | 1x HVS across ITP+CE capillary<br>1x HVS to offset bifurcation point by 2 kV | 1x HVS of CE instrument<br>1x HVS to avoid electrical current across the aux. capillary during injection to CEC | 1x HVS | 1x HVS of CE instrument and relay for voltage switching | 1x HVS and relay for voltage switching | custom-made HVS with 12 ports | 2x commercial CE instruments<br>Independent operation of both dimensions | 1x HVS of CE instrument<br>Manual voltage switch |
| Analyte transfer | Injection to CE capillary by splitting proportional to the current distribution over the CE and ITP capillary.<br>ITP capillary was flushed with LE prior to CE | Blocking of ITP capillary outlet, voltage switching across ITP + aux. capillary to aux. + CEC capillary and +3 kV at end of aux. capillary.<br>ITP and aux. capillary were flushed with LE | CE started by LE injection at bifurcation point via aux. capillary from pump (manual operation) | Voltage switching across ITP+CE capillary to aux. +CE capillary | Voltage switching across ITP to ITP+CE | Voltage switching across ITP to CE | Switching of the valve to other position | Voltage switching ITP to CE |
| Intermediate detection + position | Visual | Visual (dye as marker) | UV/Vis detection in front of bifurcation point | $C^4D$ in front of bifurcation point | $C^4D$ in front of bifurcation point | $C^4D$ on common section | UV/Vis in front of valve | $C^4D$ on common section |
| Final detection | UV/Vis +<br>ESI-QqQ-MS | UV/Vis+<br>ESI-Q-MS | ESI-TOF-MS | ESI-qTOF | $C^4D$ + ESI-QqQ | ESI-qTOF | ESI-qTOF | ESI-Q-MS |

| Sample injection | Syringe | Hydrodynamic | Valve (manual) | Hydrodynamic | Syringe | Hydrodynamic | Hydrodynamic | Hydrodynamic |
|---|---|---|---|---|---|---|---|---|
| Hydrodynamic mode | Semi-closed | Semi-closed | Open | Open | Closed | Open | Open | Open |
| Capillary ITP | PTFE<br>320 µm x 15 cm | BFS<br>220 µm x 42 cm<br>+<br>220 µm x 27cm[b)] | poly(vinyl alcohol) coated<br>200 µm x (5 + 15) cm | LN coating<br>100 µm x 20 cm<br>+<br>50 µm x 40 cm[b)] | PTFE<br>800 µm x 9 cm | BFS<br>100 µm x 35 cm<br>+<br>100 µm x 35 cm | 1st dim. CE: BFS<br>50 µm x 38.2 cm<br>+<br>50 µm x 52.8 cm | BFS<br>75 µm x 65.0 cm<br>+<br>75 µm x 27.8 cm |
| Capillary CE | PTFE<br>70 cm x 45 µm | BFS<br>75 µm x 37 cm<br>16 cm with C18<br>+ 220 µm x<br>27 cm [b)] | poly(vinyl alcohol) coated<br>50 µm x 20cm | LN coating<br>50 µm x 30 cm<br>+ 50 µm x<br>40 cm[b)] | PTFE<br>300 µm x 16 cm | BFS<br>50 µm x 35 cm +<br>50 µm x 35 cm | 2nd dim. CE: BFS<br>50 µm x 55.1 cm<br>+<br>50 µm x 40.2 cm | BFS<br>75 µm x 65.0 cm<br>+<br>50 µm x 13.5 cm |
| Electrolyte system | L-S-L | L-S-L | L-S-L | L-S-L | T-S-T | BGE-S-BGE | - | L-S-L |
| LE | 10 mM sodium phosphate in 60% MeOH, pH 7.2 | 20 mM $NH_4OAc$<br>in 75 % MeOH, pH 5.0 | 10 mM triethylamine | 10 mM $NH_4OAc$<br>pH 4.5 | 10 mM $NH_4OAc$<br>+ 20 mM HOAc<br>pH 4.5 | 10 mM imida-zole + 25 mM oxalic acid in 80 % DMSO | BGE of 1st dim. CE: 10 mM phosphoric acid, pH 2.5 | 10 mM $(NH_4)_2CO_3$ +<br>115 mM $NH_4OH$<br>pH 10.2 |
| TE | 10 mM histidine in 60% MeOH<br>pH 7.2 | 20 mM beta-alanine<br>in 75 % MeOH<br>pH 5.0 | 10 mM HOAc | acetic acid<br>10 mM | 10 mM HOAc<br>pH 3.1 | 10 mM taurine + 15 mM oxalic acid in 80 % DMSO | - | 10 mM KOH +<br>135 mM $NH_4OH$ |
| BGE | As LE | As LE | As LE | As LE | As TE | 20 mM oxalic acid in 20 % 2-propanol | BGE of 2nd dim. CE: 10 % acetic acid | As LE |
| EOF modifier | None | None | Capillary coating | LN coating | None | None | None | None |
| ITP conditions | 60 µA | 15 kV + 3 mbar counterflow | 24 kV | 14 kV across ITP + CE capillary | 300 µA | 30 kV (+ and – 15 kV regarding the MS) | CE1: 20 kV | 12 kV + 70 mbar |
| ITP conditions | 60 µA | 15 kV + 3 mbar counterflow | 24 kV | 14 kV across ITP + CE capillary | 300 µA | 30 kV (+ and – 15 kV regarding the MS) | CE1: 20 kV | 12 kV + 70 mbar |
| CE conditions | 20 kV | 15 kV | 10 kV (ITP + CE dimension) | 14 kV | 40 µA | 15 kV | CE2: 20 kV | 15 kV |

| | Reinhoud | Mazereeuw | Peterson | Kler | Piešťanský | Kler | Kohl | Graf / This setup |
|---|---|---|---|---|---|---|---|---|
| CE conditions | 20 kV | 15 kV | 10 kV (ITP + CE dimension) | 14 kV | 40 µA | 15 kV | CE2: 20 kV | 15 kV |
| Electrolyte optimization | Experimental + literature data CE and ITP were optimized individually | n.g. | n.g. | Simulation + ITP-MS experiments | Experimental approach | Simulations | - | Simulation + experimental verification of CE and ITP step |
| Nature of analytes | Cationic analytes | Cationic analytes | Cationic analytes | Cationic analytes | Cationic analytes | Cationic analytes | Cationic analytes | Anionic analytes |
| Sample | Mixture of anthracyclines | Neostigmine, salbutamol, fenoterol | Angiotensin peptides | Angiotensin | Pheniramine phenylephrine paracetamol | 20 amino acids | BSA tryptic peptide sample | Glyphosate and metabolites |
| Drawbacks | Band broadening by flushing step of ITP capillary, reduced by small ID of CE capillary. | Band broadening by flushing of ITP capillary, potential clogging of capillaries due to blocking by septa. | Flushing during CE step → band broadening possible. | Removal of fast migrating electrolytes prior to CE not possible. | Multi material setup → different EOFs, distortions of zones possible.<br>Band broadening by hydrodynamic analyte transfer to MS. | Potential clogging of capillaries due to blocking. | Valve materials not stable to perform many experiments at high separation voltage/currents → max. 15 µA.<br>Valve is prone to leakages. Band broadening due the valve's dead volumes. | Separation dimensions hydrodynamic open, manual switching |
| Comments | CE capillary is inserted far into the ITP capillary through a septum at the cathode compartment<br>→ voltage drop across the CE-MS capillary always present. | During the ITP focusing, the<br>CEC capillary outlet is disconnected from the ground. | Stacked sample is flushed back and forth over the bifurcation point, no membranes or blocking of capillaries needed. | Modified commercial system with additional vial holder. | Electrode compartments with hydrodynamic-ally closed (membranes).<br>Manual flushing of electrolyte chambers and capillaries or | Home-made multivial holder.<br>Manual blocking and deblocking of capillaries was necessary.<br>None-aqueous setup to allow the stacking of 20 amnio acids in the ITP step. | Complete spatial separation of the dimensions enabling almost unlimited selection of separation modes, BGE systems, capillary treatments. | Hydroxide ions as terminator. High degree of automation. Only voltage switching was a manual step. |

| | | | | |
|---|---|---|---|---|
| | 3 valves were used to 1) disconnect TE buffer from the ITP capillary prior to flush, 2) and 3) for replacing TE with LE in the ITP capillary.<br>The ITP capillary is closed by a membrane at the cathode compartment to prevent hydrodynamic flow.<br>MeOH addition to the BGE to prevent adsorption of the analytes.<br>Electrolyte chambers made of PMMA | | automatized by syringes<br>→ difficult change of electrolyte system.<br>For CE coupling a polysulphone elution block was necessary + syringe pump → band broadening by hydrodynamic flow. | To increase the switching precision in 2D experiments the migration velocity of the specific analyte was calculated from single-point intermediate detection data. |
| Further analytes analyzed with the same instrumentation | | | pheniramine [17]<br>varenicline [18]<br>serotonin [19]<br>(all separated as cations) | |

Abbreviations: aux.: auxiliary; BFS: bare fused silica; CEC: capillary electrochromatography; dim.: dimension; ESI: electro spray ionization; HVS: high voltage supply; LE: leading electrolyte, n.g.: not given; PMMA: poly(methyl methacrylate); PTFE: polytetrafluoroethylene; TE: terminating electrolyte.

[a)] Grouped as in Table A4

[b)] The same capillary was used in both dimensions

## References Table A3


[1] Reinhoud, N. J., Tinke, A. P., Tjaden, U. R., Niessen, W. M. A., van der Greef, J., *J. Chromatogr. A*. 1992, *627*, 263-271, DOI: 10.1016/0021-9673(92)87206-n.

[2] Tinke, A. P., Reinhoud, N. J., Niessen, W. M. A., Tjaden, U. R., van der Greef, J., *Rapid Commun. Mass Spectrom.* 1992, *6*, 560-563, DOI: 10.1002/rcm.1290060905.

[3] Stegehuis, D. S., Tjaden, U. R., van der Greef, J., *J. Chromatogr. A*. 1992, *591*, 341-349, DOI: 10.1016/0021-9673(92)80251-o.

[4] Mazereeuw, M., Spikmans, V., Tjaden, U. R., van der Greef, J., *J. Chromatogr. A*. 2000, *879*, 219-233, DOI: 10.1016/s0021-9673(00)00259-4.

[5] Peterson, Z. D., Bowerbank, C. R., Collins, D. C., Graves, S. W., Lee, M. L., *J. Chromatogr. A*. 2003, *992*, 169-179, DOI: 10.1016/s0021-9673(03)00235-8.

[6] Bowerbank, C. R., Lee, M. L., *J. Microcolumn. Sep.* 2001, *13*, 361-370, DOI: 10.1002/mcs.10019.

[7] Chen, S., Lee, M. L., *Anal. Chem.* 2000, *72*, 816-820, DOI: 10.1021/ac990727+.

[8] Kler, P. A., Posch, T. N., Pattky, M., Tiggelaar, R. M., Huhn, C., *J. Chromatogr. A*. 2013, *1297*, 204-212, DOI: 10.1016/j.chroma.2013.04.046.

[9] Piešťanský, J., Maráková, K., Kovaľ, M., Mikuš, P., *J. Chromatogr. A*. 2014, *1358*, 285-292, DOI: 10.1016/j.chroma.2014.06.083.

[10] Tomáš, R., Kovaľ, M., Foret, F., *J. Chromatogr. A*. 2010, *1217*, 4144-4149, DOI: 10.1016/j.chroma.2010.02.021.

[11] Everaerts, F. M., Beckers, J. L., Verheggen, T. P. E. M., Isotachophoresis: theory, instrumentation and applications. Elsevier, Amsterdam 1976.

[12] Kler, P. A., Huhn, C., *Anal. Bioanal. Chem.* 2014, *406*, 7163-7174, DOI: 10.1007/s00216-014-8152-6.

[13] Kohl, F. J., Montealegre, C., Neusüß, C., *Electrophoresis*. 2016, *37*, 954-958, DOI: 10.1002/elps.201500579.

[14] Römer, J., Kiessig, S., Moritz, B., Neusüß, C., *Electrophoresis*. 2021, *42*, 374-380, DOI: 10.1002/elps.202000180.

[15] Hühner, J., Jooß, K., Neusüß, C., *Electrophoresis*. 2017, *38*, 914-921, DOI: 10.1002/elps.201600457.

[16] Graf, H. G., Rudisch, B. M., Ude, L., Müller, L., Huhn, C., *J. Sep. Sci.* 2022, *45*, 3887-3899, DOI: 10.1002/jssc.202200519.

[17] Piešťanský, J., Maráková, K., Kovaľ, M., Havránek, E., Mikuš, P., *Electrophoresis*. 2015, *36*, 3069-3079, DOI: 10.1002/elps.201500351.

[18] Piešťanský, J., Maráková, K., Veizerová, L., Galba, J., Mikuš, P., *Anal. Chim. Acta*. 2014, *826*, 84-93, DOI: 10.1016/j.aca.2014.04.003.

[19] Piešťanský, J., Matuskova, M., Cizmarova, I., Majerova, P., Kovac, A., Mikuš, P., *J. Chromatogr. A*. 2021, *1648*, 462190, DOI: 10.1016/j.chroma.2021.462190.

Table A4. Overview on column-coupled ITP/CE applications sorted by electrolyte format and year of publication. For applications with final mass spectrometric detection, see Table A3. Since only a limited number of authors contributed to the topic, a grouping was made according to the (co-)authors often mentioned. (BGE-S-BGE format)

| Author | Year | Ref | Group[1)] | Instrument | FD[2)] | ID[2)] | Mode | Format | Switching | Analytes |
|---|---|---|---|---|---|---|---|---|---|---|
| Troška | 2013 | [1] | k/m | K+G [2, 3] | CD | CD | BGE-S-BGE | PMMA chip | current switching, replacement of TE by BGE (procedure not given) | nitrite and nitrate |
| Horčičiak | 2012 | [4] | k/m | K+G [2, 3] | CD | CD | BGE-S-BGE | PMMA chip | current switching, replacement of TE by BGE (procedure not given) | glyphosate |
| Ginterová | 2012 | [5] | k | EA 202 A | UV | CD | BGE-S-BGE | two PTFE cap. | current switching + washing ITP cap. with BGE | histamine, 2-phenyl-ethylamine, tyramine |
| Marák | 2012 | [6] | k | EA 202A | UV | CD | BGE-S-BGE | two PTFE cap. | current switching, replacement of TE by BGE (procedure not given) | bromate |
| Pantůčková | 2010 | [7] | b | EA 100 | UV | CD | BGE-S-BGE | two PTFE cap. | current switching + washing ITP cap. with BGE, optical control of switching time | 5-methyltetra-hydrofolate |
| Horáková | 2007 | [8] | k | EA 102 | UV | CD | BGE-S-BGE | two PTFE cap. | current switching | benzoic acid |
| Hamoudová | 2004 | [9] | p | EA 100 | UV | CD | BGE-S-BGE | two PTFE cap. | current switching + washing ITP cap. with BGE | flavonoids and phenolic acids |
| Kvasnička | 2003 | [10] | v | EA 100 | UV | CD | BGE-S-BGE | two PTFE cap. | current switching + washing ITP cap. with BGE | imazalil |
| Urbánek | 2002 | [11] | p | EA 100 | UV | CD | BGE-S-BGE | two PTFE cap. | current switching + washing ITP cap. with BGE | flavonoids |

cap.: capillaries; PMMA: poly(methyl methacrylate); PTFE: polytetrafluoroethylene

1) Abbreviations of (co-)authors used to group the CE/ITP-methods: k/m: Kaniansky + Masár; k: Kaniansky; g: van der Greef; m: Mikuš + Havránek; l: Lee + Chen b: Křivánková + Boček + Foret; p: Polášek; h: Hirokawa; v: Kvasnička + Voldřich

2) FD: final detection method; ID: intermediate detection method; CD: conductivity detection; CS Isot.: CS isotachophoretic analyzer, n.g. not given. K+G: Kaniansky + Graß 2001 (references [2, 3]); EA100. EA101, EA102, EA103 EA 202A are different versions of the same column-coupled CE/CE device from Villa-Labeco (Slowakei, Spišská Nová Ves) derived form the setup described by Everaerts et al. [12].

Continuation of Table A4. (L-S-L format)

| Author | Year | Ref | Group[1)] | Instrument | FD[2)] | ID[2)] | Mode | Format | Switching | Analytes |
|---|---|---|---|---|---|---|---|---|---|---|
| Xu | 2010 | [13] | h | Hirokawa 2008 | linear imaging UV detector | | L-S-L | chip | current switching electrokinetic injection of LE | DNA |
| Hirokawa | 2008 | [14] | h | MCE-2010 | | | L-S-L | chip | current switching electrokinetic injection of LE | DNA fragments |
| Bowerbank | 2001 | [15] | l | see [16] | UV | UV | L-S-L | two BFS capillaries | current switching + back pressure multi-injection | angiotensins |
| Chen | 2000 | [16] | l | home-built | UV | | L-S-L | 2 x BFS cap. + T-piece, syringe pump | current switching + back pressure multi-injection | angiotensin |
| Mazereeuw | 1994 | [17] | g | Prince CE | UV | visual | L-S-L | 3 x BFS capillary different inner diameters | current switching + back pressure | angiotensin |
| Stegehuis | 1992 | [18] | g | Isotachophor; Bromma | LIF | UV | L-S-L | PTFE + BFS cap. | hydrodynamic or electro-kinetic, washing TE with LE away | *o*-phthaldialdehyde and fluorescein isothiocyanate derivatives of amino acids. |
| Stegehuis | 1991 | [19] | g | Isotachophor; Bromma | UV/LIF | UV | L-S-L | PTFE + BFS cap. | electrokinetic injection, washing TE away | derivatives of amino acids |
| Foret | 1990 | [20] | b | home-built | UV | visual | L-S-L | Chip+1 cap. | washing TE away | nucleotides and amaranth (dye) |

Continuation of Table A4. (mainly T-S-T format)

| Author | Year | Ref | Group[1)] | Instrument | FD[2)] | ID[2)] | Mode | Format | Switching | Analytes |
|---|---|---|---|---|---|---|---|---|---|---|
| Mikuš | 2013 | [21] | m | EA 103 (modified) | UV | DI1:CD DI2:CD or UV | T-S-T | three PTFE cap. | current switching | phthalic acid |
| Pantůčková | 2007 | [22] | b | EA 100 | CD (UV) | CD | L-S-L or T-S-T | PTFE+BFS cap. | current switching | iodine |
| Kvasnička | 2003 | [23] | v | EA 100 | UV | CD | T-S-T | two PTFE cap. | current switching | lysozyme |
| Kvasnička | 2000 | [24] | v | EA 100 | UV | CD | T-S-T or BGE-S-BGE | two PTFE cap. | current switching | fumaric acid |
| Fanali | 2000 | [25] | k | EA 101 | UV | CD | T-S-T or BGE-S-BGE | two PTFE cap. | current switching | 2,4-dinitrophenyl-labeled amino acids |
| Kaniansky + Graß 2001 | 2000 | [2, 3] | k/m | new setup | CD | CD | T-S-T | PMMA chip | current switching | nitrite, fluoride, and phosphate |
| Procházková | 1999 | [26] | b | EA 100 | UV | CD | T-S-T | PTFE + BFS cap. | current switching | orotic acid |
| Danková | 1999 | [27] | k | Labeco-Villa | UV | CD | T-S-T | two PTFE cap. | current switching | tryptophan |
| Procházková | 1998 | [28] | b | EA 100 | UV | CD | T-S-T | two PTFE cap. | current switching | L-ascorbic acid |
| Blatný | 1997 | [29] | v | EA 101 | UV | CD | T-S-T | two PTFE cap. | current switching | Fe(III)-EDTA |
| Křivánková | 1997 | [30] | b | EA 100 | UV | CD | T-S-T | two PTFE cap. | current switching | hippurate |
| Kaniansky | 1996 | [31] | k | CS Isot. | UV | CD | T-S-T | two PTFE cap. | current switching | nitrophenols |
| Kaniansky | 1994 | [32] | k | EA 100 | UV | CD | T-S-T | PTFE + BFS cap. | current switching | paraquat and diquat |
| Kaniansky | 1994 | [33] | k | CS Isot. | CD | CD | T-S-T | two PTFE cap. | current switching | inorganic anions |
| Kaniansky | 1993 | [34] | k | prototype of EA100 | UV | UV | T-S-T | cap. fluorinated ethylene-propylene | current switching | sulphanilate, 3,5-dinitrosalicylate |
| Křivánková | 1991 | [35] | b | CS Isot. (modified) | CD/UV | CE | T-S-T | two PTFE cap. | current switching | halofuginone |
| Kaniansky | 1990 | [36] | k | CS Isot. (modified) | UV | CD | T-S-T | two PTFE cap. | current switching | nitrophenols and 2,4-dinitrophenyl-labelled amino acids |

Continuation of Table A4. (T-S-T format)

| Author | Year | Ref | Group[1)] | Instrument | FD[2)] | ID[2)] | Mode | Format | Switching | Analytes |
|---|---|---|---|---|---|---|---|---|---|---|
| Piešťanský | 2017 | [37] | m | EA 102 | UV | CD | T-S-T[a)] + HEC, chiral selector, propan-2-ol | two PTFE cap. | current switching | varenicline |
| Piešťanský | 2017 | [38] | m | EA 102 | UV | CD | | two PTFE cap. | current switching | serotonin |
| Frano | 2016 | [39] | see [27] | EA 101 | UV | CD | T-S-T[a)] + HEC, chiral selector | two PTFE cap. | current switching | DNA fragment |
| Mikuš | 2013 | [40] | m | EA 102 | LIF | CD | T-S-T[a)] | two BFS cap. | current switching | quinine |
| Mikuš | 2012 | [41] | m | EA 102 | UV | CD | T-S-T[a)] | two BFS cap. | current switching | quinine |
| Mikuš | 2011 | [42] | m | EA 102 | UV | CD | T-S-T[a)] | two BFS cap. | current switching | quinine |
| Kvasnička | 2011 | [43] | v | EA 101 | CD | CD | T-S-T[a)] | two PTFE cap. | current switching | phytic acid and lower inositolphosphates |
| Knob | 2010 | [44] | k | EA 202A | UV | CD | T-S-T[b)] | two PTFE cap. | current switching | brominated phenols |
| Mikuš | 2008 | [45, 46] | m | EA 101 | UV | CD | T-S-T[a)] | two BFS cap. | current switching | amlodipine, celiprolol |
| Kvasnička | 2006 | [47] | v | EA 101 | UV | CD | T-S-T[a)] | two PTFE cap. | current switching | domoic acid |
| Kvasnička | 2005 | [48] | v | EA 101 | CD | CD | T-S-T[a)] | two PTFE cap. | current switching | chlorate, chlorite, bromate |
| Masár | 2005 | [49] | k/m | K+G [2, 3] | CD | CD | T-S- T[c)] | PMMA chip | current switching | sulfite |
| Flottmann | 2004 | [50] | | ItaChrom II-M | UV | CD | T-S-T[a)] | two PTFE cap. | current switching | sorbate and ascorbate |
| Praus | 2004 | [51] | | CS Isot. | CD | CD | T-S-T[a)] | two PTFE cap. | current switching | chlorite |
| Bodor | 2002 | [52] | k/m | K+G [2, 3] | CD | CD | T-S-T[a)] | PMMA chip | current switching | bromate |
| Bodor | 2001 | [53] | k/m | K+G [2, 3] | CD | CD | T-S-T[a)] | PMMA chip | current switching | nitrite, fluoride, phosphate |
| Bodor | 2001 | [54] | k/m | K+G [2, 3] | CD | CD | T-S-T[a)] | PMMA chip | current switching | benzoate, sorbate |
| Danková | 2001 | [55] | k | EA 101 | UV | CD | T-S-T[b)] | n.g. | current switching | orotic acid |
| Kvasnička | 1996 | [56] | v | CS ZKI 02 | UV | CD | T-S- T[c)] | two PTFE cap. | current switching | EDTA |
| Hirokawa | 1993 | [57] | | lab-made | UV | UV+ poten-tial | T-S-T, BGE-S-BGE | PTFE + BFS cap. | common section with 2 valves | different benzoic acids derivatives, picric acid, and others |
| Foret | 1992 | [58] | b | see [20] | UV | CD | T-S-T[a)] | PTFE+BFS cap. | current switching | cytochrome |

[a)] T-S-T but different concentration of compounds in TE used in the CE dimension
[b)] T-S-T but different counter ion in TE used in the CE dimension
[c)] T-S-T but different counter ion and different coion concentration in TE used in the CE dimension

## References Table A4


[1] Troška, P., Chudoba, R., Danč, L., Bodor, R., Horčičiak, M., Tesařová, E., Masár, M., *J. Chromatogr. B*. 2013, *930*, 41-47, DOI: 10.1016/j.jchromb.2013.04.042.

[2] Graß, B., Neyer, A., Jöhnck, M., Siepe, D., Eisenbeiß, F., Weber, G., Hergenröder, R., *Sens. Actuators B Chem.* 2001, *72*, 249-258, DOI: 10.1016/s0925-4005(00)00643-2.

[3] Kaniansky, D., Masár, M., Bielčiková, J., Iványi, F., Eisenbeiss, F., Stanislawski, B., Grass, B., Neyer, A., Jöhnck, M., *Anal Chem*. 2000, *72*, 3596-3604, DOI: 10.1021/ac991236s.

[4] Horčičiak, M., Masár, M., Bodor, R., Danč, L., Bel, P., *J. Sep. Sci.* 2012, *35*, 674-680, DOI: 10.1002/jssc.201100942.

[5] Ginterová, P., Marák, J., Staňová, A., Maier, V., Ševčík, J., Kaniansky, D., *J. Chromatogr. B*. 2012, *904*, 135-139, DOI: 10.1016/j.jchromb.2012.07.018.

[6] Marák, J., Staňová, A., Vaváková, V., Hrenáková, M., Kaniansky, D., *J. Chromatogr. A*. 2012, *1267*, 252-258, DOI: 10.1016/j.chroma.2012.07.075.

[7] Pantůčková, P., Křivánková, L., *Electrophoresis*. 2010, *31*, 3391-3399, DOI: 10.1002/elps.201000193.

[8] Horáková, J., Petr, J., Maier, V., Znaleziona, J., Staňová, A., Marák, J., Kaniansky, D., Ševčík, J., *J. Chromatogr. A*. 2007, *1155*, 193-198, DOI: 10.1016/j.chroma.2007.01.075.

[9] Hamoudová, R., Urbánek, M., Pospíšilová, M., Polášek, M., *J. Chromatogr. A*. 2004, *1032*, 281-287, DOI: 10.1016/j.chroma.2004.01.014.

[10] Kvasnička, F., Dobiáš, J., Klaudisová-Chudáčková, K., *Cent. Eur. J. Chem.* 2003, *1*, 91-97, DOI: 10.2478/bf02479260.

[11] Urbánek, M., Blechtová, L., Pospíšilová, M., Polášek, M., *J. Chromatogr. A*. 2002, *958*, 261-271, DOI: 10.1016/s0021-9673(02)00316-3.

[12] Everaerts, F. M., Beckers, J. L., Verheggen, T. P. E. M., Isotachophoresis: theory, instrumentation and applications. Elsevier, Amsterdam 1976.

[13] Xu, Z., Murata, K., Arai, A., Hirokawa, T., *Biomicrofluidics*. 2010, *4*, 14108, DOI: 10.1063/1.3366719.

[14] Hirokawa, T., Takayama, Y., Arai, A., Xu, Z., *Electrophoresis*. 2008, *29*, 1829-1835, DOI: 10.1002/elps.200700590.

[15] Bowerbank, C. R., Lee, M. L., *J. Microcolumn. Sep.* 2001, *13*, 361-370, DOI: 10.1002/mcs.10019.

[16] Chen, S., Lee, M. L., *Anal. Chem.* 2000, *72*, 816-820, DOI: 10.1021/ac990727+.

[17] Mazereeuw, M., Tjaden, U. R., van der Greef, J., *J. Chromatogr. A*. 1994, *677*, 151-157, DOI: 10.1016/0021-9673(94)80554-7.

[18] Stegehuis, D. S., Tjaden, U. R., van der Greef, J., *J. Chromatogr. A*. 1992, *591*, 341-349, DOI: 10.1016/0021-9673(92)80251-o.

[19] Stegehuis, D. S., Irthu, H., Tjaden, U. R., van der Greef, J., *J. Chromatogr. A*. 1991, *538*, 393-402, DOI: 10.1016/s0021-9673(01)88860-9.

[20] Foret, F., Sustacek, V., Boček, P., *J. Microcolumn Sep.* 1990, *2*, 229-233, DOI: 10.1002/mcs.1220020505.

[21] Mikuš, P., Kovaľ, M., Maráková, K., Piešťanský, J., Havránek, E., *Talanta*. 2013, *103*, 294-300, DOI: 10.1016/j.talanta.2012.10.047.

[22] Pantůčková, P., Urbánek, M., Křivánková, L., *Electrophoresis*. 2007, *28*, 3777-3785, DOI: 10.1002/elps.200700189.

[23] Kvasnička, F., *Electrophoresis*. 2003, *24*, 860-864, DOI: 10.1002/elps.200390108.

[24] Kvasnička, F., Voldřich, M., *J. Chromatogr. A*. 2000, *891*, 175-181, DOI: 10.1016/s0021-9673(00)00513-6.

[25] Fanali, S., Desiderio, C., Ölvecká, E., Kaniansky, D., Vojtek, M., Ferancová, A., *J. High. Resolut. Chromatogr.* 2000, *23*, 531-538, DOI: 10.1002/1521-4168(20000901)23:9<531::Aid-jhrc531>3.0.Co;2-z.

[26] Procházková, A., Křivánková, L., Boček, P., *J. Chromatogr. A*. 1999, *838*, 213-221, DOI: 10.1016/s0021-9673(99)00114-4.

[27] Danková, M., Kaniansky, D., Fanali, S., Iványi, F., *J. Chromatogr. A*. 1999, *838*, 31-43, DOI: 10.1016/s0021-9673(98)00974-1.

[28] Procházková, A., Křivánková, L., Boček, P., *Electrophoresis*. 1998, *19*, 300-304, DOI: 10.1002/elps.1150190226.

[29] Blatný, P., Kvasnička, F., Kenndler, E., *J. Chromatogr. A*. 1997, *757*, 297-302, DOI: 10.1016/s0021-9673(96)00668-1.

[30] Křivánková, L., Vraná, A., Gebauer, P., Boček, P., *J. Chromatogr. A*. 1997, *772*, 283-295, DOI: 10.1016/s0021-9673(97)00126-x.
[31] Kaniansky, D., Masár, M., Marák, J., Madajová, V., Onuska, F. I., *J. Radioanal. Nucl. Chem.* 1996, *208*, 331-350, DOI: 10.1007/bf02039770.
[32] Kaniansky, D., Iványi, F., Onuska, F. I., *Anal. Chem.* 1994, *66*, 1817-1824, DOI: 10.1021/ac00083a007.
[33] Kaniansky, D., Zelenský, I., Hybenová, A., Onuska, F. I., *Anal. Chem.* 1994, *66*, 4258-4264, DOI: 10.1021/ac00095a022.
[34] Kaniansky, D., Marák, J., Madajová, V., Šimuničová, E., *J. Chromatogr. A*. 1993, *638*, 137-146, DOI: 10.1016/0021-9673(93)83422-o.
[35] Křivánková, L., Foret, F., Boček, P., *J. Chromatogr. A*. 1991, *545*, 307-313, DOI: 10.1016/s0021-9673(01)88721-5.
[36] Kaniansky, D., Marák, J., *J. Chromatogr. A*. 1990, *498*, 191-204, DOI: 10.1016/s0021-9673(01)84247-3.
[37] Piešťanský, J., Maráková, K., Galba, J., Kováč, A., Mikuš, P., *J. Sep. Sci.* 2017, *40*, 2292-2303, DOI: 10.1002/jssc.201700098.
[38] Piešťanský, J., Maráková, K., Mikuš, P., *Molecules*. 2017, *22*, 1668, DOI: 10.3390/molecules22101668.
[39] Frano, M., Dzuganova, K., Kois, P., Masar, M., *Electrophoresis*. 2016, *37*, 3084-3088, DOI: 10.1002/elps.201600336.
[40] Mikuš, P., Veizerová, L., Piešťanský, J., Maráková, K., Havránek, E., *Electrophoresis*. 2013, *34*, 1223-1231, DOI: 10.1002/elps.201200556.
[41] Mikuš, P., Maráková, K., Veizerová, L., Piešťanský, J., Galba, J., Havránek, E., *J. Chromatogr. Sci.* 2012, *50*, 849-854, DOI: 10.1093/chromsci/bms083.
[42] Mikuš, P., Maráková, K., Veizerová, L., Piešťanský, J., *J. Sep. Sci.* 2011, *34*, 3392-3398, DOI: 10.1002/jssc.201100633.
[43] Kvasnička, F., Čopíková, J., Ševčík, R., Václavíková, E., Synytsya, A., Vaculová, K., Voldřich, M., *Electrophoresis*. 2011, *32*, 1090-1093, DOI: 10.1002/elps.201000578.
[44] Knob, R., Marák, J., Staňová, A., Maier, V., Kaniansky, D., Ševčík, J., *J. Chromatogr. A*. 2010, *1217*, 3446-3451, DOI: 10.1016/j.chroma.2010.03.006.
[45] Mikuš, P., Maráková, K., Marák, J., Nemec, I., Valasková, I., Havránek, E., *J. Chromatogr. B*. 2008, *875*, 266-272, DOI: 10.1016/j.jchromb.2008.06.024.
[46] Mikuš, P., Maráková, K., Marák, J., Planková, A., Valasková, I., Havránek, E., *Electrophoresis*. 2008, *29*, 4561-4567, DOI: 10.1002/elps.200800079.
[47] Kvasnička, F., Ševčík, R., Voldřich, M., *J. Chromatogr. A*. 2006, *1113*, 255-258, DOI: 10.1016/j.chroma.2006.02.072.
[48] Kvasnička, F., Janda, V., Rousová, D., Manda, J., Kollerová, L., *Cent. Eur. J. Chem.* 2005, *3*, 137-145, DOI: 10.2478/bf02476244.
[49] Masár, M., Danková, M., Ölvecká, E., Stachurová, A., Kaniansky, D., Stanislawski, B., *J. Chromatogr. A*. 2005, *1084*, 101-107, DOI: 10.1016/j.chroma.2004.08.134.
[50] Flottmann, D., Hins, J., Meissner, T., Dietrich, C., Rettenmaier, C., *Chromatographia*. 2004, S253–S256, DOI: 10.1365/s10337-004-0241-9.
[51] Praus, P., *Talanta*. 2004, *62*, 977-982, DOI: 10.1016/j.talanta.2003.10.021.
[52] Bodor, R., Kaniansky, D., Masár, M., Silleová, K., Stanislawski, B., *Electrophoresis*. 2002, *23*, 3630-3637, DOI: 10.1002/1522-2683(200210)23:20<3630::Aid-elps3630>3.0.Co;2-8.
[53] Bodor, R., Madajová, V., Kaniansky, D., Masár, M., Jöhnck, M., Stanislawski, B., *J. Chromatogr. A*. 2001, *916*, 155-165, DOI: 10.1016/s0021-9673(00)01080-3.
[54] Bodor, R., Žúborová, M., Ölvecká, E., Madajová, V., Masár, M., Kaniansky, D., Stanislawski, B., *J. Sep. Sci.* 2001, *24*, 802-809, DOI: 10.1002/1615-9314(20010901)24:9<802::Aid-jssc802>3.0.Co;2-1.
[55] Danková, M., Strašík, S., Molnárová, M., Kaniansky, D., Marák, J., *J. Chromatogr. A*. 2001, *916*, 143-153, DOI: 10.1016/s0021-9673(00)01079-7.
[56] Kvasnička, F., Míková, K., *J. Food Compos. Anal.* 1996, *9*, 231-242, DOI: 10.1006/jfca.1996.0029.
[57] Hirokawa, T., Ohmori, A., Kiso, Y., *J. Chromatogr. A*. 1993, *634*, 101-106, DOI: 10.1016/0021-9673(93)80316-z.
[58] Foret, F., Szoko, E., Karger, B. L., *J. Chromatogr. A*. 1992, *608*, 3-12, DOI: 10.1016/0021-9673(92)87100-m.

# Appendix II

This appendix contains additional information that has not been peer reviewed.

Part A presents alternative detection electronics for the intermediate in-chip $C^4D$ based of the electronics of the Open$C^4D$.

Part B provides additional information on the development of the first-dimension ITP electrolyte system using a CE-$C^4D$ setup.

Part A: Open$C^4D$ electronics as an alternative to the in-chip $C^4D$ based on CDCD.

Part B: ITP-$C^4D$ measurements of glyphosate and its metabolites

# Part A: OpenC$^4$D electronics as an alternative to the in-chip C$^4$D based on CDCD

In addition to the CDCD-based electronics for the in-chip C$^4$D, a modified version of the OpenC$^4$D electronics was designed based on the information provided by Francisco and do Lago [1]. The layout of the detection head, shown in Figure 1, was changed to fit on a single printed circuit board while keeping its circuit. The electrodes made from vias in the original layout were replacement by spring contact pins (811-S1-006-10-016101, Preci-Dip, Delémont, Switzerland) to connect the C$^4$D geometry in the microfluidic chip with the electronics. The supply unit was identical to the one described in Section S4.2 of the Supporting Information of reference [2]

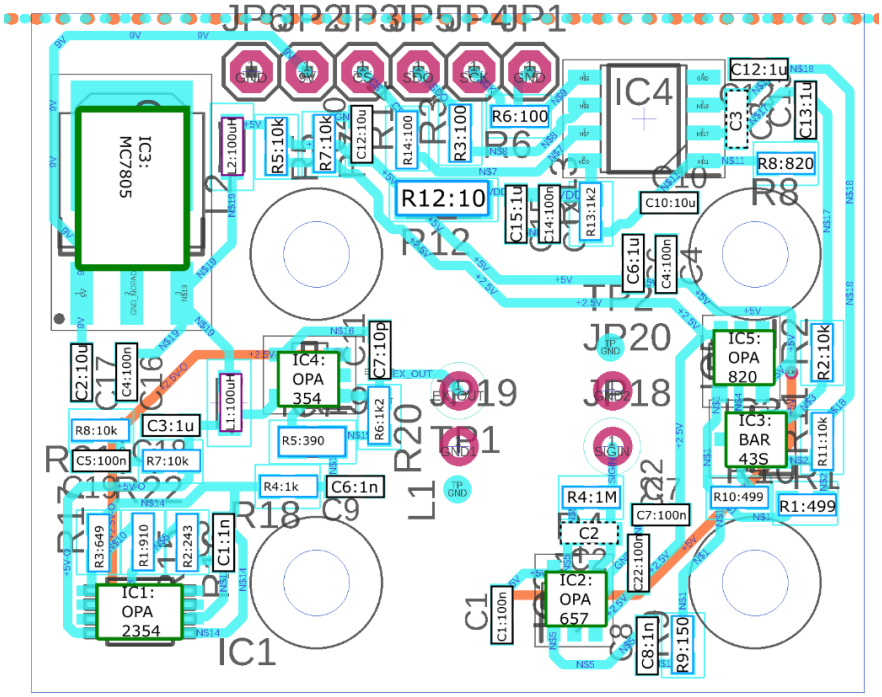


Figure 1 Scheme of the redesigned openC$^4$D printed circuit board. The electrical circuit is identical to the published electrical circuit from do Lago.

### Annotations to the sealings at the chip-capillary connection

To overcome leaching effects (described in [2]) from the sealings used at the capillary-chip connections, the nitrile butadiene rubber sealing should be replaced by a sealing material, which can better withstand alkaline conditions, like ethylene propylene diene monomer rubber.

## References


[1] Francisco, K. J., do Lago, C. L., *Electrophoresis*. 2009, *30*, 3458-3464, DOI: 10.1002/elps.200900080.

[2] Graf, H. G., Rudisch, B. M., Ude, L., Müller, L., Huhn, C., *J. Sep. Sci.* 2022, *45*, 3887-3899, DOI: 10.1002/jssc.202200519.

## Part B: ITP-$C^4D$ measurements of glyphosate and its metabolites

### Samples, BGEs and electrophoretic separation by ITP

The aqueous leading electrolyte (LE) and terminating electrolyte (TE) were prepared from filtered aqueous stock solutions just before the measurement. The LE consisted of 10 mM FA and 92 mM $NH_4OH$. The TE consisted of 5 mM proline, 92 mM $NH_4OH$ and 5 mM $Ba(OH)_2$. The samples were prepared from aqueous 10 mM stock solutions in 92 mM $NH_4OH$. The separation was performed in a bare fused silica capillary with 75 µm id and 50 cm length. The effective length was 33.3 cm. Prior to its first use, the capillary was purged with MeOH, 1 M aqueous HCl, 1 M aqueous NaOH and water for 20 min each at 1 bar. Just before a set of measurement the capillary was rinsed at 1 bar with water for 5 min and LE for 30 min. Prior to each analysis, the capillary was flushed with LE for 3 min at 1 bar. The sample was injected for 30 s at 75 mbar followed by an injection of TE for 18 s at 50 mbar. A voltage of -20.0 kV (slope -6 kV/s) and a pressure of 50 mbar was applied for 15 min to achieve ITP separation. Since the forming ITP becomes stationary under the selected conditions, the ITP stack must be slowly moved towards the $C^4D$. For this purpose, the voltage was lowered to -15.0 kV and the pressure was increased to 85 mbar. The temperature was set to 25°C. The chemicals used and their abbreviations are as given in [1]. Proline (PRO) (≥99 %) from Fluka (Buchs, Switzerland) and barium hydroxide octahydrate (≥98 %) from Sigma-Aldrich (Steinheim, Germany) were used.

### Simulations using Spresso

Simulations of ITP separations were performed with the software Spresso 3 [2] using the following parameters: current: -10 µA; simulation time: 600 s; domain length: 800 mm; circular channel geometry with 75 µm id; injection width: 10 mm; injection location: 30 mm; number of grid points: 12,000; spatial discretization: ‘SLIP’; moving frame: yes; prepare grid: no; adaptive grid speed: 0; clustering level: 0; ionic strength dependence: no; pressure head: 0; hydraulic resistance coefficient: 32. The Taylor-Aris dispersion coefficient was set to 0.

**ITP-$C^4D$ measurements**

The simulated ITP separation plotted in Figure 2A shows the concentration of the analytes versus the position in the capillary. It seemed possible to separate phosphate, originating from glyphosate degradation or from extraction media, from all other target analytes except from *N*-acetyl glyphosate. The separation from the ITP stack was achieved by optimizing the pH as well as the composition of the leading (LE) and terminating electrolyte (TE) to provide phosphate and *N*-acetyl glyphosate with a higher mobility than the leading ion formate. Therefore, both migrate zone electrophoretically in front of the ITP stack. Proline served as the terminating ion. The isotachopherograms of different selections of analytes recorded by $C^4D$, displayed in Figure 3, well corroborated with the simulation. In all experiments the migration orders were as predicted by the simulation, but the separation of phosphate was not successful as an additional ITP step was observed which is only present when phosphate was added to the analyte mixture, Figure 3B. This leads to the assumption that the electrophoretic mobility of formic acid taken from literature was higher than that of phosphate at the chosen pH. This is possibly also the reason why an ITP step was observed when the sample contained *N*-acetyl glyphosate, compare GLPA Mix in Figure 3A. The method was also successfully applied to river water spiked with glyphosate, AMPA and sarcosine, see isotachopherogram "$ITP_{exp}$ (spiked river water)" depicted in Figure 3B. Differences in migration time between Figure 3A and B may result from the fact that different batches of capillaries were used and a different number of measurements were performed prior to the experiments shown which can influence the EOF. Blank runs revealed isotachopherograms with three ITP steps at -0.3 V, -1.1 V and -1,5 V. The widest step (-0.3 V) was possibly caused by a contamination of the solutions by atmospheric $CO_2$, although $Ba(OH)_2$ was added to the TE to precipitate carbonate as $BaCO_3$ [3]. The other two steps $I^1$ and $I^2$ were wider in case of new electrolyte vials which led to the conclusion that leaching from glass vials under alkaline conditions caused these impurities.

As can be deduced from the experimental isotachopherograms, carbonate seemed to be a more suitable leading ion. The step assigned to carbonate at the chosen conditions was lower than the step assigned to phosphate and higher than the one of glyphosate. Only *N*-acetyl glyphosate and the rarely reported HMPA degradation product of glyphosate were not included in the ITP stack. Using carbonate as the leading ion, the dissolution of atmospheric $CO_2$ is also less problematic.

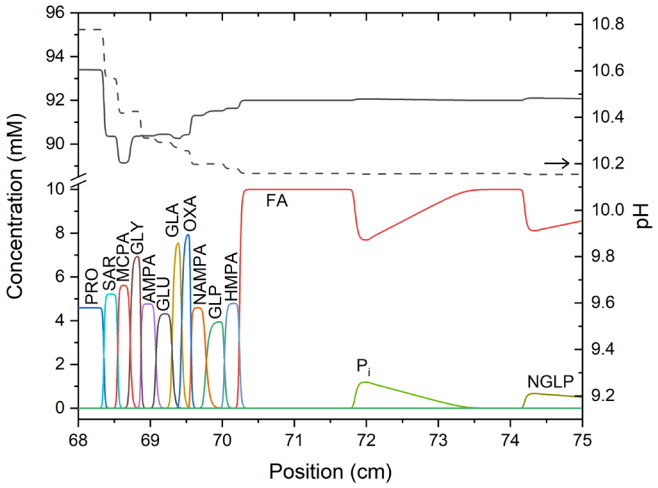


Figure 2. Concentration profile of an ITP simulated with Spresso based on data published in [1] of SAR, MCPA, GLY, AMPA, GLU, GLA, OXA, NAMPA, GLP, HMPA, $P_i$, and NGLP ($c$ = 1 mM). Injection position: 3 cm, injection length: 1 cm, current: -10 µA, simulation time 600 s, domain length: 80 cm, capillary geometry: circular, 75 µm id. LE: 10 mM FA and 92 mM $NH_3$, TE: 5 mM Pro and 92 mM $NH_3$. The abbreviations are as given in [1] or as given in Table 1 of the thesis.

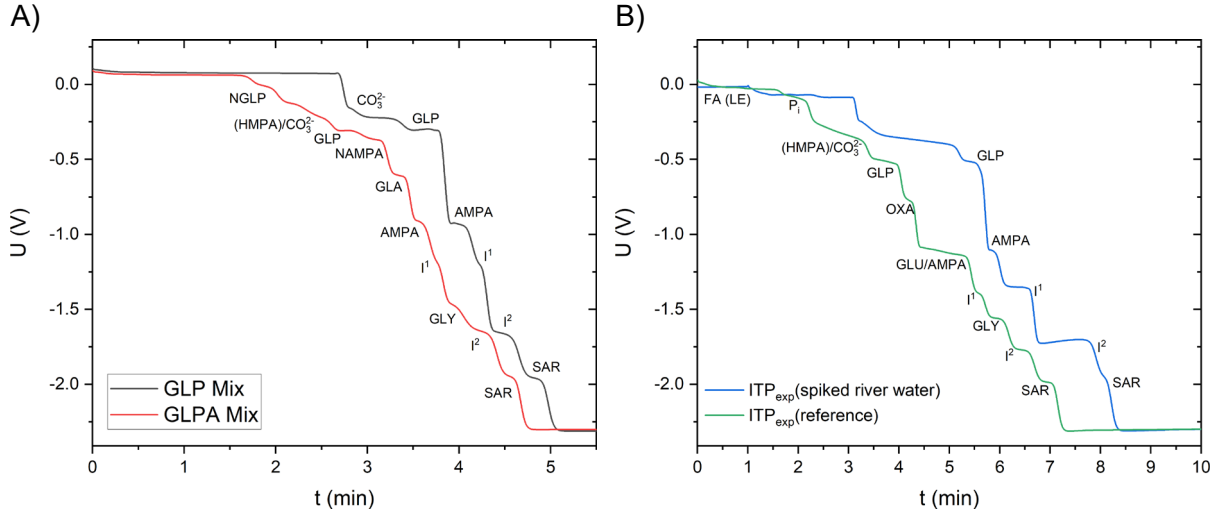


Figure 3. A) Isotachopherogram of the mixture “GLP Mix” (GLP, AMPA and SAR each 1 mM) and the mixture “GLPA Mix” (GLP, AMPA, SAR, NGLP, HMPA, NAMPA, GLA, GLY each 1 mM) respectively dissolved in 92 mM $NH_3$. B) Isotachopherogram of a refence mix (2 mM $H_3PO_4$ ($P_i$) and HMPA, GLP, OXA, GLU, AMPA, GLY, SAR each 1 mM) in 92 mM $NH_3$ and of a spiked filtered river water sample diluted to 62 % river water, 70.7 mM $NH_3$ and AMPA, GLY, SAR each 0.77 mM. Sample injection: 75 mbar x 30 s, TE plug injection after sample injection: 50 mbar x 18 s, separation: 15 min and 50 mbar at -20 kV, afterwards 85 mbar and -15 kV. Capillary: bare fused silica $l$ = 50 cm, $id$ = 75 µm. Detection: $C^4D$ at 800 kHz, 60 % amplitude, head stage gain on, $l_{eff}$ = 33.3 cm. LE: 10 mM FA and 92 mM $NH_3$, TE: 5 mM Pro and 92 mM $NH_3$ and 5 mM $Ba(OH)_2$. Leaching from glass vials under alkaline conditions caused the impurities $I^1$ and $I^2$. The abbreviations are as given in [1] or as given in Table 1 of the thesis.

## References


[1] Graf, H. G., Biebl, S. M., Müller, L., Breitenstein, C., Huhn, C., *J. Sep. Sci.* 2022, *45*, 1128-1139, DOI: 10.1002/jssc.202100952.

[2] Bercovici, M., Lele, S. K., Santiago, J. G., *J. Chromatogr. A*. 2009, *1216*, 1008-1018, DOI: 10.1016/j.chroma.2008.12.022.

[3] Mala, Z., Gebauer, P., Bocek, P., *Electrophoresis*. 2011, *32*, 1500-1507, DOI: 10.1002/elps.201100098.

# Appendix III

Paper 1:

Graf, H. G., Rudisch, B. M., Manegold, J., Huhn, C., Advancements in capacitance-to-digital converter-based $C^4D$ technology for detection in capillary electrophoresis using amplified excitation voltages and comparison to classical and open-source $C^4Ds$. *Electrophoresis* 2021, *42*, 1306-1316, DOI: 10.1002/elps.202000394

+ Supporting Information and Manual for CDCDs

Paper 2:

Graf, H. G., Biebl, S. M., Müller, L., Breitenstein, C., Huhn, C., Capillary electrophoresis applied for the determination of acidity constants and limiting electrophoretic mobilities of ionizable herbicides including glyphosate and its metabolites and for their simultaneous separation. *Journal of Separation Science* 2022; *45*, 1128-1139, DOI: 10.1002/jssc.202100952

+ Supporting Information

Paper 3:

Graf, H. G., Rudisch, B. M., Ude, L., Müller, L., Huhn, C., Picomolar detection limits for glyphosate by two-dimensional column-coupled isotachophoresis/capillary electrophoresis mass spectrometry. *Journal of Separation Science* 2022; *45*, 3887-3899, DOI: 10.1002/jssc.202200519

+ Supporting Information

# Appendix III

**Paper 1:**

Graf, H. G., Rudisch, B. M., Manegold, J., Huhn, C., Advancements in capacitance-to-digital converter-based $C^4D$ technology for detection in capillary electrophoresis using amplified excitation voltages and comparison to classical and open-source $C^4Ds$. *Electrophoresis* 2021, *42*, 1306-1316, DOI: 10.1002/elps.202000394

**Hannes Georg Graf**
**Benjamin Maximilian Rudisch**
**Johanna Manegold**
**Carolin Huhn**

Institute of Physical and Theoretical Chemistry, Eberhard Karls Universität Tübingen, Tübingen, Germany

Received December 30, 2020
Revised February 28, 2021
Accepted March 8, 2021

Research Article

# Advancements in capacitance-to-digital converter-based C$^4$D technology for detection in capillary electrophoresis using amplified excitation voltages and comparison to classical and open-source C$^4$Ds

This work introduces new hardware configurations for a capacitively coupled contactless conductivity detector (C$^4$D) based on capacitance-to-digital conversion (CDC) technology for CE. The aim was to improve sensitivity, handling, price, and portability of CDC-based C$^4$D detectors (CDCD) to reach LODs similar to classic C$^4$Ds with more sophisticated electric circuits. To achieve this, a systematic study on the CDCDs was carried out including a direct comparison to already established C$^4$D setups. Instrumental setups differing in electrode lengths, measurement modes, and amplification of excitation voltages were investigated to achieve LODs for alkali metal ions of 4 to 12 μM, similar to LODs obtained by classic C$^4$D setups. Lowest LODs were achieved for a setup with two 10 mm electrodes at a distance of 0.2 mm and an excitation voltage of 24 V. The detection head was exceptionally lightweight with only 2.6 g and covered only 20 mm of the capillary on total. This allowed the use of multiple detectors along the separation path to enable spatial tracking of analytes during separation. The entirely battery-powered detector assembly weighs less than 200 g, and the data are transmitted wirelessly for possible portable applications. The freely accessible hardware and software were optimized for fully automated measurements with real time data plotting and allowed handling multidetector setups. The new developments were applied to quantify the potassium salt of glyphosate in its herbicide formulation.

**Keywords:**
Automated measurements / Capacitance-to-digital conversion / Capacitively coupled contactless conductivity detection / Glyphosate formulation analysis / Multidetector setup
DOI 10.1002/elps.202000394

Additional supporting information may be found online in the Supporting Information section at the end of the article.

## 1 Introduction

The miniaturization of the analytical separation techniques increases separation efficiency and speed of the separation. It helps to decrease running costs, to enhance portability as well as to reduce sample, solvent, and reagent consumption and finally the amount of waste generated during the separation process [1]. On the one hand, this led to the development of microchip separation systems [2–4] and Lab-on-a-Chip technologies [5] and on the other hand to portable separation systems [6]. The latter not only requires miniaturization of the separation path, but also of the entire setup including liquid handling, driving force (pressure, voltage) and detection head. One promising separation technique for miniaturization is CE, since the instrumentation is simple and its applicability for portable systems has already been shown [7–9]. Common detection systems for CE are UV absorbance [10], MS [11], laser or LED-induced fluorescence [12,13], electrochemical detection [14], or capacitively coupled

**Correspondence**: Professor Carolin Huhn, Institute of Physical and Theoretical Chemistry, Eberhard Karls Universität Tübingen, Auf der Morgenstelle 18, Tübingen, Germany.
**E-mail**: carolin.huhn@uni-tuebingen.de

**Abbreviations:** **CDC**, capacitance-to-digital conversion; **CDCD**, CDC-based detector; **dd$H_2O$**, doubly distilled water; **GPTMS**, 3-(glycidoxypropyl)trimethoxysilane; **IC**, integrated circuit; **PCB**, printed circuit board

**Color online**: See article online to view Fig. 1 in color.

contactless conductivity detection ($C^4D$) [15]. In principle, the most universal detection system for CE is $C^4D$ due to the separation of charged analytes. $C^4D$ technology is used to measure the change of the complex conductivity (admittance) between electrodes in the presence of an external excitation signal [16,17]. Different detectors were presented: an axial geometry of $C^4D$ electrodes for CE was reported independently by da Silva and do Lago [18] as well as by Zemann et al. [19]. The electrodes were either made of silver paint or consisted of parts of hypodermic needles, the latter enabling to freely position the detection head along the capillary. In both cases, the removal of the protective outer coating of the capillary was not necessary. In addition to home-built $C^4Ds$, both commercial $C^4D$ and an open-source project, called Open$C^4D$, were introduced [15,20]. Descriptions of the working principle, development, and the universal applicability of $C^4Ds$ can be found in [15] and references therein.

Capacitance-to-digital conversion (CDC) technology is similar to $C^4D$, because both technologies use a similar working principle [16,17,21]. This leads to the fact, that the output value of the CDC is not only affected by changes in capacitance, but it is also influenced by the capacitance and resistance to ground as well as by parallel and serial resistances to the capacitor to be measured [21]. The impact to the output value by the serial resistance can be exploited by using the CDC-technology for a $C^4D$. It can be seen from alternating current theory that CDC-technology does not distinguish between a change in output value resulting from a change in capacitance or a change in conductivity when the phase shift between the excitation and the pick-up voltage is not considered.

CDC-technology as a detection unit has been used in various applications. Takeuchi et al. used a CDC with an integrated circuit (IC) on an evaluation board, together with two 2 mm long electrodes on a 1.45 mm polyimide coated glass tube as replacement for a conventional galvanic bipolar pulse conductance detector for suppressed ion chromatography [22]. Kiplagat et al. used the same evaluation board in a portable ion chromatographic system [23]. The detection head used, was equipped with 10 mm electrodes made from hypodermic needles. For metal cations separated by ion chromatography in a 75 μm id fused silica capillary, the LOD was in the range of 1–2 μM. Drevinskas et al. used a similar setup for conductivity detection in CE. They utilized a CDC-IC together with an Arduino-based microcontroller. The influence of electrode length, measurement mode (single-ended versus differential), as well as different power supplies were investigated for best LOQ, ranging from 250 to 500 nM for alkali metal ions, and baseline stability [24,25]. This detector was also applied in a portable CE system [26], a CE system integrated into a drone [27] and in a setup for multichannel separations [28]. A microcontroller with a similar CDC-IC was equipped with planar electrodes with an interdigital finger design for the detection of the size and speed of microdroplets [29]. Another application for microdroplets is described by Isgor et al., they analyzed the content of microdroplets using coplanar electrodes [30].

In this work, we introduce for the first time a CDC-based $C^4D$ detector (CDC-IC: AD7745) in combination with an operational amplifier (LT1360) for enhanced excitation voltages up to 24 V and therefore lower LODs. We also provide a more systematic and extensive study of instrumental configurations compared to previous studies of the CDC-based $C^4D$ detectors (CDCD). The parameters considered are electrode length and the use of a differential versus single-ended measurement mode. To assess the performance, a direct comparison between the new CDCD configurations presented here, the Open$C^4D$ and a commercial $C^4D$ is provided. Further important advancements of the developed CDCD setup here were ease of handling, the possibility of battery supply and wireless data transmission, as well as compact design, maximum flexibility with regard to positioning the detector head along the capillary, and a high degree of automation with real time data plotting. As model application, the analysis of glyphosate and potassium in a herbicide formulation is presented.

## 2 Materials and methods

### 2.1 Chemicals

L-Histidine (His) (USP grade) and glyphosate (>99.7%) were purchased from Fluka (Buchs, Switzerland). 2-(*N*-morpholino)ethane sulfonic acid monohydrate (MES) (>99.5%), potassium dihydrogen phosphate ($KH_2PO_4$) (≥98.0%), and sodium hydroxide (≥98.0%) were purchased from Sigma-Aldrich (Steinheim, Germany), lithium chloride monohydrate (LiCl) (≥99%) and tris(hydroxymethyl)aminomethane (Tris) (99.8–100.1%) were delivered by Merck (Darmstadt, Germany). Hydrochloric acid and (3-glycidoxypropyl)trimethoxysilan (GPTMS) (97%) were purchased from Thermo Fisher Scientific (Schwerte, Germany), and methanol for LC-MS (99.95%) was bought from Th. Geyer (Renningen, Germany). Roundup Powerflex was purchased from Bayer (Leverkusen, Germany). Further, doubly distilled water (dd$H_2O$) from a purification system from ELGA LabWater (Celle, Germany) was used.

### 2.2 Instrumentation

CE-analyses were performed using a Prince 560 capillary electrophoresis system from Prince Technologies (Emmen, The Netherlands) with WPrince 7.1.02.10.01 software. For conductivity detection, different self-developed CDCDs were used as well as an Open$C^4D$ ($OC^4D$), see [20]. Further, a commercial $C^4D$ (eDAQ), an ET120 $C^4D$ Headstage for CE and an ER225 Contactless Conductivity $C^4D$ System, all from eDAQ (Denistone East, Australia), were used for comparison and as a secondary detector. The eDAQ was used with the included PowerChrom 2.8.3 software with $C^4D$-Profiler for the determination of optimal settings. The CDC-IC AD7745 was from Analog Devices (Norwood, MA). A replica of an

 

Arduino Nano, a NRF24L01+ radio module and battery charger TP4056 were purchased from Makershop (Armsheim, Germany). The operational amplifier LT1360 and the voltage regulator LT1761-5 were ordered from Linear Technologies (Milpitas, CA). The voltage regulator LP2992IM5-5.0 was from Texas Instruments (Dallas, TX). The lithium polymer batteries, two EREMIT 3.7 V 4.000 mAh High Cap., equipped with an integrated protective circuitry and alligator claps, were purchased from Eremit (Eschborn, Germany). The printed circuit boards (PCB) were developed with the software Eagle from Autodesk (Mill Valley, CA) or KiCad and manufactured by Multi Circuit Boards (Brunnthal, Germany). Small electronic parts were purchased from Mouser (Mansfield, TX) or Reichelt (Sande, Germany). During the development for automated measurements, a 7100 Agilent CE System (Waldbronn, Germany) was used. Origin 2020 from OriginLab (Northampton, MA) was used for peak evaluation and data smoothing with a five-point window adjacent averaging function. Further calculations were performed with Excel 2019 from Microsoft (Redmond, WA).

### 2.3 Sample preparation and electrophoretic separation

#### 2.3.1 Detector evaluation

The BGE was an aqueous 20 mM MES/His buffer (pH 6.1). Model analyte stock solutions of 60 mM were made for $KH_2PO_4$, Tris, and LiCl (dried at 120°C overnight for dehydration). A mixture with a concentration of 3000 μM for each of the three substances was made and diluted prior to injection. All solutions were stored at –18°C. The separation was performed in a bare fused silica capillary from Polymicro Technologies (Phoenix, AZ) with 50 μm id and 50 cm length. Prior to the first use, the capillary was purged with MeOH, 1 M HCl, 1 M NaOH, and $ddH_2O$ for 20 min each at 1.5 bar. Prior to each analysis, the capillary was sequentially flushed at 1 bar with 0.1 M NaOH for 2 min, $ddH_2O$ for 1 min, and BGE for 3 min. The sample was injected for 5 s at 50 mbar. The separation voltage was set to 14.0 kV (slope 6 kV/s). The resulting current was 2.6 μA. The CDCD or the $OC^4D$ were mounted at an effective length ($L_{eff}$) of 31.5 mm. The eDAQ was mounted at $L_{eff}$ = 33.5 mm and was configured for an excitation frequency of 200 kHz at an amplitude of 100% and an activated head stage gain. For differential measurements with the CDCD, a reference capillary (50 μm id) filled with BGE was used.

#### 2.3.2 Model application

The CE-separation of a sample of Roundup PowerFlex, a glyphosate potassium salt containing herbicide formulation, was carried out in the same 20 mM MES/His buffer. The sample was diluted 1:20 000 with $ddH_2O$ and stored at –18°C. The separation was performed in a bare silica fused capillary with a length of 65 cm and an id of 50 μm. The position of the CDCD was at $L_{eff}$ = 45.5 cm.

For the determination of $K^+$, the capillary was purged at 1.5 bar prior to the first usage with MeOH, 1 M HCl, 1 M NaOH, and $ddH_2O$ for 20 min each. Prior to each run, the capillary was flushed at 1 bar for 2.5 min with 0.1 M NaOH, for 1.5 min with $ddH_2O$, and for 5 min with BGE. The separation voltage was set to 20 kV.

For the determination of glyphosate, the capillary was preconditioned prior to the first run with 1 M NaOH for 20 min at 1.5 bar and filled with a 3 mM glyphosate solution and immersed for approximately 60 h at room temperature to achieve a surface coating with glyphosate as the binding to bare fused silica is very strong and more or less irreversible at pH 6.1. No leaching was observed, which is demonstrated by the high migration time precision of <1.5% RSD ($n$ = 15) [31]. After immersion, the capillary was immediately used for CE separation. Between runs, flushing with BGE for 5 min at 0.75 bar was sufficient. The sample was injected at 50 mbar for 5 s, followed by injecting a plug of BGE for 5 s × 50 mbar. During separation –20 kV and 50 mbar were applied. The glass vials containing samples with glyphosate were coated with GPTMS to prevent its adsorption to the surface using a procedure adopted from Shao et al. [32]: 10 min ultrasonication in 1 M NaOH, 1 M HCl, $ddH_2O$. After each step, the vials were rinsed with $ddH_2O$. The cleaned vials were then immersed in a mixture of 2 mL GPTMS and 18 mL $ddH_2O$ and ultrasonicated for 10 min. After another 30 min, the mixture was removed and the vials left empty. The whole procedure was repeated on the following day.

### 2.4 Capacitance detection system design

A scheme of the entire CDCD assembly is shown in Fig. 1A with its components. On the CE side, two detection devices were mounted. Each consisted of the detection head on the capillary and a modular supply unit. The data were transmitted wirelessly to the master device which was connected to a computer. The wireless connection was established automatically after an initial learning step. A home-written Python 3 program with graphical user interface was used for data acquisition allowing automated and manual measurements with up to five detectors simultaneously. The data were plotted in real time. For automated measurements, the trigger from the CE could be connected either to one of the detection devices or to the master device. The trigger was designed to work with different instruments (a 7100 Agilent CE System requiring an additional module [see Supporting information] and a Prince 560 capillary electrophoresis system).

The detection device consisted of two parts: the detection head and the supply unit. A schematic diagram of the main part of the circuit of the detection head is depicted in Fig. 1B and was adapted from the circuitry published by Drevinskas et al. [25]: only the main component, the CDC-IC AD7745, and its voltage supply, LT1761-5 (see Supporting information), were identical to the published circuitry. The excitation

 

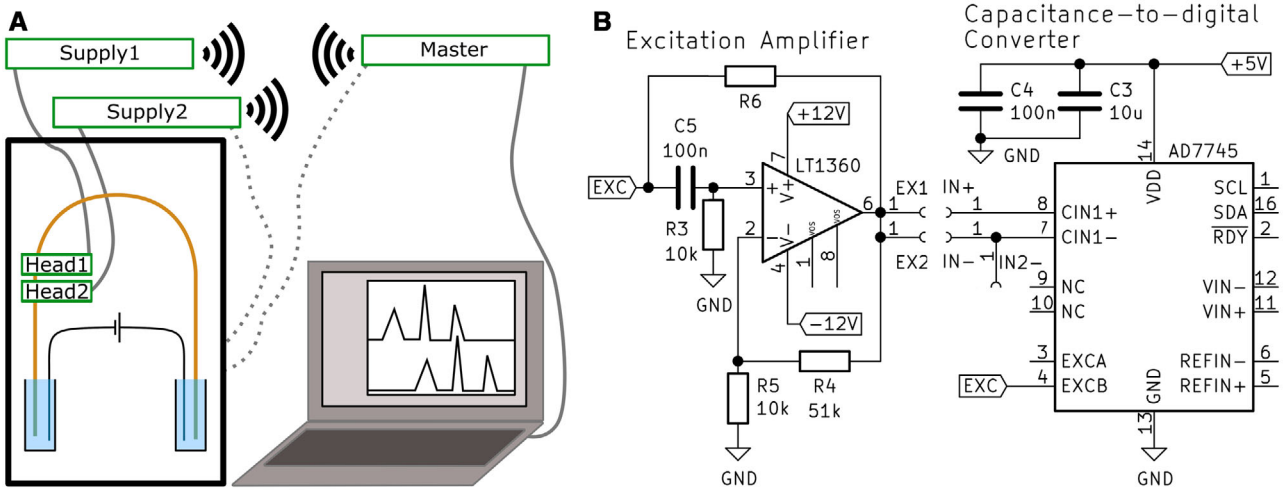


**Figure 1.** (A) Schematic diagram of the CDCD assembly. On the CE side, two detection devices were mounted. Each consisted of the detection head (Head1, Head2) mounted on the capillary and a modular supply unit (Supply1, Supply2). The data were transmitted wirelessly from the detection device to the master device (Master) connected via USB to a computer. Additionally, the trigger from the CE can be connected either to one of the detection devices or to the master device (dotted lines). (B) Schematic diagram of the main circuit parts of the detection head. Resistors without values are jumpers. For more details, see Supporting information.

voltage (EXCB) of the CDC-IC was set to a 5 V amplitude and a 32 kHz square wave signal. For some setups tested in this study, an operational amplifier (LT1360) was added to allow a higher excitation voltage. The 6.1-fold amplification was determined by the resistors R4 and R5 but was limited to 4.8 by the supply voltage of +12 V and –12 V. Without the amplifier mounted, the CDC output was connected directly to the excitation electrodes by bridging R6. The electrodes had common $C^4D$ electrode geometry and were made from hypodermic needles (0.6 mm od, 0.4 mm id, 0.2 mm gap) [19,33,34]. Compared to Drevinskas et al., the electrodes were mounted perpendicular to the PCB to allow stacking several detectors along the separation path. Further, the detection head could be exchanged easily in order to test different configurations. In case of differential measurements, a second electrode pair was mounted. The grounded shielding of the detection head was made from adhesive copper foil. To prevent short circuits, the PCB was covered by transparent adhesive tape and the electrodes were covered by heat shrink tubing. The CDC capacitive input channel was programed for a conversion time of 109.6 ms. Digital data were acquired at a rate of 9.1 Hz by an Arduino Nano microcontroller board. The Arduino Nano was part of the supply unit, which was connected to the detection head via a ribbon cable.

The supply unit consisted of a custom-made PCB, an Arduino Nano, and an NRF24L01+ radio module. The custom-made PCB supplied voltages, enabled the configuration of the detector identification and the use of wireless data transmission through switches, and had a terminal block for trigger signals from the CE system together with connections to all other modules. More detailed information about the detection head and the supply unit can be found in the Supporting information. The latest software and hardware are published on GitHub: https://github.com/AGHuhn/CDC_C4D

## 3 Results and discussion

### 3.1 Optimization of CDCDs

To investigate the capabilities of CDCDs, a CE-separation of equimolar mixtures of $KH_2PO_4$, LiCl, and Tris was defined as the reference system [25]. The concentrations ranged between 3 and 1500 μM. As BGE, a 20 mM MES/His electrolyte (pH 6.1) was chosen since it proved advantageous for the CE-$C^4D$ [15,35–38]. Over our entire investigation high migration time precision (<1.6% RSD [$n = 3$], 0.8% on average) was achieved.

To characterize the CDCDs, the LODs and the sensitivity (based on the slope of the calibration curve using the peak area) were determined. A further parameter was the plate number to estimate the size of the detection window. All figures of merit are summarized in Table 1 and partially displayed in Fig. 2. To estimate LOD and LOQ via a *S/N* of 3 and 10, the *S/N* for every concentration was calculated based on the signal height of analyte peaks and the peak-to-peak noise. Linear regression between the two points nearest to the associated *S/N* was made and the concentration corresponding to the *S/N* was determined. The slope of the calibration curve of the peak area was determined for the range 250 μM (approx. LOQ of $Li^+$ for most detectors) to 1500 μM. The plate number $N$ was calculated from the full width at half maximum $FWHM$ and the migration time $t_M$ (peak maximum) using $N = 8 \times \ln(2) \times (t_M/FWHM)^2$.

Drevinskas et al. showed that a shielding around the entire detector resulted in a low noise. They also demonstrated that the electrode length has a crucial impact on the *S/N*: longer electrodes reveal higher *S/N* [24,25]. For this reason and for the sake of simplicity, we started with two 20 mm long electrodes with shielding from the surroundings and used the

 

**Table 1.** Overview over all figures of merit for the CDCDs, the $OC^4D$, and the eDAQ

| Detector Configuration | | 2×05 -S (shielded) | 2×10 | 2×15 | 2×20 | 4×10 -S, differential | 4×20 | 2×10 -SA (shielded plus amplified) | 2×15 | 2×20 | 4×10 -SA, differential | 4×20 | $OC^4D$ | eDAQ |
|---|---|---|---|---|---|---|---|---|---|---|---|---|---|---|
| E/P (mm) | | 5/5 | 10/10 | 15/15 | 20/20 | 10/10 | 20/20 | 10/10 | 15/15 | 20/20 | 10/10 | 20/20 | | |
| LOD (μM) | $Li^+$ | 1013 | 93.3 | 197.2 | 291.5 | 62.9 | 59.8 | 3.9 | 8.3 | 8.8 | 8.7 | 6.6 | 7.6 | 3.7 |
| | $TrisH^+$ | - | 156.4 | 376.4 | 655.8 | 92.4 | 152.5 | 12.2 | 16.4 | 22.3 | 20.7 | 15.4 | 12.3 | 8.3 |
| LOQ (μM) | $K^+$ | - | 206 | 597 | 1181 | 132 | 172 | 9.9 | 10.4 | 24.1 | 18.1 | 14.0 | 14.7 | 8.9 |
| | $Li^+$ | - | 406 | 1188 | - | 300 | 359 | 17.8 | 23.1 | 42.4 | 32.9 | 27.3 | 27.0 | 14.5 |
| | $TrisH^+$ | - | 709 | - | - | 497 | 637 | 37 | 50 | 75 | 66 | 53 | 46.9 | 28.5 |
| $Li^+$ 125 μM | Height (a.u.) | - | 0.267 | 0.270 | 0.257 | 0.263 | 0.252 | 1.288 | 1.338 | 1.160 | 1.141 | 1.141 | | |
| | S/N | - | 3.8 | 2.1 | 1.4 | 5.0 | 4.6 | 61.3 | 46.1 | 27.6 | 32.6 | 40.8 | 33.76 | 66.4 |
| | $N$ ($10^3$) | - | 20.8 ± 3.1 | 17.9 ± 3.4 | 30.5 ± 10.8 | 22.3 ± 2.2 | 23.8 ± 6.8 | 23.5 ± 0.8 | 21.8 ± 0.9 | 23.1 ± 1.4 | 22.7 ± 0.5 | 24.3 ± 0.1 | 56.4 ±5.2 | 71.1 ±2.0 |
| $Li^+$ 500 μM | Height (a.u.) | 0.583 | 0.811 | 0.796 | 0.712 | 0.732 | 0.730 | 3.263 | 3.558 | 3.418 | 3.325 | 3.405 | | |
| | *S/N* | 2.0 | 11.6 | 6.1 | 3.8 | 13.8 | 13.3 | 155.4 | 122.7 | 81.4 | 95.0 | 121.6 | 81.49 | 168.0 |
| | $N$ ($10^3$) | 20.5 ± 6.9 | 12.6 ± 0.8 | 12.2 ± 0.3 | 14.7 ± 1.1 | 13.0 ± 0.4 | 13.2 ± 0.4 | 14.8 ± 0.4 | 13.5 ± 0.7 | 13.9 ± 0.6 | 14.4 ± 0.3 | 14.3 ± 0.3 | 19.5 ±0.3 | 28.7 ±0.8 |
| Noise (a.u.) | | 0.286 | 0.070 | 0.131 | 0.186 | 0.053 | 0.055 | 0.021 | 0.029 | 0.042 | 0.035 | 0.028 | | |
| Slope* (a.u. ± %) | | - | 4.52 ± 1.7 | 4.06 ± 3.6 | 4.16 ± 7.0 | 4.79 ± 5.4 | 3.88 ± 3.0 | 17.56 ± 2.7 | 24.64 ± 7.6 | 21.54 ± 2.8 | 16.22 ±5.5 | 19.39 ± 3.2 | | |

*Slope of peak area for $Li^+$

The CDCD setups are compared regarding: shielding configuration; measurement modes of the CDC (single-ended (2 electrodes, 2×) and differential mode (4 electrodes, 4×; reference electrodes: connected to negative input of CDC; inserted capillary filled with BGE)); length of excitation (E); and pick-up (P) electrodes. LOD and LOQ of $K^+$, $Li^+$, and $TrisH^+$, if the upper calibration range limit is not exceeded (1500 μM); peak heights, *S/N*, and plate number (*N*) for a peak caused by a 125 and 500 μM $Li^+$ sample; peak-to-peak noise; slope of the calibration curve of the peak area (250–1500 μM).

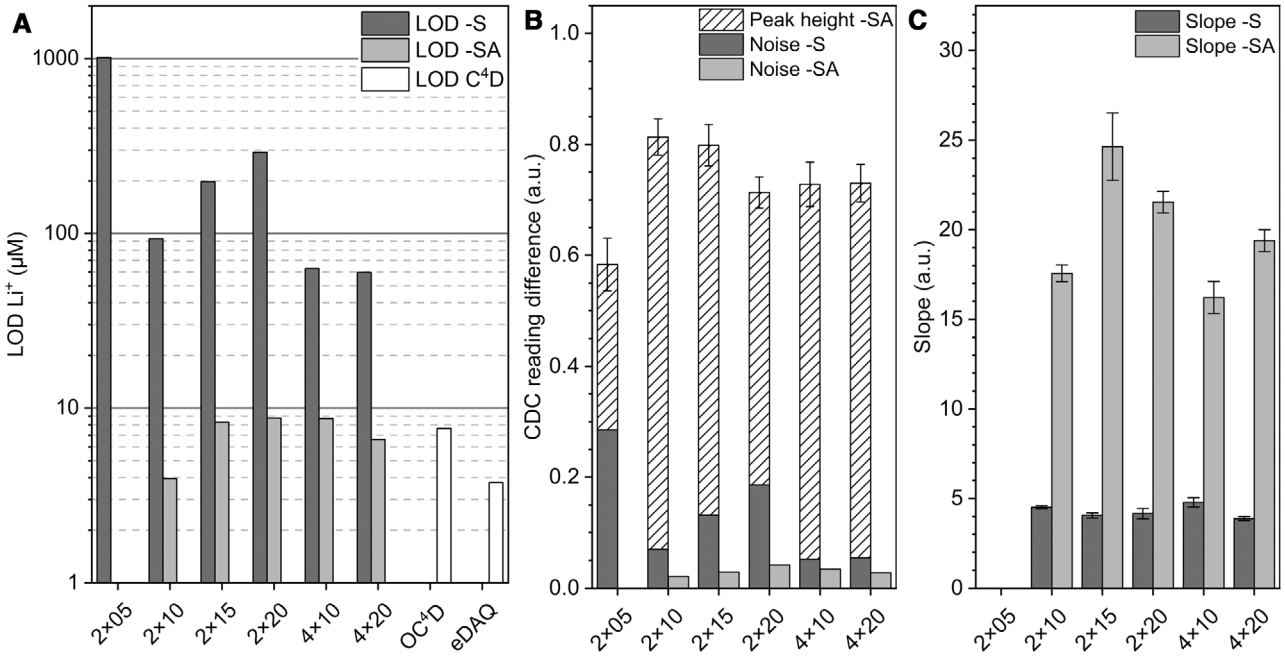


**Figure 2.** (A) LOD ($S/N = 3$, $Li^+$) (B) peak-to-peak noise (plain bars) and peak height ($n = 3$, 500 µM $Li^+$, hatched bars) as well as (C) slope of the calibration curve of the peak area (sensitivity for $Li^+$, $n = 3$) using shielded (-S, gray) and shielded plus amplified (-SA, light gray) CDCDs, $OC^4D$ and commercial $C^4D$ (eDAQ) determined from a CE separation of $K^+$, $Li^+$, and $TrisH^+$. Common nomenclature in (A,B,C): For CDCD, 2× (single-ended mode) and 4× (differential mode) represent the number of electrodes and 05, 10, 15, 20 represents the electrode length in mm. Detector settings: CDCD: excitation voltage: 32 kHz, square wave, amplitude 5 V (-S) and 24 V (-SA); $L_{eff} = 31.5$ cm. $OC^4D$: excitation voltage: 1.1 MHz, sinus wave, amplitude 5 V; $L_{eff} = 31.5$ cm. eDAQ: excitation voltage: 200 kHz, 100% amplitude, activated head stage gain; $L_{eff} = 33.5$ cm. Separation conditions: 20 mM MES/His-BGE, injection: 5 s × 50 mbar, fused silica capillary (50 cm × 50 µm id), separation voltage: 14 kV.

CDC-IC in single-ended mode instead of a differential measurement mode, which would have required two additional electrodes and a reference capillary.

To judge the results obtained during the optimization process, the following figures of merit were determined: LOD of $Li^+$ (Fig. 2A), peak-to-peak noise (Fig. 2B, plain bars), sensitivity (Fig. 2C), and the plate numbers indicating the size of the detection window, see Table 1. The following instrumental parameters were varied: the length XX (in mm) of the excitation and pick-up electrode ("2×XX" for single-ended mode); the use of the differential mode measurement of the CDC-IC using a 4-electrode setup ("4×"); as well as amplifying the peak-to-peak square wave excitation voltage of the CDC from 5 to 24 V (light gray bars, "-SA"). Gray bars or "-S" indicate results measured with shielded detectors without amplifier. For example, a CDCD in single-ended measurement mode with two electrodes of 10 mm length, with shielding and amplification is labeled "CDCD 2×10-SA." Detailed information and figures of merit of all setups are summarized in Table 1.

### 3.1.1 Electrode lengths, symmetry, and detection head shielding

The requirement for a more compact detector led to a reevaluation of the influence of the electrode length in smaller steps compared to the publication of Drevinskas et al. [24,25]. Setups with the same length (5, 10, 15, 20 mm) for both excitation and pick-up electrode were investigated first. Regarding the noise, the signal height of analyte peaks and the LOD for all detectors, a reduction of the overall electrode length was advantageous. Results from experiments with different length of excitation and pick-up electrode showed similar behavior. The positioning of the longer electrode proved to be irrelevant for LODs. An exception was observed for the CDCD 2×05-S detector: this setup showed the highest noise of all detectors and the lowest peak height of all setups, see, for example, hatched bars in Fig. 2B for a 500 µM $Li^+$ sample. The slope of the calibration curve of the peak area was similar for all other detectors (3.9–4.5 a.u.), revealing a similar sensitivity corroborating findings of Drevinskas et al. (*S/N* for 2×05; 2×15) [24]. During the study, the effectiveness of the shielding of the detector's head was confirmed. The CDCD 2×20-S showed a 3.7-times lower LOD compared to the same detection head without grounded shielding. With the fine tuning of electrode lengths in our study, we were able to lower the LOD and enhance the *S/N*: shorter electrodes were beneficial since they were easier to mount and the section of the capillary covered by the detector was shorter allowing a more freely positioning of the detector along the migration path. The lowest LOD with 93 µM was achieved for the CDCD 2×10-S.

 

Detectors with 5 mm electrodes were discarded because of their high noise, high LOD, and low sensitivity. No advantages of setups with different length of the excitation and pick-up electrode were observed, they were not further investigated.

#### 3.1.2 Differential measurements

It was possible to conduct differential measurements with the CDC-IC. For this, the detection head was equipped with four identical electrodes. The pair of electrodes connected to the negative input channel of the IC was placed around a capillary filled with BGE. The differential setup proved to be particularly advantageous for the detector with higher noise (CDCD 2×20-S). Due to lower noise achieved in differential measurement mode, the LODs for CDCD 2×10-S and CDCD 2×20-S were reduced by a factor of 1.5 and 4.9 reaching an LOD of approximately 60 μM $Li^+$. The sensitivity was 23% higher for the CDCD 4×10-S than for the CDCD 4×20-S, see Table 1, again demonstrating the positive effect of shorter electrodes. The lower LODs obtained in the differential measurement mode was also described by Drevinskas for CDCD with 20 mm and an excitation voltage of 3.3 V, however, shorter electrodes were not investigated [25].

#### 3.1.3 Amplification

Finally, the influence of the amplification of the peak-to-peak excitation voltage of the CDC-IC from 5 to 24 V with an operational amplifier was investigated for the shielded detectors (2×10-S, 2×15-S, 2×20-S) in single-ended as well as in differential (4×10-S, 4×20-S) measurement mode, compare Table 1. An amplification of the signal of 4.8 would be expected if the excitation voltage and the signal height increase to the same extent. This was reached in our CE-experiments with an increase in peak heights for 125 and 500 μM $Li^+$ by factors in the range of 4.3 to 4.9 and of 4 to 4.8, compare Table 1. The slope of the calibration curve (peak area) revealed a gain between 3.4 and 5.2, in general more pronounced for the CDCDs with 20 mm electrodes. The RSD of the slope of the calibration curve was in a similar range for all setups independent of the use of an amplifier. This means that the amplification did not improve the minimal distinguishability of two concentrations due to a higher response as the influence of the CE separation on the precision of the slope can be assumed to be similar for all setups. The impact of amplification on the *S/N* (125 and 500 μM $Li^+$) for single-ended setups was 2.2-fold higher than for differential setups and about 30% higher for detectors with 20 mm compared to those with 10 mm electrodes (see Table 1). Concerning the shielded setups and the shielded plus amplified setups, the noise reduction ranged between a factor of 4.4 for the 2×20 detectors and 1.5 for the 4×10 detectors.

To summarize, the signal heights and areas increased to the same extent as the excitation voltage and the noise for both single-ended and differential setups were reduced. The peak-to-peak noise for the shielded plus amplified detectors after applying a five-point moving average function was between 21 and 42 a.u. This matched well with the 5- to 10-fold specified resolution of 4 aF (equals a.u.) of the CDC-IC (AD7745) [21].

#### 3.1.4 Summary of the optimization process

The LOD for $Li^+$ reached with all amplified CDCDs, displayed in Fig. 2A and summarized in Table 1, were between 3.9 and 8.8 μM. Overall, LODs reached in this study were in the same order of magnitude for the amplified setups. The CDCD 2×10-SA showed the lowest noise. It was also the most compact and simplest setup of the detectors with amplifier. It provided the lowest LOD of 3.9 μM for $Li^+$. A measurement with a concentration just above the LOD is depicted in Fig. 3A.

#### 3.1.5 Detection window

A narrow detection window is desired to reach a higher spatial resolution and, thus, separation efficiency with the related precision in determining migration times. In Table 1, the plate number for all CDCDs are summarized for the $Li^+$ peak when injecting a 125 and 500 μM solution. Due to the better LOD, only detectors with amplifiers were discussed. The peak caused by a 500 μM $Li^+$ sample, was already that broad, that the limiting factor was the electrophoretic separation and not the detection. This resulted in plate numbers of 14 000 to 15 000 (500 μM) and 22 000 to 24 000 (125 μM) for peaks caused by $Li^+$. No significant effect of the electrode length on the plate number was observed.

### 3.2 Comparison of CDCDs to established $C^4D$

#### 3.2.1 Comparison regarding the LOD

To judge the performance of the CDCDs, the LOD and the plate number were compared to those achieved by the $OC^4D$ and the $C^4D$ from eDAQ; all data are summarized in Table 1 and Fig. 2. With all shielded plus amplified CDCDs and both $C^4Ds$, the LODs for $Li^+$ were between 3.7 and 8.8 μM. The LOD of the CDCD 2×10-SA (with lowest LOD of all CDCDs of 3.9 μM) was not significantly different from the commercial $C^4D$ from eDAQ (LOD 3.7 μM) for a $Li^+$ sample. The $OC^4D$ reached LODs of 7.6 μM. The eDAQ, which was always mounted as a secondary detector on the same capillary, showed a SD of 1.0 μM ($n = 4$) at the LOD. A direct comparison to literature values is difficult as different injection volumes, capillary dimensions, effective lengths, and BGE concentrations were used. LODs ($S/N = 3$) for $C^4Ds$ in literature (mostly LODs for $K^+$) were reported between 0.1 and 3.7 μM (LOQs of 0.3 to 12.3 μM) [20,39–50]. Reported LODs for $Li^+$ were between 0.8 and 4.0 μM [20,49]. Using

 

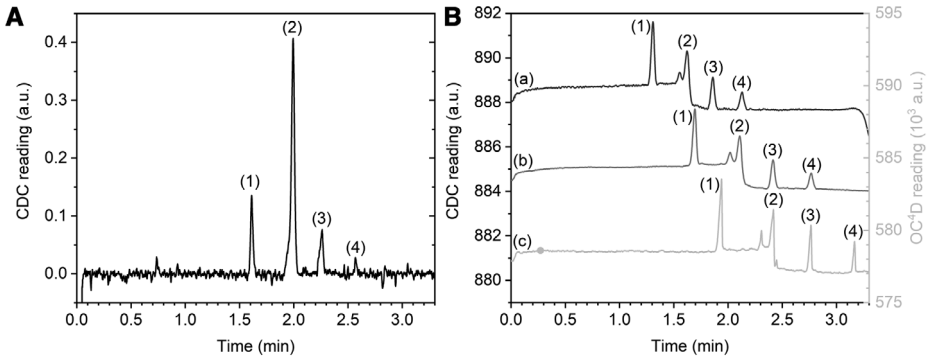


**Figure 3.** Electropherograms of the separations of $K^+$ (1), $Na^+$ (2) impurity, $Li^+$ (3) and $TrisH^+$ (4) in a 20 mM MES/His BGE, see Fig. 2 for experimental details. (A) Baseline-subtracted electropherogram at analyte concentrations of 6.25 μM recorded by the CDCD 2×10-SA at $L_{eff}$ = 31.5 cm. (B) Electropherograms at analyte concentrations of 125 μM recorded by a multidetection setup (see Section 3.3) consisting of: (A) CDCD 2×10-SA at $L_{eff}$ = 24.5 cm, (B) CDCD 2×15-SA at $L_{eff}$ = 31.5 cm (–14 a.u. offset), and (C) an $OC^4D$ (light gray, right scale, $L_{eff}$ = 36 cm). Excitation electrodes of the CDCDs pointed to each other.

a very similar detection setup and measuring conditions, Drevinskas et al. calculated LOQs for $K^+$ (0.31 μM), $Na^+$ (0.25 μM), and $TrisH^+$ (0.55 μM). A direct comparison of the data presented for the shielded plus amplified CDCDs, determined via the $S/N = 3$ criterion for the peak height to data presented by Drevinskas et al. [25] is difficult, as the authors calculated their LOQs from the calibration curve of the corrected peak area, which disregards to some extend the noise of the detector. Additionally, the lowest measured concentration of the calibration curve to determine the LOD was about the 25-fold LOD. According to DIN 32 645:2008-11, the LOD can only be determined from a calibration curve in the range of zero to the ten times the LOD. Therefore, the lowest measured concentration by Drevinskas et al. is too high for a good estimate of the LOD. In literature, LODs ($S/N = 3$) of 0.6 and 0.8 μM for $K^+$ and $Li^+$ were published for the $OC^4D$ using a 10 mM MES/His BGE [20]. The LODs are 7.5- to 9.5-fold lower than those obtained in this study for the $OC^4D$, presumably due to different measurement conditions but not detector performance.

### 3.2.2 Comparability of CDCDs and eDAQ for quantitative analysis

For the quantitative comparison of the CDCDs (CDCD 4×20-SA) with the eDAQ, the RSD of the ratio of the peak areas for $Li^+$ at a concentration of 125 to 1500 μM (called RSD(CDCD/eDAQ), $n = 3$) was calculated, see Table S1 in the Supporting information. This ratio proved robust if both detectors were installed to the same capillary and when they recorded the same run concurrently but at different effective lengths. With an RSD(CDCD/eDAQ) ≤0.7%, it is clear that both detectors performed comparatively. The precision of the peak area was similar for the CDCD and the eDAQ reaching 2.2 to 8.9% RSD ($n = 3$) for $Li^+$. This corresponds well to literature values (2.7–7%) [39–41,43,44]. The high values of the RSD of the peak areas compared to those of RSD(CDCD/eDAQ) showed, that the variation between repeated CE-runs is more pronounced than the variation between both detector types. The repeatability of the CE-separation depends on injection precision, the changes of EOF between runs and the electrophoretic mobility, caused by shifts in the BGE composition during a series of measurements. Analogous observations were made for all detectors under investigation.

### 3.2.3 Comparison regarding the plate number and peak shapes

A comparison of the plate numbers revealed 2.4 to 3.1 times lower plate numbers for the CDCD 2×10-SA (23 000 at 125 μM $Li^+$) versus the $OC^4D$ (56 000 at 125 μM $Li^+$) and the eDAQ (71 000 at 125 μM $Li^+$). This points to a narrower detection window of the $OC^4D$ and the eDAQ compared to those of the CDCDs. This correlates with a higher precision in determining migration times and higher resolution. Another reason for the lower plate numbers of the CDCD compared to those of the $C^4Ds$ can be the different excitation frequencies of the detectors. The frequencies were set to 32, 1100, and 200 kHz for the CDCDs, $OC^4D$, and the eDAQ, respectively. For $C^4D$, it is known that the plate number is reduced when using longer electrodes at low excitation frequencies [33].

The shape of analyte peaks when injecting samples with concentrations above 250 μM depended on the detector: the CDCDs showed symmetrical peaks whereas with the $C^4Ds$ triangular peaks were recorded due to electrodispersion. We presume that the CDCDs have a broader detection window compared to the C4Ds. The integration over a larger capillary segment results in a smoothing effect with respect to the shape of the peak.

### 3.2.4 Comparison of instrumental aspects

The CDCDs presented here had a noticeably light weight (1.7–2.6 g depending on the configuration) and a more

 

**Table 2.** Comparison of size, power consumption, and weights of shielded CDCDs with (CDCD-SA) or without (CDCD-S) amplification, $OC^4D$ and eDAQ

| Detector | Size of detection head (mm) | Covered capillary section (mm) | Power consumption of detection device + master device | Weight of detection head (g) | Weight w/o battery (g) |
|---|---|---|---|---|---|
| CDCD-SA | 10 × 25 × 21 | 21 | 94 mA @ 7.2 V + 34 mA @ 5 V | 2.6 | 24.1 |
| CDCD-S | 10 × 25 × 21 | 21 | 34 mA @ 7.2 V + 34 mA @ 5 V | 1.7 | 20.9 |
| $OC^4D$ | 21 × 30 × 13 | 13 | 34 mA @ 12 V + 34 mA @ 5 V | 11.5 | - |
| eDAQ | 27 × 13 × 31 | 27 | - | 19.0 | - |

For CDCD: total battery weight: 172 g; dimensions supply unit: 97 × 22 × 22 $mm^3$.

compact detection head compared to the $OC^4D$ and the eDAQ. This allowed the capillary to carry the detection head without the need for further support, so that it could be positioned freely along the capillary facilitating handling. The section of the capillary occupied by the detection head was shorter with the $OC^4D$ than with the CDCD. A shorter detection head is favorable for multidetector setups as detectors can in principle be positioned more closely to each other, then only limited by possible interferences between detectors (see Section 3.3). The setups developed here were power supplied by batteries, allowed wireless data transfer, and offered the further advantage to use up to five detectors in parallel (see Section 3.3), as well as to connect a trigger either to a detection device or to the master device wired via USB to the computer. The trigger was optimized to work for an Agilent 7100 CE System or a Prince 560 CE. The entire detection device, including the batteries weighed less than 200 g using two 4000 mAh batteries; a protective housing, if regarded as necessary, would weigh approximately 20 g. In contrast, both $C^4Ds$ used for comparison needed mains power and a wired data communication. The power consumption of the CDCDs with amplifier plus the belonging master device (680 + 170 mW) was only about 1.5-times higher compared to the $OC^4D$ (580 mW [detector] + 170 mW [microcontroller]) despite the integration of wireless data transmission. The nonamplified CDCDs (250 + 170 mW) were about twice as power efficient as the detectors with amplification. Further, the manufacturing of the CDCDs was simple. The cost of the CDCD assembly with one detection device and an $OC^4D$ (60–80 EUR) was similar but may differ for the power supply. A summary of instrumental parameters is given in Table 2 for all detectors.

### 3.3 Multidetector setup

Several detectors can be placed along the capillary. Care must be taken to avoid interferences between them when the distance becomes too short. We determined the minimum distance required for interference-free multidetector setups. Using two CDCDs (CDCD 2×10-SA, CDCD 2×15-SA), it was crucial that the excitation or the pick-up electrodes pointed to each other. This allowed a minimal distance between the PCBs of 5 cm without affecting the LOD. A shorter distance decreased LODs due to interferences and, therefore, higher noise. No such restrictions were observed for setups combining a CDCD with an $OC^4D$/eDAQ or combining two $OC^4Ds$.

A multidetector setup consisting of the two single-ended CDCDs with the lowest LODs (CDCD 2×10-SA, CDCD 2×15-SA) and an $OC^4D$ were used to allow spatial tracking of the migrating analytes in the reference system (electropherograms see Fig. 3B). The distances between the detectors were 7.0 and 4.5 cm. The excitation electrodes of the CDCDs pointed to each other. This setup allowed to determine the speed of migration, which is constant in CE separations, as well as the migration direction of the analytes [51]. The time at which an analyte should pass the $OC^4D$ was calculated from the speed based on the signals and positions of the CDCDs and the distance between the $OC^4D$ and the CDCD next to it. On average, depending on the analyte, the measured time was 0.16 to 0.61 s shorter than the calculated time and the SD was 0.10 to 0.18 s ($n = 5$). Spatially, this means that the analyte has exceeded the position of the $OC^4D$ by only 49 to 111 μm on average (corresponding to a SD of 21 to 51 μm). The precise determination of the location of analytes along the separation path is necessary for setups where the analytes are transferred, for example, to an additional separation dimension, for fractionation or for stopped-flow experiments. Similar to our results, excellent linearity ($R^2 = 1.0$) was reported for the evaluation of the detector position as a function of the detection time by Caslavska et al. [52]. Multidetector setups with up to 16 $C^4Ds$ were described in literature but were mainly applied to validate simulations of CE separations. The $C^4D$ setups used in literature were more spacious. A direct comparison of LODs was not possible due to missing statements. Also, it was not stated if any interferences between the detectors were observed [53]. Further, multidetector setups were used to record concurrent CE separations of anions and cations using different sample injection modes [54].

### 3.4 Quantification of glyphosate in a herbicide formulation

To demonstrate the applicability of the CDCDs to real samples, the content of glyphosate and potassium was determined in the herbicide Roundup PowerFlex via external calibration, see Fig. 4 for electropherograms. A BGE of 20 mM MES/His (pH 6.1) proved suitable for the separation of

 

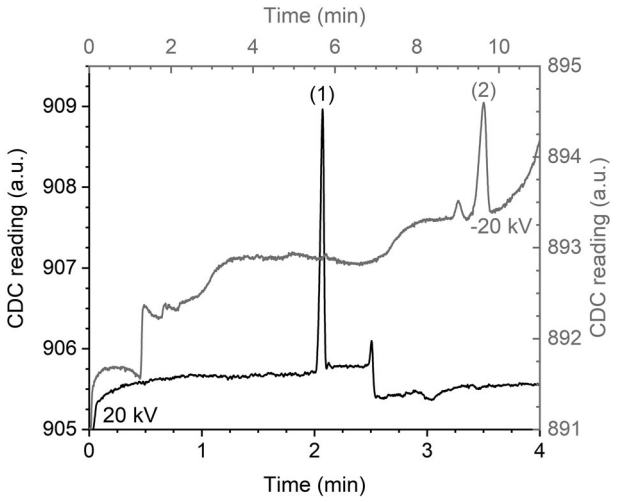


**Figure 4.** Electropherograms of CE-separations of a 1:20 000 dilution of the herbicide Roundup PowerFlex (nominal concentrations in the commercial product: 4.6 M $K^+$ and 3.2 M glyphosate) for the determination of the content of $K^+$ (Peak (1), 230 μM in injected solution) and glyphosate (Peak (2), 161 μM in injected solution). Separation in 20 mM MES/His BGE at 20 kV or –20 kV plus 50 mbar pressure. Detection: CDCD 2×10-SA (conversion time: 109.6 ms; excitation voltage: 32 kHz, square wave, amplitude 24 V, $L_{eff}$ = 45.5 cm). Bare fused silica capillary: 65 cm × 50 μm. Injection: 5 s × 50 mbar.

glyphosate because it was doubly charged at pH 6.1 ($pK_a$ values: 2.0, 2.6, 5.6, and 10.6 [55]). For detection, the CDCD 2×10-SA was used (see discussion in Section 3.1.4). The results obtained for both analytes showed excellent linearity ($R^2 > 0.99$) in the concentration range 62.5 to 250 μM for glyphosate and 125 to 1500 μM for $K^+$. The LOD was estimated based on $S/N = 3$ to 10 μM for glyphosate and 7 μM for $K^+$. The migration time precision was <1.2% RSD ($n$ = 3). The RSD of the peak area was <10% ($n$ = 3). The concentration of $K^+$ and glyphosate in the herbicide formulation was determined via a calibration curve in triplicate at two dilutions (1:20 000 and 1:10 000). The results were: 4.6 M ± 3.4% for $K^+$ and 3.2 M ± 1.3% for glyphosate. According to the datasheet, the nominal concentration was approximately 2.84 M of the glyphosate potassium salt, which is 11% lower than measured for the sample. The deviation is possibly due to the high dilution of the samples, the high viscosity of the herbicide formulation, possibly some matrix effects or simple deviations between labeling and actual content.

## 4 Concluding remarks

In this study, we presented different setups of portable CDCDs combined with an operational amplifier. To obtain best LODs and a compact detection head, a systematic study was conducted regarding electrode length, the use of a differential measurement mode, and different excitation voltages. To judge the performance of the CDCDs, a direct comparison to the OpenC$^4$D and a commercial C$^4$D was carried out. For the fully optimized CDCD with two electrodes of 10 mm length and a square wave excitation voltage with a frequency of 32 kHz and an amplitude of 24 V, LODs ($S/N = 3$) for $K^+$ and $Li^+$ were approximately 4 μM. Similar results were obtained for the commercial C$^4$D. The LODs for the OpenC$^4$D were twice as high. Depending on the measurement conditions, LODs between 0.1 and 3.7 μM (LOQs of 0.3 to 12.3 μM) (mostly for $K^+$) were reported for C$^4$Ds in literature [20,39–50].

Compared to the other C$^4$Ds used in this study, the detection head had a low weight of only 2.6 g. Therefore, the detection head can easily be carried by the CE capillary itself so it can be freely positioned along the separation path. To enhance handling compared to currently available detectors, the CDCD setups were battery powered and used wireless data transmission. With their compact design, low weight of less than 200 g including batteries, low power consumption of the detection device of approximately 680 mW (less than 250 mW when LODs above 40–60 μM were sufficient) it was well suited for portable systems, even with multiple detectors for timing events. Additionally, the CDCD was low priced with 80 EUR, and the simple assembly proved beneficial. For convenience, full automation for measurements with commercial CE systems was implemented. The hardware and software were optimized for real time data plotting and is provided as open source. It was also shown that multidetector setups to enable spatial tracking of analytes during separation were possible.

*We thank for the support from the Excellence Initiative, a jointly funded program of the German Federal and State governments, organized by the German Research Foundation (DFG). We thank Prof. F.-M. Matysik and his team, Institute of Analytical Chemistry at the University of Regensburg, for providing the OpenC$^4$D.*

*Open access funding enabled and organized by Projekt DEAL.*

*The authors have declared no conflict of interest.*

### Data availability statement

The data that support the findings of this study are available from the corresponding author upon reasonable request.

## 5 References

[1] Pena-Pereira, F. (Ed.), *Miniaturization in Sample Preparation*, De Gruyter, Warsaw, 2015, pp. 1–28.

[2] Henry, C. S. (Ed.), *Microchip Capillary Electrophoresis*, Humana Press, Totowa, NJ 2006, pp. 1–10.

[3] Wuethrich, A., Quirino, J. P., *Anal. Chim. Acta* 2019, *1045*, 42–66.

[4] Piendl, S. K., Geissler, D., Weigelt, L., Belder, D., *Anal. Chem.* 2020, *92*, 3795–3803.

[5] Trietsch, S. J., Hankemeier, T., van der Linden, H. J., *Chemometr. Intell. Lab.* 2011, *108*, 64–75.

 

[6] Lewis, A. P., Cranny, A., Harris, N. R., Green, N. G., Wharton, J. A., Wood, R. J. K., Stokes, K. R., *Meas. Sci. Technol.* 2013, *24*, 042001.

[7] Kubáň, P., Nguyen, H. T. A., Macka, M., Haddad, P. R., Hauser, P. C., *Electroanalysis* 2007, *19*, 2059–2065.

[8] Seiman, A., Jaanus, M., Vaher, M., Kaljurand, M., *Electrophoresis* 2009, *30*, 507–514.

[9] Koenka, I. J., Kung, N., Kubáň, P., Chwalek, T., Furrer, G., Wehrli, B., Muller, B., Hauser, P. C., *Electrophoresis* 2016, *37*, 2368–2375.

[10] de Jong, G. (Ed.), *Capillary Electrophoresis–Mass Spectrometry (CEMS)*, Wiley-VCH, Weinheim 2016.

[11] Klampfl, C. W., *Electrophoresis* 2009, *30*, S83–S91.

[12] Casto, L. D., Do, K. B., Baker, C. A., *Anal. Chem.* 2019, *91*, 9451–9457.

[13] Pan, J. Z., Fang, P., Fang, X. X., Hu, T. T., Fang, J., Fang, Q. *Sci. Rep.* 2018, *8*, 1791.

[14] Kim, J. H., Kang, C. J., Kim, Y. S., *Biosens. Bioelectron.* 2005, *20*, 2314–2317.

[15] Kubáň, P., Hauser, P. C., *TrAC Trends Anal. Chem.* 2018, *102*, 311–321.

[16] Brito-Neto, J. G. A., da Silva, J. A. F., Blanes, L., do Lago, C. L., *Electroanalysis* 2005, *17*, 1198–1206.

[17] Zhang, M., Stamos, B. N., Amornthammarong, N., Dasgupta, P. K., *Anal. Chem.* 2014, *86*, 11538–11546.

[18] Fracassi da Silva, J. A., do Lago, C. L., *Anal. Chem.* 1998, *70*, 4339–4343.

[19] Zemann, A. J., Schnell, E., Volgger, D., Bonn, G. K., *Anal. Chem.* 1998, *70*, 563–567.

[20] Francisco, K. J., do Lago, C. L., *Electrophoresis* 2009, *30*, 3458–3464.

[21] Analog Devices Inc. *24-Bit Capacitance-to-Digital Converter with Temperature Sensor*, AD7745/AD7746, Product datasheet, Norwood, 2005.

[22] Takeuchi, M., Li, Q., Yang, B., Dasgupta, P. K., Wilde, V. E., *Talanta* 2008, *76*, 617–620.

[23] Kiplagat, I. K., Kubáň, P., Pelcová, P., Kubáň, V., *J. Chromatogr. A* 2010, *1217*, 5116–5123.

[24] Drevinskas, T., Kaljurand, M., Maruška, A., *Electrophoresis* 2014, *35*, 2401–2407.

[25] Drevinskas, T., Maruška, A., Briedis, V., *Electrophoresis* 2015, *36*, 292–297.

[26] Drevinskas, T., Telksnys, L., Maruška, A., Gorbatsova, J., Kaljurand, M., *Electrophoresis* 2018, *39*, 2877–2883.

[27] Drevinskas, T., Maruška, A., Girdauskas, V., Dūda, G., Gorbatsova, J., Kaljurand, M., *Anal. Methods* 2020, *12*, 4977–4986.

[28] Maruška, A., Drevinskas, T., Stankevičius, M., Bimbiraitė-Survilienė, K., Kaškonienė, V., Jonušauskas, L., Gadonas, R., Nilsson, S., Kornyšova, O., *Anal. Methods* 2021, *13*, 141–146.

[29] Elbuken, C., Glawdel, T., Chan, D., Ren, C. L., *Sens. Actuators A* 2011, *171*, 55–62.

[30] Isgor, P. K., Marcali, M., Keser, M., Elbuken, C., *Sens. Actuators B* 2015, *210*, 669–675.

[31] Wimmer, B., Pattky, M., Zada, L. G., Meixner, M., Haderlein, S. B., Zimmermann, H. P., Huhn, C., *Anal. Bioanal. Chem.* 2020, *412*, 4967–4983.

[32] Shao, X., Shen, Y., O'Neill, K., Lee, M. L., *J. Chromatogr. A* 1999, *830*, 415–422.

[33] Tůma, P., Opekar, F., Štulík, K., *Electrophoresis* 2002, *23*, 3718–3724.

[34] Kubáň, P., Hauser, P. C., *Electrophoresis* 2004, *25*, 3387–3397.

[35] Kubáň, P., Hauser, P. C., *Electrophoresis* 2013, *34*, 55–69.

[36] Kubáň, P., Hauser, P. C., *Electrophoresis* 2015, *36*, 195–211.

[37] Kubáň, P., Hauser, P. C., *Electrophoresis* 2017, *38*, 95–114.

[38] Kubáň, P., Hauser, P. C., *Electrophoresis* 2019, *40*, 124–139.

[39] Ďurč, P., Foret, F., Pokojová, E., Homola, L., Skřičková, J., Herout, V., Dastych, M., Vinohradská, H., Kubáň, P., *Anal. Bioanal. Chem.* 2017, *409*, 3507–3514.

[40] Greguš, M., Foret, F., Kubáň, P., *Electrophoresis* 2015, *36*, 526–533.

[41] Kubáň, P., Greguš, M., Pokojová, E., Skřičková, J., Foret, F., *J. Chromatogr. A* 2014, *1358*, 293–298.

[42] Greguš, M., Foret, F., Kindlová, D., Pokojová, E., Plutinský, M., Doubková, M., Merta, Z., Binková, I., Skřičková, J., Kubáň, P., *J. Breath Res.* 2015, *9*, 027107.

[43] Mori, M., Ishikawara, F., Tomoda, T., Yamada, S., Okamoto, M., Itabashi, H., Seki, Y., Matsumoto, R., Shoho, Y., Martha, L., Sumino, H., Murakami, M., *J. Chromatogr. B* 2016, *1012–1013*, 178–185.

[44] Sáiz, J., Duc, M. T., Koenka, I. J., Martín-Alberca, C., Hauser, P. C., García-Ruiz, C., *J. Chromatogr. A* 2014, *1372C*, 245–252.

[45] Kubáň, P., Kobrin, E.-G., Kaljurand, M., *J. Chromatogr. A* 2012, *1267*, 239–245.

[46] Huang, T., Kang, Q., Zhu, X., Zhang, Z., Shen, D., *Anal. Methods* 2013, *5*, 6839–6847.

[47] Kobrin, E. G., Lees, H., Fomitšenko, M., Kubáň, P., Kaljurand, M., *Electrophoresis* 2014, *35*, 1165–1172.

[48] Nogueira, T., Lago, C. L. D., *Microchem. J.* 2011, *99*, 267–272.

[49] Chang Guo, C., Lei Guang, L., Yu Jun, S., Yu Ping, L., *Electrochim. Acta* 2009, *54*, 6959–6962.

[50] Kubáň, P., Evenhuis, C. J., Macka, M., Haddad, P. R., Hauser, P. C., *Electroanalysis* 2006, *18*, 1289–1296.

[51] Jorgenson, J. W., Lukacs, K. D., *Anal. Chem.* 1981, *53*, 1298–1302.

[52] Caslavska, J., Koenka, I. J., Hauser, P. C., Thormann, W., *Electrophoresis* 2016, *37*, 699–710.

[53] Stojkovic, M., Koenka, I. J., Thormann, W., Hauser, P. C., *Electrophoresis* 2014, *35*, 482–486.

[54] Mai, T. D., Hauser, P. C., *J. Chromatogr. A* 2012, *1267*, 266–272.

[55] Sprankle, P., Meggitt, W. F., Penner, D., *Weed Sci.* 1975, *23*, 229–234.

 

# Appendix III

**Supporting Information to Paper 1:**

Graf, H. G., Rudisch, B. M., Manegold, J., Huhn, C., Advancements in capacitance-to-digital converter-based $C^4D$ technology for detection in capillary electrophoresis using amplified excitation voltages and comparison to classical and open-source $C^4Ds$. *Electrophoresis* 2021, *42*, 1306-1316, DOI: 10.1002/elps.202000394

# Supporting information to:
# Advancements in capacitance-to-digital converter-based C4D technology for detection in capillary electrophoresis using amplified excitation voltages and comparison to classical and open-source C4Ds

Hannes G. Graf,[1] Benjamin M. Rudisch,[1]Johanna Manegold,[1] Carolin Huhn[1]*

[1] Institute of Physical and Theoretical Chemistry, Eberhard Karls Universität Tübingen, Tübingen, Germany.

*Correspondence should be addressed to the following author:
Professor Carolin Huhn; Institute of Physical and Theoretical Chemistry;
Eberhard Karls Universität Tübingen; Auf der Morgenstelle 18;
carolin.huhn@uni-tuebingen.de

## Capacitance detection system design

The detection device consisted of two parts: a detection head and a supply unit.

### Detection head

A schematic diagram of the detection head circuit is depicted in Figure S1A and was adapted from the circuitry published by Drevinskas *et al.* [1]. The scheme of top and bottom of the detection head's PCB is depicted in Figure S1B and C. The main component was the CDC-IC: AD7745. For stabilization of the 5 V supply voltage, an LT1761-5 voltage regulator was used. The external circuit for LT1761-5, consisting of the capacitors C1 and C2, and for the AD7745, consisting of C3, C4 and the resistors R1 and R2, were in accordance with their datasheet from the manufacturer. The excitation voltage of the CDC (EXCB pin: 32 kHz, 5 V amplitude, square wave signal) was amplified for some setups (CDCD A) by an operational amplifier LT1360, which was used in non-inverting amplification mode. The 6.1-fold amplification was set by the resistors R4 and R5 but was limited to 4.8 by the supply voltage of +12 V and -12 V. The direct current (DC) voltage of the excitation voltage was capacitively decoupled by C5 and R3 allowing to use of the positive and negative amplification range of the operational amplifier (up to ± 15 V). For simulating the DC decoupling and dimensioning C5 and R3 –R5, the program LTspice XVII from Linear Technology (Milpitas, CA, USA) was used. If the amplifier was not mounted, R3 – R5 and C5 were not installed, the CDC output was connected directly to the excitation electrodes by bridging R6. The capacitors C6 and C7 were reserved. The electrodes had common $C^4D$ electrode geometry and were made from hypodermic needles (0.6 mm OD, 0.4 mm ID, 0.2 mm gap). The excitation electrode was mounted on the PCB at EX1 through a via (id = 0.65 mm). Similarly, the pick-up electrode was mounted on a separate PCB, which was produced as part of the detection head's PCB and had to be separated prior to its use. These PCBs with golden side plating are shown in Figure S1B and C between the two dark gray vertical lines. The side plating connected to the via was soldered to the IN+ pad. Between the two electrodes, a layer of transparent adhesive tape with a small hole, which was necessary for the passage of the capillary, was installed for insulation. In case of differential measurements, the second electrode pair was mounted in the same way and connected to EX2 and IN-. The grounded shielding of the detection head consisted of adhesive copper foil. To prevent short circuits the PCB was covered by transparent adhesive tape and the electrodes were covered by heat shrink tubing. Individual parts of the copper foil were soldered together to increase the conductivity. Grounding took

place via the gold-plated side of the detection head. The 24-bit ADC of the CDC continuously acquired the output charge, and the corresponding digital data were stored in the IC register. The CDC capacitive input channel was programed for the longest available conversion time of 109.6 ms. Digital data were therefore acquired at a rate of 9.1 Hz by an Arduino Nano microcontroller board via a two-wire interface (I²C). The Arduino Nano was part of the supply unit, which was connected to the detection head via a ribbon cable on JP1.

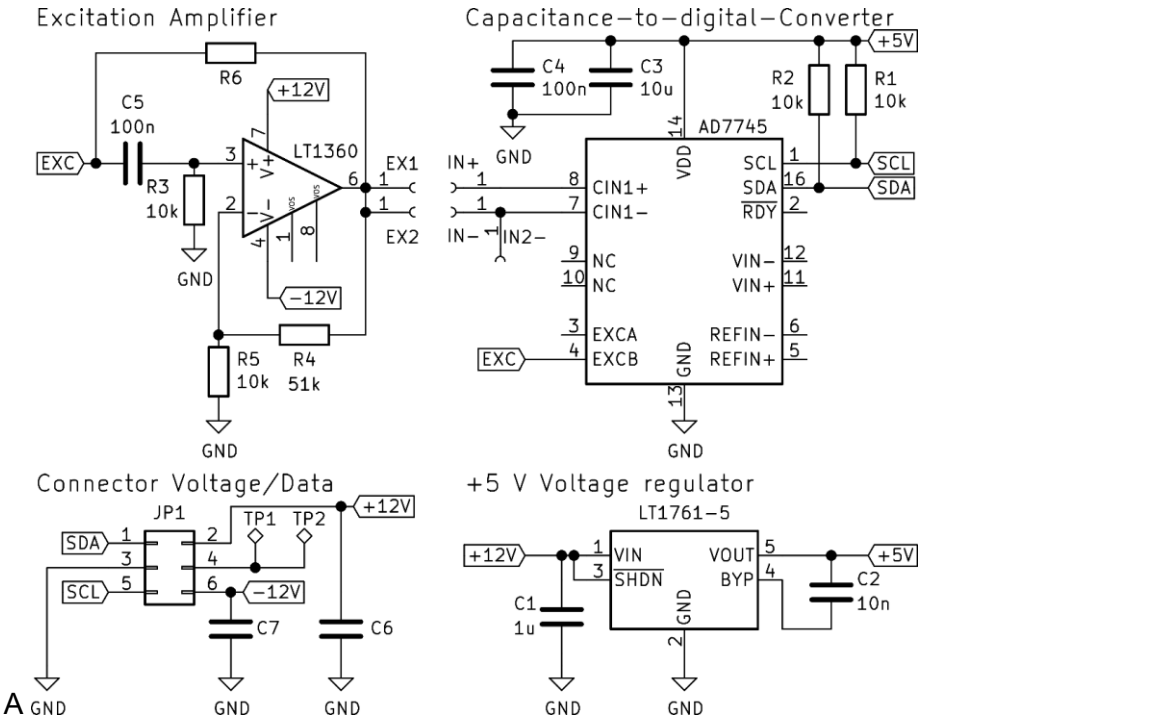


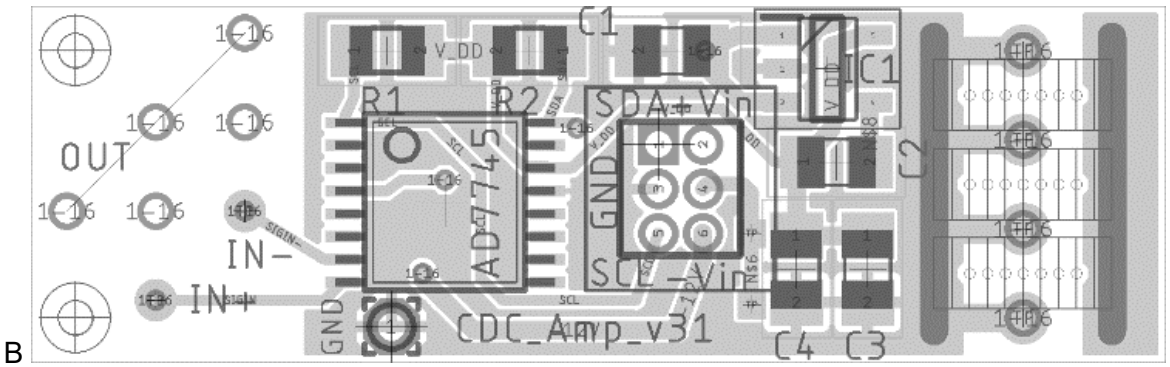


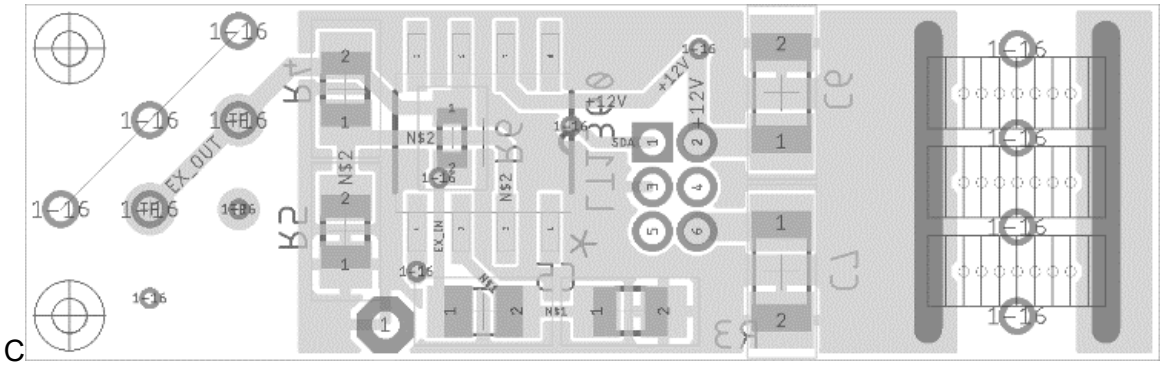


*Figure S1: A) Schematic diagram of the detection head's circuit. Capacitors without values are reserved. Resistor R6 is a jumper. B) and C) Scheme of the top and bottom of the PCB of the detection head. The two dark gray vertical bars at the right side indicate the two plated-through slots. The horizontally dotted lines indicate perforation lines, at which the 4 small PCBs for mounting the pick-up electrode can be separated after separation along the plated-through slots.*

## Supply unit

The schematic diagram of the circuit of the supply unit is displayed in Figure S2A together with schemes of the top and the bottom of the PCB in Figure S2B and C. The base of the supply unit was a custom-made PCB containing sockets for a power supply (6 – 16 V; JP1 or VIN+/VIN-), for an Arduino Nano (JP2 and JP3), for a NRF24L01+ radio module (JP5) (requiring C1) and pins for the connection to the detection head (JP4) as well as a PCB terminal block for a trigger signal with an additional 5 V output (JP6). Furthermore, the PCB supplied the voltages for the detection head and the Arduino Nano. If no amplifier on the detection head was used, it was directly supplied by the input voltage by bridging R3 and R5, otherwise an LP2992IM5-5.0 voltage regulator (IC2) and an isolated DC/DC-converter AM2D-0512DZ were installed to provide +12 V and -12 V. For the LP2992IM5-5.0 C10, C11, C15 and C16 were necessary. The IC1, an LT1761ES5-5 voltage regulator, was required to supply the Arduino and the radio module with voltage. The capacitors C20, C21, C24 and C25 were installed. The resistors R1 and R2 provided the possibility to track the input voltage of the detection system, which was convenient for the battery-powered setup. R3 and R5 were jumpers and allowed different ways of supplying IC1 with voltage either from the input voltage or from the +12 V line of the DC/DC-converter, in this study the latter was used. Similarly, R4 and R6 allowed to connect ground to the negative input voltage or to the common pin of the DC/DC-converter or connect all three of them as realized in this study. Dip switch (S1) was used for configuring the detector allowing to use more than one detector at a time and activating the wireless data transmission. Pushing the reset switch S2 or the one on the Arduino was necessary to apply configuration changes. Capacitors C12, C13, C22, C23 were reserved.

## Master device

The data were sent wirelessly to a master device which was the same as the supply unit, but only used the socket for the Arduino, the radio module (needs C1), and the PCB terminal block for the trigger. The Arduino of the master device was connected to a computer for recording data and power supply. A home-written Python 3 program with graphical user interface was used for data acquisition allowing automated and manual measurements with up to five detectors simultaneously.

The cost of one supply unit, one detection head and one master device were 25 EUR, 22 EUR and 13 EUR. Further, a set of batteries (24 EUR) was required resulting in a total of 84 EUR (70 EUR without amplifier).

## Configuration

For all measurements, the power was provided by two lithium polymer batteries (3.7 V each) connected in series to obtain a supply voltage of 7.2 V. For measurements without amplifier (CDCD SA) the following electronic components were installed on the detection head: AD7745 with LT1761-5, JP1, C1 – C4, R1 – R2. R6 was bridged. On the supply unit, the following parts were needed: pins on VIN+ and VIN- to clamp on the batteries, Arduino Nano (JP2, JP3); JP4; radio module on JP5 with C1; IC1 with C20, C21, C24, C25; S1; S2; R3 – R6 bridged. For measurements with amplifier (CDCD A) all electronic parts were installed on the detection head and R6 was left free. Some changes were also required on the supply unit: IC2 was equipped with an LP2992IM5-5.0; C10, C11, C15 and C16 were installed, T1 was mounted and R3 was left open. The latter led to IC1 being supplied by the +12 V rail of the DC/DC converter. Also, the detection head was supplied with ±12 V. When supplying IC1 directly from the battery (R3 bridged and R5 left open) this setup proved more power efficient with a power consumption of only 99 mA at 7.2 V instead of 144 mA at 7.2 V.

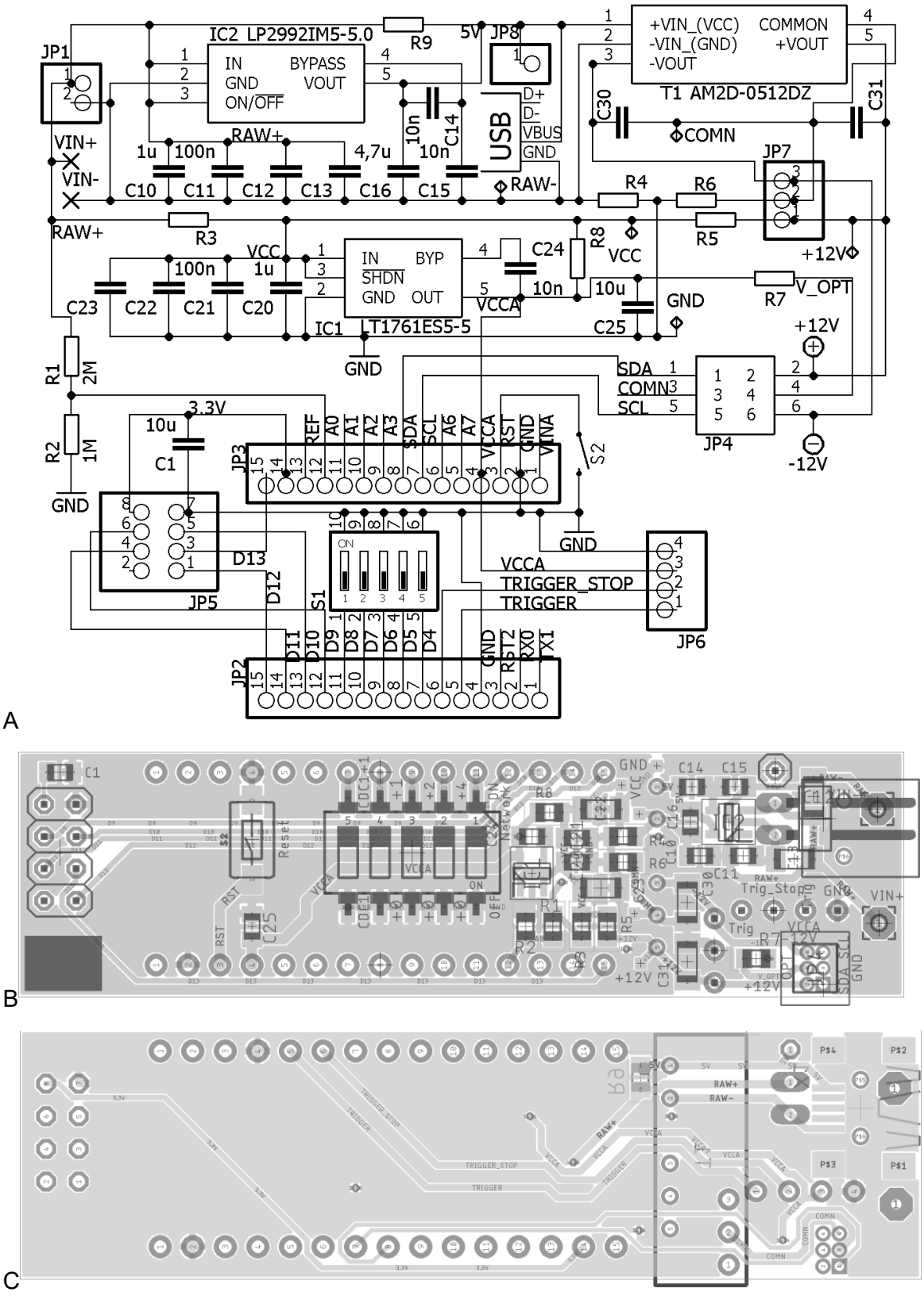


*Figure S2: A) Schematic diagram of the supply unit's circuit. Capacitors without values are reserved. Resistors without values are jumpers. B) and C) Scheme of the top and bottom of the supply unit's PCB.*

## Alternative configurations

The following configurations were also possible but not used in this study: the AD7745 could also be supplied with voltage directly from IC1 on the supply unit by connecting the test pad TP2 with the wiring to the VDD pin of the AD7745 and bridging of R7 on the supply unit. At IC2 it was also possible to mount an LT1761ES5-5, which necessitated C14, a 10 µF capacitor at

C16 and C15 was left free. The 5 V supply for the Arduino Nano and the DC/DC-converter could also be established by a USB-port on the supply unit, if R3, R8 and R9 were bridged. IC1, IC2 and the associated capacitors must not be fitted. This configuration is only possible for CDCDs with amplification. If a USB cable was connected to the Arduino, a wired data communication to the computer is possible, but led to 4.7 V on the 5 V rail, which led to a reduced supply voltage for the amplifier.

A

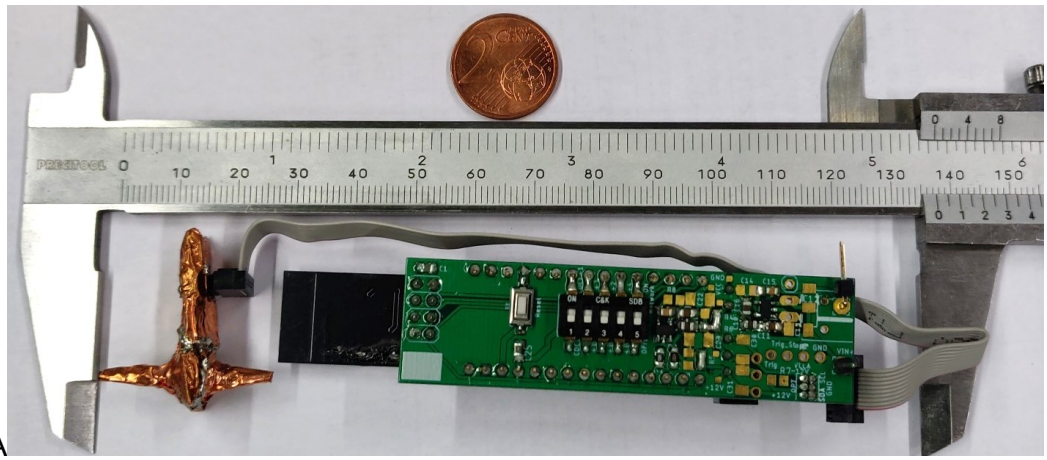

B

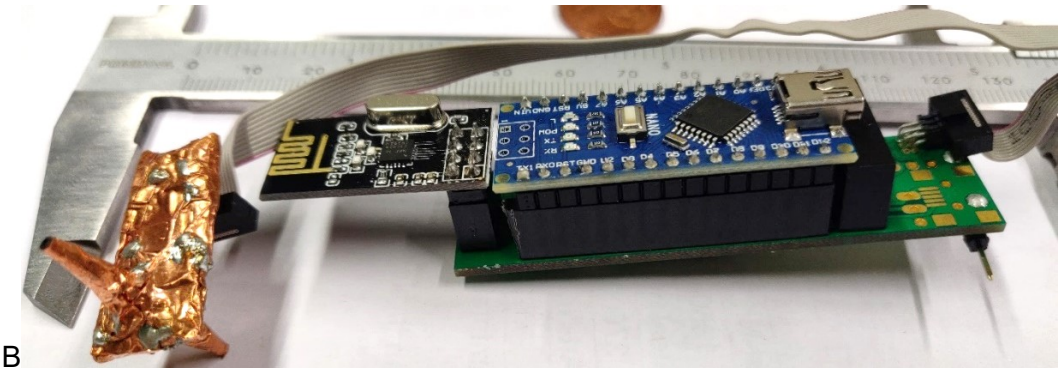

C

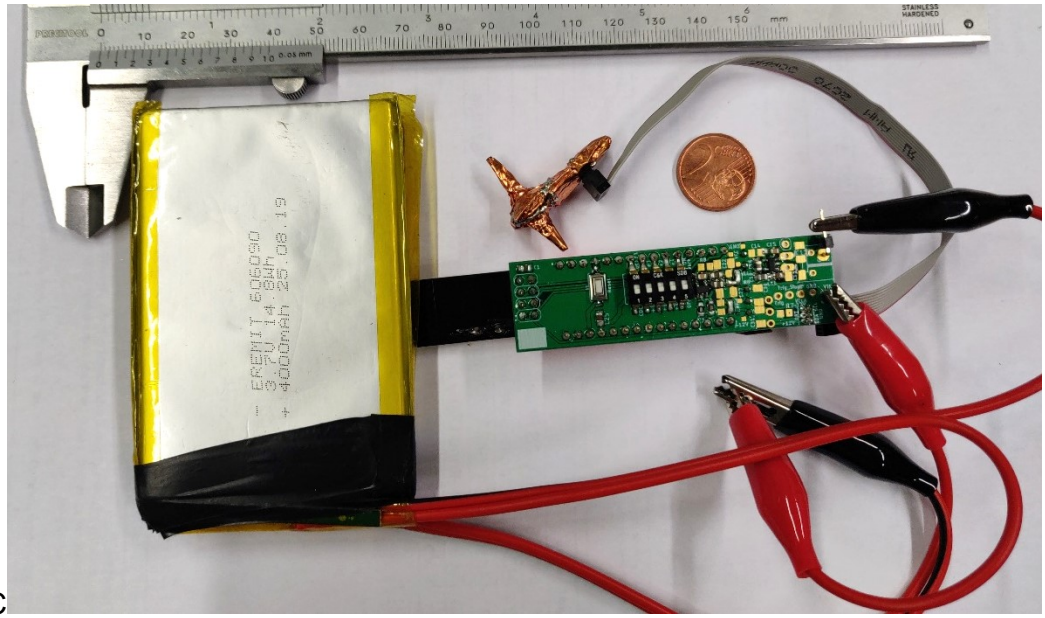

*Figure S3. Photo of the detection device CDCD 2×10-SA and the corresponding supply unit. (A) Top view of the supply unit. (B) Bottom view of the supply unit with the NRF24L01+ radio module and the Arduino. (C) Complete detector device including batteries.*

## Trigger module for the 7100 Agilent CE System

The trigger module for the 7100 Agilent CE consisted out of a PCB designed in-house, equipped with the resistors R1 – 4, two transistors Q1, Q2 (BC 847) a 4-pin terminal block (JP3), a male (JP1) and a female (JP2) D-Sub 9 connector. The latter allowed the passthrough to further devices triggered by the CE, like a mass spectrometer. The schematic diagram of the trigger module's circuit is displayed in Figure S4.

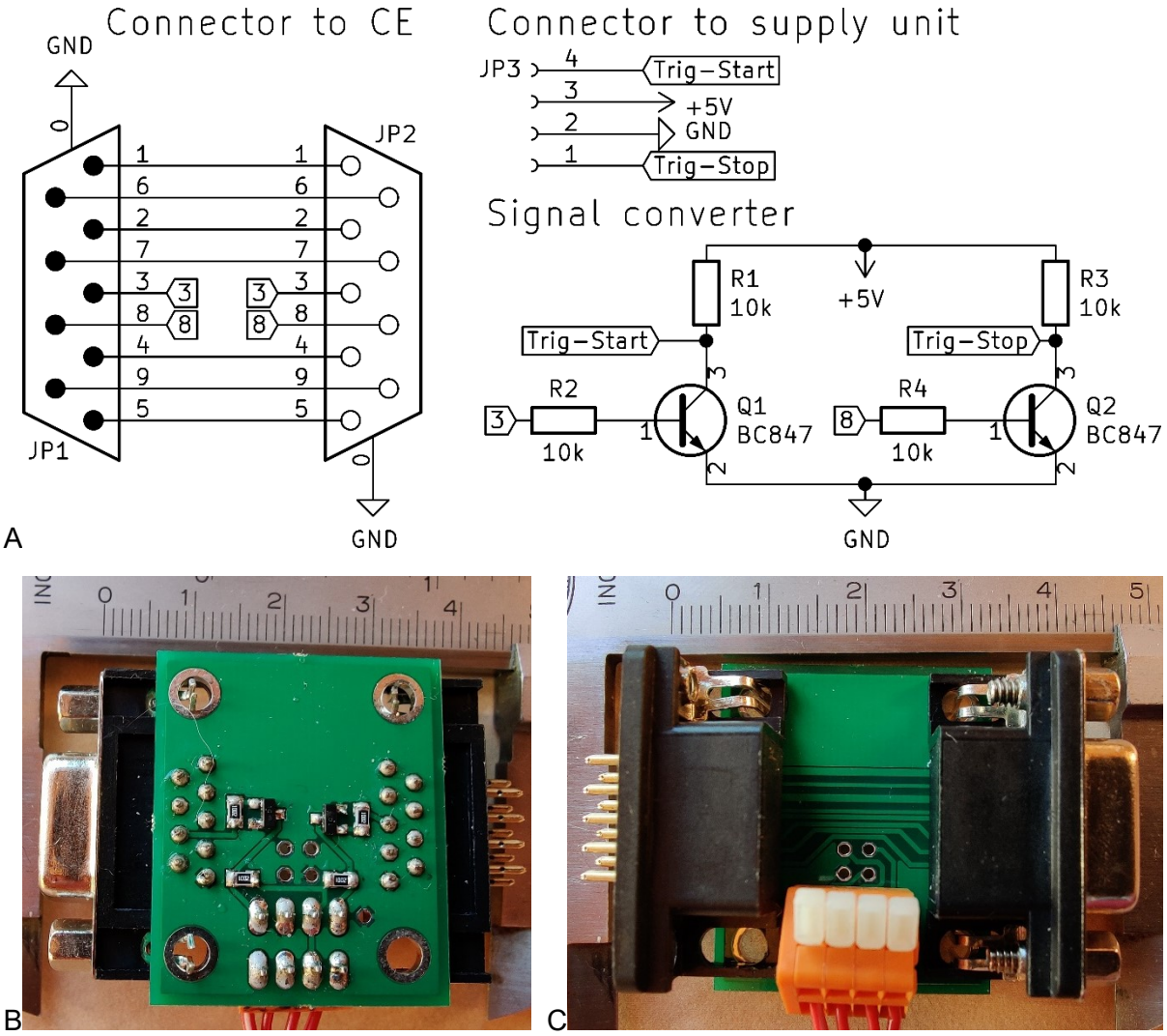


*Figure S4: (A)Schematic diagram of the trigger module's circuit for the 7100 Agilent CE System. (B) and (C) photos of the top and bottom of the module.*

# Detector response for large conductivity changes

For large changes in conductivity, e.g. caused during the flushing steps (Figure S5), different electrode lengths led to different measured changes in the capacitance values. For example, the transition from almost non-conductive ddH2O to low-conductive BGE showed a slightly negative correlation between changes in capacitance values and electrode length, except for the CDCD 2×05. Sorting the results obtained from the non-amplified setups by increasing capacitance change results in the order 2×05 ≈ 2×20 < 2×15 < 2×10. The corresponding RSD over all detectors was 5 %.

As can be seen from Figure S5B, an overshoot in measured capacitance was visible when instead of a transition from ddH2O to BGE a transition from ddH2O to highly conductive 100 mM NaOH solution passed the detector (in either direction). This is possibly due to the maximum capacitance value already reached for solutions with a lower conductivity. This effect is known from flushing with solutions of different conductivity (data not shown). At the transition, the ddH2O and the 100 mM NaOH mix. The measured capacitance changes due to the transition of ddH2O to 100 mM NaOH showed a positive correlation concerning the overall electrode length.

When using amplified excitation voltages, higher capacitance changes were observed at the transition from ddH2O to BGE. Comparing amplified to non-amplified setups revealed a ratio in the range of 4.0 to 6.9, compare Figure S5A, whereas a single-ended setup with shorter electrodes proved superior. The transition from ddH2O to 100 mM NaOH showed analogous behavior with ratios between 5.0 and 6.0. The CDCD 4×10-SA showed a gain as high as 13.9 for unknown reasons. All in all, for large conductivity changes the measured capacitance changes increased to the same extent as the excitation voltage for both single-ended and differential setups.

The duration of the transition from ddH2O to BGE during flushing at 1 bar (approx. 4 s) was also examined. No discernible correlation to the type of CDCD could be observed, compare Figure S5.

The most pronounced response to the transition from ddH2O to BGE was observed for CDCD 2×10-SA (396 a.u.). The conductivity and measured capacitance increased monotonously over a limited conductivity range. However, the response to the transition from ddH2O to 100 mM NaOH exceeded this range and the already described overshoots could be observed. The CDCD 2×20-SA and both differential setups with amplifier (4×10-SA, 4×20-SA) showed the highest response with capacitance changes of 1293 a.u. to 1333 a.u..

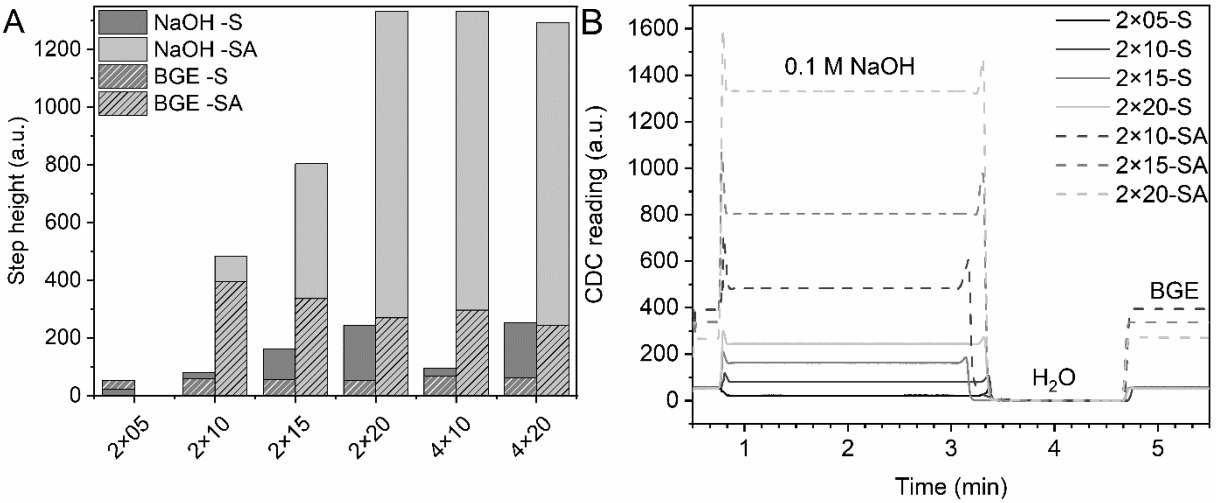


*Figure S5. (A) Step height caused by the transition from ddH2O to aqueous 0.1 M NaOH (plain) or to BGE (hatched) during flushing. See Figure 2 of the main document for further information. (B) Capacitance change observed when consecutively flushing 0.1 M NaOH solution, ddH2O (set as 0 a.u.) and BGE between separations for the shielded (solid, S) and shielded plus amplified (dashed, SA) detectors. The 2×05 is only shown without amplification.*

# Data to section: Comparability of CDCDs and eDAQ for quantitative analysis

*Table S1: RSD of the peak area (n = 3) of the CDCD 4×20-SA (RSD(CDCD)), of the eDAQ (RSD(eDAQ)) and of the ratio of the peak area CDCD/eDAQ (RSD(CDCD/eDAQ)) at different concentrations of $Li^+$.*

| c(Li+) (µM) | RSD(CDCD) (%) | RSD(eDAQ) (%) | RSD(CDCD/eDAQ) (%) |
|---|---|---|---|
| 125 | 3.1 | 3.2 | 0.5 |
| 250 | 2.2 | 2.6 | 0.5 |
| 500 | 4.4 | 4.8 | 0.6 |
| 750 | 2.2 | 2.8 | 0.7 |
| 1500 | 9.1 | 8.9 | 0.3 |

## References

[1] Drevinskas, T., Maruska, A., Briedis, V., *Electrophoresis* 2015, *36,* 292-297.

# Appendix III

**Manual for CDCDs to Paper 1:**

Graf, H. G., Rudisch, B. M., Manegold, J., Huhn, C., Advancements in capacitance-to-digital converter-based $C^4D$ technology for detection in capillary electrophoresis using amplified excitation voltages and comparison to classical and open-source $C^4Ds$. *Electrophoresis* 2021, *42*, 1306-1316, DOI: 10.1002/elps.202000394

# Manual CDCD

## Content

# Introduction

This manual describes the use and setup of the CDC-based $C^4D$ (CDCD).
The CDCD provide 4 different types of use, which distinguish between the use of an amplifier on the detection head and the use of wireless data transmission. The configurations are summarized in the table below. Depending on the chosen configuration, the assembly of the hardware differs. All configurations can also be realized in a differential measurement mode setup.

*Table 1: Configurations of CDCDs*

| Configuration | Wired data transmission (only one detector) | Wireless data transmission (up to 8 detectors, needs master device) |
|---|---|---|
| Without amplifier (needs link at the bottom of the detection head) | 1 | 3 |
| With amplifier (needs fully equipped bottom of the detection head) | 2 | 4a-4d |

## Setup for the first time a CDCD-set

1. Chose the desired configuration of the CDCDs according to Table 1.
2. Build according to the chapters “Building instructions for detection head” and “Building instructions for the supply unit” the required units.
3. Configure according to the chapter “Initial configuration” the CDCDs

## Use of preconfigured CDCDs

There are 4 different types of use, which distinguish between the use of an amplifier and the use of wireless data transmission, see Table 1.

Information: The Arduino Nanos must be preconfigured according to the section “Configuration” before use.

### Wired data transmission

- Set switches 2,3,4 to ON; set the remaining switches to OFF
- Connect the Arduino’s USB port on the detection device to the PC
- Start the Software

### Wireless data transmission, battery powered setups

- Connect Master device to PC
- On the detection unit: set switch 5 to “ON”, use switches 2-4 to set a unique id. Apply changes by pressing the momentary switch and wait until the Arduino restarts (see section “Coding”)
- Supply the detection unit by voltage (6 - 16V) at the ports mark ports in Figure 11.

# Additional Information

## Coding

The coding on the supply unit of the detection device must be unique, the coding can be changed at any time and must by applied by resetting the Arduino (disconnect the device from power or use one of the momentary switches).

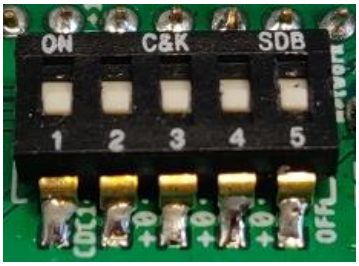


*Figure 1:DIP-switches on the supply unit*

Switches 2-4: Set the detection device ID according to: switch 2 adds 1 to CDC1 → CDC2; switch 3 adds 2, switch 4 adds 4.

All possibilities:

| S 2 | S 3 | S 4 | Name | S 2 | S 3 | S 4 | Name |
|---|---|---|---|---|---|---|---|
| OFF | OFF | OFF | CDC1 | OFF | OFF | ON | CDC5 |
| ON | OFF | OFF | CDC2 | ON | OFF | ON | CDC6 |
| OFF | ON | OFF | CDC3 | OFF | ON | ON | CDC7 |
| ON | ON | OFF | CDC4 | ON | ON | ON | CDC8 |

Switch 5: OFF: Configuration mode; except switches 2 to 4 are set to ON
→ Usage without amplifier and wireless communication → CDC1
ON: wireless communication is activated

## Trigger

The trigger can be connected via a 4-pin terminal block. The trigger can be connected to any detection device or to the master. However, preferably on the master.

Two trigger mods are supported (change requires reprogramming)

- Prince Trigger-Mode (2 wire connection) (line 11: ce_ms = false)
  - The trigger $T_G$ is connected to GND via a switch of the CE. Every change in potential is evaluated as a trigger, the maximum pulse length must not exceed 4 s. Start and stop triggers take place at the same cable.
- Agilent Trigger-Mode (4 wire connection) (line 11: ce_ms = true)
  - Adapter board with 2x D-SUB 9 ports (male and female) and small parts is necessary

## Measurement mode

The detection head can also be equipped with a second pair of electrodes to allow a differential measurement setup. This requires also a change in the software for the Arduinos.

- Single-ended measurement mode (2 electrodes) (line 13: differential = false)
- Differential measurement mode (4 electrodes) (line 13: differential = true)

## LEDs:

Wireless data communication:

- LED on Master and detection device flash fast (approx. 10 Hz): Connection established successfully
- LED on Master and detection device flash slow: establishing connection
- LED on detection device flash slow: detection device searches for master
- LED on detection device is not flashing: detection head cannot be addressed (see: Known hardware problems)

# Software

## Required basic software

- Python 3.X along with PyQt5; matplotlib and pySerial
  → Anaconda Python 3.X : https://www.anaconda.com/distribution/
- System path “python” should be created in Windows (can be created automatically during installation, check the box next to “Add Anaconda to my PATH environment variable”)
- After installation of “Anaconda” add installation of “pySerial” via: Enter in command line (search for “cmd” in Windows): `conda install -c anaconda pyserial` confirm after some time by entering “y”. Installation is completed after the message “All requested Packages already installed”, close the window.
- To check the installation of the driver for the Arduino connect it to the PC. For troubleshooting have a look at: https://sparks.gogo.co.nz/ch340.html or https://www.makershop.de/ch340-341-usb-installieren/ or search in the web for “CH340 driver”

## Measurement software

0. Connect the USB port of the Arduino of the master to the PC and supply the detection devices with power. When operating without radio: Connect the detection device’s Arduino to the PC.
1. Launch python software, pleas wait a moment until the UI appears.

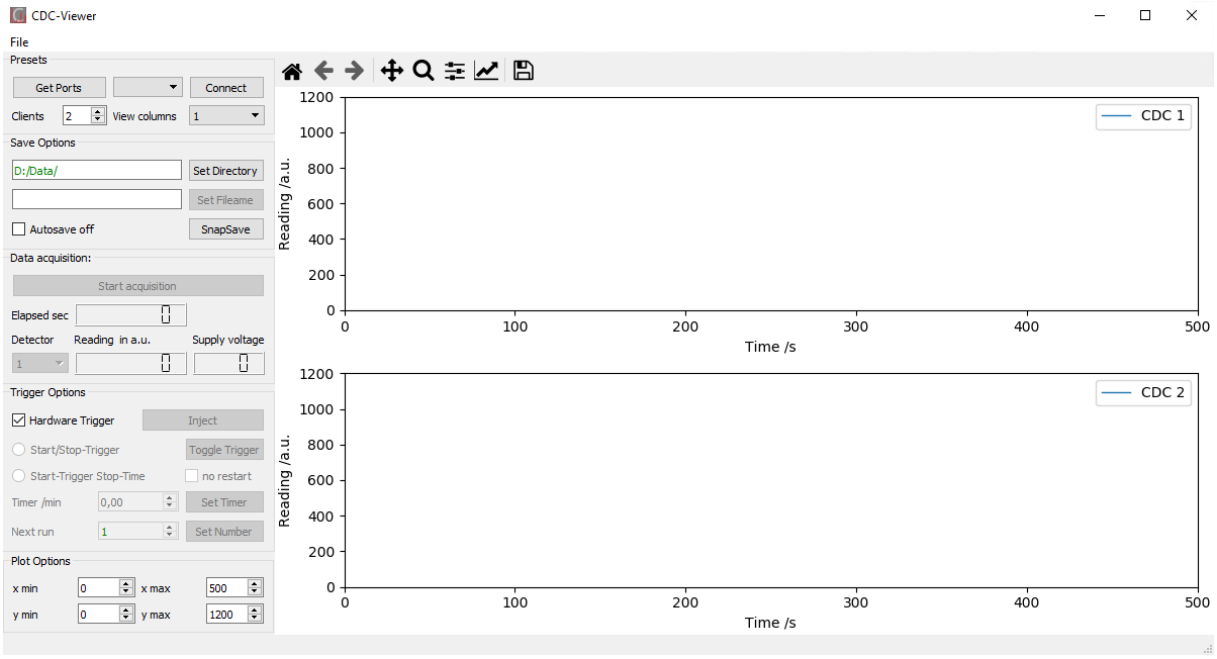


*Figure 2. Software UI*

2. Choose serial port of the Arduino and apply by clicking “Connect”, if port is not known, have a look at: Serial Monitor, COM-Port
3. Set number of detection devices (Clients), corresponds to the highest ID assigned via the DIP switches, and chose desired columns of plots, “0” disables live plot.
4. Save options: (Duplicates in the file name will result in the file being overwritten)
   1. Autosave mode:
      - Select Folder
      - Enter any desired filename without file extension (min. 3 letters) apply by clicking “Set Filename”. Successful application is reported by green text color

Information: The chosen filename will be extended by _RX_DY whereas X increments the measurements (X is display in the box “Next run” / “Current run”) and Y denotes the number of the detection device (selected by the DIP switches)

2. Manual mode (Check “disable Autosave”)
    - Save current plots via “SnapSave”
      Information: The chosen filename will be extended by _DY, Y denotes the number of the detection device (selected by the DIP switches)
      Information: “SnapSave” is also available in autosave mode

5. Data acquisition:
    a) “Start acquisition” start the data acquisition
    b) The combobox “Detector” allows to select a specific detector by its id.
    c) “Reading in a.u.” displays the received value form the selected detector device in dependence of elapsed time since the last reset (“Elapsed sec”). “Supply voltage” displays the belonging voltage of the batteries.
6. Trigger Options:
    a) In autosave mode, the “Inject” button can be used to start a recording manually. Afterwards, the same button, now labeled “Stop run”, stops the recording by clicking. This button works in any case, despite of a connected hardware trigger or the checkbox “Hardware-Trigger” is checked or unchecked.
       See also section “Trigger”
    b) Unchecking the checkbox “Hardware-Trigger” deactivates the trigger from hardware, the “Inject” / “Stop run” button are working anyway.
    c) Start/Stop-Trigger: (preselected)
       Start and stop of a measurement are defined by a trigger event at the beginning and the end of the measurement.
    d) Start-Trigger Stop-Time:
       Start via trigger event and stop after a predefined period
        - Activation is only possible if the duration (“Timer /min”) is set to a value different form “0” and is applied by clicking “Set Time”.
        - If “no restart” is checked, only the first trigger event is recognized. Only a single measurement with the set duration is recorded. Following triggers are disregarded.
    e) Further options:
        - “Current run” / “Next run” informs about the number of the next/current measurement, green text color. Adjustment is possible by changing the number. After applying with “Set Number”, the text color is green again.
        - “Toggle Trigger” can be used in case of an error with the trigger. This button can be used to toggle whether the next trigger event is a start or a stop signal.
7. Plot:
   Joint adaptation of the plot area in x and y direction of all diagrams.

## Known software issues

Information: All data is at any time recorded to a backup-directory which is in the temp folder in the root directory of the python script. The data is named: YYYY-mm-dd_HH-MM-SStemp_DX.csv

1.) Live-Plots stops working: no effect on measurement data if values in “Reading in a.u.” and / or “Elapsed sec” change.
2.) In case of errors regarding the matplotlib library: Enter in the Windows command line successively the following commands:
    - pip uninstall matplotlib
    - python -m pip install --upgrade pip
    - pip install matplotlib

## Serial Monitor, COM-Port

Software: Arduino IDE (https://www.arduino.cc/en/Main/Software)

Accessing the serial monitor:

1. Connect the PC to the USB port on the Arduino Nano
2. Open Arduino IDE
3. Select the COM port at Tools >Ports> COM X
    - If the port is not known: unplug the Arduino, display the port list, remind and close it. Plug in the Arduino and select the new entry in the port list. At the bottom right you should see Arduino Nano, ATmega328 (Old Bootloader) on COM X.
    - If not: Select Tools > Board > Arduino Nano and select Tools > processor > ATmega328 (Old Bootloader)

Open the serial monitor (magnifying glass at the top right), select 19200 baud in the new window at the bottom right

# Configuration

## Initial configuration

In the initial configuration, the software is installed on the Arduinos and the detection sets are defined. The definition of the detection sets pairs all detection devices with a fixed master so that several sets can be used at the same time without crosstalk.

## Preparatory steps

1. Make sure the Arduino IDE (https://www.arduino.cc/en/Main/Software) is installed
2. Copy the contents of the Arduino\libraries folder into the libraries folder of the working directory of the Arduino software (`%USERPROFILE%\Documents\Arduino`)
   The following folders are then contained in Arduino\libraries: RF24-master, SBNetwork-master
3. To check the installation of the driver for the Arduino connect the bare Arduino to the PC. For troubleshooting have a look at: https://sparks.gogo.co.nz/ch340.html or https://www.makershop.de/ch340-341-usb-installieren/ or search in the Web for „CH340 driver“
4. Define a set ID, this must be unique in the laboratory and must be entered later identically in all Arduinos of a detector set

## Upload and configuration for the detection devices

Information: Start with the configuration of the detection device's Arduinos. Only connect one Arduino on the PC during configuration.

Connect the PC to the USB port on the Arduino Nano with installed custom-made PCB (set all switches to OFF) and radio module

1. Open the file „CDC_Funk_MC_Multi_v19.ino“ at Arduino\CDC_Funk_MC_Multi_v19
2. Select the COM port at Tools > Ports > COM X
   2.1. If the port is not known: unplug the Arduino, display the port list, remind and close it. Plug in the Arduino and select the new entry in the port list
3. At the bottom right you should see Arduino Nano, ATmega328 (Old Bootloader) on COM X. If not: Select Tools > Board > Arduino Nano and select Tools > processor > ATmega328 (Old Bootloader)
4. Check if line 10 contains the following: bool client = true; // Save bool for client/master
5. Set the desired trigger mode in line 11: for Prince: ce_ms = false; for Agilent: ce_ms = true
6. Set the desired measurement mode in line 13: for single-ended mode: differential = false, for differential measurement mode: differential = true
7. Upload CDC_Funk_MC_Multi_v19.ion with the arrow button „→„ or use Sketch > Upload; Success is confirmed by a message “Upload completed” below the sketch.
8. Set the detection device ID according to: switch 2 adds 1 to CDC1 → CDC2; switch 3 adds 2, switch 4 adds 4; switch 5 on ON activates the radio module.
   All options:

| S 2 | S 3 | S 4 | Name | S 2 | S 3 | S 4 | Name |
|---|---|---|---|---|---|---|---|
| OFF | OFF | OFF | CDC1 | OFF | OFF | ON | CDC5 |
| ON | OFF | OFF | CDC2 | ON | OFF | ON | CDC6 |
| OFF | ON | OFF | CDC3 | OFF | ON | ON | CDC7 |
| ON | ON | OFF | CDC4 | ON | ON | ON | CDC8 |

   Leave switch 5 on OFF for configuration
   It is only necessary for the configuration of the CDC8 that a detector is plugged in and supplied with voltage.

9. Open the serial monitor (magnifying glass at the top right), select 19200 baud in the new window at the bottom right

   The output should be:

```
Firmware:CDC_Funk_MC_Multi_v19
Hello at CDCX
SetupRadio is active
Enter 'N_X' to reset the wireless device and set it to client-master-set X
Prince Trigger-Mode (2 wire connection)
CDCX
…
```

   If X does not correspond to the set value: set the switches again and press the reset button on the Arduino.

   For CDC8 a different output is displayed:

```
Firmware:CDC_Funk_MC_Multi_v19

Hello at CDC 8
Please make sure that a detector with power supply is connected to configure
CDC8 or use a CDC in USB-only mode, in the latter case CDC is always named
CDC1
„„„„ Enter 'N_X' to reset the wireless device and set it to client-master-set
X
Prince Trigger-Mode (2 wire connection)
Init...Get offset
…
done
CDC1;373;0;8396142
```

10. Configuration of the set ID „S“: Enter N_“S“ in the input field above the output in the serial monitor and confirm with „Enter“

    The output should be: (here: „S“ = 9 and X = 2)

```
Erasing device configuration data...Done
SBNetwork Version 1.0.5
====================
Try to read device config from internal flash...Failed
Creating new device config and stroing it to internal flash...
Done
Device MAC = 0x5 0x4 0x4 0x9 0x2
Master MAC = 0x0 0x0 0x0 0x0 0x0
NetKey = 0
Initializing NRF24L01 transmitter...Done
Try to connect to master...Warning - Not paired to a master
```

11. Unplug the USB cable from the Arduino and set switch 5 to ON, radio is activated, connect the detection head

For additional detection devices it is in general possible to skip the steps 2 – 7. Doublecheck step 8 for each detection device to prevent identical IDs.

## Upload and configuration for the master

Start analogously to steps 1-4 of section „Upload and configuration for the detection devices„:

5. Set line 10 for a master to: bool client = false; // Save bool for client/master
6. Set the desired trigger mode in line 11 : for Prince: ce_ms = false; for Agilent: ce_ms = true
7. Upload CDC_Funk_MC_Multi_v19.ion with the arrow button „→„ or use Sketch > Upload; Success is confirmed by a message „Upload completed“ below the sketch.
8. Open the serial monitor (magnifying glass at the top right), select 19200 baud in the new window at the bottom right

   Output:

```
Firmware:CDC_Funk_MC_Multi_v19
Enter 'N_X' to reset the wireless device and set it to client-master-set X
„„„„ PRESS 'E' to handle the switch of adding new clients
Hello at CDC0
Prince Trigger-Mode (2 wire connection)
SBNetwork Version 1.0.5
====================

Try to read device config from internal flash...Done
Device MAC = 0x5 0x4 0x4 0x8 0x0
Master MAC = 0x0 0x0 0x0 0x0 0x0
NetKey = 0
Masterstorage Slot 0 0x5 0x4 0x4 0x8 0x1
Masterstorage Slot 1 0x0 0x0 0x0 0x0 0x0
Masterstorage Slot 2 0x0 0x0 0x0 0x0 0x0
Masterstorage Slot 3 0x0 0x0 0x0 0x0 0x0
Masterstorage Slot 4 0x0 0x0 0x0 0x0 0x0
Masterstorage Slot 5 0x0 0x0 0x0 0x0 0x0
Masterstorage Slot 6 0x0 0x0 0x0 0x0 0x0
Masterstorage Slot 7 0x0 0x0 0x0 0x0 0x0
Masterstorage Slot 8 0x0 0x0 0x0 0x0 0x0
Masterstorage Slot 9 0x0 0x0 0x0 0x0 0x0
Initializing NRF24L01 transmitter...Done
```

9. Configuration of the set ID „S“: Enter N_“S“ in the input field above the output in the serial monitor and confirm with „Enter“

   The output should be: (here: „S“ = 9)

```
Erasing device configuration data...Done
SBNetwork Version 1.0.5
====================

Try to read device config from internal flash...Failed
Creating new device config and stroing it to internal flash...
Done
Device MAC = 0x5 0x4 0x4 0x9 0x0
Master MAC = 0x0 0x0 0x0 0x0 0x0
NetKey = 0
Creating new Master Storage
Masterstorage Slot 0 0x0 0x0 0x0 0x0 0x0
Masterstorage Slot 1 0x0 0x0 0x0 0x0 0x0
Masterstorage Slot 2 0x0 0x0 0x0 0x0 0x0
Masterstorage Slot 3 0x0 0x0 0x0 0x0 0x0
Masterstorage Slot 4 0x0 0x0 0x0 0x0 0x0
Masterstorage Slot 5 0x0 0x0 0x0 0x0 0x0
Masterstorage Slot 6 0x0 0x0 0x0 0x0 0x0
Masterstorage Slot 7 0x0 0x0 0x0 0x0 0x0
Masterstorage Slot 8 0x0 0x0 0x0 0x0 0x0
Masterstorage Slot 9 0x0 0x0 0x0 0x0 0x0
Initializing NRF24L01 transmitter...Done
„„„„„„
Configuration:Master client-master-set-number:9 Device-Number: 0
„„„„„„
```

10. Activation of the automatic detection device adding (all detection device that should not be connected to the master must not be in use): Enter „E“ in the input field above the output in the serial monitor and confirm with Enter
    Output:

    ```
    „„„„„„
    Activating AutomaticClientAdding
    „„„„„„
    ```

11. Power one detection device after the other. The master's output displays:

    ```
    Received 'SEARCH_MASTER'. Send MasterACK...Done
    Received 'PAIRING_REQUEST'. Send PairingACK... Done
    Storing new MAC to MasterStorage... Done
    CDC1;8388608;0;13195058
    …
    Received 'SEARCH_MASTER'. Send MasterACK...Done
    Received 'PAIRING_REQUEST'. Send PairingACK... Done
    Storing new MAC to MasterStorage... Done
    CDC2;8388608;0;13030720
    ```

    etc.
12. Enter „E“ in the input field above the output in the serial monitor and confirm with Enter to disable the automatic detection device adding, after adding all detector devices.
    Output:

    ```
    „„„„„„
    Deactivating AutomaticClientAdding
    „„„„„„
    ```

13. Disconnect the master from the USB cable
14. Configuration is finished

## Follow-up configuration – detection device

Note: Only connect one Arduino on the PC during configuration.

1. Connect the PC to the USB port on the Arduino Nano with installed custom-made PCB (switch 4 on OFF) and radio module
2. Open Arduino IDE
3. Select the COM port at Tools > Ports > COM X
   - If the port is not known: unplug the Arduino, display the port list, remind and close it. Plug in the Arduino and select the new entry in the port list
4. Set the detection device ID according to: switch 2 adds 1 to CDC1 → CDC2; switch 3 adds 2, switch 4 adds 4; switch 5 on ON activates the radio module.

   All options:

| S 2 | S 3 | S 4 | Name | S 2 | S 3 | S 4 | Name |
|---|---|---|---|---|---|---|---|
| OFF | OFF | OFF | CDC1 | OFF | OFF | ON | CDC5 |
| ON | OFF | OFF | CDC2 | ON | OFF | ON | CDC6 |
| OFF | ON | OFF | CDC3 | OFF | ON | ON | CDC7 |
| ON | ON | OFF | CDC4 | ON | ON | ON | CDC8 |

   Leave switch 5 on OFF for configuration

   It is only necessary for the configuration of the CDC8 that a detector is plugged in and supplied with voltage.

5. Open the serial monitor (magnifying glass at the top right), select 19200 baud in the new window at the bottom right

   The output should be:

```
 Hello at Number: X
„„„„ PRESS 'N_4' to reset the wireless device and set it to client-master-set
4,
if no confirmation is displayed, retry it with disabled Network
Init...done
CDCX
```

   If X does not correspond to the set value: set the switches again and press the reset button.

6. Configuration of the set ID *S*: Enter N_*S* in the input field above the output in the serial monitor and confirm with “Enter”

   The output should be: (here: *S* = 9 and X = 2)

```
Erasing device configuration data...Done
SBNetwork Version 1.0.5
====================
Try to read device config from internal flash...Failed
Creating new device config and stroing it to internal flash...
Done
Device MAC = 0x5 0x4 0x4 0x9 0x2
Master MAC = 0x0 0x0 0x0 0x0 0x0
NetKey = 0
Initializing NRF24L01 transmitter...Done
Try to connect to master...Warning - Not paired to a master
```

7. Unplug the USB cable from the Arduino and set switch 5 to ON, radio is activated, connect the detection head

## Reset of the master device

Note: all previously trained detector devices will be deleted

Procedure analogous to steps 1 - 3 of the “Follow-up configuration – detection device”

4. All coding switches are set to OFF or are not installed.
5. Open the serial monitor (magnifying glass at the top right), select 19200 baud in the new window at the bottom right

   Output:

```
Firmware:CDC_Funk_MC_Multi_v19
„„„„ Enter 'N_X' to reset the wireless device and set it to client-master-set
X
„„„„ PRESS 'E' to handle the switch of adding new clients
Hello at CDC 0
Prince Trigger-Mode (2 wire connection)
SBNetwork Version 1.0.5
====================

Try to read device config from internal flash...Done
Device MAC = 0x5 0x4 0x4 0x9 0x0
Master MAC = 0x0 0x0 0x0 0x0 0x0
NetKey = 0
Masterstorage Slot 0 0x5 0x4 0x4 0x8 0x1
Masterstorage Slot 1 0x0 0x0 0x0 0x0 0x0
Masterstorage Slot 2 0x0 0x0 0x0 0x0 0x0
Masterstorage Slot 3 0x0 0x0 0x0 0x0 0x0
Masterstorage Slot 4 0x0 0x0 0x0 0x0 0x0
Masterstorage Slot 5 0x0 0x0 0x0 0x0 0x0
Masterstorage Slot 6 0x0 0x0 0x0 0x0 0x0
Masterstorage Slot 7 0x0 0x0 0x0 0x0 0x0
Masterstorage Slot 8 0x0 0x0 0x0 0x0 0x0
Masterstorage Slot 9 0x0 0x0 0x0 0x0 0x0
Initializing NRF24L01 transmitter...Done
CDC1;556;0;8396837
```

6. Configuration of the set number *S*: Enter N_*S* in the input field above the output in the serial monitor and confirm with “Enter”
   Output: (here: *S* = 9)

   Output:

```
Erasing device configuration data...Done
SBNetwork Version 1.0.5
====================

Try to read device config from internal flash...Failed
Creating new device config and stroing it to internal flash...
Done
Device MAC = 0x5 0x4 0x4 0x9 0x0
Master MAC = 0x0 0x0 0x0 0x0 0x0
NetKey = 0
Creating new Master Storage
Masterstorage Slot 0 0x0 0x0 0x0 0x0 0x0
Masterstorage Slot 1 0x0 0x0 0x0 0x0 0x0
Masterstorage Slot 2 0x0 0x0 0x0 0x0 0x0
Masterstorage Slot 3 0x0 0x0 0x0 0x0 0x0
Masterstorage Slot 4 0x0 0x0 0x0 0x0 0x0
Masterstorage Slot 5 0x0 0x0 0x0 0x0 0x0
Masterstorage Slot 6 0x0 0x0 0x0 0x0 0x0
Masterstorage Slot 7 0x0 0x0 0x0 0x0 0x0
Masterstorage Slot 8 0x0 0x0 0x0 0x0 0x0
Masterstorage Slot 9 0x0 0x0 0x0 0x0 0x0
Initializing NRF24L01 transmitter...Done
„„„„„„
Configuration:Master client-master-set-number:9 Device-Number: 0
„„„„„„
```

7. Activation of the automatic detection device adding (all detection device that should not be connected to the master must not be in use): Enter “E” in the input field above the output in the serial monitor and confirm with Enter
   Output:

```
„„„„„„
Activating AutomaticClientAdding
„„„„„„
```

8. Power one detection device after the other. The master’s output displays:

```
Received 'SEARCH_MASTER'. Send MasterACK...Done
Received 'PAIRING_REQUEST'. Send PairingACK... Done
Storing new MAC to MasterStorage... Done
CDC1;8388608;0;13195058
…
Received 'SEARCH_MASTER'. Send MasterACK...Done
Received 'PAIRING_REQUEST'. Send PairingACK... Done
Storing new MAC to MasterStorage... Done
CDC2;8388608;0;13030720
```

   etc.

9. Enter “E” in the input field above the output in the serial monitor and confirm with Enter to disable the automatic detection device adding, after adding all detector devices.
   Output:

```
„„„„„„
Deactivating AutomaticClientAdding
„„„„„„
```

10. Disconnect the master from the USB cable
11. Configuration is finished

## Add additional detection devices to a master

Prepare the detection device with the same set ID as all other detection device according to the item “Upload and configuration for the detection devices” or “Follow-up configuration – detection device”.

Then continue according to “Reset of the master” WITHOUT performing step 6

Note: Another client can be added in while other clients are in operation

# Hardware

A CDCD-set can consist out of two different devices which in turn consist of individual units:

1.) Detection device:
    - detection head
    - supply unit
2.) Master device (only needed with wireless data transmission)

A CDCD-set consist of a master device and up to 8 detection devices.

The different hardware configurations of the detection head and the supply unit are described in the chapters “Building instructions for detection head” and “Building instructions for the supply unit”

## Known hardware problems

| Error pattern | Solution |
|---|---|
| Data is received very rarely (frequency below 10 Hz) | Try another position of the master or detection device supply unit |
| The Arduino's pins get warm | Check whether there is no short circuit (start with: 3V3 against GND on the Arduino if there is a connection, remove the radio module and check again. If there is no more short circuit: replace the radio module) |

## Building instructions for detection head

1. Detach of the 4 mini-PCBs on the right of Figure 3 the result is shown in Figure 4.

A B

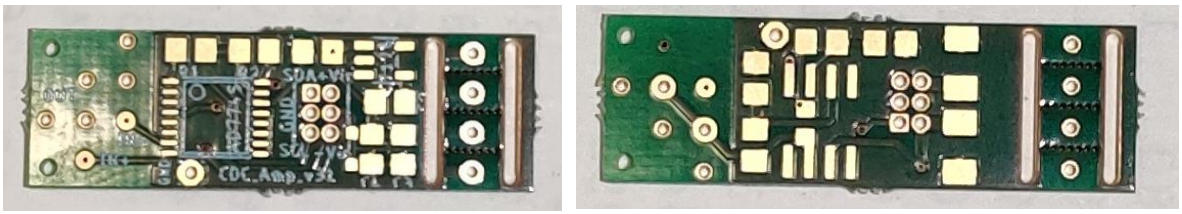

*Figure 3: Images of the (A) top and (B) bottom of the entire detection head's PCB.*

A B

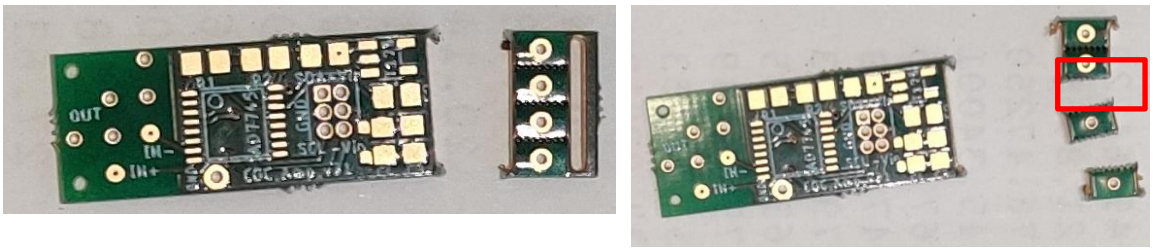

*Figure 4: Images of the detection head circuit board with detached mini circuit boards. One of the further used mini PCBs is outlined in red.*

2. Solder the required components according to Table 2 onto the larger PCB. The schematics is displayed in Figure 5. The equipped top and bottom of the detection head's PCB with and without installed amplifier can be found in Figure 6.

A B

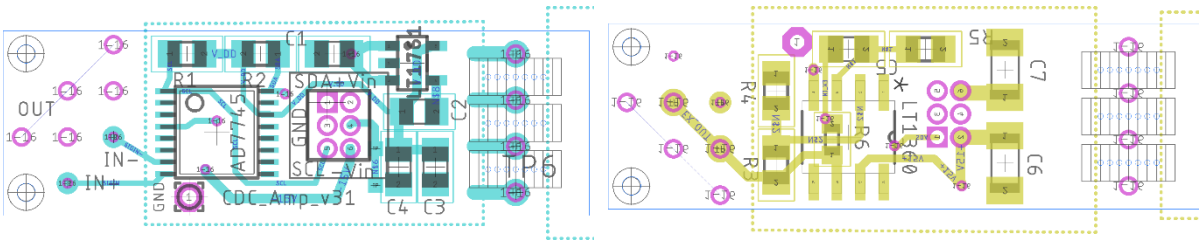


*Figure 5: Schematics of the (A) top and (B) bottom of the detection head's PCB.*

*Table 2: Components of the detection head*

Top:

| Part | Value | Package |
|---|---|---|
| AD7745 | AD7745 | TSSOP16 |
| LT1761-5 | LT1761 | SOT23-5 |
| C1 | 1u | C0805 |
| C2 | 10n | C0805 |
| C3 | 10u | C0805 |
| C4 | 100n | C0805 |
| JP1 | FTSH-103-01-F-D | |

Bottom:

Configuration 1 and 3 (no Amplifier):

solder pads of R6 together

Configuration 2 and 4 (with amplifier):

| Part | Value | Package |
|---|---|---|
| LT1360 | LT1360CS8PBF | |
| C5 | 100n | C0805 |
| R3 | 51k | R0805 |
| R4 | 10k | R0805 |
| R5 | 10k | R0805 |
| C6 | reserved | C1206K |
| C7 | reserved | C1206K |

Information: The head could also be supplied by the 5 V line of the Arduino, if the jumper Vopt|VA on the supply unit of the detection unit is connected and the test pad next to the upper pad of C4 is linked, see Figure 5

A 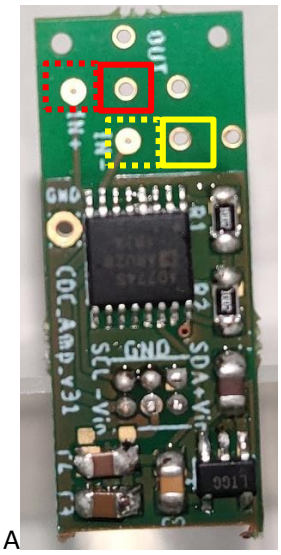

B 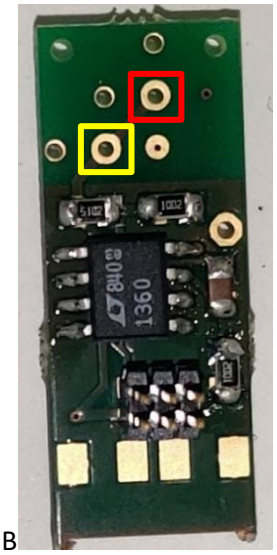

C 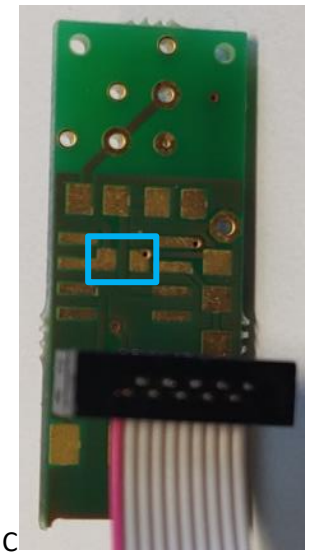

*Figure 6: Images of the equipped (A) top and (B+C) bottom of the detection head's PCB with (B) and without (C) amplifier (link between the two pads in the blue box is missing)*

3. Prepare the cannula segments by cutting a cannula to the desired length. Inset a capillary during cutting. Use cannulas with inner diameter of 0.4 mm (outer diameter 0.6, Gauge 23).

*Figure 7: A pair of cannulas cut to a length of 10 mm each on a 360 µm outer diameter capillary.*

4. Solder one cannula segment to the PCB of the detection head (outlined in red in Figure 6) and one to the mini-PCB. The soldering joint must be on the side with the larger soldering pad this is also the side where the electrode sticks out. The other side of the electrode should be at the same level as the PCB. The result is shown in Figure 8. For setups in differential measurement mode, a second pair of electrodes are mounted in the same way but to the yellow outlined boxes in Figure 6

A 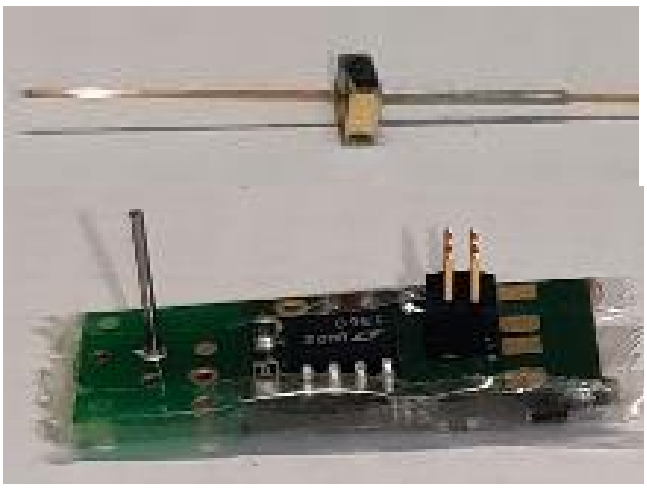
B 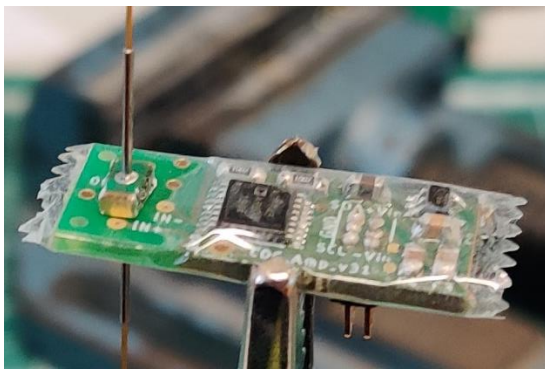

*Figure 8: (A) mini-PCB and large PCB equipped with electrodes. The larger PCB is wrapped in transparent adhesive tape to prevent short circuits. The mini-PCB with an electrode is equipped with a capillary. (B) Both PCBs just before soldering them together (golden side of the mini-PCB and the pad next to the label IN+)*

5. After wrapping the larger PCB in transparent adhesive tape, punch a hole with a needle in the tape, where the capillary must pass it.

6. Solder the mini-PCB to the larger PCB, it is important to solder the golden side connected electrically to the electrode of the mini-PCB to the pad connected to the input of the CDC-IC. The mounting pad IN+ is dotted outlined in red in Figure 6. The tape covering the mounting pad has not to be removed since it will melt during the soldering process anyway. Insert a capillary trough both electrodes while soldering.

7. Use heat shrink tubing to cover the electrodes and carefully wrap the PCBs with a layer of transparent adhesive tape. Keep the tape away from the golden side of the large PCB.

A

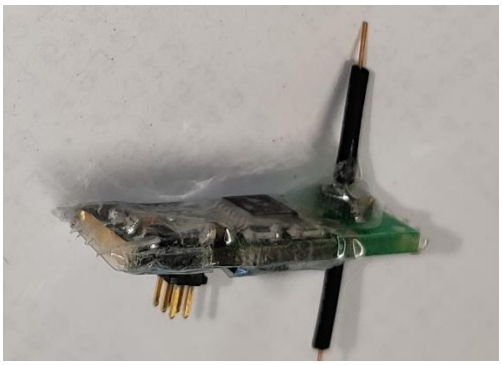

B

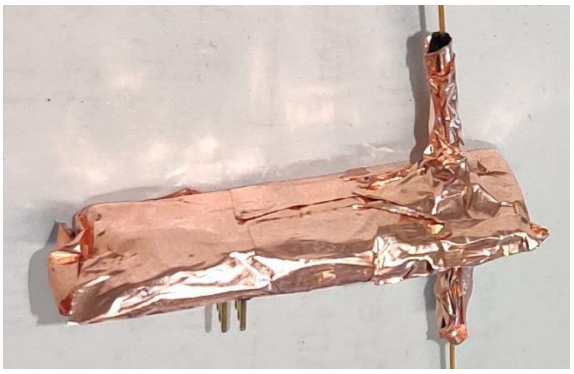

*Figure 9: detection head (A) before and (B) after wrapping with adhesive copper foil*

8. Wrap the detector carefully with adhesive copper foil, solder it to the golden side of the large PCB to connect it to ground. If necessary, solder the individual layers of the outer copper layer together to ensure proper electrical connection among themselves.

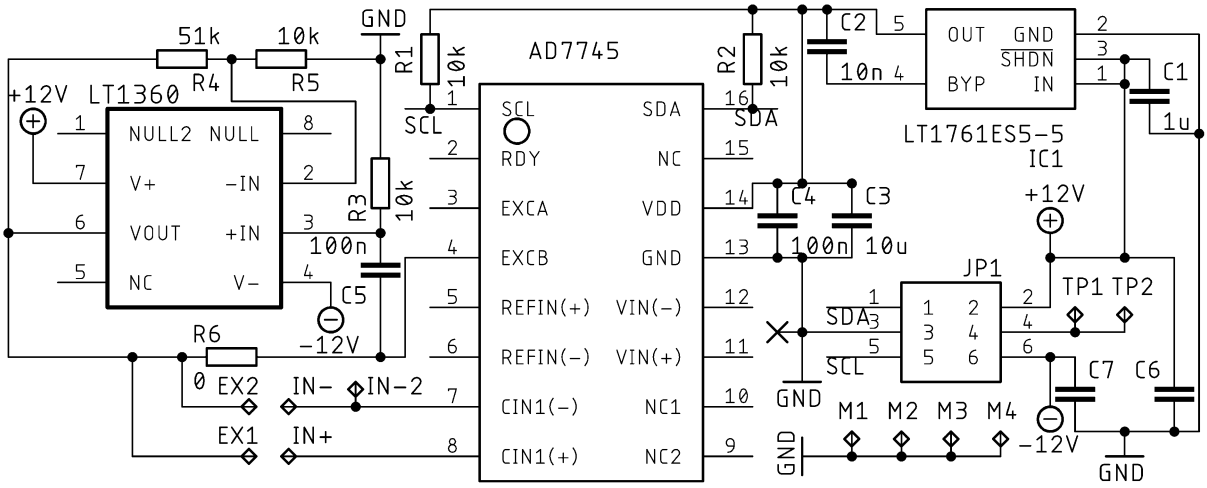


*Figure 10. Schematic diagram of the detection head's circuit. Capacitors without values are reserved. Resistor R6 is a jumper.*

## Building instructions for the supply unit

The supply unit consists except for a PCB described below out of an Arduino Nano and a NRF24L01+ radio module. It provides pins for the connection to the detection head as well as an optional PCB terminal block for a trigger signal with an additional 5 V output. The DIP-switches on the supply unit are used for configuration.

The necessary components on the supply unit depending on the desired configuration can be taken from the figures in this section.

Fully annotated PCB of a supply unit:

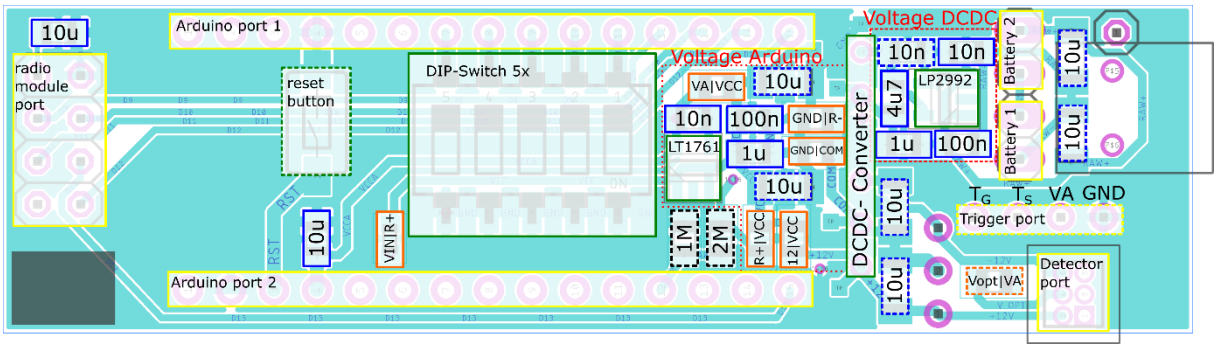


Color code: yellow: connectors; green: IC, buttons, and switches; black: resistors; blue: capacitors; orange: jumpers

Information: the dashed outlined 1 MΩ and 2 MΩ resistors are optional and allow tracking of the battery voltage.

Information: the dashed outlined reset button and the trigger port PCB block terminal are optional as well as all dashed outlined 10 µF capacitors.

Information: the dashed outlined 10 nF capacitor in Voltage DCDC is necessary if LP2992-5 is replaced by an LT1761-5. Further, the solid outlined 10 nF capacitor must not be installed and the 4.7 µF capacitor must be replaced by a 10 µF capacitor.

Information: The detection head can also be supplied directly from the 5 V supplying the Arduino by linking the dashed outlined jumper Vopt|VA

## Supply unit of a master device

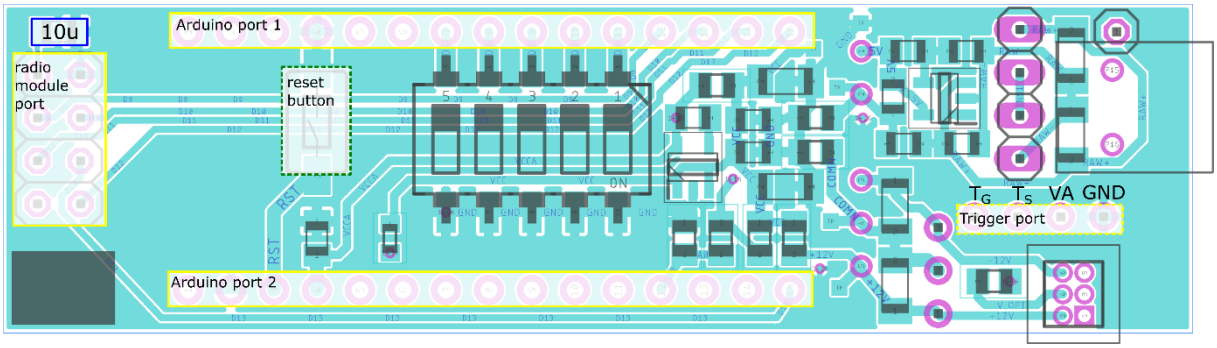

## Supply units for wired data transmission

Configuration 1: Use of only one client without radio and without amplifier [performance not tested]

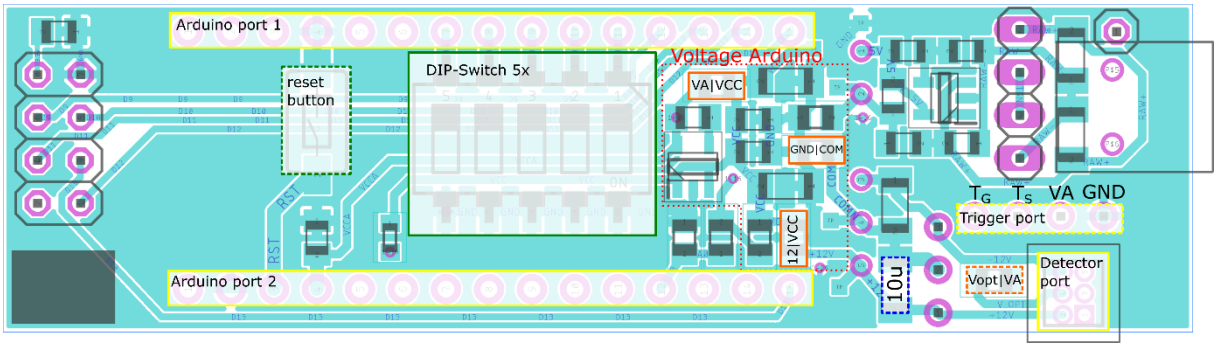


Configuration 2: Use of only one client without radio and with amplifier [performance not tested]

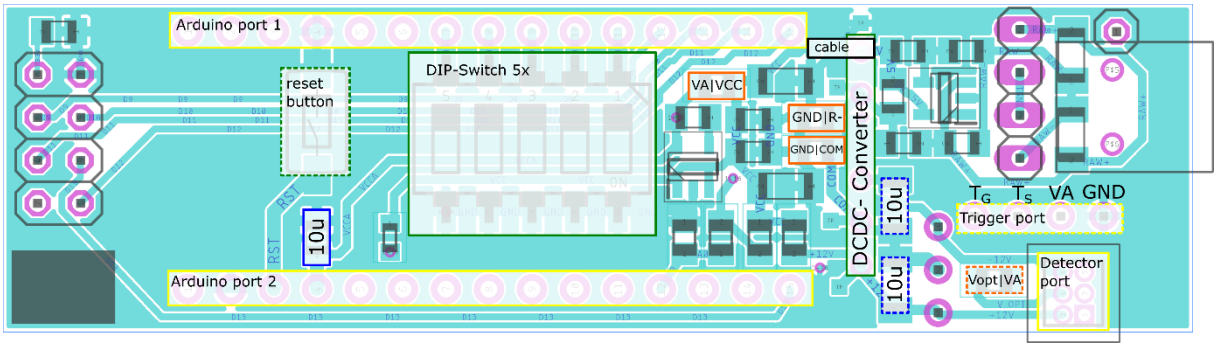


## Supply units for wireless data transmission and battery supply:

Configuration 3: Usage without amplifier

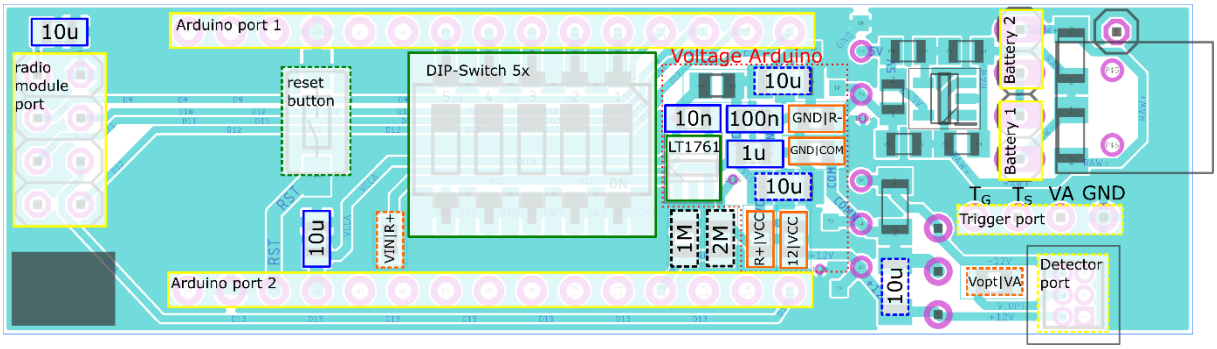


Configuration 4: Usage with amplifier

a) galvanic separation from the input voltage (the setup is powered entirely through the DCDC-Converter):

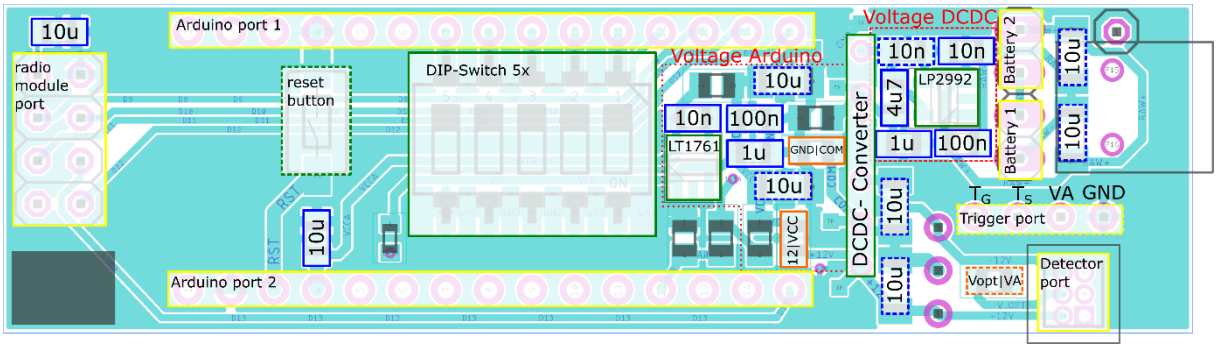

b) Supply Arduino via LT1761 from batteries

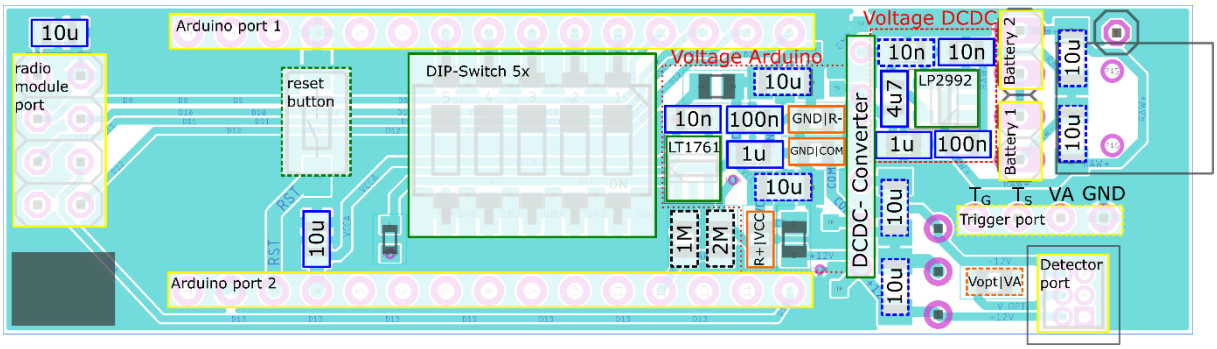


c) Supply Arduino via its own voltage regulator [performance not tested]

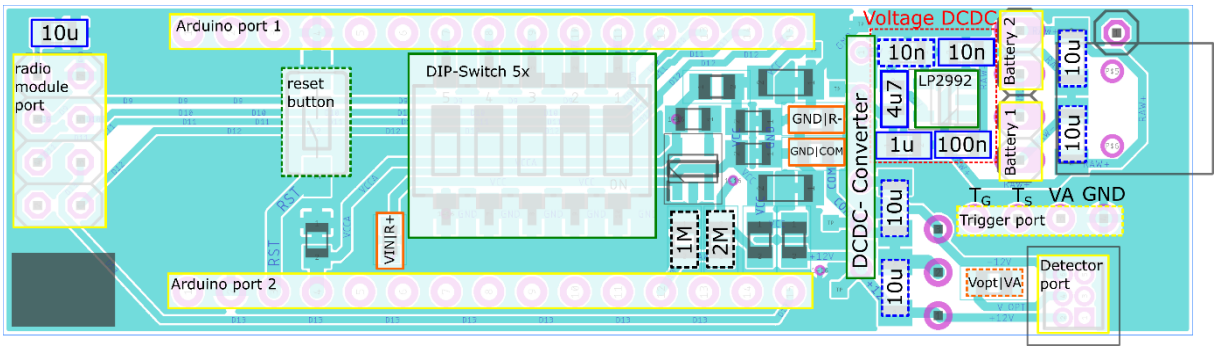


d) Supply Arduino via LP2992: (this setup also allows a wired or wireless data transmission which is powered via the 5 V line of the Arduino (Configuration 2)) [performance not tested]

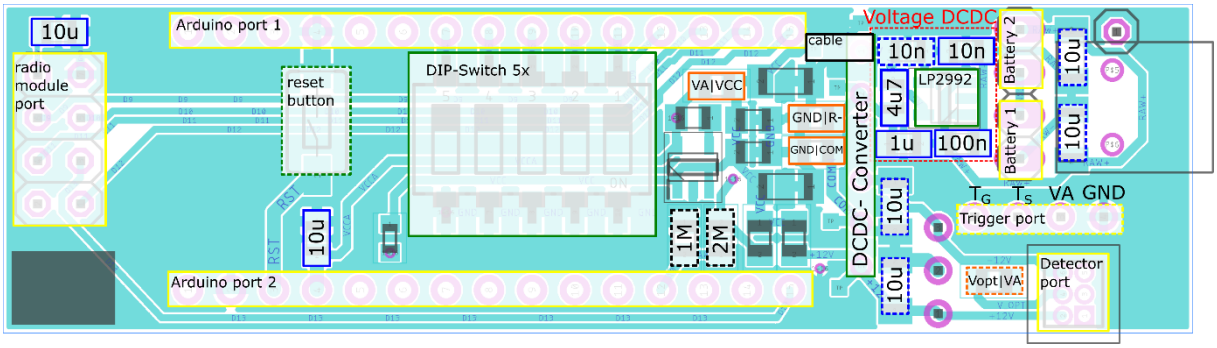

## Images of a supply unit in configuration 4d, Arduino is supplied via LP2992

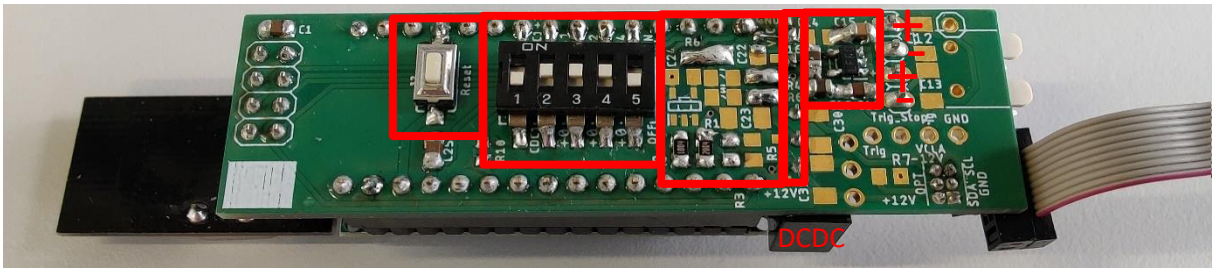


*Figure 11. Supply unit of detection device – top*
*Left: Reset-Taster*
*Center left: DIP-switch. switch 2-4 to configure id; switch 5: enable radio module (switch on OFF)*
*Center: Area for voltage regulator for Arduino and resistors (with values 1M, 2M), here Arduino powered directly from LP2992 (VA|VCC are linked and a wire is installed between the test pad next to the print VCC and Pin 1 of the DCDC; see top right corner)*
*Center right: DCDC solder pads*
*Right: Area for voltage regulator for DCDC-converter*
*"+" and "-" denote the polarities of two in series connected ports for the batteries (3.7 V each)*

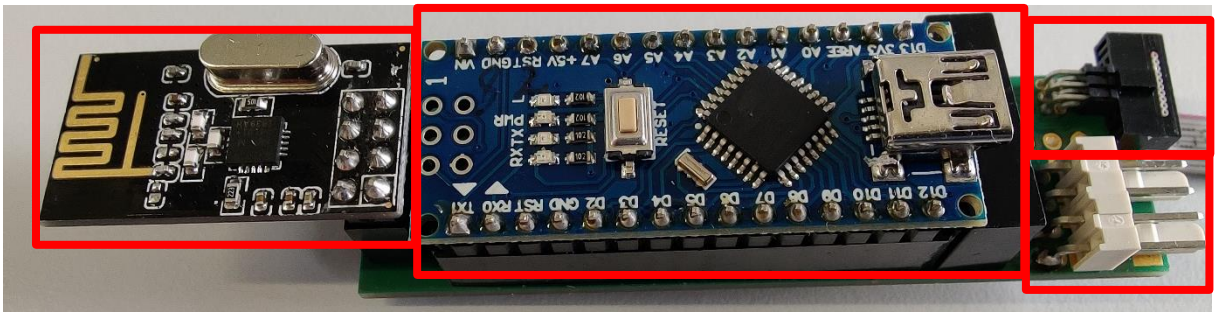


*Figure 12. Supply unit of detection device – bottom, equipped Left: radio module*
*Center: Arduino Nano*
*Top right: connector for 10-core ribbon cable to detection head*
*Bottom right: two connectors to attach the necessary pair of batteries (2x 3.7 V)*

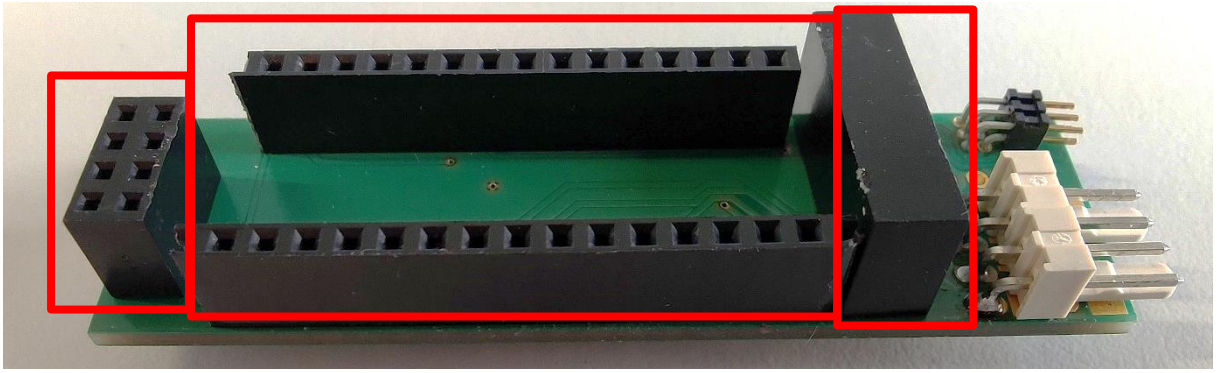

*Figure 13. Supply unit of detection device – bottom*
*Left: 2x4 socket for radio module*
*Center: 2x 1x15 socket for Arduino Nano*
*Right: DCDC-Converter*

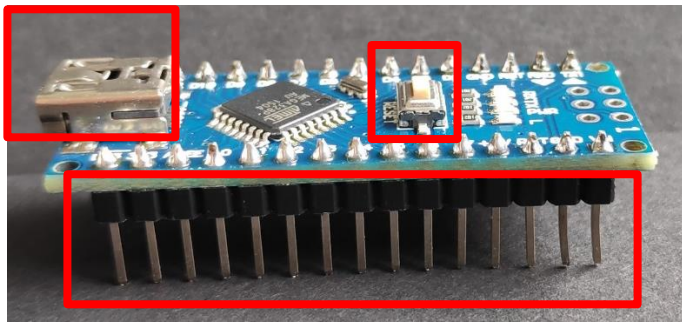

*Figure 14. Arduino Nano Top*
*Left: Mini-USB port for configuration or communication and supply in case of wired data communication*
*Top right: Reset-Button, restarts Arduino*
*Bottom: Pins*

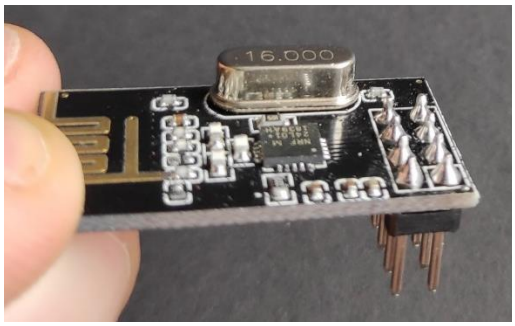

*Figure 15.Radio module (NRF24L01)*
*Bottom right: Pins 2x4*

## Scheme of the supply unit's circuit

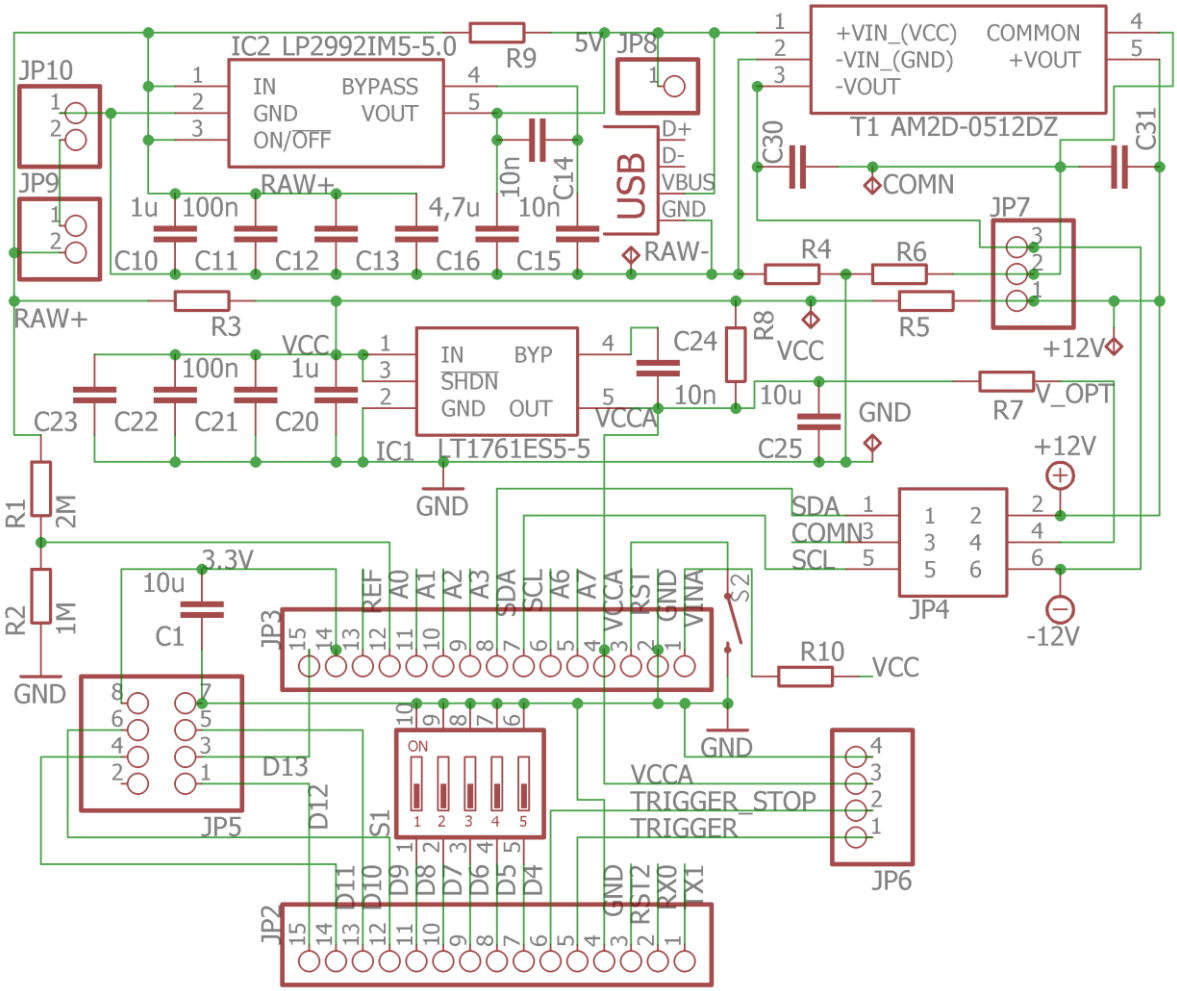

# Appendix III

**Paper 2:**

Graf, H. G., Biebl, S. M., Müller, L., Breitenstein, C., Huhn, C., Capillary electrophoresis applied for the determination of acidity constants and limiting electrophoretic mobilities of ionizable herbicides including glyphosate and its metabolites and for their simultaneous separation. *Journal of Separation Science* 2022; *45*, 1128-1139, DOI: 10.1002/jssc.202100952

Received: 2 December 2021 | Revised: 30 December 2021 | Accepted: 31 December 2021

DOI: 10.1002/jssc.202100952

JOURNAL OF SEPARATION SCIENCE

RESEARCH ARTICLE

# Capillary electrophoresis applied for the determination of acidity constants and limiting electrophoretic mobilities of ionizable herbicides including glyphosate and its metabolites and for their simultaneous separation

**Hannes Georg Graf** | **Sonja Maria Biebl** | **Linda Müller** | **Christina Breitenstein** | **Carolin Huhn**

Institute of Physical and Theoretical Chemistry, Eberhard Karls Universität Tübingen, Tübingen, Germany

**Correspondence**
Carolin Huhn, Institute of Physical and Theoretical Chemistry, Faculty of Science, Eberhard Karls Universität Tübingen, Auf der Morgenstelle 18, 72076 Tübingen, Germany.
Email: carolin.huhn@uni-tuebingen.de

**Funding information**
Deutsche Forschungsgemeinschaft, Grant/Award Number: SFB 1253/1 2017; Collaborative Research Center 1253 CAMPOS (Project 4: Floodplain Biogeochemistry)

Thermodynamic acidity constants and limiting ionic mobilities were determined for polyprotic non-chromophore analytes using capillary electrophoresis with capacitively coupled contactless conductivity detection. It was not necessary to work with buffers of identical ionic strength as ionic strength effects on effective electrophoretic mobilities were corrected by modeling during data evaluation (software AnglerFish). The mobility data from capillary electrophoresis coupled to conductivity detection were determined in the pH range from 1.25 to 12.02 with a high resolution (36 pH steps). With this strategy, thermodynamic acidity constants and limiting ionic mobilities for various acidic herbicides were determined, sometimes for the first time. The model analytes included glyphosate, its metabolites, and its acetylated derivates (aminomethyl phosphonic acid, glyoxylic acid, sarcosine, glycine, *N*-acetyl glyphosate, *N*-acetyl aminomethyl phosphonic acid, hydroxymethyl phosphonic acid). The obtained data were used in simulations to optimize separations by capillary electrophoresis. Simulations correlated very well to experimental results. With the new method, the separation of glyphosate from interfering components like phosphate in beer samples was possible.

**KEYWORDS**
analyte mixtures, conductivity detection, dissociation constant, simulation, transformation products

## 1 | INTRODUCTION

One of the key parameters of ionizable organic and inorganic compounds is their acidity (acid dissociation) constant, in the negative decadic logarithmic form indicated as $pK_a$. From a pharmaceutical and (eco)toxicological point of view, it influences their solubility, sorption, dissolution

**Article Related Abbreviations:** AcOH, acetic acid; AMPA, aminomethyl phosphonic acid; $C^4D$, capacitively coupled contactless conductivity detection; HMPA, hydroxymethyl phosphonic acid; MCPA, 2-methyl-4-chlorophenoxyacetic acid; $NH_4AcO$, ammonium acetate

rate, reaction kinetics, complexation, transfer across biological membranes, the speed of reaching the site of action, metabolism, protein binding, or receptor interactions. It is therefore one of the first parameters to be determined in the development of an active agent [1]. For their metabolites, especially for (microbial) transformation products in the environment, the knowledge on ionization constants is limited. Metabolites are often more acidic than their precursors, as metabolism has the goal of increasing water solubility in order to remove substances from the organism.

To determine p$K_a$ values, any physicochemical measure can be used which is affected by the pH. Potentiometric, spectroscopic, electrophoretic, or solubility-based methods, as well as theoretical methods, were used [2–6]. Potentiometric titrations are most often used because of their short analysis time (~20 min), but they have high requirements for the analyte's purity and fairly high LODs mostly around 0.5 mM [3, 4]. UV-visible (UV-Vis) spectrophotometry is more sensitive and can be applied when the spectra of neutral and ionized forms differ from each other in wavelength or intensity. Extreme pH values are accessible [3]. The chemical shift induced by ionization is utilized by nuclear magnetic resonance spectroscopy. Its great advantage is its applicability for mixtures including structurally related impurities. It is also possible to determine individual p$K_a$ values of functional groups, even in case of similar chemical shifts. The major drawbacks of this method are a systematic error when using constant volume titration [5, 6] and the expensive equipment.

For mixtures, capillary electrophoresis (CE) is well suited because it is a separation technique and the electrophoretic mobility of an ion is a function of the pH. Already in 1991, Beckers et al. used CE-UV to determine absolute mobilities and p$K_a$ values [7]. The advantages of using CE for p$K_a$ determination are its applicability for a broad range of analytes as a sufficient solubility in water is probably the only relevant criterion for analytes' physicochemical properties (depending, of course, on the detection method applied). The sample can be impure, the solubility in water can be low, prior knowledge of the analyte concentration is not required and the sample consumption is low. Further, the high degree of automation enables multiplexed assays [8, 9]. Two illustrative examples demonstrated CE's capabilities in p$K_a$ determination: (1) the identification of the main tautomer of 5-azacytosine derivatives, a potential antiviral agent, in combination with density functional theory calculations [10] and (2) the possibility to identify the effect of substituent positions on the charge of drugs under physiological conditions [11]. Two major strategies evolved: (1) the p$K_a$ of monoprotic acids or bases can rapidly be determined from two CE runs at different pH by injecting the analyte together with a reference compound of similar p$K_a$ ($\Delta$p$K_a$ < 1). The runs are performed with the substances fully or partially ionized in the background electrolyte (BGE) [12]. (2) However, for compounds with more complex speciation due to several acidic and/or basic functional groups, this method cannot be applied. Then, pH-dependent mobility measurements are required. In most studies, the ionic strength was kept constant over the entire pH range in order to avoid changes in electrophoretic mobility caused by effects other than the pH [13, 14]. For mobility and p$K_a$ determinations at very acidic conditions, the measured effective electrophoretic mobilities were corrected to constant ionic strength using Debye-Hückel-Onsager theory [15–17]. Recently, Maly et al. developed the software AnglerFish which corrects the electrophoretic mobilities for ionic strength effects at all pH values [18].

In this study, the negative decadic logarithmic thermodynamic acidity dissociation constants (p$K_a^\circ$) and limiting electrophoretic mobilities ($\mu_{lim}$) of various, mostly acidic herbicides like 2-methyl-4-chlorophenoxyacetic acid (MCPA), glufosinate , and glyphosate with its impressive pH speciation including its transformation products were determined at pH 1.25–12.02. The extremely wide pH range was enabled due to correcting electrophoretic mobilities concerning ionic strength effects by the AnglerFish software. Capacitively coupled contactless conductivity detection ($C^4D$) was used to enable their analyses despite the lack of a chromophoric system. The new data were finally used to optimize CE separations by simulations.

## 2 | MATERIALS AND METHODS

### 2.1 | Chemicals

We included herbicides, their transformation products, and other ionizable substances as model analytes: glyphosate (analytical grade), aminomethyl phosphonic acid (AMPA, 99 %), glycine (≥ 98 %), glyoxylic acid monohydrate (98 %), 4-methylmorpholine (≥99.5 %), 2-methyl-4-chlorophenoxyacetic acid (99.2 %), oxamic acid (≥ 98 %), and sarcosine (≥ 98 %) were purchased from Sigma-Aldrich (Steinheim, Germany). Glufosinate ammonium was purchased from Fluka (Buchs, Switzerland), *N*-acetyl aminomethyl phosphonic acid (*N*-acetyl AMPA) (95.5 %) and hydroxymethyl phosphonic acid (HMPA, 98.6 %) from Dr. Ehrensdorfer (Augsburg, Germany), and *N*-acetyl glyphoate (95 %) from Toronto Research Chemicals (Toronto, Canda).

Chemicals for BGEs were acetic acid (AcOH, 100%), aqueous ammonia solution ($NH_4OH$) for LC-MS 25%, ammonium acetate ($NH_4AcO$, ≥ 98%), formic acid (98–100%), phosphoric acid 85% (suprapur), *p*-toluenesulfonic acid (>98%), tricine (>99%) from Merck (Darmstadt,

Germany), and 2-(*N*-morpholino)ethane sulfonic acid monohydrate (>99.5%) from Fluka. Beta-alanine and 3-(*N*-morpholino)propane sulfonic acid (≥99.5%) were purchased from Alfa Aesar (Karlsruhe, Germany). Lithium hydroxide monohydrate (98.5–101.5%) was delivered by Sigma-Aldrich.

Capillaries were conditioned using hydrochloric acid 32% (Thermo Fisher Scientific, Schwerte, Germany), methanol (for LC-MS), and solutions of sodium hydroxide (≥98.0%, Merck). Propan-2-ol (for LC-MS) used in the sheath liquid was ordered from Carl Roth (Karlsruhe, Germany). Double-distilled water from a purification system from ELGA LabWater (Celle, Germany) was used in all solutions.

## 2.2 | Selection of analytes

We chose glyphosate as a challenging model analyte because of its many functional groups. In addition, it has no chromophore system precluding the use of spectrophotometric techniques as well as UV-Vis detection in CE. As glyphosate is the herbicide most heavily applied worldwide, also its transformation products from different degradation pathways are of interest [19, 20]. Glyphosate is either transformed into AMPA and glyoxylic acid by glyphosate oxidoreductase or into sarcosine and phosphate by carbon-phosphorus lyase. Further, glyphosate can be acetylated to *N*-acetyl glyphosate by glyphosate *N*-acetyltransferase in genetically modified crops which further degrades to *N*-acetyl AMPA. Glycine originates either from glyoxylic acid or sarcosine [21–26]. Another metabolite, rarely detected, is HMPA, which was observed in surface water [24]. Due to their similar physicochemical characteristics, the herbicides glufosinate and MCPA as well as oxamic acid, formed during ozonation from the herbicide chloridazon [27], were also included in this study. *N*-Methylmorpholine was included as a neutral to basic model compound. Its $pK_a^\circ$ and $\mu_{lim}$ are of interest since it is a promising BGE compound for CE but no data are available for simulation in literature.

## 2.3 | Instrumentation and methods

CE-$C^4D$ was performed using a Prince 560 capillary electrophoresis system from Prince Technologies (Emmen, The Netherlands) with WPrince 7.1.02.10.01 software. For conductivity detection, a commercial $C^4D$, an ET120 $C^4D$ Headstage for capillary electrophoresis, and an ER225 Contactless Conductivity $C^4D$ System, all from eDAQ (Denistone East, Australia), were used. The optimum settings for the detector were determined with the $C^4D$-Profiler, which is part of the PowerChrom 2.8.3 control software. The best settings for the $C^4D$ were a frequency of 300 kHz, an amplitude of 100%, and an activated head stage gain. These settings were applied when using BGEs in the pH range between 4 and 10. Higher frequencies (up to 1200 kHz) and lower amplitudes were necessary for other pH values. Fused silica capillaries were purchased from Polymicro Technologies (Phoenix, AZ, USA).

CE-MS was performed with a 7100 CE coupled via a commercial sheath liquid CE-ESI-MS interface, equipped with a platinum needle, to a 6150 single quadrupole mass spectrometer, all from Agilent Technologies (Waldbronn, Germany; Santa Clara, CA, USA). A coaxial sheath liquid flow, composed of 0.1% formic acid in 50% v/v propan-2-ol, was provided during analyses. It was supplied via splitter (1:100) by a 1200 series isocratic pump (Agilent Technologies) at a flow rate of 5 µL/min. The MS was operated in selected ion monitoring mode using the following operation parameters: capillary voltage, 3500 V negative; nebulizer pressure, 5 psi (during injection 1 psi); drying gas flow, 11 L/min; and drying gas temperature, 150°C. The exact masses of the pseudomolecular ions $[M\text{-}H]^-$ of the 12 acidic model analytes (see Table 1) were monitored simultaneously with an optimized fragmentor voltage of 125 V. The peak width was set to 0.3 min. Nitrogen gas was supplied by an NGM 44-LC/MS generator (cmc instruments, Eschborn, Germany). The control of the CE and MS instruments, as well as the data acquisition, were performed by ChemStation Rev. C. 01.05 software (Agilent Technologies).

The pH measurements were conducted with a WTW inoLab pH 7110 equipped with the pH-electrode SenTix 81. A 3-point calibration of the pH meter was carried out with buffers at pH 4.01, 7.00, and 10.01 from Carl Roth (Karlsruhe, Germany). Filtration of solutions was performed with 45 µm PTFE filters (Macherey-Nagel, Düren, Germany).

## 2.4 | Design of experiment and data evaluation

The determination of $pK_a^\circ$ and $\mu_{lim}$ values was performed by the free software AnglerFish [18]. Besides experimentally determined effective electrophoretic mobilities of the analytes in BGEs of different pH, it requires the BGEs' composition and initial estimates of the $pK_a^\circ$ and $\mu_{lim}$. Estimates of the $pK_a^\circ$ values were obtained via the website chemicalize.com from ChemAxon [28].

pH values in the range of pH 1 to 12 were selected with an increment of about 0.3 using the software PeakMaster [29]. The BGEs for the pH range 2–12 (ionic strength 10 mM; pH 12.02: 12 mM) were adopted from the model

BGEs described in the AnglerFish software [18]. For lower pH, BGEs with an ionic strength of 15 to 68 mM were used. After preparation, the pH values of the BGEs were controlled using a pH-electrode. The solutions were used immediately for CE measurements.

The effective electrophoretic mobility $\mu_{eff}$ was calculated from triplicate runs using the migration times $t_m$ of each analyte and the detection time of the injection zone with water as the electroosmotic flow (EOF) marker $t_{EOF}$. Using PeakMaster, we verified that the eigenmobility of the injection zone was negligible for all BGEs selected in our study [30]. The migration path length $l_m$ was determined as the distance between the inlet and the detector position ($l_{eff}$ = 33.3 cm) minus the length of half the sample plug ($l_{S/2}$ = 0.3 cm) and the BGE plug ($l_{BGE}$ = 1.6 cm) injected behind the sample. The plugs' lengths were calculated via Hagen-Poiseuille's law assuming that the solutions' viscosity equals the one of water at 25°C (0.891 mPa s). The electric field strength $E$)was 300 V/cm. The effective electrophoretic mobilities were then calculated as $\mu_{eff} = l_m \times (t_m^{-1} - t_{EOF}^{-1}) \times E^{-1}$. To compensate for slight errors in the preparation of the BGEs, the actual concentration of the weak base was recalculated by AnglerFish based on the measured pH.

## 2.5 | Samples, BGEs, and electrophoretic separations by CE-C$^4$D

The BGEs were prepared from aqueous filtered stock solutions. Each buffer consisted of lithium hydroxide and a second compound to achieve the desired pH. The final concentrations, the intended and measured pH values are given in Table S1. BGEs with pH > 8 were degassed at 50 mbar for 10 min prior to their use to reduce $CO_2$/carbonate concentrations. To avoid excessive currents for separations below pH 1.7, some parameters had to be adapted. They are added in parentheses in the following workflow. The samples were prepared from aqueous 10 mM analyte stock solutions and diluted with BGE. Analyte concentrations were 385 to 455 μM of each analyte and 75 –90% v/v BGE. Due to its low solubility in water, the MCPA concentration was limited to 96 μM. Separations were performed in a bare fused silica capillary with 50(25) μm id and 50 cm length. The effective length was 33.3 cm. Prior to its first use, the capillary was purged with methanol, 1 M aqueous hydrochloric acid solution, 1 M aqueous sodium hydroxide solution, and water for 30(60) min, each at 1 bar. At the transition between two BGEs, the capillary was flushed with 1 M aqueous sodium hydroxide solution and water, 5(10) min each, and 20(40) min with the new BGE at 1(2) bar. Prior to each analysis, the capillary was flushed at 1(2) bar with BGE for 5(10) min. The sample was injected for 7.2(21) s at 50(100) mbar followed by injecting a BGE plug for 18(36) s at 50(100) mbar. The separation was driven by a voltage of 15.0 kV (slope 6 kV/s) and a pressure of 70(150) (350 at pH < 1.7 for *N*-acetyl glyphosate, *N*-acetyl AMPA) mbar. The temperature was set to 25°C. Depending on the BGE's pH, the separation was achieved within 4–18 min. For the verification of simulations using a BGE at pH 9.5, the BGE plug injected after the sample plug was elongated to 1 min and the conditioning prior to each run was altered to rinsing subsequently with 0.1 M aqueous sodium hydroxide solution for 2 min, water for 1 min and BGE for 3 min, each at 1 bar.

## 2.6 | Samples, BGEs, and electrophoretic separation by CE-MS

The BGE for CE-MS (pH 6.1) contained 20 mM $NH_4OH$ and 20.78 mM AcOH. It was prepared from filtered stock solutions of 100 mM AcOH and 100 mM $NH_4AcO$ in water. The model samples were prepared from aqueous 10 mM analytes stock solutions in aqueous 10 mM $NH_4AcO$. The degassed beer (SUPERFREUNDE – Pils; SUPERFREUNDE, Hamburg, Germany) was filtered with a 45 μm PTFE filter (Macherey-Nagel, Düren, Germany). The final injected solution contained 80:20 v/v beer:water, 10 mM $NH_4AcO$, and spiked analyte. Separations were performed in a bare fused silica capillary with 50 μm id and 60 cm length. The capillary tip was sanded with 4000-grit sandpaper to an angle of 45° to improve the electrospray process. Prior to the first use, the capillary was purged with water and BGE for 10 min, each at 1 bar. The capillary was rinsed with BGE for 7 min at 1 bar between two runs. Samples were injected for 10 s at 50 mbar followed by a BGE plug injection for 7 s at 50 mbar. The separation was performed at 15.0 kV and pressure support of 70 mbar. The temperature was set to 25°C.

## 2.7 | Simulations using PeakMaster

The free software PeakMaster [29] was used to simulate CE separations. In order to select suitable separation conditions, the migration time of neutral species was first roughly estimated by using the EOF mobility in bare fused silica capillaries. After an experiment under the previously selected conditions, the migration time of water was determined and entered into PeakMaster to adjust the simulated electropherograms. Water was a suitable EOF-marker as the simulations showed a negligible eigenmobility of the injection zone for the selected BGE compositions.

## 3 | RESULTS AND DISCUSSION

### 3.1 | Choice of separation and detection methods for the determination of thermodynamic acidity constants and limiting electrophoretic mobilities

The selected analytes, compare Section 2.2, are mostly acids and have a negative charge over a wide pH range. Therefore, in capillaries with a negatively charged surface, such as bare fused silica capillaries, the movement of the EOF and the migration of the analytes take place in opposite directions. Ideally, the effective electrophoretic mobility of the analyte is determined from the migration times of the analyte and the EOF recorded in the same run. This requires either the reversal of the EOF by a positively charged capillary surface or a reversal of the separation voltage together with a counter-flow (EOF + pressure) high enough to bring both analytes and EOF marker to the detector. The use of a coated capillary to achieve a positively charged capillary surface was not considered because of the insufficient stability of coatings over a wide pH range [31].

There are also some restrictions regarding the detection methods: only one of the model analytes has a chromophore group, so only indirect UV-Vis detection would be an option, requiring a probe ion in the BGE. Mass spectrometry was not considered as a detection method since influences on pH and migration velocities by ions from the sheath liquid of the CE-MS interface cannot be excluded completely [32]. We chose to use CE-$C^4D$ with a positive separation voltage and pressure support of usually 70 mbar and a bare fused silica capillary as described in Section 2.5.

### 3.2 | Determination of thermodynamic acidity constants and limiting electrophoretic mobilities

The pH dependence of the effective electrophoretic mobilities of all analytes including the fit by Anglerfish software is shown in Figure 1. The error bars of the determined effective electrophoretic mobilities were too small to be shown in the figure. Despite some challenges during the detection of peaks, see Section 3.3, excellent electrophoretic mobility data at a high resolution were acquired for analytes with challenging properties proven by $R^2 \geq 0.98$ of the fit for all analytes. This allowed determining precisely $pK_a^\circ$ and $\mu_{lim}$ data by the AnglerFish software (see Table 1). A narrow gradation in pH helped to identify the analyte peaks and reduced the influences by outliers and undetectable analyte peaks on the results.

### 3.3 | Influences on peak detection

The most challenging task during the evaluation was the low resolution between the peak caused by the EOF marker and the analyte when the effective electrophoretic mobility of the analyte was close to zero. In addition, some analyte peaks were not observed at specific pH values due an insufficient conductivity difference between the BGE and the analyte (e.g. AMPA pH 3.54–4.17; glufosinate pH 2.65 + 3.24; MCPA pH 5.35–8.32; oxamic acid pH 2.65–3.24,4.48, 4.77; glyoxylic acid pH 1.86; glycine pH 8.99, 10.525; *N*-acetyl AMPA pH 1.80, 2.66, 3.03). The most critical analyte in this regard was oxamic acid in the range from pH 2.65 to 3.24 since its $pK_a^\circ$ is 1.9. Further, distortions of the peaks by superposition with system peaks (e.g. glyphosate pH 11.35, 11.67; AMPA pH 11.05, 12.02; HMPA pH 9.93–11.87) were observed. At pH 7.41, HMPA and oxamic acid comigrate. To reduce comigration of analytes, several runs were made with subsets of analytes, or analytes were excluded, when no changes in the effective electrophoretic mobility were expected in a specific pH range (glyoxylic acid at pH 9.93 and 10.25; oxamic acid pH > 8.4; MCPA pH > 11.35).

The mobility of phosphate was measured in the pH range of 3.8–10.8 as well as in a tosylate BGE at pH 2.1. Data for *N*-methylmorpholine were evaluated between pH 4.5 and 9.7 as only one $pK_a^\circ$ was predicted. For both analytes, a lower pH increment was used where no significant mobility change was expected (compare Figure 1) to reduce experimental effort.

### 3.4 | Comparison of thermodynamic acidity constants data and limiting electrophoretic mobilities data to literature data

The $pK_a^\circ$ values determined in our study are in excellent agreement with available data from literature or simulation, see Figure 2. No distinct deviation between the literature data and the identity function $pK_a^\circ$(CE-$C^4D$) = $pK_a$(lit) were observed. As expected, the deviations in the simulation data were clearly the greatest.

To judge the quality of our $\mu_{lim}$ data, we calculated the relative deviation between literature data and our data and compared it to the relative error of the fit function provided by AnglerFish, see Table 2. For glyoxylic acid and phosphate, the relative error of the fit is similar to the relative deviation corroborating no significant difference between literature data and our results. In contrast, a significant difference is given for glycine because the relative deviation is approximately twice the relative error. Compared to the

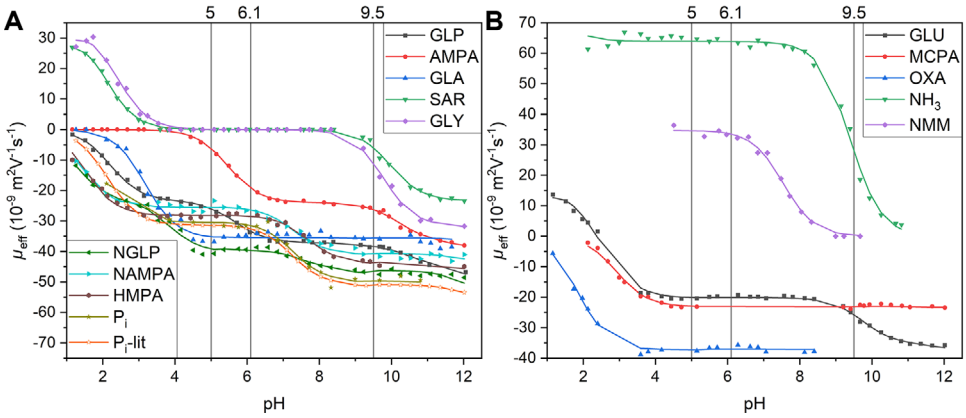


**FIGURE 1** pH-dependent change in the effective electrophoretic mobilities (points) and fits by AngerFish (lines) of (A) glyphosate and its transformation products (abbreviations see Table 1) including experimental and literature (-lit) data for phosphate as well as of (B) other model analytes at an ionic strength of 10 mM (pH > 2). Vertical lines indicate pH values suitable for separations which were tested

**TABLE 1** Thermodynamic acidity constants $pK_a^\circ$ and limiting electrophoretic mobilities $\mu_{lim}$ ($10^{-9}$ $m^2V^{-1}s^{-1}$) for different charge numbers of +1 to −3. Only the higher absolute charge numbers relevant for the specific $pK_a^\circ$ are indicated. Abbreviations of the model analytes are given as used in figures

| Model analyte | $R^2$ | | +1 | −1 | −2 | −3 |
|---|---|---|---|---|---|---|
| *Glyphosate and its transformation products* | | | | | | |
| Glyphosate (GLP) | 0.998 | $\mu_{lim}$ | – | 26.4 ± 0.1 | 45.5 ± 0.1 | 60.1 ± 0.3 |
| | | $pK_a^\circ$ | – | 2.25 ± 0.01 | 5.77 ± 0.02 | 10.55 ± 0.05 |
| Aminomethyl phosphonic acid (AMPA) | 0.999 | $\mu_{lim}$ | – | 27.2 ± 0.1 | 45.0 ± 0.2 | – |
| | | $pK_a^\circ$ | – | 5.51 ± 0.01 | 10.31 ± 0.03 | – |
| Glyoxylic acid (GLA) | 0.979 | $\mu_{lim}$ | – | 39.1 ± 0.5 | – | – |
| | | $pK_a^\circ$ | – | 3.22 ± 0.06 | – | – |
| Sarcosine (SAR) | 0.997 | $\mu_{lim}$ | 36.5 ± 0.5 | 26.3 ± 0.3 | – | – |
| | | $pK_a^\circ$ | 2.02 ± 0.02 | 10.00 ± 0.02 | – | – |
| Glycine (GLY) | 0.996 | $\mu_{lim}$ | 37.3 ± 1.0 | 35.1 ± 0.8 | – | – |
| | | $pK_a^\circ$ | 2.35 ± 0.05 | 9.81 ± 0.05 | – | – |
| *N*-Acetyl glyphosate (NGLP) | 0.989 | $\mu_{lim}$ | – | 26.1 ± 1.0 | 48.4 ± 0.6 | 62.7 ± 0.5 |
| | | $pK_a^\circ$ | – | 1.14 ± 0.13 | 3.97 ± 0.11 | 7.80 ± 0.24 |
| *N*-Acetyl AMPA (NAMPA) | 0.982 | $\mu_{lim}$ | – | 28.7 ± 0.4 | 49.4 ± 0.4 | – |
| | | $pK_a^\circ$ | – | 1.41 ± 0.07 | 7.40 ± 0.08 | – |
| Hydroxymethyl phosphonic acid (HMPA) | 0.990 | $\mu_{lim}$ | – | 31.4 ± 0.2 | 52.8 ± 0.4 | – |
| | | $pK_a^\circ$ | – | 1.57 ± 0.03 | 7.77 ± 0.07 | – |
| Phosphoric acid ($P_i$) | 0.979 | $\mu_{lim}$ | – | 33.7 ± 1.2 | 59.7 ± 1.3 | n.d. |
| | | $pK_a^\circ$ | – | 1.98 ± 0.16 | 7.39 ± 0.17 | n.d. |
| *Model substances* | | | | | | |
| Glufosinate (GLU) | 0.997 | $\mu_{lim}$ | 21.1 ± 0.9 | 23.3 ± 0.2 | 43.3 ± 0.4 | – |
| | | $pK_a^\circ$ | 1.88 ± 0.07 | 2.90 ± 0.07 | 9.87 ± 0.05 | – |
| MCPA | 0.990 | $\mu_{lim}$ | – | 26.2 ± 0.1 | – | – |
| | | $pK_a^\circ$ | – | 2.96 ± 0.02 | – | – |
| Oxamic acid (OXA) | 0.990 | $\mu_{lim}$ | – | 40.8 ± 0.3 | – | – |
| | | $pK_a^\circ$ | – | 1.90 ± 0.02 | – | – |
| Ammonia | 0.992 | $\mu_{lim}$ | 68.4 ± 0.8 | – | – | – |
| | | $pK_a^\circ$ | 9.35 ± 0.05 | – | – | – |
| *N*-Methylmorpholine (NMM) | 0.994 | $\mu_{lim}$ | 38.2 ± 0.5 | – | – | – |
| | | $pK_a^\circ$ | 7.49 ± 0.04 | – | – | – |

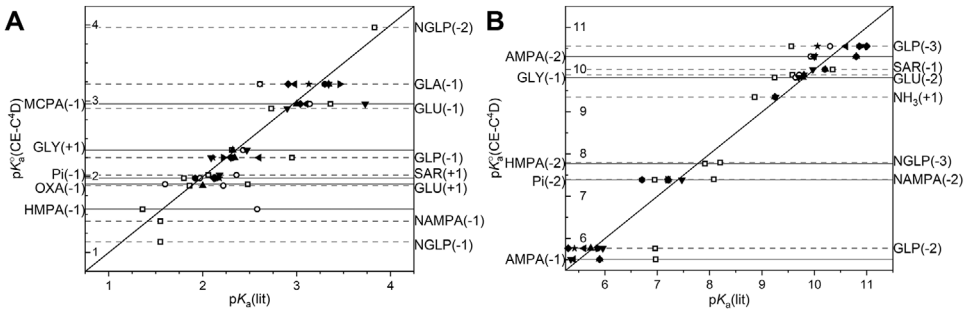


**FIGURE 2** Graphical comparison of $pK_a^\circ$ values determined by CE-$C^4D$ ($pK_a^\circ$(CE-$C^4D$)) in this study with simulated (unfilled symbols) and literature (filled symbols) data in the $pK_a$ range of (A) 0.75–4.25 and (B) 5.25–11.5. If $pK_a^\circ$(CE-$C^4D$) = $pK_a$(lit) then these points are on the identity function (diagonal line). Solid/dashed lines indicate analytes and their higher absolute charge number for the specific $pK_a^\circ$ (in parentheses) on the left/right axis. For abbreviations see Table 1. Raw data and literature values with references are summarized in Table S2

**TABLE 2** Comparison of our data and literature data for limiting electrophoretic mobilities $\mu_{lim}$ ($10^{-9}$ $m^2V^{-1}s^{-1}$) including the relative error of the fit function and the relative deviation between our results and literature data

| Model analyte | | +1 | –1 | –2 | –3 |
|---|---|---|---|---|---|
| Glyoxylic acid | **CE-$C^4D$** | | **39.1 ± 0.5** | | |
| | literature | | 39.6 [33] | | |
| | rel. error/rel. deviation (%) | | 1.3/1.3 | | |
| Glycine | **CE-$C^4D$** | **37.3 ± 1.0** | **35.1 ± 0.8** | | |
| | literature | 39.5 ± 0.4 [34] | 37.4 [35] | | |
| | rel. error/rel. deviation (%) | 2.7/5.6 | 2.3/6.1 | | |
| Phosphate | **CE-$C^4D$** | | **33.7±1.2** | **59.7 ± 1.3** | **n.d.** |
| | literature | | 34.6 [36]<br>35.1 [33] | 61.4 [33] | 71.5 [33] |
| | rel. error/rel. deviation (%) | | 3.6/2.6<br>3.6/4.0 | 2.2/2.8 | |
| Ammonia | **CE-$C^4D$** | **68.4 ± 0.8** | | | |
| | literature | 76.2 [36] | | | |
| | rel. error/rel. deviation (%) | 1.2/10.2 | | | |

literature, our data show a lower $\mu_{lim}$ for both the anionic and cationic species.

The $\mu_{lim}$ for ammonia in literature is more than 10% higher compared to the value calculated from our CE-$C^4D$ data. The reason for this is the short migration time of less than 1.7 min for $NH_4^+$ at all pH levels ($EOF_{max.}$ = 4.2 min). This can certainly be improved by using methods designed for cations, for example, our method with lower pressure support. In connection with uncertainties in migration time, migration path length as well as the actual separation voltage curve, this can lead to noticeable uncertainties in the calculated effective electrophoretic mobility. All other determined values have lower uncertainties since the underlying migration times were significantly longer. Using phosphate as an example, Figure 1A shows the good agreement between the data from our study and the data from the literature.

## 3.5 | Optimization of electrophoretic separations and their experimental verification

To find suitable separation conditions providing ideally baseline separation of all analytes, it is necessary to first select a pH, where all target analytes show sufficient differences in their effective electrophoretic mobilities. Further, it is beneficial, if all analytes have a mobility high enough to ensure separation from neutral matrix compounds. The simplest way to estimate suitable pH values is by plotting the effective electrophoretic mobility of the analytes as well as potentially interfering components (here: phosphate [32]) against the pH as done in Figure 1. To achieve stable separation conditions and high migration time repeatability a pH should be chosen where the slopes of the curves in the $\mu$(pH)-plot are low (ideally zero) to avoid a significant

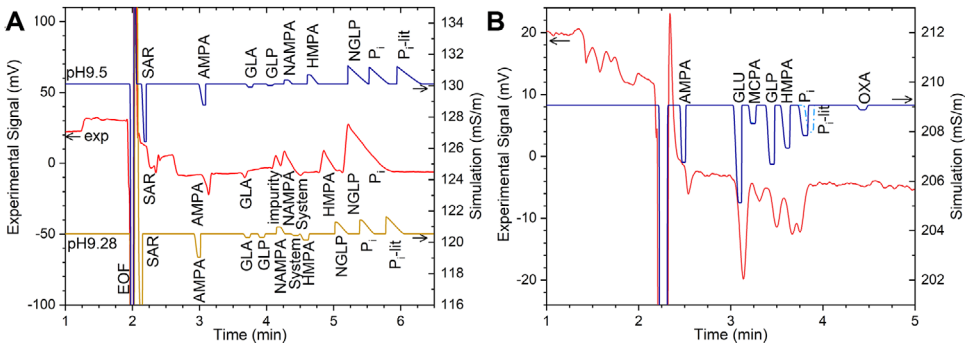


**FIGURE 3** Experimental and simulated electropherograms after injection of the sample for 0.12 min at 50 mbar (~6.4 mm sample plug) at (A) pH 9.5 or pH 9.28 and (B) pH 5.0. The following parameters were used for (A) and [B]: sample concentration of 250 μM in 20 % BGE [500 μM in 1% BGE, 125 μM MCPA]. BGE: 8.3 mM AcOH + 21.8 mM $NH_4OH$ [10 mM AcOH + 20 mM $NH_4AcO$], separation voltage: 15 kV [and 70 mbar]. Bare fused silica capillaries with a length of 50 cm and an id of 50 μm were used. Detection: $C^4D$ at 300 kHz [800 kHz], 100% [60%] amplitude, head stage gain on, low pass: 5 Hz [off], $l_{eff}$ = 33.3 cm, $l_{mig}$ = 28 cm [30.5 cm]. For (A) simulation for pH 9.5 is offset by +40 mS/m. After 20 measurements the pH was changed from pH 9.5 to 9.28 partly due to $CO_2$ dissolution (2.5 mM $H_2CO_3$ based on pH change). For abbreviations see Table 1

mobility change by minimal pH changes in the BGE. Additionally, moderately acidic conditions are advantageous as the BGE composition is not altered due to the dissolution of $CO_2$ from air into the BGE forming carbonate.

As can be seen from Figure 1A, glyphosate itself as well as most of its metabolites are charged over a wide pH range. However, below pH 9, one of the two main metabolites of glyphosate, AMPA or sarcosine, is uncharged prohibiting their separation from neutral matrix components. For this reason and because of the sufficient differences in effective electrophoretic mobility of all metabolites, a pH of 9.5 was chosen for CE-$C^4D$ measurements, but with the disadvantage that the BGE's pH may change due to $CO_2$ dissolution. We also carried out CE-$C^4D$ separations at pH 5.0 and CE-MS at pH 6.1, including only analytes charged at the respective pH.

### 3.5.1 | CE-$C^4D$ measurements at pH 9.5

A comparison of the simulated and experimental electropherograms from conductivity data of a separation of sarcosine, AMPA, glyoxylic acid, glyphosate, *N*-acetyl AMPA, HMPA, *N*-acetyl glyphosate, and phosphate at a pH of 9.5 is shown in Figure 3A. In the simulation, the signals caused by sarcosine and HMPA show a slightly lower migration time than in the experimental electropherogram revealing a relative error of 8 and 3%, respectively. In this case, the comparatively high deviation for sarcosine is caused by the strong dependence of its effective electrophoretic mobility on the pH as can be seen from Figure 1A. For AMPA and glyoxylic acid, simulation and experiment corresponded well (relative error 2%). No peak caused by glyphosate was observed in the experimental electropherogram although the simulation showed a small change in conductivity. Obviously, this change was too small to be recorded by $C^4D$ for this BGE composition. Unfortunately, an impurity comigrated with glyphosate, which was also present in blank measurements. Migration times of *N*-acetyl AMPA and *N*-acetyl glyphosate were identical between simulation and experiment. However, in comparison to the simulation, the peak of *N*-acetyl glyphosate was twice as intense (both in peak height and peak area). This can be traced back to a partial overlap with the peak from phosphate. The phosphate signal itself was larger than expected presumably due to the mineralization of some analytes. This increase was only observed when injecting analytes with a phosphonate group. We included phosphate in the simulated electropherogram using our data (inorganic phosphate [$P_i$]) and literature data ($P_i$-lit). It is evident that the data from the literature deviate more from the experimental electropherogram.

To judge the influence of $CO_2$ dissolution on the pH in alkaline BGEs, the BGE's pH was measured prior to and after 20 CE runs. Inlet and outlet vial solutions were merged to compensate for pH changes due to electrolysis. The measured pH of 9.28 indicated that 2.5 mM $H_2CO_3$ was present from the atmospheric $CO_2$ as calculated by PeakMaster. With this composition, the separation was simulated again resulting in the third electropherogram in Figure 3A. Comparing both simulations and the $C^4D$ data, no differences in the peaks of sarcosine, glyphosate, and *N*-acetyl AMPA were observed. While the peak of HMPA was positive in the simulation for pH 9.5 and the $C^4D$ data, it was negative for the simulation for pH 9.28. Simulation data for pH 9.28 better correlated with the experimental data for glyoxylic acid, while the simulation data for pH 9.5 better correlated for AMPA. The system peak appearing

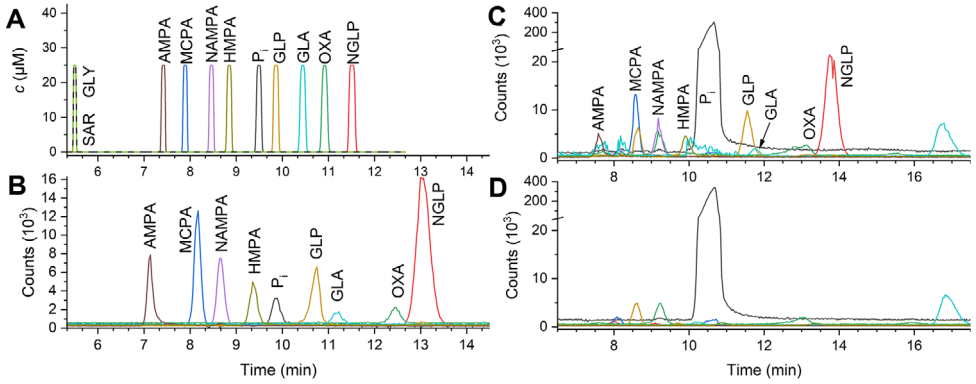


**FIGURE 4** (A) Simulated and (B) experimental electropherograms by CE-MS analysis after injection of a mixture of analytes ($c$ = 25 µM, each) for 10 s × 50 mbar (~7.3 mm) in water (curve of $[P_i\text{-H}]^-$ offset by −1524; SAR and GLY only in simulation) and (C) beer as well as (D) the unspiked beer sample. All samples contained 10 mM $NH_4AcO$. Injected beer samples were diluted to 80% v/v beer by the aqueous solutions added. Separations were performed at 15 kV and 70 mbar pressure in a bare fused silica capillary with a length of 60 cm and an id of 50 µm at pH 6.1 in 20 mM $NH_4AcO$ and 0.78 mM AcOH, see also Sections 2.3 and 2.6. For (A) the migration time of uncharged substances was set to 5.5 min. For abbreviations see Table 1

in the simulation for pH 9.28 due to $H_2CO_3$ in the BGE corresponded well with a peak visible in the $C^4D$ traces. All in all, the simulation at a pH of 9.5 aligned better with the $C^4D$ data revealing that the pH change cannot be fully explained by $CO_2$ dissolution in the BGE.

To summarize, a separation of the analytes glyphosate, AMPA, *N*-acetyl glyphosate, *N*-acetyl AMPA, glyoxylic acid, sarcosine, HMPA, and phosphate can be performed successfully at a pH of 9.5. As predicted by simulation, the analytes were well separated, except the peaks for *N*-acetyl glyphosate and phosphate. However, glyphosate could not be detected due to insufficient conductivity differences to the BGE, which would be solvable by using a BGE with another coion, for example, formiate. For trace analysis, MS detection can be applied as the BGE compounds are volatile.

### 3.5.2 | CE- $C^4D$ measurements at pH 5.0

To detect glyphosate and overcome the dissolution of $CO_2$, CE-$C^4D$ measurements were carried out at pH 5.0. We separated a mixture of herbicides and degradation products, namely: glyphosate, MCPA, glufosinate as well as AMPA, HMPA, phosphate, and oxamic acid. A good correlation between the simulated and experimental electropherogram is visible in Figure 3B. The maximum relative migration time difference does not exceed 2% for all analytes. A 2.4% shorter migration time in the experiment compared to the simulation for AMPA can be attributed to the strong mobility dependency of AMPA at the selected pH as can be deduced from Figure 1. The relative migration time difference for phosphate (1.3 %) using our data ($P_i$) versus literature data ($P_i$-lit) (2.9 %) between simulation and experiment clearly shows that the data obtained in this study allow a better prediction of its migration time. For oxamic acid, the difference in its mobility to the BGE coions was too low to result in a signal.

### 3.5.3 | CE-MS measurements at pH 6.1

In addition to CE-$C^4D$, CE-MS analysis was performed for all metabolites of glyphosate. To avoid the influence on the BGE's pH by $CO_2$ dissolution, acidic conditions were chosen with the drawback that glycineand sarcosine are not separated from neutral substances. The simulation by PeakMaster (Figure 4A) showed a complete separation of all metabolites of glyphosate except glycineand sarcosine which are uncharged at pH 6.1 (see Figure 1). MCPA and oxamic acid were also included in the simulation, revealing no superposition with other analytes. The simulation was successfully reproduced by CE-MS with regard to the migration order for an aqueous sample but impressively also in a spiked beer sample, see Figure 4B,C. Both glycineand sarcosine were not included in the samples since no separation from neutral compounds was predicted. In the unspiked beer sample, only a peak for phosphate was visible, compared to Figure 4D. Slightly longer migration times for all analytes were observed when injecting (un)spiked beer samples. These may be due to adsorption of matrix components and thus a reduced EOF, which would necessitate optimized rinsing steps. Other reasons are field amplification phenomena or transient sample-induced isotachophoresis. Despite fragmentor voltage optimization, both *N*-acetyl AMPA and *N*-acetyl glyphosate showed in-source decay as the masses of $[M\text{-H}]^-$ for AMPA and glyphosate were observed at the

migration times of their acetylated derivates. Differences between the electropherograms in Figure 4A,B are mainly caused by coupling CE to MS via the sheath liquid interface: ions from the sheath liquid migrate into the capillary and influence the separation conditions since the sheath liquid's composition is different from the BGE [32]. Baseline separation and a good migration time precision with an RSD below 1.4% for all analytes were reached for an aqueous standard analyte mixture (2.5 μM ($n = 3$) or 25 μM ($n = 6$)). The peak area precision did not exceed an RSD of 16% ($n = 3$; $c = 2.5$ μM) or 20% ($n = 6$; $c = 25$ μM). It was possible to achieve a LOQ of 0.25 μM (~42 μg/L) for glyphosate with an injection over 15 s at 100 mbar when only glyphosate was measured in selected ion monitoring mode, see electropherogram in Figure S1. See et al. described similar LOQs for CE-$C^4D$ at a pH of 6.3 for glyphosate and AMPA in spiked tap water samples at comparable separation conditions [37]. In comparison, when analyzing water samples, a non-derivatization normal phase LC-MS method with SPE pretreatment achieved LOQs in the range of 20 ng/L for glyphosate, glufosinate, and AMPA [38]. HILIC-LC-MS methods showed LOQs of 20 μg/kg for glyphosate and some of its degradation products in peas and soya cake [39].

## 4 | CONCLUDING REMARKS

In this study, we successfully established a universal CE-$C^4D$ method to record electropherograms of analytes over a large pH range (pH 1.25–12.02) which was applied to analytes being strong acids up to moderate bases. Besides acceptable solubility in water, there are no particular restrictions with regard to the type of analytes amenable: the number of dissociation states is only limited by the pH steps per pH range, there is no need for a chromophore as in other CE methods [40, 41] or for applying UV-Vis spectrophotometry. In combination with the free software AnglerFish [18], the negative decadic logarithmic thermodynamic acidity constants ($pK_a^\circ$) and limiting electrophoretic mobilities ($\mu_{lim}$) of analytes can be determined from CE-$C^4D$ data even in buffers of varying ionic strength. The BGEs were prepared from just ten common buffer chemicals. We performed separations in BGEs of up to 36 different pH values for different herbicides to obtain effective electrophoretic mobility data with a very high resolution over a large pH range. With our resolution of three pH steps per one pH unit, the minimum resolved $pK_a^\circ$ difference was one and enabled the characterization of analytes with complex pH-speciation. Migration times of EOF and analytes are determined simultaneously with our method so effective electrophoretic mobilities can be determined with high precision. The analysis by CE-$C^4D$ can easily be automated and its analyte consumption is extremely low (approximately 1 μg). The method presented here is very cost-effective with the simultaneous injection of several analytes. Analytes can be characterized also with impurities present. The possibility to add an internal standard for quality control is another advantage of our procedure.

For many of the model analytes, $pK_a^\circ$ and $\mu_{lim}$ were determined for the first time. In literature, the separation conditions are often determined in an experimental approach, sometimes based on available $pK$ $pK_a$data [32, 37, 42]. By simulation, it was easy to find optimal separation conditions for up to nine chemically very similar analytes at different pH values and verify them experimentally. We were able to separate glyphosate and all its transformation products except glycine by CE-$C^4D$ at pH 9.5. Furthermore, MCPA, oxamic acid, and glyphosate with all its transformation products except sarcosine and glycine were analyzed in aqueous samples as well as in a spiked beer sample by CE-MS at pH 6.1. For aqueous samples good migration time precision with a maximum RSD of < 1.4% ($n = 6$) was observed. When monitoring glyphosate in selected ion monitoring mode, a LOQ of 0.25 μM (~42 μg/L) was reached.

## ACKNOWLEDGMENTS

This work was supported by the Collaborative Research Center 1253 CAMPOS (Project 4: Floodplain Biogeochemistry), funded by the German Research Foundation (DFG, Grant Agreement SFB 1253/1 2017).

Open access funding enabled and organized by Projekt DEAL.

## CONFLICT OF INTEREST

The authors have declared no conflict of interest.

## DATA AVAILABILITY STATEMENT

All data that support the findings of this study are included in the manuscript except the underlying electropherograms from CE-$C^4D$.

## ORCID

*Carolin Huhn* https://orcid.org/0000-0001-6865-1043

## REFERENCES

1. Prankerd RJ. Critical compilation of $pK_a$ values for pharmaceutical substances. Profiles Drug Subst Excip Relat Methodol. 2007;33:1–33.
2. Pathare B, Tambe V, Patil V. A review on various analytical methods used in determination of dissociation constant. Int J Pharm Pharm Sci. 2014;6:26–34.
3. Albert A, Serjeant EP. The determination of ionization constants. 3rd ed. Chapman and Hall: New York; 1984.

4. Benet LZ, Goyan JE. Potentiometric determination of dissociation constants. J Chromatogr A. 1967;56:665–80.
5. Reijenga J, van Hoof A, van Loon A, Teunissen B. Development of methods for the determination of p$K_a$ values. Anal Chem Insights. 2013;8:53–71.
6. Bezencon J, Wittwer MB, Cutting B, Smiesko M, Wagner B, Kansy M, Ernst B. p$K_a$ determination by $^1$H NMR spectroscopy - an old methodology revisited. J Pharm Biomed. Anal. 2014;93:147–155.
7. Beckers JL, Everaerts FM, Ackermans MT. Determination of absolute mobilities, pK values and separation numbers by capillary zone electrophoresis. J Chromatogr A. 1991;537:407–428.
8. Poole SK, Patel S, Dehring K, Workman H, Poole CF. Determination of acid dissociation constants by capillary electrophoresis. J Chromatogr A. 2004;1037:445–54.
9. Nowak P, Wozniakiewicz M, Koscielniak P. Application of capillary electrophoresis in determination of acid dissociation constant values. J Chromatogr A. 2015;1377:1-12.
10. Geffertova D, Ali ST, Solinova V, Krecmerova M, Holy A, Havlas Z, Kasicka V. Investigation of the acid-base and electromigration properties of 5-azacytosine derivatives using capillary electrophoresis and density functional theory calculations. J Chromatogr A. 2017;1479:185-193.
11. Solinova V, Brynda J, Sicha V, Holub J, Gruner B, Kasicka V. Determination of acidity constants, ionic mobilities, and hydrodynamic radii of carborane-based inhibitors of carbonic anhydrases by capillary electrophoresis. Electrophoresis 2021;42:910–919.
12. Fuguet E, Rafols C, Bosch E, Roses M. Fast high-throughput method for the determination of acidity constants by capillary electrophoresis: I. Monoprotic weak acids and bases. J Chromatogr A. 2009;1216:3646–51.
13. Jia Z, Ramstad T, Zhong M. Medium-throughput p$K_a$ screening of pharmaceuticals by pressure-assisted capillary electrophoresis. Electrophoresis 2001;22:1112–8.
14. Ishihama Y, Oda Y, Asakawa N. Microscale determination of dissociation constants of multivalent pharmaceuticals by capillary electrophoresis. J Pharm Sci. 1994;83:1500–1507.
15. Koval D, Kasicka V, Jiracek J, Collinsova M. Physicochemical characterization of phosphinic pseudopeptides by capillary zone electrophoresis in highly acidic background electrolytes. Electrophoresis 2003;24:774–781.
16. Zuskova I, Novotna A, Vcelakova K, Gas B. Determination of limiting mobilities and dissociation constants of 21 amino acids by capillary zone electrophoresis at very low pH. J Chromatogr B. 2006;841:129–134.
17. Ehala S, Grishina AA, Sheshenev AE, Lyapkalo IM, Kasicka V. Determination of acid-base dissociation constants of very weak zwitterionic heterocyclic bases by capillary zone electrophoresis. J Chromatogr A. 2010;1217:8048–8053.
18. Maly M, Boublik M, Pocrnic M, Ansorge M, Lorincikova K, Svobodova J, Hruska V, Dubsky P, Gas B. Determination of thermodynamic acidity constants and limiting ionic mobilities of weak electrolytes by capillary electrophoresis using a new free software AnglerFish. Electrophoresis 2020;41:493–501.
19. Benbrook CM. Trends in glyphosate herbicide use in the United States and globally. Environ Sci Eur. 2016;28:1–15.
20. Valle AL, Mello FCC, Alves-Balvedi RP, Rodrigues LP, Goulart LR. Glyphosate detection: methods, needs and challenges. Environ Chem Lett. 2018;17:291–317.
21. Rueppel ML, Brightwell BB, Schaefer J, Marvel JT. Metabolism and degradation of glyphosphate in soil and water. J Agric Food Chem. 1977;25:517–28.
22. Modification of the residue definition of glyphosate in genetically modified maize grain and soybeans, and in products of animal origin. EFSA J. 2009;7:1310.
23. Jayasumana C, Gunatilake S, Senanayake P. Glyphosate, hard water and nephrotoxic metals: are they the culprits behind the epidemic of chronic kidney disease of unknown etiology in Sri Lanka? Int J Environ Res Public Health. 2014;11:2125–2147.
24. Conclusion on the peer review of the pesticide risk assessment of the active substance glyphosate. EFSA J. 2015;13:4302.
25. Zhan H, Feng Y, Fan X, Chen S. Recent advances in glyphosate biodegradation. Appl Microbiol Biotechnol. 2018;102:5033–5043.
26. Kaczynski P, Lozowicka B, Wolejko E, Iwaniuk P, Konecki R, Dragowski W, Lozowicki J, Amanbek N, Rusilowska J, Pietraszko A. Complex study of glyphosate and metabolites influence on enzymatic activity and microorganisms association in soil enriched with *Pseudomonas fluorescens* and sewage sludge. J Hazard Mater. 2020;393:122443.
27. Fleischer S, Weiss SC, Lucke T, Seitz W, Schulz W, Weber WH Formation of Oxamic Acid During Drinking Water Treatment. Ozone: Science & Engineering. 2015;37:441–449.
28. https://chemicalize.com/. Accessed November 22, 2021.
29. Maly M, Dovhunova M, Dvorak M, Gerlero GS, Kler PA, Hruska V, Dubsky P. Generalized model of the linear theory of electromigration and its application to electrokinetic chromatography: Theory and software PeakMaster 6-Next Generation. Electrophoresis 2019;40:683–692.
30. Stedry M, Jaros M, Hruska V, Gas B. Eigenmobilities in background electrolytes for capillary zone electrophoresis: III. Linear theory of electromigration. Electrophoresis 2004;25:3071–3079.
31. Hajba L, Guttman A. Recent advances in column coatings for capillary electrophoresis of proteins. TrAC Trends Anal Chem. 2017;90:38–44.
32. Wimmer B, Pattky M, Zada LG, Meixner M, Haderlein SB, Zimmermann HP, Huhn C. Capillary electrophoresis-mass spectrometry for the direct analysis of glyphosate: method development and application to beer beverages and environmental studies. Anal Bioanal Chem. 2020;412:4967–4983.
33. Hirokawa T, Nishino M, Aoki N, Kiso Y, Sawamoto Y, Yagi T, Akiyama J-I. Table of isotachophoretic indices. J Chromatogr A. 1983;271:D1–106.
34. Vcelakova K, Zuskova I, Kenndler E, Gas B. Determination of cationic mobilities and p$K_a$ values of 22 amino acids by capillary zone electrophoresis. Electrophoresis 2004;25:309–17.
35. Hirokawa T, Gojo T, Kiso Y. Isotachophoretic determination of mobility and p$K_a$ by means of computer simulation. J Chromatogr A. 1986;369:59-81.
36. Jaros M, Hruska V, Stedry M, Zuskova I, Gas B. Eigenmobilities in background electrolytes for capillary zone electrophoresis: IV. Computer program PeakMaster. Electrophoresis 2004;25:3080-5.
37. See HH, Hauser PC, Ibrahim WA, Sanagi MM. Rapid and direct determination of glyphosate, glufosinate, and aminophosphonic acid by online preconcentration CE with contactless conductivity detection. Electrophoresis 2010;31:575–582.
38. Pan S, Chen X, Li X, Jin M. Nonderivatization method for determination of glyphosate, glufosinate, bialaphos, and their main

metabolites in environmental waters based on magnetic metal-organic framework pretreatment. J Sep Sci. 2019;42:1045–1050.
39. Dias J, Lopez SH, Mol H, de Kok A. Influence of different hydrophilic interaction liquid chromatography stationary phases on method performance for the determination of highly polar anionic pesticides in complex feed matrices. J Sep Sci. 2021;44:2165–76.
40. Zrncic M, Babic S, Mutavdzic Pavlovic D. Determination of thermodynamic p$K_a$ values of pharmaceuticals from five different groups using capillary electrophoresis. J Sep Sci. 2015;38:1232–1239.
41. Jerez G, Kaufman G, Prystai M, Schenkeveld S, Donkor KK. Determination of thermodynamic p$K_a$ values of benzimidazole and benzimidazole derivatives by capillary electrophoresis. J Sep Sci. 2009;32:1087–95.
42. Iwamuro Y, Iio-Ishimaru R, Chinaka S, Takayama N, Kodama S, Hayakawa K. Analysis of phosphorus-containing amino acid-type herbicides by capillary electrophoresis/mass spectrometry using a chemically modified capillary having amino groups. Health Sci J. 2010;56:606–12.

## SUPPORTING INFORMATION

Additional supporting information may be found in the online version of the article at the publisher's website.

**How to cite this article:** Graf HG, Biebl SM, Müller L, Breitenstein C, Huhn C. Capillary electrophoresis applied for the determination of acidity constants and limiting electrophoretic mobilities of ionizable herbicides including glyphosate and its metabolites and for their simultaneous separation. J Sep Sci. 2022;45:1128–1139.
https://doi.org/10.1002/jssc.202100952

# Appendix III

**Supporting Information to Paper 2:**

Graf, H. G., Biebl, S. M., Müller, L., Breitenstein, C., Huhn, C., Capillary electrophoresis applied for the determination of acidity constants and limiting electrophoretic mobilities of ionizable herbicides including glyphosate and its metabolites and for their simultaneous separation. *Journal of Separation Science* 2022; *45*, 1128-1139, DOI: 10.1002/jssc.202100952

## Supporting Information to:

# Capillary electrophoresis applied for determination of acidity constants and limiting electrophoretic mobilities of ionizable herbicides including glyphosate and its metabolites and for their simultaneous separation

Hannes Georg Graf, Sonja Maria Biebl, Linda Müller, Christina Breitenstein, Carolin Huhn

This Supporting Information includes in Table S1 an overview of the composition of all BGEs used for p$K_a$ and $\mu_{lim}$ determination including their desired and measured pH.

In Table S2, a comparison is made between the p$K_a$ values determined in our study and data available from literature or simulation data. It is the raw data for Figure 2A and B of the manuscript.

A CE-MS electropherogram monitoring only glyphosate in SIM mode is shown in Figure S1 when injecting analytes at a concentration close to the limit of quantification.

**Table S1.** Composition of BGEs at different desired pH values ($pH_{desired}$) and the measured pH values of the BGE ($pH_{meas}$). All concentrations are given in mM.

| $pH_{desired}$ | $pH_{meas}$ | Ionic strength | *p*-Toluenesulfonic acid | Phosphoric acid | Formic acid | Acetic acid | 2-(*N*-Morpholino)-ethanesulfonic acid | 3 (*N*-Morpholino)-propanesulfonic acid | Tricine | Glycine | β-Alanine | Lithium hydroxide |
|---|---|---|---|---|---|---|---|---|---|---|---|---|
| 1.25 | 1.26 | 68 | | 515.00 | | | | | | | | |
| 1.54 | 1.54 | 33 | | 152.8 | | | | | | | | |
| 1.86 | 1.73 | 15 | | 41.85 | | | | | | | | |
| 2.07 | | 9 | | 19.64 | | | | | | | | |
| 2.07* | 2.10 | 13 | 14.5 | | | | | | | | | 5.00 |
| 2.37 | | 10 | | 15.13 | | | | | | | | 5.00 |
| 2.37* | 2.42 | 10 | 9.7 | | | | | | | | | 5.00 |
| 2.65 | 2.65 | 10 | | 12.65 | | | | | | | | 7.30 |
| 3.03 | | 10 | | 10.92 | | | | | | | | 8.70 |
| 3.24 | | 10 | | | 39.11 | | | | | | | 9.30 |
| 3.24* | | 10 | 9.93 | | | | | | | | | 9.30 |
| 3.54 | 3.54 | 10 | | | 24.83 | | | | | | | 9.70 |
| 3.85 | | 10 | | | | 83.35 | | | | | | 9.90 |
| 4.16 | | 10 | | | | 45.79 | | | | | | 10.00 |
| 4.48 | 4.51 | 10 | | | | 27.15 | | | | | | 10.00 |
| 4.77 | | 10 | | | | 18.90 | | | | | | 10.00 |
| 5.08 | | 10 | | | | 14.30 | | | | | | 10.00 |
| 5.35 | | 10 | | | | | 60.00 | | | | | 10.00 |
| 5.63 | | 10 | | | | | 36.60 | | | | | 10.00 |
| 5.97 | | 10 | | | | | 22.13 | | | | | 10.00 |
| 6.27 | | 10 | | | | | | 87.58 | | | | 10.00 |
| 6.56 | 6.58 | 10 | | | | | | 49.69 | | | | 10.00 |
| 6.83 | | 10 | | | | | | 31.02 | | | | 10.00 |
| 7.10 | | 10 | | | | | | 21.42 | | | | 10.00 |
| 7.41 | 7.48 | 10 | | | | | | | 59.74 | | | 10.00 |
| 7.72 | | 10 | | | | | | | 34.42 | | | 10.00 |
| 8.04 | | 10 | | | | | | | 21.63 | | | 10.00 |
| 8.32 | | 10 | | | | | | | 16.06 | | | 10.00 |
| 9.00 | | 10 | | | | | | | | 65.48 | | 10.00 |
| 9.30 | 9.22 | 10 | | | | | | | | 37.57 | | 10.00 |
| 9.67 | | 10 | | | | | | | | | 43.48 | 10.00 |
| 9.93 | 10.01 | 10 | | | | | | | | | 28.08 | 10.00 |
| 10.25 | | 10 | | | | | | | | | 18.43 | 10.00 |
| 10.53 | | 10 | | | | | | | | | 14.16 | 10.00 |
| 10.80 | | 10 | | | | | | | | | 11.59 | 10.00 |
| 11.05 | 11.09 | 10 | | | | | | | | | 9.95 | 10.00 |
| 11.35 | | 10 | | | | | | | | | 8.01 | 10.00 |
| 11.67 | | 10 | | | | | | | | | 4.94 | 10.00 |
| 12.02 | 12.02 | 12 | | | | | | | | | | 11.73 |

* alternative composition, it was used when the conductivity difference between the analyte and the default BGE was too low to be detect by $C^4D$

**Table S2.** Comparison of acidity constants p$K_a$. Data from our study are highlighted in bold and data from simulations in italic. Simulated data were obtained via the website chemicalize.com from ChemAxon (Budapest, Hungary) and ACD/Labs software (Toronto, ON, Canada). Literature data based on the database in PeakMaster [1, 2], on potentiometric titrations (pt), quantum calculations (qc) or from literature, where the techniques was not given (n.g.), was included. In addition, the ionic strength *I* is given, where possible. Only the higher absolute charge numbers relevant for the specific p$K_a$ are indicated. For abbreviations see Table 1.

| Analyte | Method | +1 | -1 | -2 | -3 |
|---|---|---|---|---|---|
| GLP | **CE-C$^4$D** | **-** | **2.25±0.01** | **5.77±0.02** | **10.55±0.05** |
| | *Sim chemicalize* | *-0.58* | *2.95* | *6.96* | *9.56* |
| | *Sim ACD/Labs* | *1.22±0.1* | *n.d.* | *n.d.* | *10.30±0.3* |
| | n.g. [3] | | 2.34 | 5.73 | n.d. |
| | n.g. [4] | 0.78 | 2.09 | 5.96 | 10.98 |
| | n.g. [5] | 0.8 | 2.3 | 5.3 | 11.0 |
| | pt [6] | <2 | 2.6 | 5.6 | 10.6 |
| | pH-metric [7] | 0.88±0.07 | 2.22±0.02 | 5.87±0.01 | 10.89±0.01 |
| | pt [8] | | 2.32±0.03 | 5.86±0.02 | 10.86±0.03 |
| | NMR [9] | | 2.11±0.02 | 5.42±0.01 | 10.06 ±0.02 |
| AMPA | **CE-C$^4$D** | **n.d.** | **5.51±0.01** | **10.31±0.03** | |
| | *Sim chemicalize* | *-0.2* | *6.97* | *9.94* | |
| | *Sim ACD/Labs* | *1.48±0.1* | *n.d.* | *9.93±0.3* | |
| | n.g. [4] | 2.4 | 5.9 | 10.8 | |
| | change in pH during titrations *I* = 0.09 M [10] | 1.85 | 5.35 | 10.0 | |
| | pt [11] | 2.35±0.05 | 5.9±0.05 | 10.8±0.05 | |
| | n.g. [5] | 1.8 | 5.4 | 10.0 | |
| GLA | **CE-C$^4$D** | | **3.22±0.06** | | |
| | *Sim chemicalize* | | *2.61* | | |
| | *Sim ACD/Labs* | | *2.61±0.54* | | |
| | PeakMaster [1, 2] | | 3.34 | | |
| | n.g. [12] | | 3.337 | | |
| | pt *I* = 1 M [13] | | 2.91 | | |
| | pt *I* = 0.5 M [14] | | 2.98 | | |
| | pH metric [15] | | 3.46±0.06 | | |
| | n.g. [16] | | 3.3 | | |
| | pt *I* = 1 M [17] | | 3.13±0.1 | | |
| SAR | **CE-C$^4$D** | **2.02±0.02** | **10.00±0.02** | | |
| | *Sim chemicalize* | *2.06* | *10.35* | | |
| | *Sim ACD/Labs* | *2.36±0.1* | *10.20±0.7* | | |
| | pt [18] | n.d. | 10.21 | | |
| | n.g. [19] | 2.18 | 9.97 | | |
| GLY | **CE-C$^4$D** | **2.35±0.05** | **9.81±0.05** | | |
| | *Sim chemicalize* | *2.31* | *9.24* | | |
| | *Sim ACD/Labs* | *2.43±0.1* | *9.64±0.13* | | |
| | PeakMaster [1, 2] | 2.32 | 9.78 | | |
| | pt *I* = 0.5 M [14] | 2.47 | 9.70 | | |
| NGLP | **CE-C$^4$D** | | **1.14±0.13** | **3.97±0.11** | **7.80±0.24** |
| | *Sim chemicalize* | | *1.55* | *3.83* | *8.20* |
| | *Sim ACD/Labs* | | *n.d.* | *n.d.* | *n.d.* |
| NAMPA | **CE-C$^4$D** | | **1.41±0.07** | **7.40±0.08** | |
| | *Sim chemicalize* | | *1.55* | *8.08* | |
| | *Sim ACD/Labs* | | *n.d.* | *n.d.* | |

| Analyte | *Method* | *+1* | *-1* | *-2* | *-3* |
|---|---|---|---|---|---|
| HMPA | **CE-C$^4$D** | | **1.57±0.03** | **7.77±0.07** | **n.d.** |
| | *Sim chemicalize* | | *1.36* | *7.91* | *14.83* |
| | *Sim ACD/Labs* | | *2.58±0.1* | *n.d.* | *n.d.* |
| $P_i$ | **CE-C$^4$D** | | **1.98±0.16** | **7.39±0.17** | n.d. |
| | *Sim chemicalize* | | *1.80* | *6.95* | *12.90* |
| | *Sim ACD/Labs* | | *1.97±0.1* | *n.d.* | *n.d.* |
| | PeakMaster [1, 2] | | 2.16 | 7.21 | 12.67 |
| | n.g. [12] | | 2.12 | 7.470 | 12.360 |
| | n.g. [20] | | 2.12 | 7.21 | 12.67 |
| | n.g. [21] | | 2.12 | 7.21 | 12.30 |
| | n.g. *I* = 0 [22, 23] | | 2.148 | 7.198 | 12.375 |
| | n.g. *I* = 0.1 M [22, 23] | | 1.92 | 6.71 | 11.52 |
| | thermometric titration [24] | | 2.18 | 7.20 | 12.32 |
| GLU | **CE-C$^4$D** | **1.88±0.07** | **2.90±0.07** | **9.87±0.05** | |
| | *Sim chemicalize* | *1.86* | *2.73* | *9.58* | |
| | *Sim ACD/Labs* | *2.22±0.1* | *n.d.* | *9.71±0.2* | |
| | n.g. [3] | 2.0 | n.d. | 9.8 | |
| | n.g. [25] | > 0.8 | > 2.9 | > 9.8 | |
| MCPA | **CE-C$^4$D** | | **2.96±0.02** | | |
| | *Sim chemicalize* | | *3.36* | | |
| | *Sim ACD/Labs* | | *3.14±0.1* | | |
| | qc [26] | | 3.00 | | |
| | n.g. [3] | | 3.73 | | |
| | n.g. [27] | | 3.04 | | |
| | n.g. [28] | | 3.1 | | |
| OXA | **CE-C$^4$D** | | **1.90±0.02** | | |
| | *Sim chemicalize* | | *2.48* | | |
| | *Sim ACD/Labs* | | *1.60±0.2* | | |
| | *Estimate* [29] | | *1.48* | | |
| $NH_3$ | **CE-C$^4$D** | **9.35±0.05** | | | |
| | *Sim chemicalize* | *8.86* | | | |
| | PeakMaster [1, 2] | 9.25 | | | |
| | n.g. *I* = 0 M [22] | 9.245 | | | |
| | n.g. *I* = 0.1M [22] | 9.26 | | | |

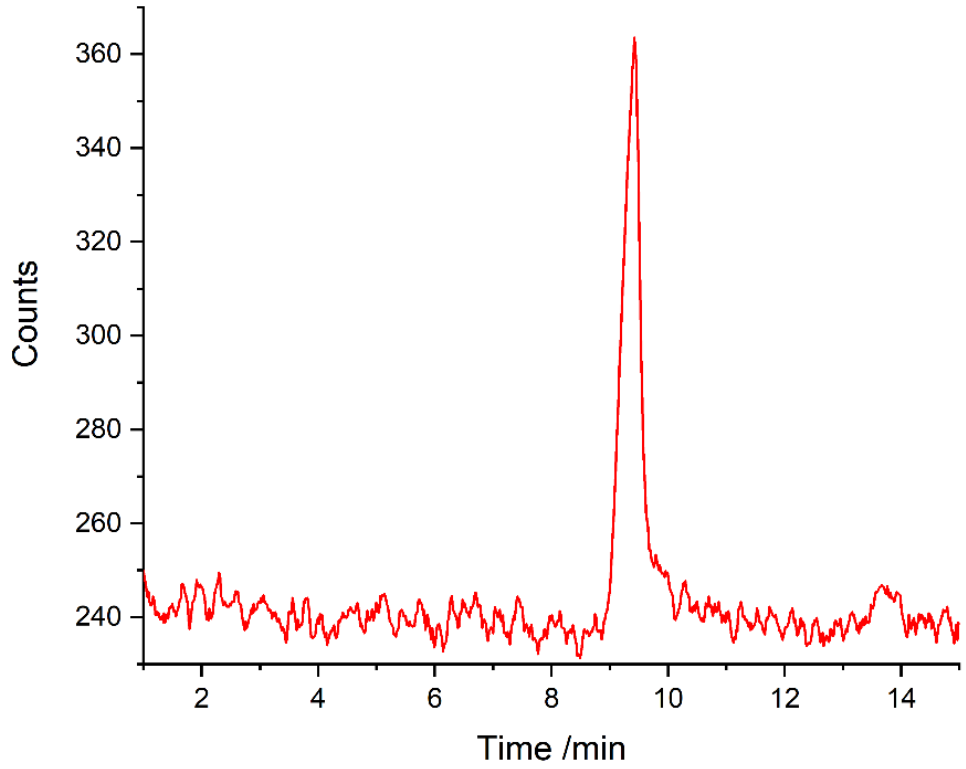


**Figure S1.** CE-MS electropherogram based on single ion monitoring of $[M-H]^-$ of glyphosate after injection of a mixture of the analytes AMPA, MCPA, *N*-acetyl AMPA, HMPA, phosphate, glyphosate, glyoxylic acid, oxamic acid and *N*-acetyl glyphosate ($c$ = 0.25 µM) in an aqueous solution of 10 mM $NH_4OAc$ for 15 s × 100 mbar. Separations were performed at 15 kV and supported by a pressure of 70 mbar in a bare fused silica capillary with a length of 60 cm and an id of 50 µm at pH 6.1 in an aqueous BGE made of 20 mM $NH_4OAc$ and 0.78 mM AcOH. The data were smoothed using a seven-point moving average function.

# References


[1] Maly, M., Dovhunova, M., Dvorak, M., Gerlero, G. S., Kler, P. A., Hruska, V., Dubsky, P., Generalized model of the linear theory of electromigration and its application to electrokinetic chromatography: Theory and software PeakMaster 6-Next Generation. *Electrophoresis*. 2019, *40*, 683-692.

[2] Jaros, M., Hruska, V., Stedry, M., Zuskova, I., Gas, B., Eigenmobilities in background electrolytes for capillary zone electrophoresis: IV. Computer program PeakMaster. *Electrophoresis*. 2004, *25*, 3080-3085.

[3] Lewis, K. A., Tzilivakis, J., Warner, D. J., Green, A., An international database for pesticide risk assessments and management. *Hum. Ecol. Risk Assess.* 2016, *22*, 1050-1064.

[4] You, J., Koropchak, J. A., Condensation nucleation light scattering detection with ion chromatography for direct determination of glyphosate and its metabolite in water. *J. Chromatogr. A*. 2003, *989*, 231-238.

[5] Chen, Z., He, W., Beer, M., Megharaj, M., Naidu, R., Speciation of glyphosate, phosphate and aminomethylphosphonic acid in soil extracts by ion chromatography with inductively coupled plasma mass spectrometry with an octopole reaction system. *Talanta*. 2009, *78*, 852-856.

[6] Sprankle, P., Meggitt, W. F., Penner, D., Adsorption, mobility, and microbial degradation of glyphosate in the soil. *Weed Sci.* 1975, *23*, 229-234.
[7] Comer, J., Chamberlain, K., Evans, A., Validation of pH-metric technique for measurement of $pK_a$ and log $P_{ow}$ of ionizable herbicides. *SAR QSAR Environ. Res.* 1995, *3*, 307-313.
[8] Wauchope, D., Acid dissociation constants of arsenic acid, methylarsonic acid (MAA), dimethylarsinic acid (cacodylic acid), and *N*-(phosphonomethyl)glycine (glyphosate). *J. Agric. Food Chem.* 1976, *24*, 717-721.
[9] Dhansay, M. A., Linder, P. W., Torrington, R. G., Modro, T. A., Organophosphorus herbicides and plant growth regulators part 1. Synthesis and protonation behaviour of glyphosate and related compounds. *J. Phys. Org. Chem.* 1990, *3*, 248-254.
[10] Chavane, V., Recherchs sur l'acide aminométhane phosphonique. *Bulletin de la Société Chimique de France*. 1948, *15*, 774 - 777.
[11] Rumpf, P., Chavane, V., Étude électrochemique de quelques acides phosphoniques aminés. *Comptes rendus des séances de l'académie des sciences*. 1947, *225*, 919-920.
[12] Hirokawa, T., Nishino, M., Aoki, N., Kiso, Y., Sawamoto, Y., Yagi, T., Akiyama, J.-I., Table of isotachophoretic indices. *J. Chromatogr. A*. 1983, *271*, D1-D106.
[13] Hiltin, A., Leussing, D. L., Reaction of ethylenediamine and *C,C,C',C'*-tetramethylethylenediamine with glyoxylate in the presence and absence of zinc(II) or nickel(II). *J. Am. Chem. Soc.* 2002, *93*, 6831-6836.
[14] Leussing, D. L., Hanna, E. M., Metal ion catalysis in transamination. IV. Nickel(II)-and zinc(II)-glyoxalate-amino acid complexes1. *J. Am. Chem. Soc.* 2002, *88*, 696-699.
[15] Öjelund, G., Wadsö, I., Thermochemistry of ionization reactions for glyoxylic acid, pyruvic acid, and alpha-ketobutyric acid. *Acta Chem. Scand.* 1967, *21*, 1408-1414.
[16] Strehlow, H., Die Kinetik der Hydratation von α-Ketocarbonsäuren. *Zeitschrift für Elektrochemie, Berichte der Bunsengesellschaft für physikalische Chemie*. 1962, *66*, 392-396.
[17] Das, S., Bhattacharyya, J., Mukhopadhyay, S., Mechanistic studies on the oxidation of glyoxylic and pyruvic acid by a $[Mn_4O_6]^{4+}$ core in aqueous media: Kinetics of oxo-bridge protonation. *Helv. Chim. Acta*. 2006, *89*, 1947-1958.
[18] Hamborg, E. S., Niederer, J. P. M., Versteeg, G. F., Dissociation constants and thermodynamic properties of amino acids used in $CO_2$ absorption from (293 to 353) K. *J. Chem. Eng. Data*. 2007, *52*, 2491-2502.
[19] Lide, R. L., Handbook of chemistry and physics. 82 Edition, CRC Press, Boca Raton, Fl 2001.
[20] Alexeyev, V., Quantitative analysis. Mir Publishers, Moscow 1969.
[21] Bassett, J., Denney, R. C., Jeffery, G. H., Mendham, J., Vogel's textbook of quantitative chemical analysis. Fifth Edition, Longman Scientific & Technical, Harlow 1989.
[22] Martell, A., Smith, R. M., Motekaitis, R., NIST standard reference database 46 version 8.0: NIST critically selected stability constants of metal complexes. 2004.
[23] Miller, A. G., Macklin, J. W., Raman spectrometric determination of the tribasic sodium phosphate hydrolysis quotient. *Anal. Chem.* 1983, *55*, 684-687.

[24] Najib, F. M., Zewar, S., Abdulla, A. M., A new sensor for thermometric titrations. *Talanta*. 2007, *71*, 141-148.
[25] Wang, K. C., Chen, S. M., Hsu, J. F., Cheng, S. G., Lee, C. K., Simultaneous detection and quantitation of highly water-soluble herbicides in serum using ion-pair liquid chromatography-tandem mass spectrometry. *J. Chromatogr. B*. 2008, *876*, 211-218.
[26] Mounir, N., El Jazouli, H., Amine, M. E., Masbouh, F., Kabli, H., Ichou, Y. A., Albourine, A., Potentiometric and quantum studies of the speciation of phenoxyacetic acids in the presence of mercury (II) and of lead (II). *Chem. Speciat. Bioavailab.* 2007, *19*, 45-56.
[27] Roberts, D. M., Dawson, A. H., Senarathna, L., Mohamed, F., Cheng, R., Eaglesham, G., Buckley, N. A., Toxicokinetics, including saturable protein binding, of 4-chloro-2-methyl phenoxyacetic acid (MCPA) in patients with acute poisoning. *Toxicol. Lett.* 2011, *201*, 270-276.
[28] Díez, C., Barrado, E., Marinero, P., Atienza, J., Study of different parameters affecting the derivatization of acidic herbicides with trimethylsulfonium hydroxide to make them suitable for gas chromatography analysis. *J. Chromatogr. A*. 2006, *1125*, 244-253.
[29] Yang, L., Liu, L., Olsen, B. A., Nussbaum, M. A., The determination of oxalic acid, oxamic acid, and oxamide in a drug substance by ion-exclusion chromatography. *J. Pharm. Biomed. Anal.* 2000, *22*, 487-493.

# Appendix III

**Paper 3:**

Graf, H. G., Rudisch, B. M., Ude, L., Müller, L., Huhn, C., Picomolar detection limits for glyphosate by two-dimensional column-coupled isotachophoresis/capillary electrophoresis mass spectrometry. *Journal of Separation Science* 2022; *45*, 3887-3899, DOI: 10.1002/jssc.202200519

Received: 28 June 2022 | Revised: 18 August 2022 | Accepted: 19 August 2022

DOI: 10.1002/jssc.202200519

JOURNAL OF SEPARATION SCIENCE

RESEARCH ARTICLE

# Picomolar detection limits for glyphosate by two-dimensional column-coupled isotachophoresis/capillary zone electrophoresis-mass spectrometry

**Hannes Georg Graf** | **Benjamin Maximilian Rudisch** | **Lukas Ude** | **Linda Müller** | **Carolin Huhn**

Institute of Physical and Theoretical Chemistry, Department of Chemistry, Eberhard Karls Universität Tübingen, Tübingen, Germany

**Correspondence**
Carolin Huhn, Institute of Physical and Theoretical Chemistry, Department of Chemistry, Eberhard Karls Universität Tübingen, Auf der Morgenstelle 18, Tübingen, Germany.
Email: carolin.huhn@uni-tuebingen.de

Capillary electrophoresis-mass spectrometry often lacks sufficient limits of detection for trace substances in the environment due to its low loadability. To overcome this problem, we conducted a feasibility study for column-coupling isotachophoresis to capillary electrophoresis-mass spectrometry. The first dimension isotachophoresis preconcentrated the analytes. The column-coupling of both dimensions was achieved by a hybrid capillary microfluidic chip setup. Reliable analyte transfer by voltage switching was enabled by an in-chip capacitively coupled contactless conductivity detector placed around the channel of the common section between two T-shaped crossings in the chip connecting both dimensions. This eliminated the need to calculate the moment of analyte transfer. A commercial capillary electrophoresis-mass spectrometry instrument with easily installable adaptations operated the setup. Prior to coupling isotachophoresis with capillary zone electrophoresis-mass spectrometry, both dimensions were optimized individually by simulations and verified experimentally. Both dimensions were able to stack/separate all degradation products of glyphosate, the most important herbicide applied worldwide. The first dimension isotachophoresis also removed phosphate, which is a critical matrix component in many environmental samples. Enrichment and separation of glyphosate and its main degradation product aminomethylphosphonic acid by the two-dimensional setup provided an excellent limit of detection of 150 pM (25 ng/L) for glyphosate.

**Article Related Abbreviations:** AMPA, aminomethylphosphonic acid; AUX, auxiliary vial housing; $C^4D$, capacitively coupled contactless conductivity detector; GLP, glyphosate; IN, inlet position of the CE instrument; LE, leading electrolyte; OUT, outlet position of the CE instrument; SAR, sarcosine; TE, terminating electrolyte; tITP, transient ITP.

**KEYWORDS**
column-coupling, conductivity detection, herbicides, intermediate detection, microfluidic chip interface

## 1 | INTRODUCTION

The LODs in CZE are not sufficient for trace analysis of substances in the environment due to the very low sample loadability. Therefore, different online sample preconcentration techniques were described [1–3]. Among them, the most robust, powerful, and universal preconcentration method uses ITP, which is based on a discontinuous electrolyte system. Analytes with a mobility inside the mobility window spanned by the leading (LE) and terminating (TE) electrolyte are sandwiched between them and adjusted in their concentrations to the leading ion. Ionic macroconstituents in the matrix can be removed by modifying this mobility window. Compared to CZE, ITP provides a clearly higher loadability [4]. Transient ITP (tITP) is performed in a single capillary and is accomplished through a coion that temporarily serves as a leading or terminating ion. The tITP stack dissipates to zone electrophoresis separation over time. Alternatively, ITP and CZE are conducted in two steps, first performing ITP and second, CZE in the same capillary. This requires removing the LE or the TE prior to the CZE step [5–7]. Higher flexibility, for example, in the choice of different capillary inner diameters and different electrolytes can be achieved by column-coupling ITP to CZE. Theoretical considerations [8–12] and examples [2, 3] for all strategies can be found elsewhere.

The first applications of column-coupled ITP/CZE were described by Kaniansky and Marák [13] using an adapted column-coupled ITP/ITP setup originally developed by Everaerts et al. [14, 15]. The modular, hydrodynamically closed setup with two capillaries of different inner diameters, each equipped with one capacitively coupled contactless conductivity detector ($C^4D$) and an additional UV-visible detector in the second dimension [14–17], was used in its commercialized version in about forty publications, the most recent of the major contributing authors are [18–22]. This setup was mostly used with a T-S-T system where the TE served as the BGE in the CZE step [13, 23]. Column-coupled ITP/CZE was also hyphenated to LIF in a setup developed and applied by Mikuš et al. for ultrasensitive detection of fluorescing compounds in multicomponent matrices [24]. In 2010, Foret et al. coupled the commercial ITP/CZE setup with an MS hydrodynamically transferring the analytes to the MS [25]. This setup was applied by Piešťanský et al. to determine pheniramine [26, 27], varenicline [28], and serotonin [29] in urine.

Earlier attempts of combining column-coupled ITP/CZE to MS used two high voltage supplies and a narrow capillary (CZE) inserted into a wider capillary (ITP). The electrokinetic transfer between both dimensions required all ITP separation potentials to be offset by +2 kV relative to the MS. After the analyte transfer, the ITP capillary was flushed with LE to provide a homogeneous BGE for the second dimension CZE [30, 31]. A similar fluidic setup was used by Peterson et al., who applied the voltage continuously from the TE vial to the MS while the ITP was flushed back and forth over the splitting point by injecting LE from a side channel. A UV-visible detector mounted just before the splitting point timed the injections [32].

In several publications, Neusüß et al. described column-coupling methods with final detection by MS. Different valves made from polyether ether ketone and a polyaryletherketone/polytetrafluoroethylene composite were used for interfacing. Depending on the separation modes coupled, at least two CE instruments were used, and up to two intermediate detectors (UV/$C^4D$) were mounted in front of the valve to calculate the arrival of analytes in the valve and transfer them to the second dimension via valve switching [33, 34]. Several studies used ITP/CZE fully integrated on microfluidic chips with conductivity detection at each column [35–37]. Further column-coupling strategies applied with other combinations of separation modes are reviewed elsewhere [17, 38].

Previous studies of our group showed that column-coupling setups benefit from a straight separation path with homogeneous surfaces and similar dimensions in both columns and the interface [39]. Our ITP-$C^4D$/CZE-MS setups published so far, used an adapted CE-MS instrument and focused on cationic analytes (mostly peptides) using the LE also as BGE in the second dimension CZE-MS forming a so-called L-S-L system which is less common in ITP/CZE compared to T-S-T systems [39]. Intermediate on-chip $C^4D$ detection on the common section between both dimensions enabled reliable analyte transfer in a non-aqueous ITP-$C^4D$/CZE-MS [40]. A commercial CE-MS instrument strongly modified by an external multivial holder and a custom-made multiport high voltage source was developed to allow a free choice of the BGE in the CZE dimension (BGE-S-BGE format) [40].

In this study, we address both instrumental and methodological aspects of a new ITP-$C^4D$/CZE-MS setup to

achieve sensitive analysis of anionic analytes. We combined the previous achievements by Kler et al. with an improved interface technology suggested by Sydes et al. [39–41] to achieve a user-friendly and compact 2D setup: A hybrid capillary microfluidic glass chip approach was used on a single adapted commercial CE-MS instrument. All components including the capillary-chip connections were modular and flexibly installed. No calculations or preliminary evaluation steps to successfully transfer the analytes were needed in our setup since we integrated an intermediate in-chip $C^4D$ placed directly on the common section of both dimensions formed between two T-crossings.

Anionic herbicides such as glyphosate (GLP) were selected as model analytes since their analysis is still challenging in environmental samples [42]. The lack of a chromophoric system and their high charge and polarity make them difficult to be analyzed by chromatographic methods. In addition to GLP, we also included its metabolites in this study (for analyte selection, see [43]) to demonstrate the broad applicability of the ITP method.

Commonly, GLP is analyzed by LC-MS/MS on C18 columns after a rather laborious derivatization step and solid phase extraction. Other chromatographic methods were used [44, 45] including anion exchange chromatography and hydrophilic interaction liquid chromatography [46, 47]. GLP can also be determined directly by coupling CZE to $C^4D$, MS, or indirect UV or use ITP-$C^4D$. After derivatization, also CZE-LIF and CZE-UV are applicable [48].

To optimize the separation conditions, the p$K_A$ values and limiting electrophoretic mobilities for GLP and its metabolites were used to simulate optimal separation conditions for CZE-MS [43]. A focus was set on simultaneously removing phosphate as the most critical matrix component, which we intended to exclude from the ITP stack [49, 50]. Finally, ITP-$C^4D$/CZE-MS measurements were conducted to analyze GLP in aqueous samples.

## 2 | MATERIALS AND METHODS

### 2.1 | Chemicals

The chemicals used for analysis were aminomethylphosphonic acid (AMPA) (99%), barium hydroxide octahydrate ($Ba(OH)_2$) (≥ 98%), glycine (GLY) (≥98%), glyoxylic acid monohydrate (98%), GLP (analytical grade) and sarcosine (SAR) (≥98%), sodium phosphate dibasic heptahydrate ($Na_2HPO_4$, inorganic phosphate) (≥99%), potassium hydroxide (KOH) (≥85%), ammonium carbonate ($(NH_4)_2CO_3$), all purchased from Sigma-Aldrich (Steinheim, Germany). Dr. Ehrensdrofer (Augsburg, Germany) supplied *N*-acetyl AMPA (99.5%) and hydroxymethylphosphonic acid (98.6%). The used *N*-acetyl GLP (NGLP) (95%) was purchased from Toronto Research Chemicals (Toronto, Canada). Proline (≥99%), was ordered from Fluka (Buchs, Switzerland). Ammonia solution for LC-MS (25%) and formic acid for LC-MS (98%) were purchased from Merck (Darmstadt, Germany). The sheath liquid was prepared with propan-2-ol (LC-MS grade) from Carl Roth (Karlsruhe, Germany). Deionized water was purified by an ELGA LabWater (Celle, Germany). Glufosinate, oxamic acid, and 2-methyl-4-chlorophenoxyacetic acid were only included in simulations.

### 2.2 | Instrumentation

#### 2.2.1 | CE-mass spectrometry

For ITP-MS and CZE-MS, a 7100 CE was coupled to a 6150 single quadrupole mass spectrometer via a sheath liquid CE-ESI-MS interface, all supplied from Agilent Technologies (Waldbronn, Germany or Santa Clara, CA, USA). A sheath liquid flow was provided during analyses via a splitter (1:100) by a 1200 series isocratic pump (Agilent Technologies). The MS simultaneously monitored the $[M-H]^-$ masses in selected ion monitoring mode with equal dwell times using the following operation parameters unlike otherwise stated: capillary voltage 3500 V negative; nebulizer pressure 5 psi; drying gas flow 10 L/min; drying gas temperature 150°C; fragmentor voltage: 125 V; peak width 0.3 min. Nitrogen gas was supplied by an NGM 44-LC/MS (CMC Instruments, Eschborn, Germany). The control of the CE and MS instruments and the data acquisition were performed by ChemStation Rev. C. 01.05 software (Agilent Technologies). All measurements were performed in a bare fused silica capillary from Polymicro Technologies (Phoenix, AZ, USA) with an inner diameter of 75 μm. The lengths are given in the figure captions. The capillary tip in the ESI sprayer was sanded with 4000-grit sandpaper to an angle of 45° improving the electrospray process. This instrumentation was also the base for the 2D ITP-$C^4D$/CZE-MS setup.

#### 2.2.2 | Fluidic setup used for ITP-conductivity detection coupled to CZE-MS

Starting with the achievements of Kler and Sydes [39–41], a new setup was established. A scheme is given in Figure 1A and photos of the realized setup are given in Section S1. The core element of the fluidic setup was a microfluidic fused silica chip produced with selective laser-induced etching technology from LightFab (Aachen, Germany), see Figure 1B,C. The chip included a double T-shaped

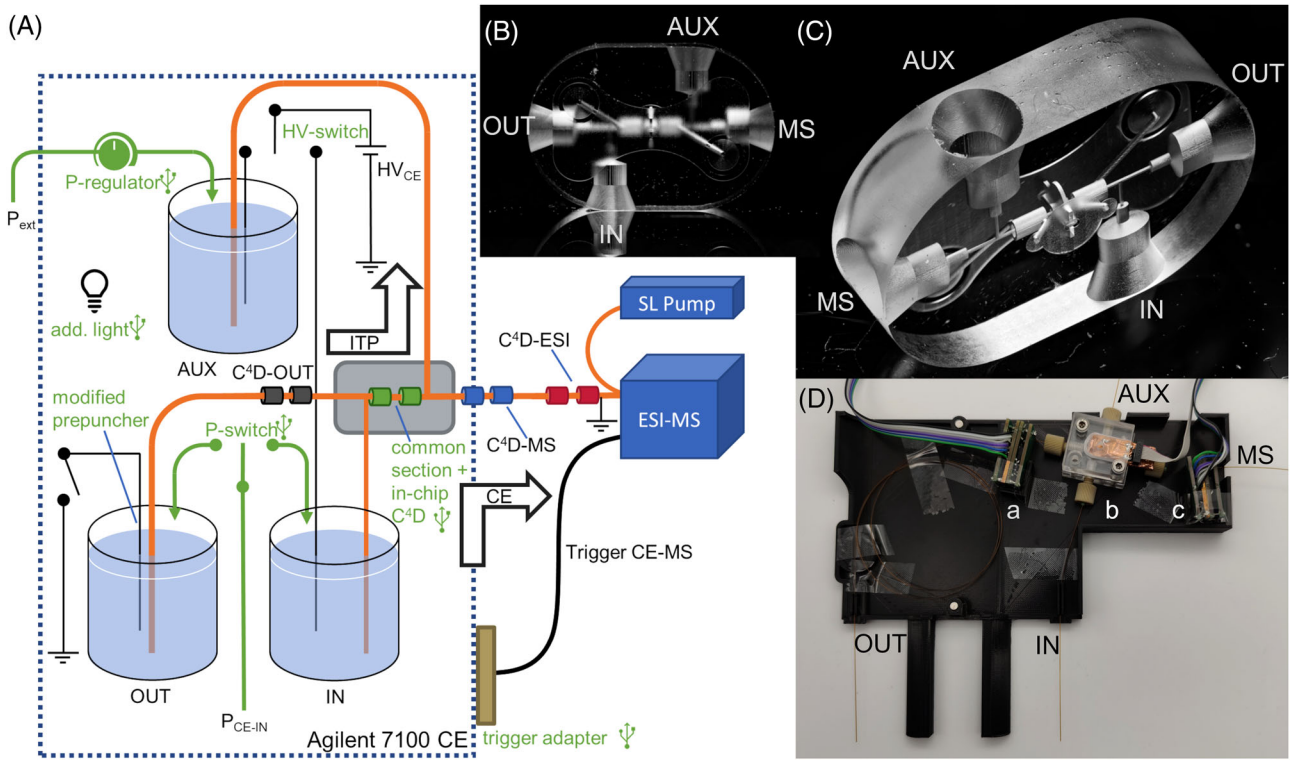


**FIGURE 1** (A) Scheme of the ITP-C$^4$D/CZE-MS setup with four capacitively coupled contactless conductivity detectors (C$^4$Ds) (one in-chip) and ESI-MS detection; gray box: microfluidic chip, amber: capillaries, green: compressed air (P) supplied by the CE instrument ($P_{CE-IN}$) or the external laboratory pressure system ($P_{ext}$), black: electric circuit, the green text indicates adaptions to the commercial CE-MS. (B) Front and (C) back view photo of the fused silica chip including a double T-shaped microfluidic structure to transfer analytes between two dimensions (common section) and a C$^4$D geometry around it. (D) Photo of the open 3D printed CE cassette with the fluidic setup including (a) C$^4$D-OUT, (b) in-chip C$^4$D, and (c) C$^4$D-MS. The capillaries are labeled according to the capillary ends

microfluidic structure (id: 100 µm) giving a 4 mm long common section of the dimensions with a volume of 31 nl. The section was surrounded by a chip-integrated geometry of a C$^4$D consisting of two tubular and one disk-shaped cavity filled with conductive silver paint. Capillaries were connected to the four ports of the chip with fittings and sleeves, all fixed in a mount. The lengths (in cm) of the capillaries were 65.0 (OUT), 13.5 (IN, id: 50 µm), 65.0 (MS), and 27.8 (AUX), for abbreviations, see Figure 1 and Section 2.2.3. Capillary ends were sanded to an angle of 90° at the chip side to ensure tight connections and the lowest possible dead volumes. The commercial CE-MS cassette was replaced by a 3D printed cassette to house the chip interface and provide maximum flexibility regarding its positioning while ensuring an easy installation in the CE, see Figure 1D. Further details can be found in Section S2.

### 2.2.3 | Adaptions to the commercial CE-MS instrument for 2D applications

When upgrading the commercial CE-MS instrument for 2D applications, we desired to make as few changes as possible to the standard CE-MS setup. Thus, the four capillaries inserted into the chip interface were installed as follows: 1) The ITP (1st dimension) was performed from the CE's outlet (OUT) to the auxiliary vial housing (AUX) which was installed in a recess of the CE's insulation plate. 2) The CZE-MS separation (2nd dimension) was performed from the CE's inlet position (IN) to the MS as in standard CZE-MS, compare Figure 1A. Therefore, the sample injection must be accomplished from OUT. This was well possible using the autosampler with a small adaptation of the CE's pressurization system for the vials. Further details can be found in Section S3.

### 2.2.4 | Detection setup

The in-chip C$^4$D used the electronics and software developed by Graf et al. [54] in the configuration with a preamplifier. The display data were smoothed by a ten-point moving average function. For maximum insight into the separation process, three optional openC$^4$Ds were used [51], which were named according to the capillary ends, compare Figure 1A. The C$^4$D-OUT was mounted 4.5 cm

in front of the first T-crossing to monitor the filling of the capillaries and the LE-TE boundary. The $C^4D$-MS was placed 8.0 cm behind the second T-crossing in the chip and aided to see if a transient ITP remained after voltage switching. Just before the ESI sprayer, the $C^4D$-ESI was placed (12.7 cm in front of the capillary end). It was used to detect counterions possibly migrating into the BGE from the sheath liquid changing its composition [52] or a possible counter-ITP migrating from the MS to the chip interface [53]. Further details can be found in Section S4.

## 2.3 | Solutions and electrophoretic separation

### 2.3.1 | Solutions and samples

The final composition of the LE, also serving as BGE in the CZE dimension, was 10 mM $(NH_4)_2CO_3$ and 115 mM $NH_4OH$ (pH 10.2) in water. The aqueous TE solution contained 10 mM KOH and 135 mM $NH_4OH$. All samples were dissolved in LE. The sheath liquid was made of 0.1% formic acid in 50% v/v propan-2-ol and provided at a flow rate of 5 μl/min.

### 2.3.2 | Settings for CZE and ITP coupled to MS

For one-dimensional measurements on a single capillary, the capillary was purged prior to its first use with BGE or LE for 5 min and between runs for 1.5 min at 1 bar each. Samples were injected as stated in the figure captions and were followed by a BGE or TE plug injected for 5 s at 50 mbar. Settings for the MS are given in Section 2.2.1 or the figure captions.

ITP-$C^4D$/CZE-MS measurements are described in Section 3.2.

## 2.4 | Simulations of capillary zone electrophoresis and isotachophoresis

The optimization of the CZE and ITP was performed by simulations with the software PeakMaster [55] and Spresso [56] using the $pK_A$ and mobility data we published previously [54]. The EOF in CZE simulations was estimated from the EOF mobility in bare fused silica capillaries. Due to pressure application in experiments, the migration time of the sample plug with uncharged matrix components was used as an EOF marker to adapt the simulations.

# 3 | RESULTS

## 3.1 | One-dimensional methods

Prior to column-coupled ITP/CZE, both CZE and ITP methods were developed independently based on preliminary simulations with PeakMaster and Spresso, see Section 2.4, and then validated by CZE-MS and ITP-MS measurements.

### 3.1.1 | Capillary zone electrophoresis-MS

As predicted by simulations, see Figure 2A, a BGE with a pH of 10.2 allowed a baseline separation of all analytes by CZE-MS, especially of GLP and its two main metabolites AMPA and SAR (see also discussion in [43]), compare Figure 2B. Due to insufficient ionization efficiency in the ESI process, glyoxylic acid was not detected. Separations at lower pH values were discarded due to insufficient robustness to small pH changes, especially for SAR and glycine, see [43]. The relatively high effective electrophoretic mobility of the slowest target ion SAR also simplified the search for a suitable terminating ion in the first-dimension ITP. When monitoring only AMPA, GLP, and SAR, LOQs were estimated to be 5 and 2 μM for GLP and AMPA, respectively, while SAR was hardly detectable, see Section S5.

### 3.1.2 | Isotachophoresis-MS

First-dimension ITP simulations focused on preconcentrating all target ions, which required a pH > 9 of the electrolytes on the one hand, and on the other hand on ensuring that the mobility of the leading ions was lower than that of phosphate ions to exclude them from the ITP stack. This should allow removing phosphate in the first dimension by front-cutting in ITP/CZE. Phosphate is critical since it is widely present in environmental samples but is also used to extract GLP from soils and sediments [50, 57]. Aiming at an L-S-L system for the 2D separation, MS-compatible electrolyte components had to be used. All desired features could be combined at a pH of the LE of 10.2 using formate or carbonate as leading ions and proline as terminating ion, see Figure 3A. The fast-migrating *N*-acetyl GLP could not be included in the ITP stack. Advantageously, both, phosphate and chloride were removed successfully migrating zone electrophoretically in the LE.

Experiments with formate as the leading ion showed that carbonate ions from atmospheric carbon dioxide,

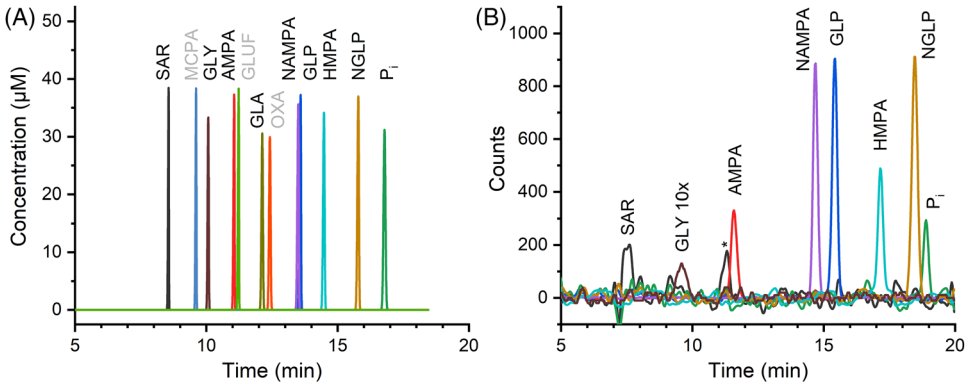


**FIGURE 2** (A) Simulated electropherogram for the separation of a mixture of aminomethylphosphonic acid (AMPA), glyoxylic acid (GLA), glyphosate (GLP), glufosinate (GLUF), glycine (GLY), hydroxymethylphosphonic acid (HMPA), 2-methyl-4-chlorophenoxyacetic acid (MCPA), *N*-acetyl AMPA (NAMPA), *N*-acetyl GLP (NGLP), oxamic acid (OXA), $Na_2HPO_4$ as inorganic phosphate ($P_i$) source and sarcosine (SAR) ($c = 50$ µM, each) dissolved in BGE, and the corresponding (B) experimental electropherogram of a subset of analytes (highlighted in Figure 2A). The pseudo molecular $[M\text{-}H]^-$ ions were recorded by MS in selected ion monitoring mode after injecting the sample for 5 s × 30 mbar and separation by CZE at +10 kV and −10 mbar pressure at the inlet. The aqueous BGE was made from 10 mM $(NH_4)_2CO_3$ and 115 mM $NH_4OH$, pH 10.2; The bare fused silica capillary had a length of 60 cm and an inner diameter of 75 µm. Drying gas was supplied at 11 L/min. The data curve of GLY in (B) was amplified by a factor of ten. No GLA signal was recorded. The $[SAR\text{-}H]^-$ trace showed a signal from an impurity marked with an asterisk. For abbreviations, see Section 2.1

dissolved in basic solutions, impaired ITP separations. The addition of barium hydroxide to the TE successfully reduced this interference and further allowed to omit proline in the TE since hydroxide proved suitable as a terminating ion. This was possible because the electrophoretic mobility of hydroxide was low using the weak base ammonia as the counterion in ITP under basic conditions. This is possible, because its mobility is proportional to the mobility of the counterion in the TE zone, for details see [58].

We decided to use carbonate in the LE, as phosphate ions were better separated from the ITP stack due to a higher difference in effective electrophoretic mobilities as compared to formate. The high buffer capacity was another advantage. Potassium hydroxide was sufficient as TE with hydroxide ions serving as terminating ions. This avoided barium salts precipitating in the ESI interface.

The isotachopherogram given in Figure 3B shows the successful separation of phosphate ($c$ = 5 mM) as an interfering ionic macroconstituent from a selection of the model analytes (GLP, AMPA, and SAR ($c = 100$ µM, each)), which cover the full mobility range of the ITP stack. All analytes migrated in the migration order predicted by simulations for this ITP electrolyte system. The detection of analytes in the low nanomolar range is shown in Figure 3C. However, at these low concentrations, the length of the individual analyte zones in peak mode ITP was so small that the analyte zones were no longer detected sufficiently separated for precise quantification as quenching effects become likely [15, 53].

## 3.2 | ITP-conductivity detection coupled to CZE-MS

In order to demonstrate the applicability of the new 2D setup, we focused on GLP and AMPA as the most important analytes present in environmental and food samples. For these analytes, a good comparison with literature data is possible. Future studies will also include degradation products and will demonstrate the applicability to environmental samples.

The ITP-$C^4D$/CZE-MS method can be divided into four steps: A) preparation of runs, B) column-coupled ITP-$C^4D$, C) analyte transfer and D) column-coupled CZE-MS. These steps are presented in the panels in Figure 4. Traces of $C^4D$ and MS detection as well as the current during voltage application are shown in Figure 5A,B for an injection of GLP and AMPA at a concentration of 50 nM. The zero point of the time scale was set to the application of voltage to the CZE-MS step, thus for ITP negative time values are given. More methodological details on the steps in ITP-$C^4D$/CZE-MS can be found in Section S6.

**Step A) Preparation of runs**

First, the entire setup was flushed with LE = BGE from AUX, see Figure 4A.

**Step B) Column-coupled ITP-$C^4D$**

After injecting the sample at OUT, the ITP step was started by applying +12 kV to AUX with respect to OUT and MS and application of 70 mbar to OUT.

In Figure 4B, the target analytes reached the first T-crossing, while faster/slower matrix ions ($M_f/M_s$)

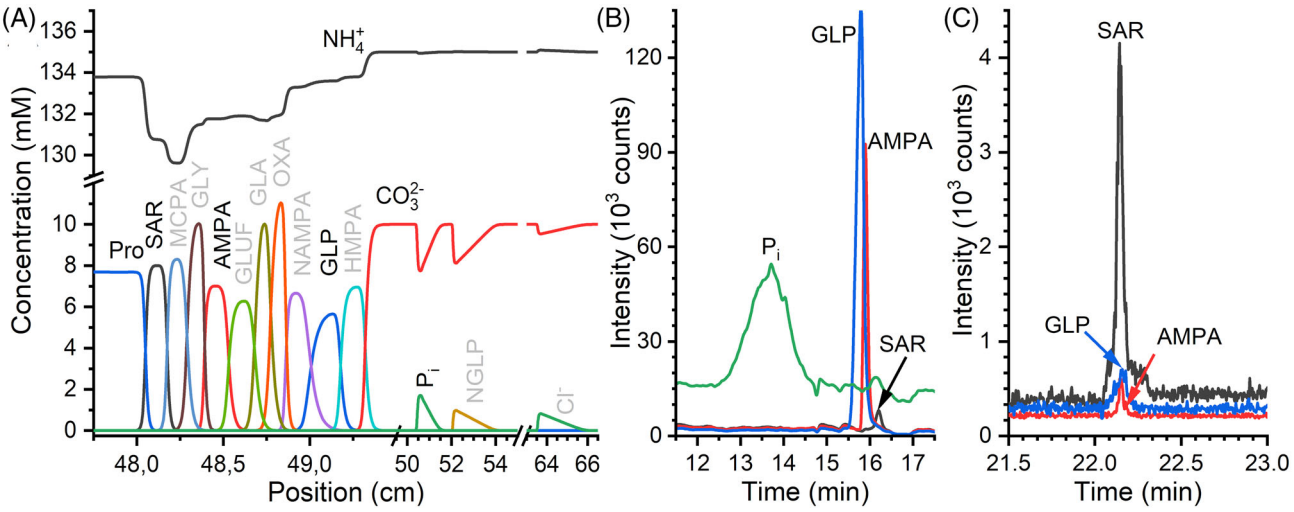


**FIGURE 3** (A) Simulated ITP with the analytes: aminomethylphosphonic acid (AMPA), glyoxylic acid (GLA), glyphosate (GLP), glufosinate (GLUF), glycine (GLY), hydroxymethylphosphonic acid (HMPA), 2-methyl-4-chlorophenoxyacetic acid (MCPA), *N*-acetyl AMPA (NAMPA), N-acetyl GLP (NGLP), oxamic acid (OXA), $Na_2HPO_4$ as inorganic phosphate ($P_i$) source, sarcosine (SAR), and chloride ($Cl^-$) ($c = 1$ mM, each) at a pH of 10.2 in the leading electrolyte (LE). LE: 10 mM carbonate, terminating electrolyte (TE): 5 mM proline (Pro), counterion: 135 mM $NH_3$. (B, C) Mass traces of $[M\text{-}H]^-$ ions recorded by ESI-MS after ITP separation. A sample mixture of (B) 100 µM AMPA, GLP, SAR, and 5 mM $Na_2HPO_4$ ($P_i$) dissolved in 135 mM $NH_4OH$ or (C) 5 nM AMPA, GLP, and SAR dissolved in LE was injected for (B) 10 s or (C) 20 s at 100 mbar and separated by ITP at (B) -12 or (C) -14 kV and (B) 75 or (C) 80 mbar pressure support. (B, C) LE: 10 mM $(NH_4)_2CO_3$, 115 mM $NH_4OH$; TE: 10 mM KOH, 135 mM $NH_4OH$. The bare fused silica capillary had a length of (B) 50 or (C) 65 cm and an inner diameter of 75 µm. The MS' capillary ESI voltage was set to (B) −3500 V or (C) -4000 V and the peak width of the MS was set to (B) 0.15 or (C) 0.05 min to achieve optimal settings for low analyte concentrations and narrow peaks in (C). For abbreviations, see Section 2.1

migrated zone electrophoretically in the LE/TE. The isotachophoretic condition in the first dimension was verified by the current decreasing continuously at constant voltage, see Figure 5A (negative time range) and by a strong sudden change in conductivity recorded by the $C^4D$-OUT at -2.0 min, see Figure 5B. This conductivity step was due to the LE-TE boundary with the stacked target analytes passing the detector in front of the chip interface.

Due to the permanent electrical connection of the MS interface to ground, an EOF was also present from AUX to MS, leading to a constant bulk flow of LE through the capillary to the MS. This ensured that anions originating from the sheath liquid did not enter the migration path as can be seen from the absence of a conductivity change in $C^4D$-ESI [52]. Ions entering this migration path during the ITP step were also flushed to the MS.

**Step C) Analyte transfer**

The in-chip $C^4D$ on the common section between the two dimensions allowed a reliable transfer of the analytes between the ITP and the CZE dimension by voltage switching. When the LE-TE boundary passed the in-chip $C^4D$, see Figure 4C, a strong change in the in-chip $C^4D$ data was observed, see Figure 5A at -1.5 min. Now, the ITP method was stopped setting the applied pressure and voltage to zero (dashed vertical line in Figure 5A). Matrix compounds migrating slower than the TE ($M_s$) and faster than the LE ($M_f$) were removed prior to the CZE separation since they were not transferred to the second dimension but remained in the OUT or AUX capillary.

**Step D) Column-coupled CZE-MS**

The CZE separation started by applying +15 kV to IN, see Figure 4D. Except TE co-transferred upon voltage switching, the CZE-MS migration path was only filled with LE. Accordingly, after the dissolution of the tITP L-S-L stack, zone electrophoretic separation starts. No pronounced conductivity change was detected by the $C^4D$-MS, which verified that the ITP quickly resolved. Only a low amount of TE was co-transferred to the CZE-MS dimension. No conductivity change was observed by $C^4D$-ESI, demonstrating that the bulk flow was high enough in each step to prevent anions from the sheath liquid entering the capillary.

AMPA and GLP were detected at 19.5 and 24.6 min. The two large peaks observed in the $m/z$ 168 trace for $[GLP\text{-}H]^-$ were recorded with similar intensity in each measurement, even in blank runs. Experiments indicated that they originate from leachates of the seal debris that was carried into the interface during capillary mounting.

A short time span between the detection of the LE-TE boundary by the in-chip $C^4D$ and stopping the ITP step is beneficial for the second dimension CZE-MS to

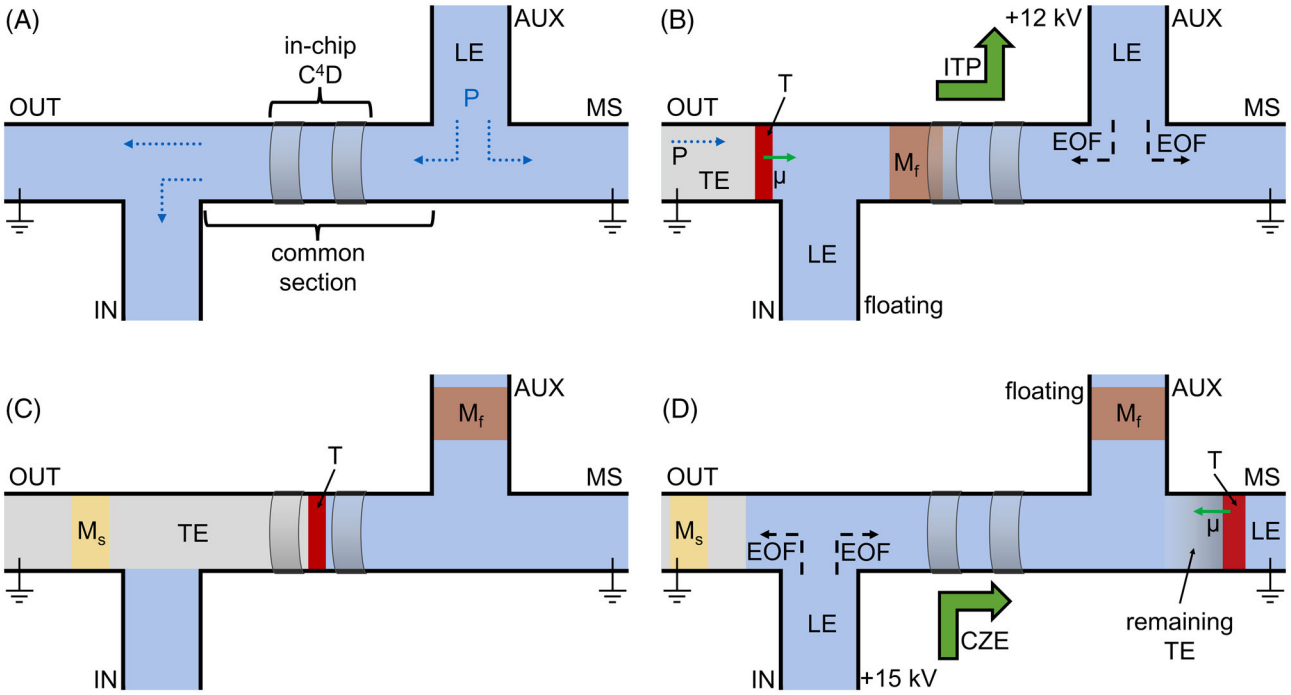


**FIGURE 4** Schematic depiction of the steps during ITP-$C^4D$/CZE-MS. Step (A) Preparation of measurements: all capillaries were purged from the auxiliary vial (AUX) with leading electrolyte (LE). Step (B) Column-coupled ITP-$C^4D$: The target analytes (T) stacked at the LE-TE boundary prior to entering the common section. Electrophoretic migration of analytes from AUX to OUT, but transport by EOF and pressure from OUT to AUX. Step (C) Analyte transfer: when the LE-TE boundary was detected by the in-chip $C^4D$, the ITP was stopped and the high voltage supply replugged. Step (D) Column-coupled CZE-MS: only the stacked target analytes reach the MS being transported by the high EOF while migrating electrophoretically towards the chip interface. $C^4D$: capacitively coupled contactless conductivity detector; T: target analytes; $M_f$, $M_s$: matrix components with electrophoretic mobility faster than the LE ($M_f$) or slower than the terminating electrolyte (TE) ($M_s$); P: pressure support; μ: migration direction of anions; OUT, IN, MS: capillary to the CE's outlet, inlet position and to the CE-MS interface, respectively, see also Figure 1A

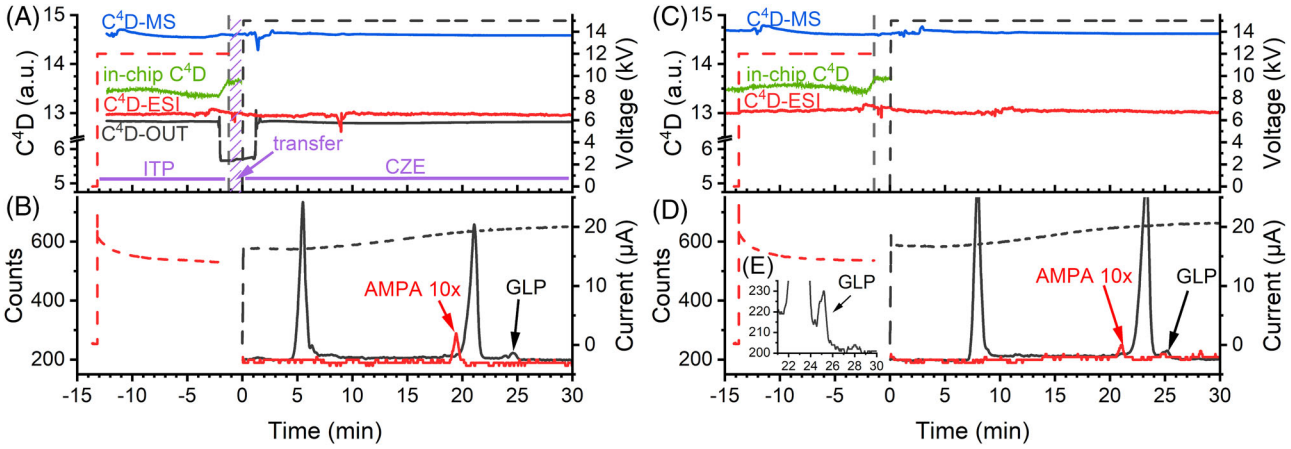


**FIGURE 5** Data acquired during ITP-$C^4D$/CZE-MS. Injection at 100 mbar for 20 s of glyphosate (GLP) and aminomethylphosphonic acid (AMPA) at a concentration of (A+B) 50 nM or (C–E) 500 pM each dissolved in the leading electrolyte (LE). In panel (A) the ITP, transfer, and CZE steps are indicated in purple. (A, C) Solid curves: capacitively coupled contactless conductivity detector ($C^4D$) traces of the detectors $C^4D$-OUT (4.5 cm in front of the first T-crossing), in-chip $C^4D$ (on the common section), $C^4D$-MS (8.0 cm behind the second T-crossing) and $C^4D$-ESI (12.7 cm in front of the MS), see Figure 1A. (A, C) Dashed curves: applied voltage by the CE. (B, D) Solid curves: MS traces from selected ion monitoring for m/z 168.1 $[GLP\text{-}H]^-$ and 110.0 $[AMPA\text{-}H]^-$. (B, D) Dashed curves: measured driving current. (E) Enlarged section of the MS trace for *m/z* 168.1 showing the GLP peak at 500 pM (84.5 ng/L, S/N = 10). For further details, see Sections 2.2.2, 2.2.4, and 3.2. The zero point of the time scale was set to the application of voltage for the CZE-MS step

lower the amount of co-transferred TE. This time span also depends on the amount of analytes/matrix components present in the ITP stack. This is shown by comparing two ITP/CZE-MS runs in Figure 5A,B versus Figure 5C,D, which only differed in the concentration of the sample. The run with a sample concentration of 500 pM (Figure 5C) was stopped 11 seconds earlier and, therefore, virtually no TE was observed in the CZE-MS dimension proven by the absence of a conductivity dip in the data of the $C^4D$-MS compared to the run after injecting a 50 nM sample (Figure 5A).

During the CZE-MS step, the LE was transported from IN to OUT driven by the EOF, which is observed by the $C^4D$-OUT revealing a strong conductivity change upon the TE-LE boundary passing at 1.2 min and the increasing current up to a certain limit during the CZE separation, see Figure 5B (positive time range). Therefore, the TE and the slower matrix ions ($M_s$) were pushed back to OUT, preventing their continuous transfer to the MS capillary by suctions effects caused by the EOF in the IN-MS path and the CE-ESI-MS interface. The faster matrix ions ($M_f$) were trapped in the AUX capillary caused by its floating potential preventing EOF and ion migration.

## 4 | DISCUSSION

This feasibility study showed that it is possible to perform column-coupling ITP-$C^4D$/CZE-MS in a hydrodynamically open migration path on a single, adapted commercial CE-MS setup with only minor additional components. This was achieved using a modular hybrid capillary microfluidic chip approach that clamped capillaries with fittings instead of gluing them as in our previous approaches [40]. The use of butt-end connections between capillaries and fluidic channels possible due to the high precision in selective laser-induced etching provided the lowest possible dead volumes and allowed a uniform separation path completely made from bare fused silica. No capillary coatings were required, instead, the system operated at high EOF conditions. The double T-shaped microfluidic structure formed a common section between both separation dimensions defining a fixed transfer volume of 31 nl. This transfer volume is easily scalable by changing the dimensions of the common section in different chip interfaces which is easily possible thanks to the selective laser-induced etching technology. This technology allowed circular cross-sections of the fluidic structure in contrast to other chip technologies, where a cross-section mismatch is present when coupling capillaries. In comparison with mono T-shaped microfluidic structures as used in [39], the double T-shaped structure allowed to remove ionic matrix components with higher mobilities than the target analytes such as phosphate and chloride. This setup forced their migration towards AUX and thus prevented their migration into the CZE-MS dimension. Future studies will investigate if multiple heart cuts refilling the common intersection are possible when an ionic macroconstituent has electrophoretic mobility in between those of analytes, similar to the work of Peterson et al. [32]. However, for environmental samples, the main macroconstituents are inorganic ions, which mostly have a very high effective electrophoretic mobility, making the L-S-L approach with front cutting an ideal solution. An alternative approach to transfer a fixed volume between two fully separated dimensions was presented by the Neusüß group using a valve with four or eight ports with transfer volumes of 4–20 nl [33, 34, 59]. Our approach has the advantage that dead volumes are minimized as low as technically possible for capillary-interface couplings. No current and liquid leakages as observed for the valve-based system (due to mechanical and electrical wear) were observed. The valve's inner surface was different from the capillaries evoking internal pressures due to EOF mismatches. In our setup, the applicable voltage was not limited, whereas the valve allowed a maximum of 25 kV [33, 34]. On the other hand, our setup does not allow us to independently operate the separation dimensions, which are not hydrodynamically separated.

In our study, an in-chip $C^4D$ with tubular electrodes surrounding the dimensions' common section was used for the first time. It enabled a reliable analyte transfer between the ITP and the CZE dimension by voltage switching, aided only by some support from the suction effect of the ESI interface. The use of a detector directly on the common section eliminated the need to calculate the arrival time of the analytes at the transfer point based on their migration speed as in most other setups [15, 34, 39, 59]. This is advantageous, especially for first dimension separations, where the migration speed changes over time such as ITP operated at a constant voltage as applied here. Effects on EOF velocities, changes in buffer pH, and so forth, are thus considered automatically, giving rise to higher robustness of the setup. This will also aid in applications to samples with a higher matrix load in the future.

Using an L-S-L system (LE is also the BGE of the CZE separation), enabled us to build a compact setup that was housed completely in a single CE instrument. Previous attempts of our group with a similar fluidic setup and a BGE dedicated to separating cationic analytes required an additional external high voltage supply, a multivial holder, and manual (de)blocking of capillaries [40]. Other 2D attempts used a second CE instrument, an additional high voltage supply [30, 31, 33, 34, 59], or required

pumps or syringes for liquid handling in hydrodynamically closed setups with membranes and a hydrodynamic analyte transfer when coupled to MS [15]. After the filling of our setup with LE, no further flushing steps of sections of the capillary network as in [30–32] were necessary, especially prior to the CZE separation, which proved advantageous regarding band broadening.

All adaptions to the CE-MS setup were modular and allowed to flexibly be installed in the CE instrument itself. This compact setup allowed to use short capillaries. A 3D printed cassette avoided mechanical stress to the fluidic system as well as an easy installation in the CE instrument similar to single capillary applications. Switching between 1D and 2D applications was thus fast and easy. Two capillaries connected to the CE's autosampler allowed maximal flexibility and especially automation. All liquid handling with flushing steps was computer-controlled and implemented by pressurization of the respective vial. In the current setup, the analyte transfer was conducted manually restricted especially due to constraints given by the CE software.

Thanks to individual optimization of both, the CZE, and the ITP step, the first ITP/CZE-MS measurements were conducted without an intense optimization phase and revealed a remarkably low LOD (S/N = 3) of 150 pM (25 ng/L) for GLP improving LODs of the individual method by a factor of 10 000. GLP was successfully separated from AMPA as predicted by the individual CZE-MS analyses, see Figure 5D,E.

Regarding the concentration range, analyses up to an analyte concentration of 50 μM (5.5 mg/L AMPA and 8.5 mg/L GLP) were conducted. The RSD of the peak area ($n = 3$) for a sample with a concentration of 500 nM was 11% for AMPA and 20% for GLP. The precision of the migration times was very good with 1.1% and 2.8%. In the future, further optimizations reducing the analysis time are intended using higher separation voltages and shorter capillaries (possibly up to a factor of two compared to the setup presented here). The LODs can further be enhanced by using higher injection volumes or using ITP capillaries with larger ids. For comparison, under optimized CZE-$C^4D$ conditions with a field-enhanced sample injection, See et al. reached a four times higher LOD of 100 ng/L for GLP [60]. For electrophoretic methods with $C^4D$, lower LODs were only demonstrated using offline preconcentrating methods. For example, dynamic supported liquid membrane tip extraction was used by See et al. achieving an LOD of ~50 ng/L [61]. See et al. combined electromembrane extraction with large volume sample stacking to improve the LOD to 64 ng/L [62]. Horčičiak et al. presented a chip-based column-coupling ITP-$C^4D$/CZE-$C^4D$ setup and reached a LOD of 2.5 μg/L in a BGE-S-BGE electrolyte system [50]. CZE-MS without derivatization and preconcentrating steps provided an LOD of 5 μg/L for GLP in our laboratory [49]. Only with chromatographic techniques, for example, LC-MS/MS in combination with derivatization and solid phase extraction with an enrichment factor > 300, an LOD below 1 ng/L was reached [63]. Our method revealed the lowest published LOD for GLP using electrophoretic separations without any additional offline pre-concentration step.

In future work, the ITP-$C^4D$/CZE-MS will be applied to all degradation products of GLP except for *N*-acetyl GLP, which should be well possible given the results of simulations and single dimension ITP-MS and CZE-MS experiments. The possibility of simultaneously removing phosphate as the most critical interfering matrix compound will be investigated with surface water samples and soil extracts.

## ACKNOWLEDGMENTS

We thank the staff at LightFab, especially Martin Hermans, for the detailed advice and our workshop for the fast and precise manufacturing of all instrumental components, especially Alexander Schnapper, Christof Binder, and Gerd Vollmer.

## CONFLICT OF INTEREST

The authors have declared no conflict of interest.

## DATA AVAILABILITY STATEMENT

All supporting data are included in the paper or the Supporting Information.

## ORCID

*Carolin Huhn* https://orcid.org/0000-0001-6865-1043

## REFERENCES

1. Šlampová A, Malá Z, Gebauer P. Recent progress of sample stacking in capillary electrophoresis (2016–2018). Electrophoresis 2019;40:40–54.
2. Breadmore MC, Grochocki W, Kalsoom U, Alves MN, Phung SC, Rokh MT, Cabot JM, Ghiasvand A, Li F, Shallan AI, Keyon ASA, Alhusban AA, See HH, Wuethrich A, Dawod M, Quirino JP. Recent advances in enhancing the sensitivity of electrophoresis and electrochromatography in capillaries and microchips (2016-2018). Electrophoresis 2019;40:17–39.
3. Malá Z, Gebauer P. Recent progress in analytical capillary isotachophoresis. Electrophoresis 2019;40:55–64.
4. Boček P, Deml M, Kaplanová B, Janák J. Analytical isotachophoresis: the concept of the separation capacity. J Chromatogr A. 1978;160:1–9.
5. Reinhoud NJ, Tjaden UR, van der Greef J. Automated isotachophoretic analyte focusing for capillary zone electrophoresis in a single capillary using hydrodynamic back-pressure programming. J Chromatogr A. 1993;641:155–62.

6. Lamoree MH, Reinhoud NJ, Tjaden UR, Niessen WM, van der Greef J. On-capillary isotachophoresis for loadability enhancement in capillary zone electrophoresis/mass spectrometry of beta-agonists. Biol. Mass. Spectrom. 1994; 23: 339–45.
7. van der Vlis E, Mazereeuw M, Tjaden UR, Irth H, van der Greef J. Combined liquid-liquid electroextraction-isotachophoresis for loadability enhancement in capillary zone electrophoresis-mass spectrometry. J. Chromatogr. A. 1995; 712: 227234.
8. Křivánková L, Gebauer P, Boček P. Some practical aspects of utilizing the on-line combination of isotachophoresis and capillary zone electrophoresis. J. Chromatogr. A. 1995; 716: 35–48.
9. Křivánková L, Gebauer P, Thormann W, Mosher RA, Boček P. Options in electrolyte systems for on-line combined capillary isotachophoresis and capillary zone electrophoresis. J. Chromatogr. A. 1993; 638: 119–35.
10. Kaniansky D, Marák J, Laštinec J, Reijenga JC, Onuska FI. Capillary zone electrophoresis with on-line isotachophoretic sample pretreatment: sample clean-up aspects. J. Microcolumn Sep. 1999; 11: 141–53.
11. Křivánková L, Pantůčková P, Boček P. Isotachophoresis in zone electrophoresis. J. Chromatogr. A. 1999; 838: 55–70.
12. Kvasnička F, Jaroš M, Gaš B. New configuration in capillary isotachophoresis–capillary zone electrophoresis coupling. J. Chromatogr. A. 2001; 916: 131–42.
13. Kaniansky D, Marák J. On-line coupling of capillary isotachophoresis with capillary zone electrophoresis. J. Chromatogr. A. 1990; 498: 191–204.
14. Everaerts FM, Verheggen T, Mikkers FEP. Determination of substances at low concentrations in complex mixtures by isotachophoresis with column coupling. J. Chromatogr. A. 1979; 169: 21–38.
15. Everaerts FM, Beckers JL, Verheggen TP, Isotachophoresis: theory, instrumentation and applications. Amsterdam: Elsevier; 1976.
16. Urbánek M, Blechtová L, Posplšilová M, Polášek M. On-line coupling of capillary isotachophoresis and capillary zone electrophoresis for the determination of flavonoids in methanolic extracts of Hypericum perforatum leaves or flowers. J. Chromatogr. A. 2002; 958: 261–271.
17. Kler PA, Sydes D, Huhn C. Column-coupling strategies for multidimensional electrophoretic separation techniques. Anal. Bioanal. Chem. 2015; 407: 119–38.
18. Procházková A, Křivánková L, Boček P. Analysis of orotic acid in human urine by on-line combination of capillary isotachophoresis and zone electrophoresis. J. Chromatogr. A. 1999; 838: 213–21.
19. Marák J, Staňová A, Vaváková V, Hrenáková M, Kaniansky D. On-line capillary isotachophoresis-capillary zone electrophoresis analysis of bromate in drinking waters in an automated analyzer with coupled columns and photometric detection. J. Chromatogr. A. 2012; 1267: 252–8.
20. Pantůčková P, Křivánková L. Analysis of 5-methyltetrahydrofolate in human blood, serum and urine by on-line coupling of capillary isotachophoresis and zone electrophoresis. Electrophoresis 2010; 31: 3391–9.
21. Kvasnička F, Čopíková J, Ševčík R, Václavíková E, Synytsya A, Vaculová K, Voldřich M. Determination of phytic acid and inositolphosphates in barley. Electrophoresis 2011; 32: 1090–3.
22. Mikuš P, Kovaľ M, Maráková K, Piešťanský J, Havránek E. Separation possibilities of three-dimensional capillary electrophoresis. Talanta 2013; 103: 294300.
23. Piešťanský J, Cizmarova I, Matuskova M, Mikuš P. Comparison of 1D a 2D ITP-MS performance parameters and application possibilities: ultratrace determination of B vitamins in human urine. Electrophoresis 2022; 43: 998–1009.
24. Mikuš P, Veizerová L, Piešťanský J, Maráková K, Havránek E. On-line coupled capillary isotachophoresis-capillary zone electrophoresis in hydrodynamically closed separation system hyphenated with laser-induced fluorescence detection. Electrophoresis 2013; 34: 1223–31.
25. Tomáš R, Kovaľ M, Foret F. Coupling of hydrodynamically closed large bore capillary isotachophoresis with electrospray mass spectrometry. J. Chromatogr. A. 2010; 1217: 4144–9.
26. Piešťanský J, Maráková K, Kovaľ M, Mikuš P. Comparison of hydrodynamically closed isotachophoresis-capillary zone electrophoresis with hydrodynamically open capillary zone electrophoresis hyphenated with tandem mass spectrometry in drug analysis: pheniramine, its metabolite and phenylephrine in human urine. J. Chromatogr. A. 2014; 1358: 285–92.
27. Piešťanský J, Maráková K, Kovaľ M, Havránek E, Mikuš P. Enantioselective column coupled electrophoresis employing large bore capillaries hyphenated with tandem mass spectrometry for ultra-trace determination of chiral compounds in complex real samples. Electrophoresis 2015; 36: 3069–79.
28. Piešťanský J, Maráková K, Veizerova L, Galba J, Mikuš P. On-line column coupled isotachophoresis-capillary zone electrophoresis hyphenated with tandem mass spectrometry in drug analysis: varenicline and its metabolite in human urine. Anal. Chim. Acta. 2014; 826: 84–93.
29. Piešťanský J, Matuskova M, Cizmarova I, Majerova P, Kovac A, Mikuš P. Ultrasensitive determination of serotonin in human urine by a two dimensional capillary isotachophoresis-capillary zone electrophoresis hyphenated with tandem mass spectrometry. J. Chromatogr. A. 2021; 1648: 462190.
30. Reinhoud NJ, Tinke AP, Tjaden UR, Niessen WMA, van der Greef J. Capillary isotachophoretic analyte focusing for capillary electrophoresis with mass spectrometric detection using electrospray ionization. J. Chromatogr. A. 1992; 627: 263–71.
31. Tinke AP, Reinhoud NJ, Niessen WMA, Tjaden UR, van der Greef J. On-line isotachophoretic analyte focusing for improvement of detection limits in capillary electrophoresis/electrospray mass spectrometry. Rapid Commun. Mass Spectrom. 1992; 6: 560–3.
32. Peterson ZD, Bowerbank CR, Collins DC, Graves SW, Lee ML. Advantages and limitations of coupling isotachophoresis and comprehensive isotachophoresis–capillary electrophoresis to time-of-flight mass spectrometry. J. Chromatogr. A. 2003; 992: 169–79.
33. Kohl FJ, Montealegre C, Neusüß C. On-line two-dimensional capillary electrophoresis with mass spectrometric detection using a fully electric isolated mechanical valve. Electrophoresis 2016; 37: 954–8.
34. Römer J, Kiessig S, Moritz B, Neusüß C. Improved CE(SDS)-CZE-MS method utilizing an 8-port nanoliter valve. Electrophoresis 2021; 42: 374–80.
35. Troška P, Chudoba R, Danč L, Bodor R, Horčičiak M, Tesařová E, Masár M. Determination of nitrite and nitrate in cere-

brospinal fluid by microchip electrophoresis with microsolid phase extraction pre-treatment. J. Chromatogr. B. 2013; 930: 41–7.
36. Bodor R, Madajová V, Kaniansky D, Masár M, Jöhnck M, Stanislawski B. Isotachophoresis and isotachophoresis — zone electrophoresis separations of inorganic anions present in water samples on a planar chip with column-coupling separation channels and conductivity detection. J. Chromatogr. A. 2001; 916: 155165.
37. Graß B, Neyer A, Jöhnck M, Siepe D, Eisenbeiß F, Weber G, Hergenröder R. A new PMMA-microchip device for isotachophoresis with integrated conductivity detector. Sens. Actuators B Chem. 2001; 72: 249–58.
38. Kohl FJ, Sánchez-Hernández L, Neusüß C. Capillary electrophoresis in two-dimensional separation systems: techniques and applications. Electrophoresis 2015; 36: 144–58.
39. Kler PA, Posch TN, Pattky M, Tiggelaar RM, Huhn C. Column coupling isotachophoresis-capillary electrophoresis with mass spectrometric detection: characterization and optimization of microfluidic interfaces. J. Chromatogr. A. 2013; 1297: 204–12.
40. Kler PA, Huhn C. Non-aqueous electrolytes for isotachophoresis of weak bases and its application to the comprehensive preconcentration of the 20 proteinogenic amino acids in column-coupling ITP/CE-MS. Anal. Bioanal. Chem. 2014; 406: 71637174.
41. Sydes D, Kler PA, Hermans M, Huhn C. Zero-dead-volume interfaces for two-dimensional electrophoretic separations. Electrophoresis 2016; 37: 3020–4.
42. Knoll S, Rösch T, Huhn C. Trends in sample preparation and separation methods for the analysis of very polar and ionic compounds in environmental water and biota samples. Anal. Bioanal. Chem. 2020; 412: 6149–65.
43. Graf HG, Biebl SM, Müller L, Breitenstein C, Huhn C. Capillary electrophoresis applied for the determination of acidity constants and limiting electrophoretic mobilities of ionizable herbicides including glyphosate and its metabolites and for their simultaneous separation. J. Sep. Sci. 2022; 45: 1128–39.
44. Koskinen WC, Marek LJ, Hall KE. Analysis of glyphosate and aminomethylphosphonic acid in water, plant materials and soil. Pest. Manag. Sci. 2016; 72: 423–32.
45. Anastassiades M, Wachtler A-K, Kolberg DI, Eichhorn E, Marks H, Benkenstein A, Zechmann S, Mack D, Wildgrube C, Barth A, Sigalov I, Görlich S, Dörk D, Cerchia G, Quick method for the analysis of highly polar pesticides in food involving extraction with acidified methanol and LC- or IC-MS/MS measurement. 2021.
46. Dias J, López SH, Mol H, de Kok A. Influence of different hydrophilic interaction liquid chromatography stationary phases on method performance for the determination of highly polar anionic pesticides in complex feed matrices. J. Sep. Sci. 2021; 44: 2165–76.
47. Jansons M, Pugajeva I, Bartkevics V. Evaluation of selected buffers for simultaneous determination of ionic and acidic pesticides including glyphosate using anion exchange chromatography with mass spectrometric detection. J. Sep. Sci. 2019; 42: 3077–85.
48. Gauglitz G, Wimmer B, Melzer T, Huhn C. Glyphosate analysis using sensors and electromigration separation techniques as alternatives to gas or liquid chromatography. Anal. Bioanal. Chem. 2018; 410: 725–46.
49. Wimmer B, Pattky M, Zada LG, Meixner M, Haderlein SB, Zimmermann HP, Huhn C. Capillary electrophoresis-mass spectrometry for the direct analysis of glyphosate: method development and application to beer beverages and environmental studies. Anal. Bioanal. Chem. 2020; 412: 4967-4983.
50. Horčičiak M, Masár M, Bodor R, Danč L, Bel P. Trace analysis of glyphosate in water by capillary electrophoresis on a chip with high sample volume loadability. J. Sep. Sci. 2012; 35: 674–80.
51. Francisco KJ, do Lago CL. A compact and high-resolution version of a capacitively coupled contactless conductivity detector. Electrophoresis 2009; 30: 3458–64.
52. Foret F, Thompson TJ, Vouros P, Karger BL, Gebauer P, Boček P. Liquid sheath effects on the separation of proteins in capillary electrophoresis/electrospray mass spectrometry. Anal. Chem. 2002; 66: 4450–8.
53. Melzer T, Wimmer B, Bock S, Posch TN, Huhn C. Challenges and applications of isotachophoresis coupled to mass spectrometry: a review. Electrophoresis 2020; 41: 1045–59.
54. Graf HG, Rudisch BM, Manegold J, Huhn C. Advancements in capacitance-to-digital converter-based $C^4D$ technology for detection in capillary electrophoresis using amplified excitation voltages and comparison to classical and open-source $C^4Ds$. Electrophoresis. 2021; 42: 1306–16.
55. Malý M, Dovhunová M, Dvořák M, Gerlero GS, Kler PA, Hruška V, Dubský P. Generalized model of the linear theory of electromigration and its application to electrokinetic chromatography: theory and software PeakMaster 6-Next Generation. Electrophoresis 2019; 40: 683-692.
56. Bercovici M, Lele SK, Santiago JG. Open source simulation tool for electrophoretic stacking, focusing, and separation. J. Chromatogr. A. 2009; 1216: 1008–18.
57. Wimmer B, Neidhardt H, Schwientek M, Haderlein SB, Huhn C. Phosphate addition enhances alkaline extraction of glyphosate from highly sorptive soils and aquatic sediments. Pest. Manag. Sci. 2022; 78: 2550–9.
58. Malá Z, Gebauer P. Methodology of analysis of very weak acids by isotachophoresis with electrospray-ionization mass-spectrometric detection: anionic electrolyte systems for the medium-alkaline pH range. Anal. Chim. Acta. 2018; 998: 67–74.
59. Hühner J, Jooß K, Neusüß C. Interference-free mass spectrometric detection of capillary isoelectric focused proteins, including charge variants of a model monoclonal antibody. Electrophoresis 2017; 38: 914–21.
60. See HH, Hauser PC, Ibrahim WA, Sanagi MM. Rapid and direct determination of glyphosate, glufosinate, and aminophosphonic acid by online preconcentration CE with contactless conductivity detection. Electrophoresis 2010; 31: 575-582.
61. See HH, Hauser PC, Sanagi MM, Ibrahim WA. Dynamic supported liquid membrane tip extraction of glyphosate and aminomethylphosphonic acid followed by capillary electrophoresis with contactless conductivity detection. J. Chromatogr. A. 2010; 1217: 5832–8.
62. See HH, Stratz S, Hauser PC. Electro-driven extraction across a polymer inclusion membrane in a flow-through cell. J. Chromatogr. A. 2013; 1300: 79–84.
63. Hanke I, Singer H, Hollender J. Ultratrace-level determination of glyphosate, aminomethylphosphonic acid and glufosinate in natural waters by solid-phase extraction followed by liquid

chromatography-tandem mass spectrometry: performance tuning of derivatization, enrichment and detection. Anal. Bioanal. Chem. 2008; 391: 2265–76.

## SUPPORTING INFORMATION

Additional supporting information can be found online in the Supporting Information section at the end of this article.

**How to cite this article:** Graf HG, Rudisch BM, Ude L, Müller L, Huhn C. Picomolar detection limits for glyphosate by two-dimensional column-coupled isotachophoresis/capillary zone electrophoresis-mass spectrometry. J Sep Sci. 2022;45:3887–3899.
https://doi.org/10.1002/jssc.202200519

# Appendix III

**Supporting Information to Paper 3:**

Graf, H. G., Rudisch, B. M., Ude, L., Müller, L., Huhn, C., Picomolar detection limits for glyphosate by two-dimensional column-coupled isotachophoresis/capillary electrophoresis mass spectrometry. *Journal of Separation Science* 2022; *45*, 3887-3899, DOI: 10.1002/jssc.202200519

# Supporting Information to:

## Picomolar detection limits for glyphosate by two-dimensional column-coupled isotachophoresis/capillary electrophoresis mass spectrometry

Hannes Georg Graf, Benjamin Maximilian Rudisch, Lukas Ude, Linda Müller, Carolin Huhn

## Content

# S1 Overview over the ITP-C$^4$D/CE-MS setup

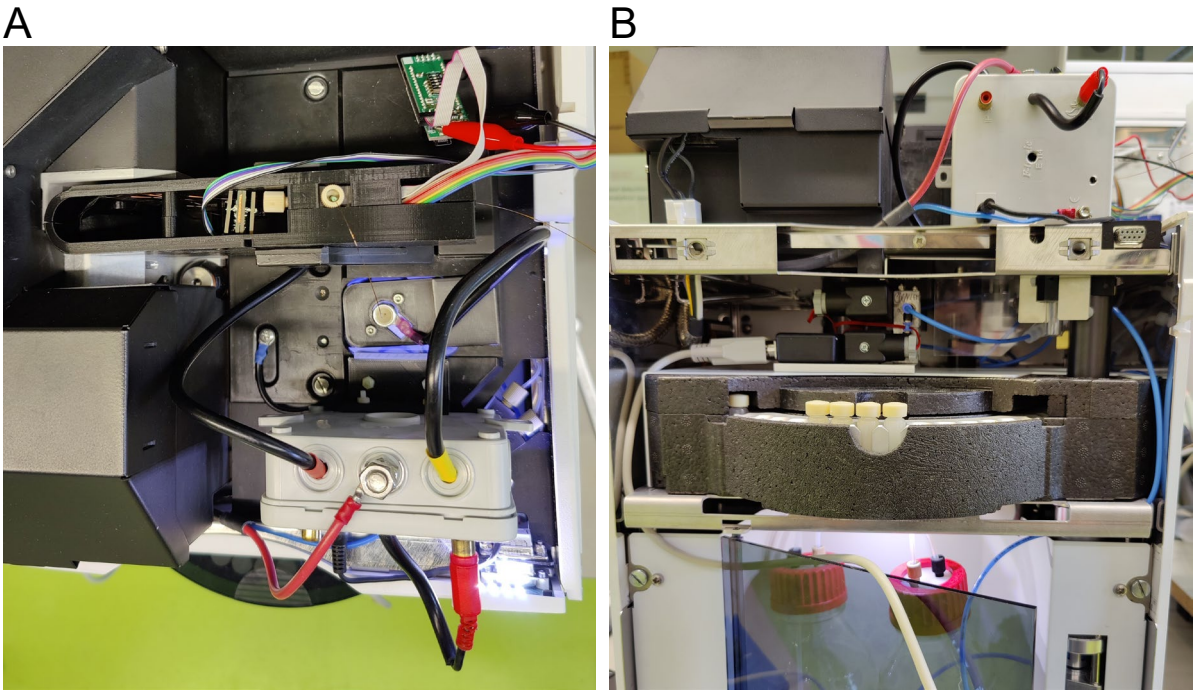


Figure S1. Photos of the ITP-C$^4$D/CZE-MS setup. (A) Top view and (B) front view on the setup place inside the CE with open top cover and removed front cover.

# S2 Fluidic setup

The core element of the hybrid capillary microfluidic setup was a microfluidic chip. In addition to microfluidic structures, it also included the geometry of a capacitively coupled contactless conductivity detector (C$^4$D). Fused silica capillaries extended the microfluidic structure to be compatible with regular CE equipment.

## S2.1 Fluidic chip

The custom-made microfluidic fused silica chip was produced from a solid block of fused silica according to CAD drawings with selective laser-induced etching technology from LightFab (Aachen, Germany). Figure S2 shows photos of the chip and Figure S3 the corresponding technical drawing. The microfluidic channel structure was double T-shaped and had an inner diameter of 100 µm. The geometry of a C$^4$D was placed between both T's and consisted of two tubular and one disk-shaped cavity. These cavities, the bone-shaped deepening (see Figure S3) and the two circular funnels attached to the cavities were filled with conductive silver paint (Art-Nr.: 5900,

Busch, Viernheim, Germany) after cleaning them with propan-2-ol and methanol, followed by a drying step. All fluids and the paint were introduced by applying reduced pressure (850 mbar) at the bottom of the chip (Figure S3, bottom drawing). Figure S4 shows a photo of the setup used for this task. By polishing the top of the chip using a 4000-grit sandpaper and cleaning its bottom side, it was ensured that there was no electrical contact between all three cavities, compare Figure S2B.

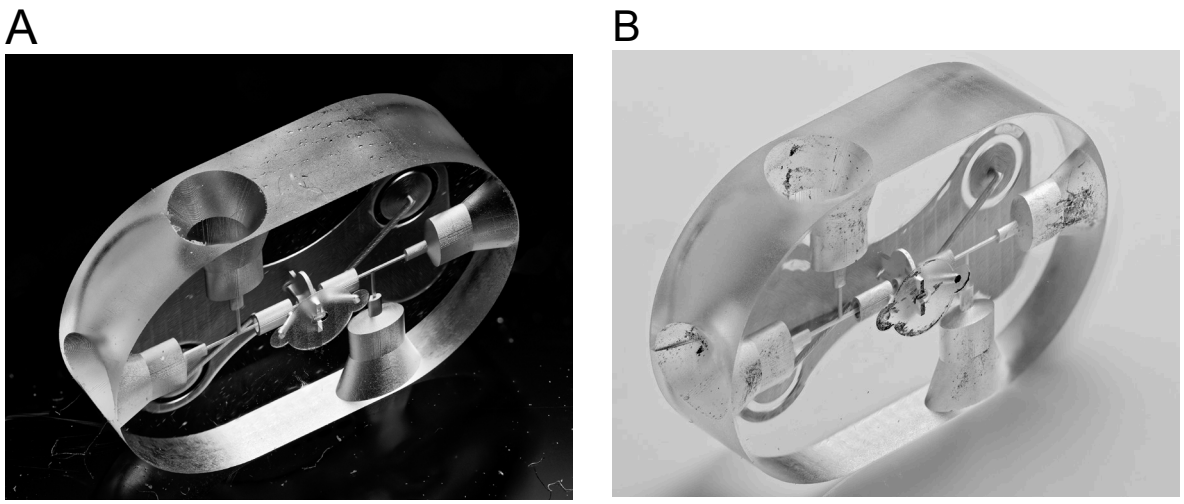


Figure S2. Photos of the microfluidic chip manufactured by selective laser-induced etching technology prior (A) and after silvering (B) of the $C^4D$ structure.

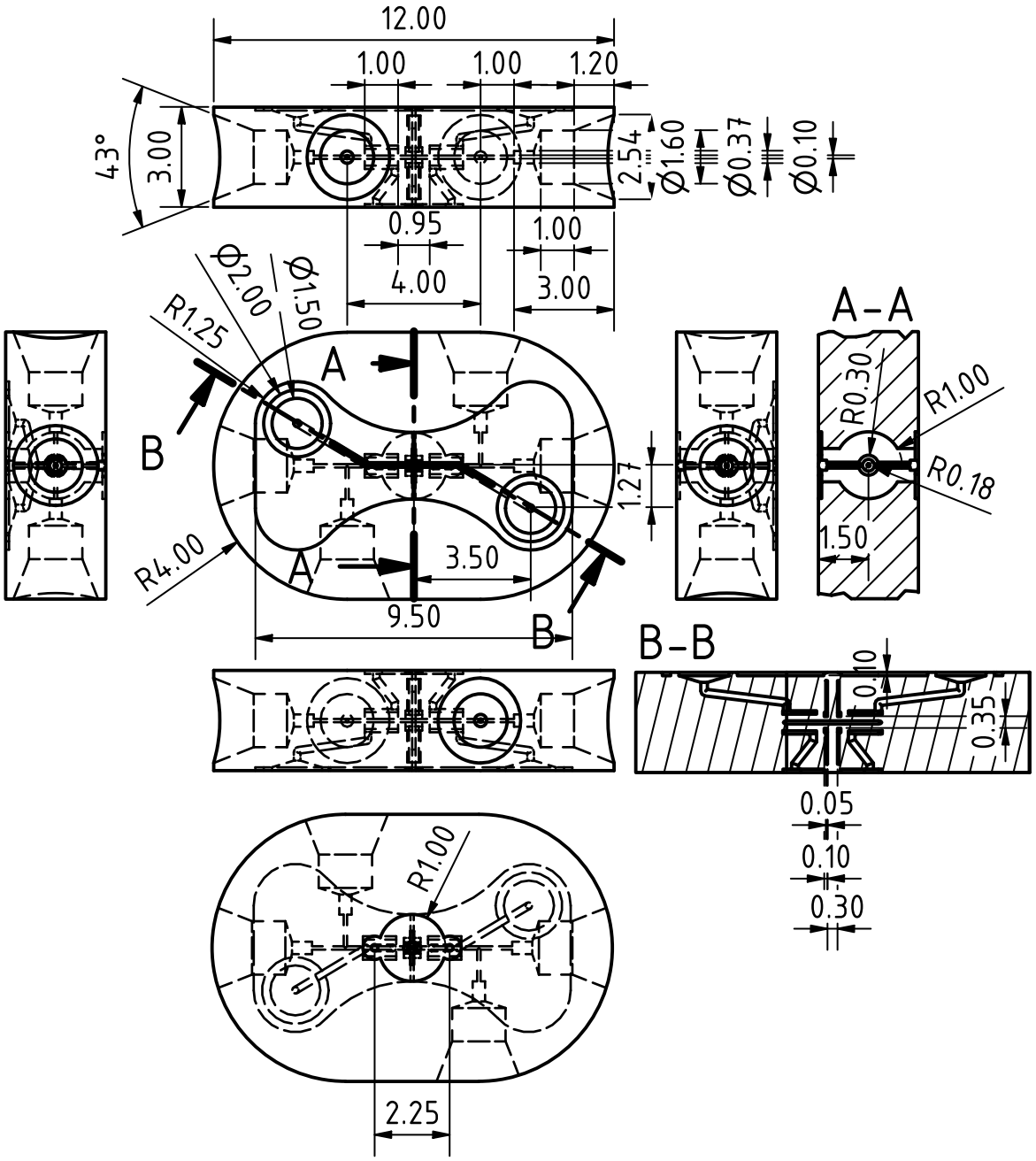


Figure S3. Microfluidic chip with double T-shaped microfluidic structure (id: 100 µm) and cavities for in-chip $C^4D$ detection on the common section between the T crossings in the center of the chip. (Scale 5:1).

Figure S4. Setup to introduce fluids in the $C^4D$ structure of the microfluidic chip. It consists of a 50 ml centrifuge tube with two holes drilled in its lid. To one of them a 1 mL syringe cylinder was installed airtight to attach the hose of a vacuum pump. The microfluidic chip was place on top of the other hole in the lid which was covered by some layers of Parafilm ensuring airtightness between the chip and the centrifuge tube lid. A punched hole in the film allowed the connection of negative pressure to the $C^4D$ structure. The glass bottle was used as stand.

## S2.2 Assembly of the microfluidic interface

To mount the capillaries and the in-chip $C^4D$ to the microfluidic chip the parts shown in Figure S5 were required. A technical exploded drawing of the interface is given in Figure S6. All capillaries were prepared by sliding a fitting and a sleeve (F-331, F-242; IDEX Health & Science, Lake Forest, IL, USA) on them. Further sealing was achieved using a piece of nitrile butadiene rubber ($d$ = 2 mm, $l$ ~ 1.5 mm) which was threaded in using a cannula (od: 0.8 mm). The capillary ends, which are to be connected to the chip, were ground to an 90° angle with a 4000-grit sandpaper while flushing with water. A capillary ready to be mounted to the chip is shown in Figure S5c and its enlargement.

To assemble the interface, the housing of the microfluidic chip (f) was placed in the orientation given in Figure S5 on top of the poly(methyl methacrylate) (PMMA) bottom cover (g) so that the four threaded M3 holes in the corners were aligned. Prior to install the microfluid chip (k) inside its housing with the bone-shaped and silvered side facing the viewer, the inlay (l) was placed inside the recess to ensure that the housing's holes aligned exactly with the microfluid structure of the chip. The four capillaries were mounted in the chip as shown in the bottom view of the assembly in Figure S5n. The capillaries were first fitted to the capillary mounts of the chip which were in a line. The fittings were only lightly tightened. After placing the stainless-steel shielding (j), to avoid direct coupling of the excitation with the pick-up electrode of the $C^4D$, on top of

chip, the in-chip C$^4$D detection head (e) was placed in its mount (d) and screwed on top of the chip housing with the Allen screws (h) after sliding the rubber rings (i) over them. Two of the golden spring contact pins of the C$^4$D detection head were place on the bone-shaped silvered surface while the other two were align to the two circular funnels of the chip. The C$^4$D detection head was wired to the supply unit of the C$^4$D (b). The supply unit transmitted the data wirelessly to the master device of the C$^4$D (a) which was connected to the computer. Technical drawings of the microfluidic chip housing, the C$^4$D's mount, the stainless-steel shield and the PMMA inlay are given in Figure S6-S10

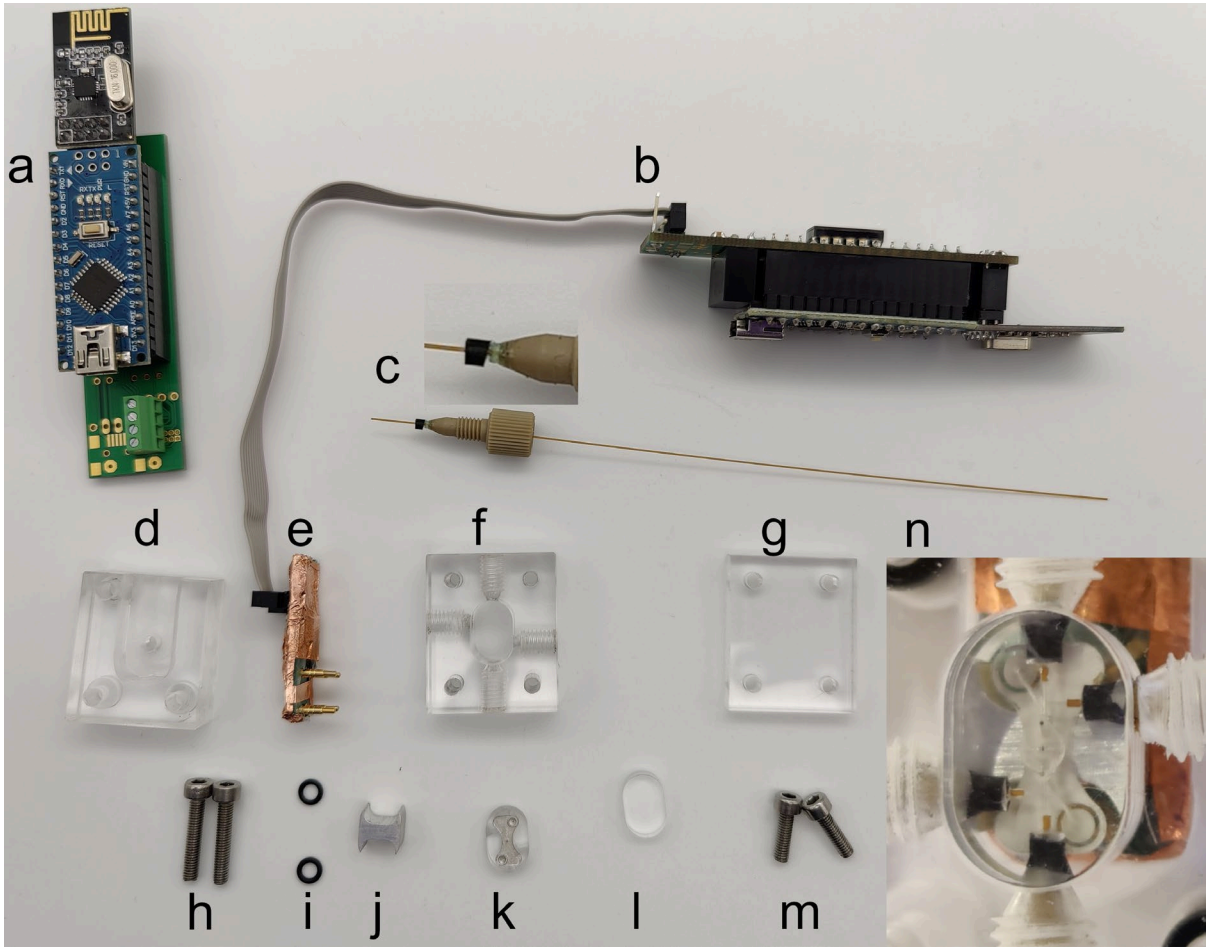


Figure S5. Overview of all parts for the microfluidic chip interface including the electronics of the in-chip C$^4$D. (a) Master device of the C$^4$D, (b) supply unit of the C$^4$D, (c) capillary with mounted sealing, sleeve and fitting, (d) C$^4$D's mount, (e) C$^4$D detection head, (f) microfluid chip housing, (g) bottom cover, (h) Allen screws (M3 x 20) and (i) rubber rings (3 × 1 mm) to slide on the Allen screws to attach the C$^4$D's mount to the chip housing, (j) stainless steel shielding, (k) microfluidic chip with silvering, (l) inlay and (m) Allen screws (M3 x 10) to mount the assembly to the cassette or bottom cover, (n) bottom view of the assembled interface without bottom cover.

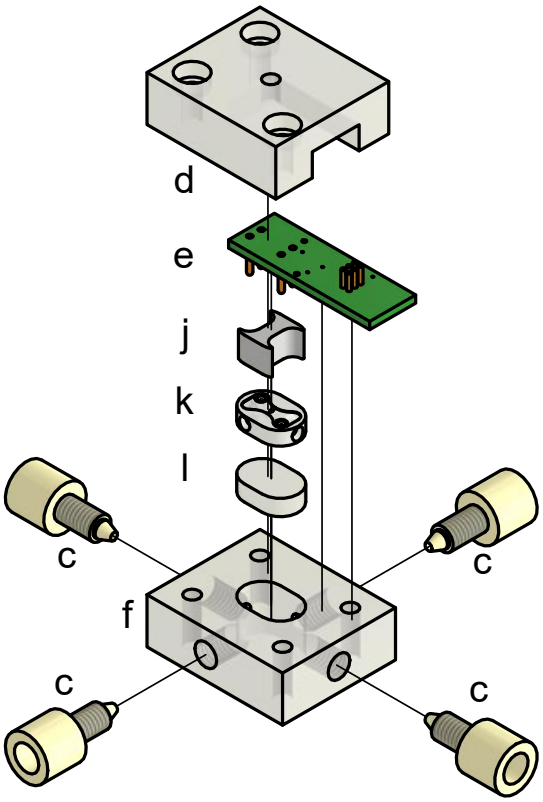


Figure S6. Exploded drawing of the microfluidic chip interface without capillaries and screws. Labels see Figure S5.

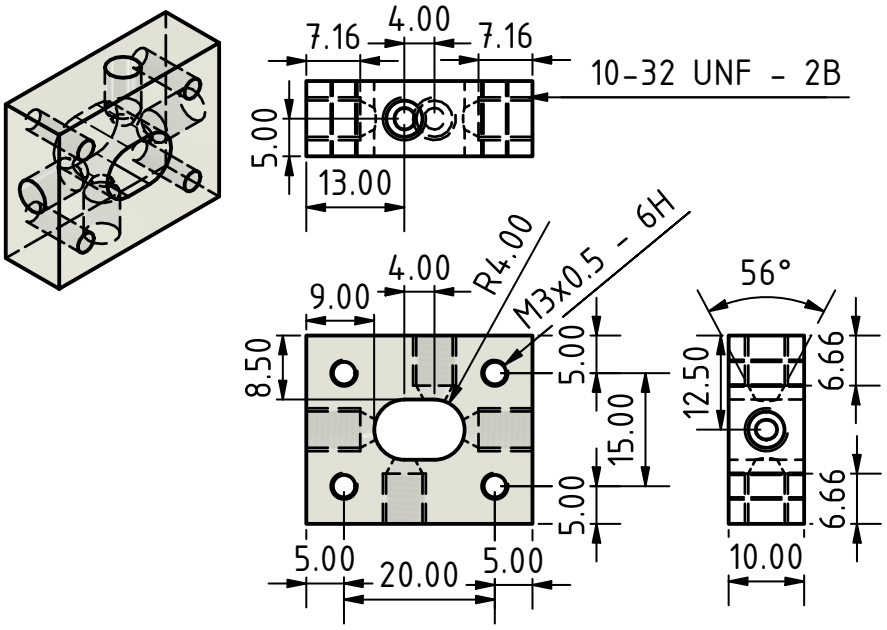


Figure S7. Technical drawing (scale: 1:1) of the microfluidic chip housing made from PMMA. Except from the thread length, all 10-32 UNF holes with conical tip were identical at the four small sides of the housing.

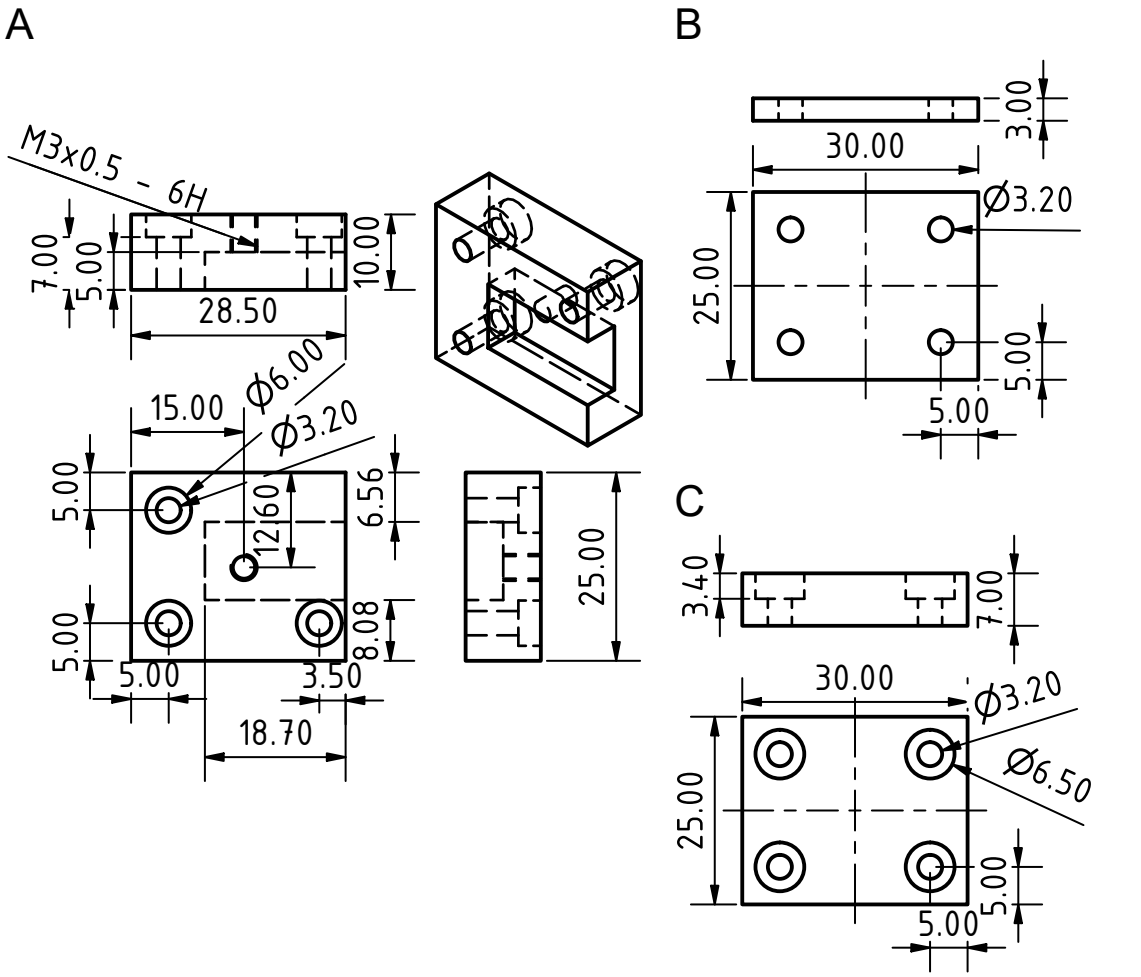


Figure S8. (A) Technical drawing of the C$^4$D's mount which was placed on top of the microfluidic chip housing and screwed in place by two M3x20 screws. (B+C) Technical drawing of the bottom cover without (B) and with (C) countersunk screw heads used only during the mounting procedure of the capillaries. Scale: 1:1, all parts were made from PMMA.

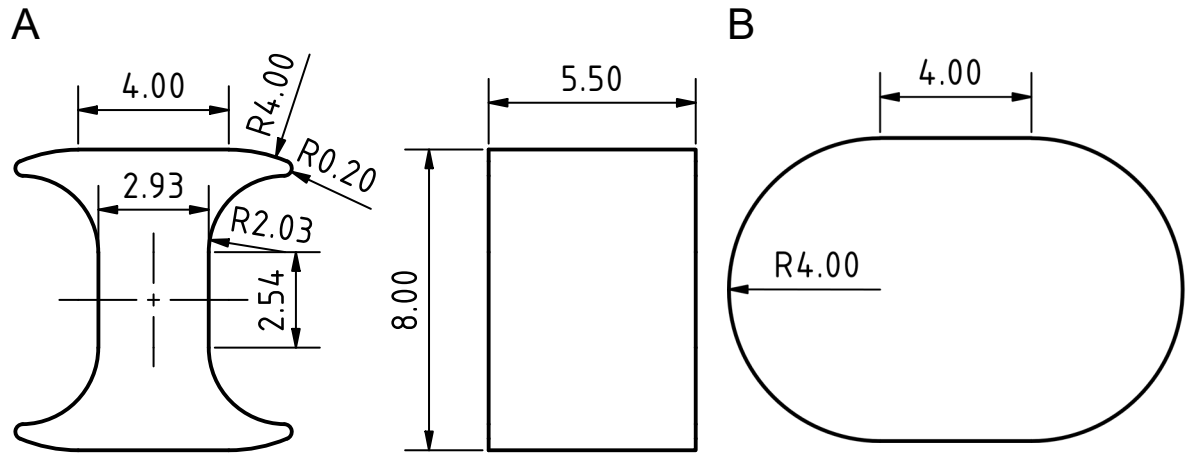


Figure S9. Technical drawings (scale: 5:1) of (A) the stainless-steel shield paced on top of the bone-shaped side of the microfluidic chip and (B) PMMA inlay (depth: 3.5 mm) placed on the opposite of the chip inside the recess of the chip housing.

# S3 Adaption of the CE-MS instrument for 2D applications

When upgrading the commercial CE-MS instrument for 2D applications, it was desired to make as few changes as possible to the commercial CE-MS instrument. A scheme with all adaptations to upgrade the CE-MS instrument to an ITP-$C^4D$/CE-MS setup is shown in Figure 1A of the manuscript. To reduce the number of adaptions, the CE-MS separation dimension was performed from the CE's inlet position (IN) to the MS as in regular CE-MS. This means that the first dimension ITP was performed form the CE's outlet (OUT) to a vial in the auxiliary vial housing (AUX) added to the setup. Therefore, the sample injection must be accomplished from the CE's outlet. This was well possible using the autosampler. However, the built-in precise compressed air system of the CE normally used for injections is only connected to the inlet position. To enable pressurization of the outlet vial, the compressed air supply of the inlet was split, and two software-controlled solenoid valves connected it either to IN or OUT or both, see Section S3.1.1 for details. The compressed air system was connected to the vials via a prepuncher, which also ensured the access of the electrodes and capillaries to the vials. Vials were sealed to maintain the applied pressure when the vial handler was in the top position. In the load position of the vial handler, a gap between the prepuncher and the electrode was present. By the CE's software, the outlet could just be set to the load position. Therefore, an elongated prepuncher was developed to seal the outlet vial already in the load position, see Section S3.1.2. At the inlet, the vial is lifted some millimeters to close this gap while applying pressure.

The auxiliary vial housing was an airtight container for a vial and equipped with an electrode and a compressed air connector to allow pressurization and application of high voltage to a vial. It was placed in a recess of the CE's insulation plate. The insulation was necessary, because the MS is set to ground and OUT can only withstand low voltages. Otherwise, flashovers can occur between the electrode and the CE's housing. Further information is given in Section S3.2.

## S3.1 Modifications at the outlet

### S3.1.1 Pressure split device

The pressure split device to connect the CE pressurization system to IN and OUT consists out of two units as can be seen in Figure S10A. The corresponding electrical circuit and a scheme of the wiring are shown in Figure S10B and C. A part list is provided in Table S1. The valve unit was installed just beneath the isolation plate in the CE. It had one compressed air supply port which was connected to the tubing of compressed air for the inlet in standard CE-MS. The supplied compressed air controlled by the CE was split and connected to two solenoid valves, allowing to choose if it is fed to IN, OUT or both. A plastic case on the valve unit housed the electronics for an optional LED stripe and a D-Sub 9 socket to connect the valve unit with the relay unit. The LED was attached via a hook-and-loop fastener under the insulation plate at the left inside and enabled an improved lightning of the vials to check their filling levels. This was useful since the valves and the plastic case mounted on a metal plate blocked the CE's integrated lightning for the vials.

The relay module allowed to switch the 12 V DC power supply of the solenoid valves by relays which were computer-operated via an Arduino Nano integrated in the unit. The module could control up to four valves or three valves plus the dimmable LED strip. The relay module must be supplied via a 12V AC/DC adapter and was connected via USB to a computer. The D-Sub 9 cable was connected to the valve unit.

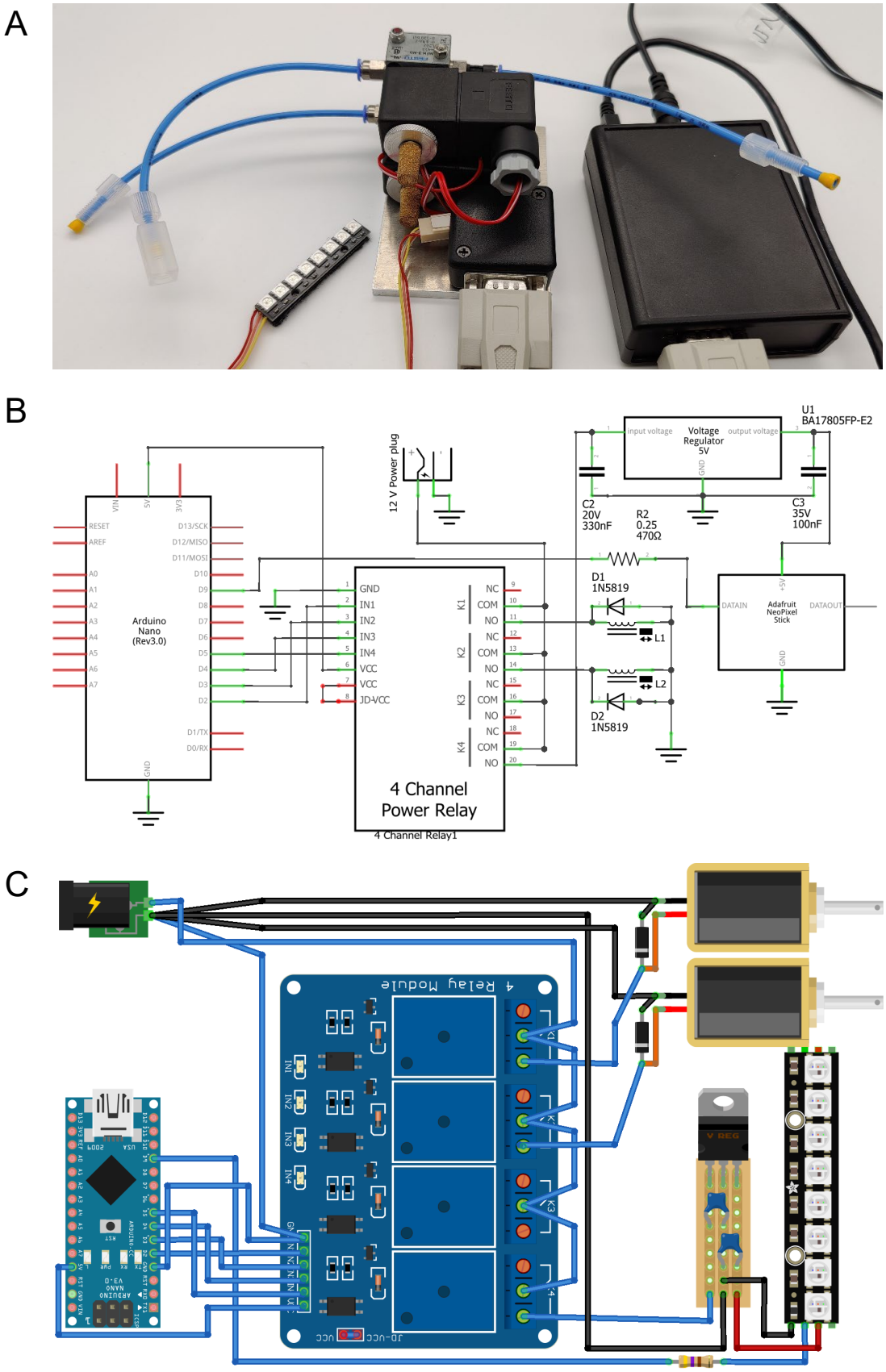


Figure S10. (A) Photo of pressure split device consisting of the valve unit (center) with the LED strip (left) and the relay unit (right). (B) Electrical circuit of the device. Flyback diodes were connected across the solenoid to eliminate voltage spike accruing when the supply current is interrupted. (C) Scheme of the wiring.

Table S1. Part list of the pressure split device consisting of the valve and the control unit

| Name | Part | Manufacturer/Supplier |
|---|---|---|
| **Valve unit** | | |
| Straight push in fitting M 5-3mm | IQSM M53 | Sang-A / Landefeld |
| T push in fitting M 5-3mm | IQSMTL M53 | Sang-A / Landefeld |
| Elbow push in fitting M 5-3mm | IQSML M53 | Sang-A / Landefeld |
| Flangeless Nut Teflon 1/8in | P-345X | IDEX |
| Flangeless Ferrule | P-300X | IDEX |
| Flangeless connector | P-620 | IDEX |
| Solenoid valve | MFH-3-M5 (4450) | Festo |
| Solenoid coil | MSFG-12 (4526) | Festo |
| Silencer M 5, sintered bronze | SD 50 | Landefeld |
| Schottky diode 1A 40V DO-41 | 1N5819 | ST MICROELECTRONICS |
| ABS-case, 40 x 40 x 20 mm | 1551PBK | Hammond Manufacturing |
| D-SUB 9 sockets female | | Reichelt |
| | | |
| **LED stick** | | |
| NeoPixel-Stick with 8 WS2812 | | Adafruit |
| Voltage regulator 25-7.5 V to 5V 1A | BA17805FP-E2 | Rohm Semiconductor |
| 3-Pin PCB connector assembly | PSS 254/3W<br>PSK 254/3W | Reichelt |
| Resistors and capacitors | | Mouser / Reichelt |
| | | |
| **Control unit** | | |
| Shell case 77 × 95 × 30 mm | 1593BB | Hammond Manufacturing |
| Relay module | DEBO RELAIS 4CH | sertronics |
| Arduino Nano | | Arduino |
| Plug-in power supply 25W 12 V / 2,08 A | GST25E12 | Mean Well |
| Barrel connector panel jack, id: 2.1 mm | HEBL 21 | Reichelt |
| D-SUB 9 socket (male) | | Reichelt |

### S3.1.2 Elongated prepuncher

To ensure airtightness of the outlet vial in its load position, an elongated stainless steel prepuncher was designed and manufactured by the workshop closing the gap between the prepuncher and the electrode. Photos and a technical drawing are given in Figure S11. If no sealing was desired, a polypropylene vial with a small hole drilled in its neck was used or no vial was loaded.

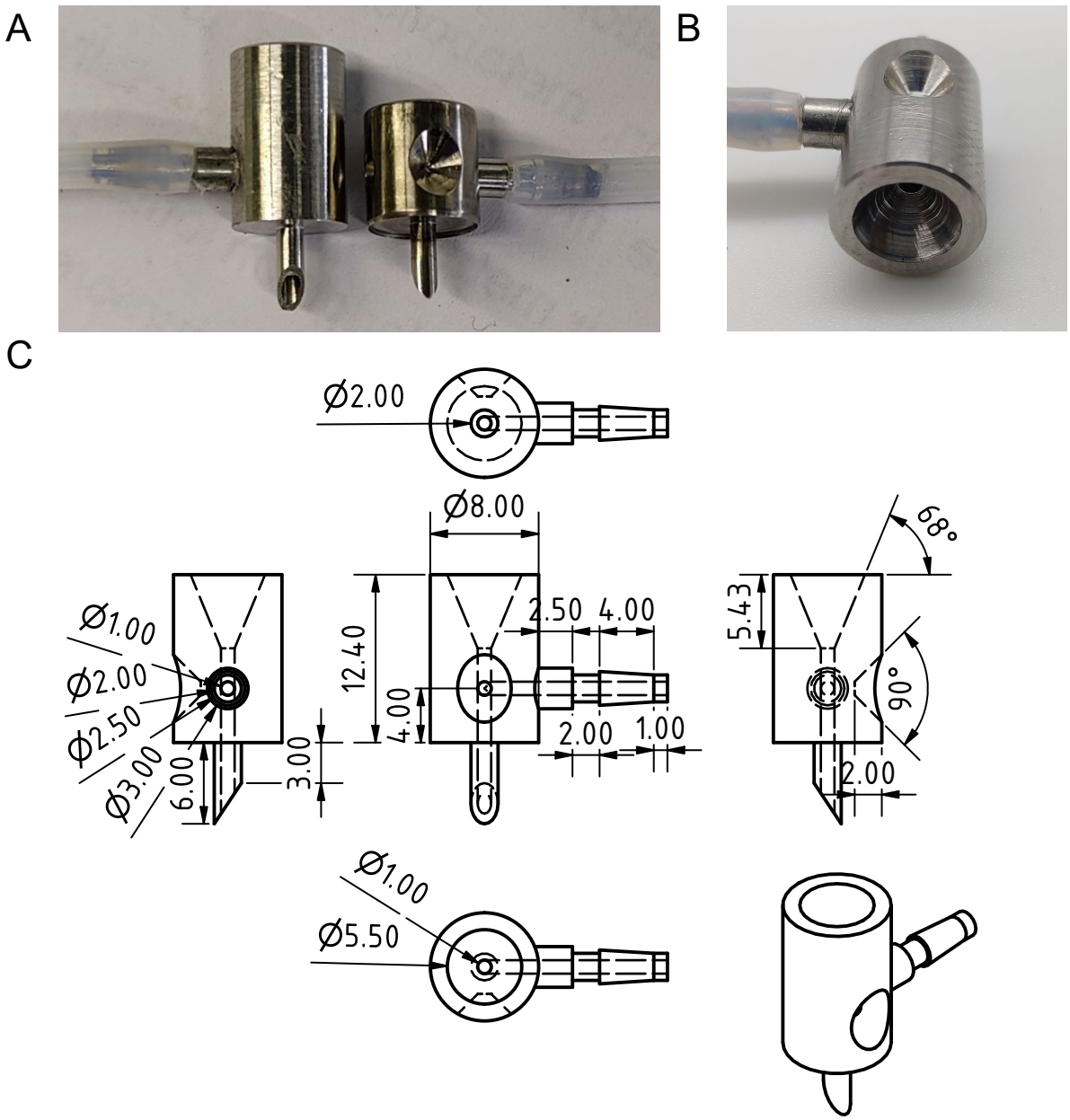


Figure S11. (A) Photo of the elongated stainless-steel prepuncher (left) and the commercial prepuncher (right). The hose fitted to the prepuncher's fittings was connected to the pressure supply of the CE. (B) Top view of the elongated prepuncher. (C) Technical drawing (scale: 2:1) of the elongated prepuncher. The prepuncher was manufactured from two turned parts, the part with the sharp tip and the fitting for the hose. Both were glued together.

## S3.2 Auxiliary vial

### S3.2.1 Auxiliary vial housing

The auxiliary vial housing allowed to house a single vial and to pressurized it with compressed air and connect it to high voltages up to 30 kV. Photos of the assembled auxiliary vial housing and its single parts are given in Figure S12. The technical drawings are presented in Figure S13. The auxiliary vial housing consisted of a PMMA

housing, a screwable bottom piece made from polyoxymethylene (POM) to place the vial in the housing and a 3D printed housing mount made from polylactic acid (PLA). The top of the vial housing had a threaded hole to mount a standard electrode from an Agilent 7100 CE (part number: G7100-60007, Agilent Technologies, Waldbronn, Germany). The end of the threaded hole had to be conical to ensure that the inner part of the electrode was pushed slightly upwards. This compressed the bushing in the electrode and sealed the capillary against the electrode. Prior to installing the electrode, a ring cable lug connected to the high voltage supply was pushed onto the thread of the electrode. The vial housing was equipped with a push-in fitting M 5 - 3mm (IQSM M53, Sang-A) to install the hose from the pressure controller, see Section S3.2.2. Alternatively, the pressure could also be supplied from the CE if the hose connected normally to IN from the pressure split device was connected to AUX disabling pressurization of IN. To reach an airtight sealing, a sealing ring (22 × 2 mm) was placed on the bottom piece. By exchanging the bottom piece either a 1.5 ml vial as used in the 7100 CE or a 4 ml vial could be place in the vial housing. The housing mount was z-shaped and was attached via Allen screws to the vial housing. The housing mount rested on support elements in a rounded rectangular recess (40 × 60 mm, R = 1 cm) in the CE's insulation plate located 27 mm apart from its front edge and 20 mm from its right edge. Thread inserts were fitted to install a support element underneath the left side of the recess, see Figure S14. This type of attachment ensured that all capillary ends were place at the same height and ensured easy access to exchange the AUX vial manually. The insulation plate was further equipped with 3 mm PMMA plates to prevent flashovers between the auxiliary vial and the CE's housing, see Figure S14.

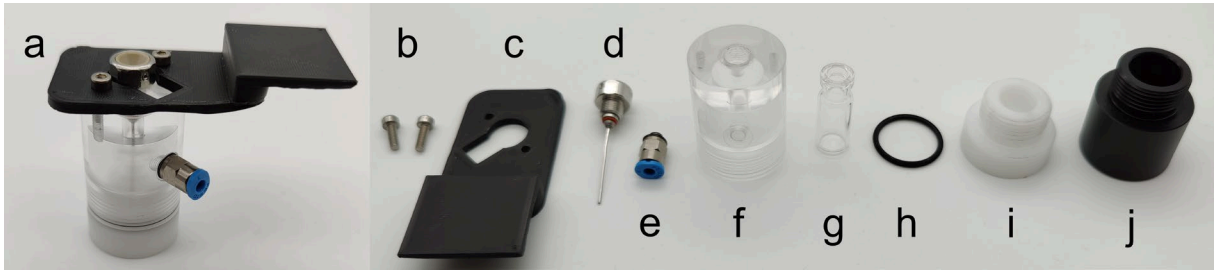


Figure S12. Assembled auxiliary vial (a) and overview of its parts. Allen screws (M3 × 10) (b) attached the housing mount (c) to the vial housing (f) which was equipped with the electrode (d) and the push-in fitting (e). A 1.5 ml or 4 ml vial (g) could be places in the bottom piece (i) or (j). Sealing was achieved with ring (h).

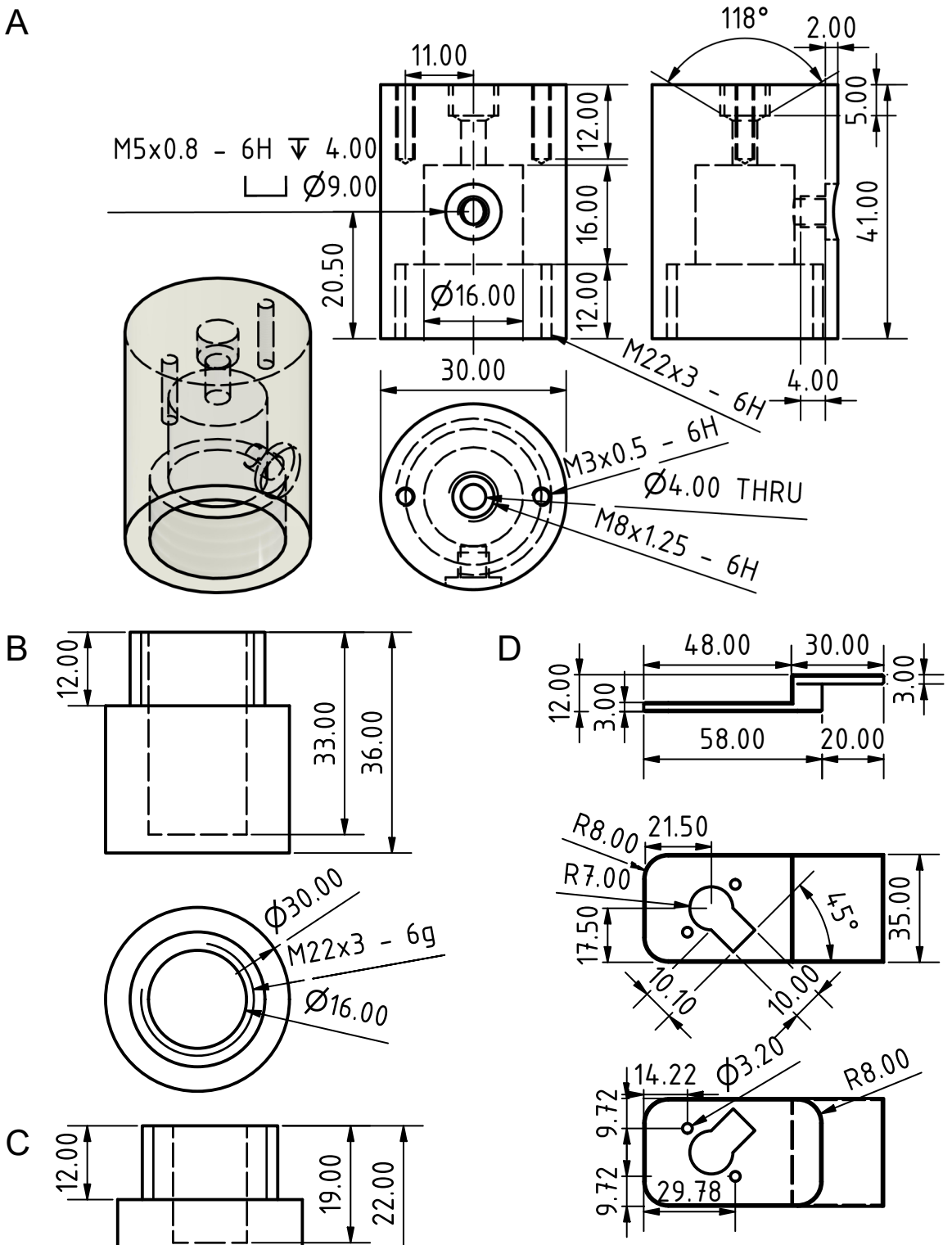


Figure S13. Technical drawing (scale: 1:1) of the PMMA vial housing (A), the POM bottom pieces for a 1.5 ml (B) or a 4 ml (C) vial and the housing mount from PLA (D,scale 1:2)

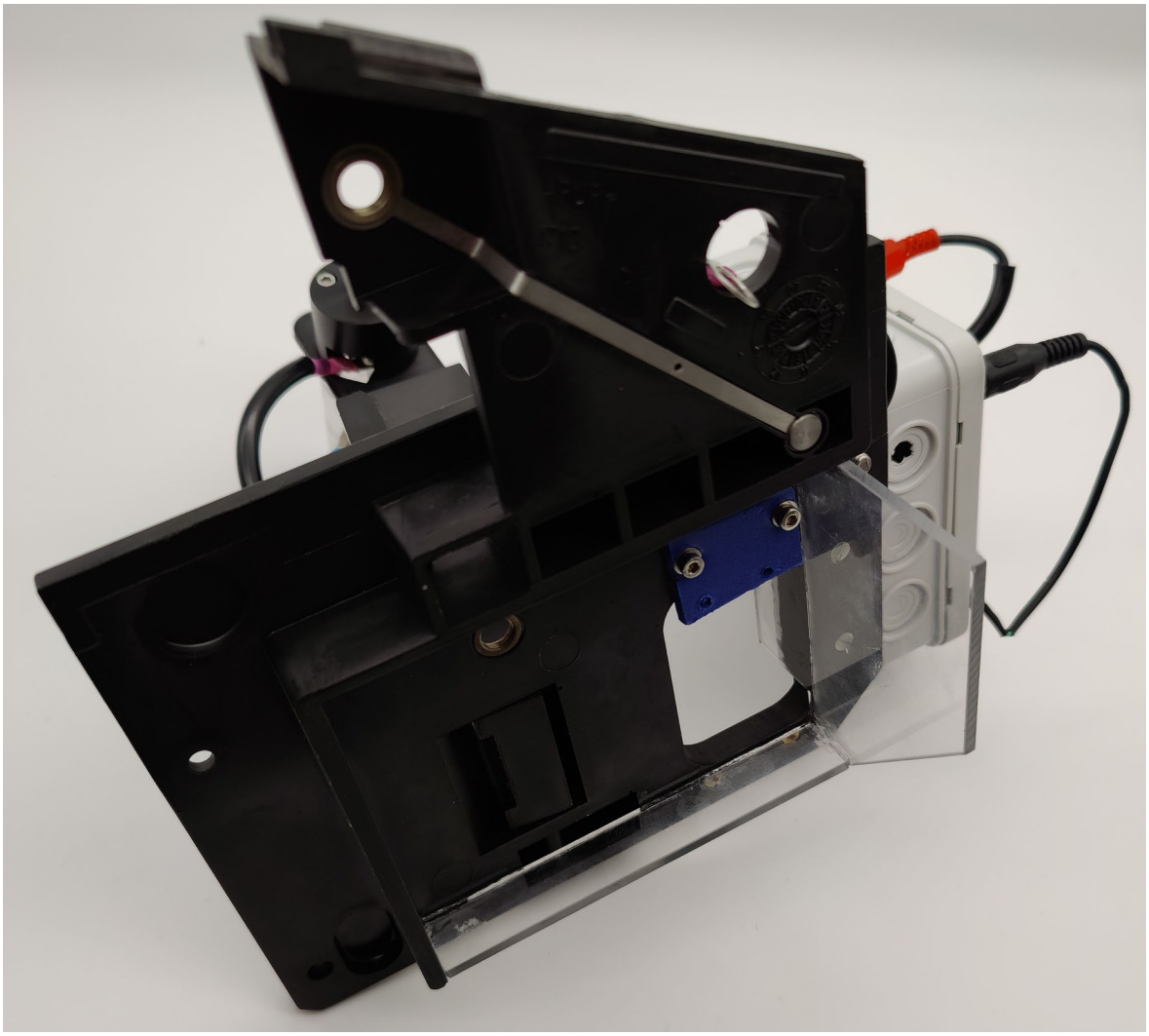

Figure S14. Photo from the bottom of the modified insulation plate with the recess, the support element (fastened with two screws, blue) and the PMMA plates glued to the insulation plate.

### S3.2.2 Pressure controller unit

To control the pressure supplied from the laboratory installation when applied to the vial in the auxiliary vial housing, a commercial pressure controller from Parker (Cleveland, OH, USA) was purchased. It had an internal vent, an effective orifice of 0.76 mm and a pressure range of up to 15 psig. To adjust and monitor the pressure by a computer, electronics were designed to convert digital data to the analog input of the pressure controller and vice versa. A photo of the setup is given in Figure S15. The schematic diagram of the electronics circuit and a scheme of the PCB layout are shown in Figure S16 and all parts are listed in Table S2.

Figure S15. Photo of the pressure controller (blue, right) with attached tubing and the electronics encased in the black box on the left.

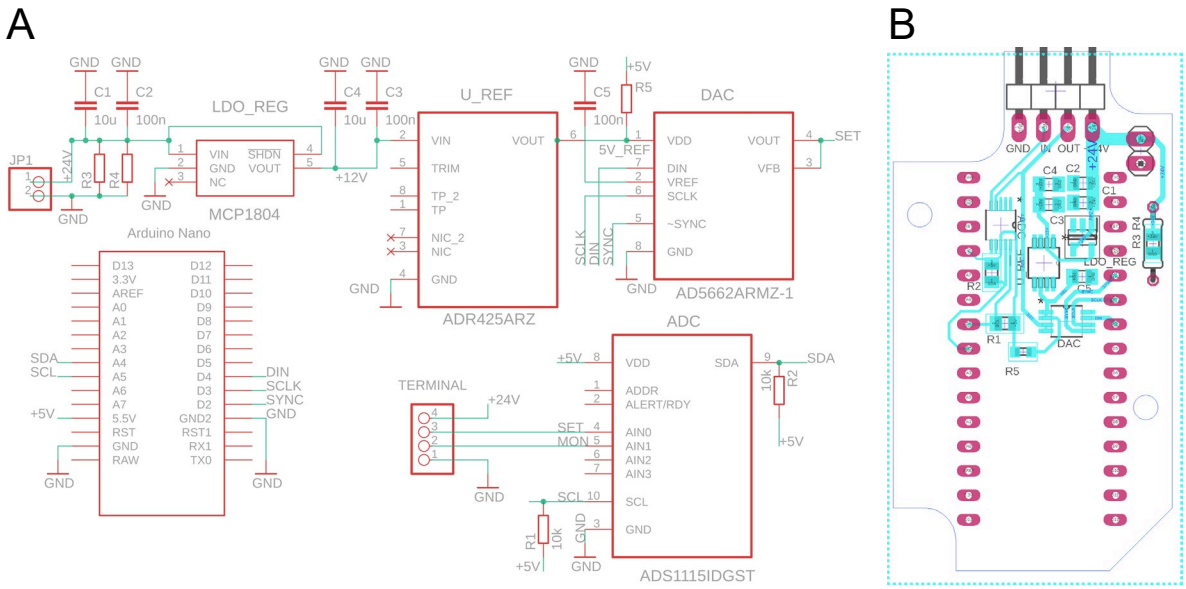


Figure S16. (A) Schematic diagram of the pressure controller unit's circuit. R5 is a jumper to enable an alternative power supply of the digital-to-analog-converter via the Arduino. R3 and R4 are reserved. (B) Scheme of the pressure controller electronics PCB layout.

Table S2. Part list for the pressure controller unit.

| Part | Part number | Manufacturer/Supplier |
|---|---|---|
| Pressure controller + metric adaptor | 990-005103-015 OEM-EP Miniature Electronic Pressure Controller | Parker |
| Straight push in fitting M 5-3mm | IQSM M53 | Sang-A |
| Mini-ABS-Case, 60 × 35 × 20 mm | | Reichelt |
| Plug-in power supply unit, 27 W, 24 V, 1.12 A | | RND electronics |
| Low dropout voltage regulator | MCP1804T-C002I/OT | Microchip |
| Ultraprecision, low noise voltage References | ADR425ARMZ | Analog Devices |
| 16-Bit digital-to-analog converter | AD5662ARMZ-1 | Analog Devices |
| 4 Channel 16-bit analog-to-digital converter | ADS1115IDGST | Texas Instruments |
| Arduino Nano | | Arduino |
| Barrel connector panel jack, id = 2.1 mm | HEBL 21 | Reichelt |

S3.2.3 Switching box

A switching box made from a junction box (100 × 100 mm) was used to connect either IN or AUX to the CE's high voltage supply. In the upper half of the box a screw (M8 × 15) with two nuts was installed to connect the ring cable lug of the CE's high voltage supply to the box. The same screw was connected to a short cable with a cinch plug which can be linked either to a cinch socket connected to IN or to AUX. In the lower half of the box, separated inside the box by a piece of plastic from the high voltage regime, a similar setup is installed to disconnect the ground potential from OUT. Here, a screw (M4 × 15) with three nuts were used. The box was fixed to the insulation plate with a plastic bracket and plastic screws so that the CE's top cover could still be closed.

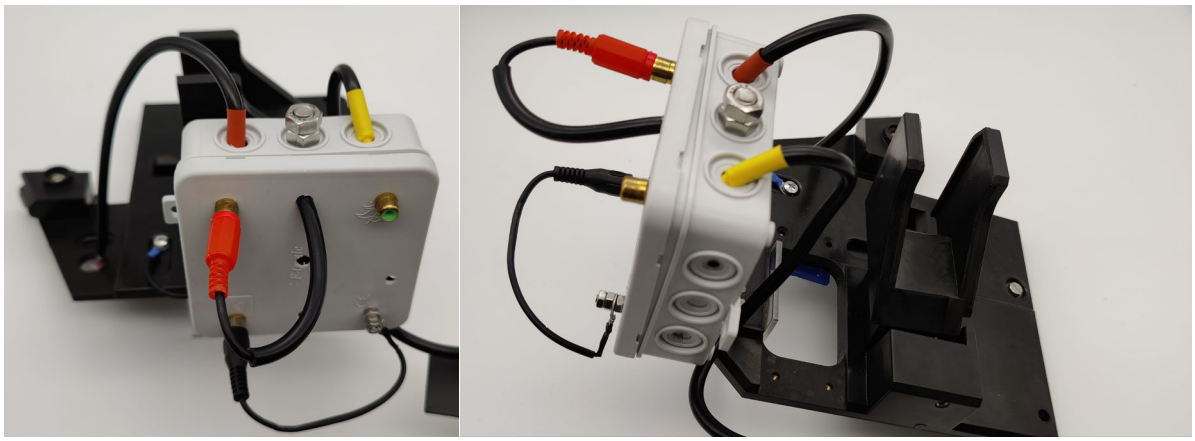

Figure S17. Photos of the switching box (gray) fixed to the insulation plate. In the configuration shown, the high voltage was connected to IN and OUT was connected to ground.

## S3.3 3D printed CE cassette

A 3D printed cassette, adopted from the commercial CE cassette for the 7100 CE, was printed from polylactic acid. It was designed to provide more space to flexibly mount all elements while maintaining fast and easy installation. Both sides of the cassette were hold together by rod magnets (4 mm od, height: 10 mm) (S-04-10-AN, Supermagnete, Gottmadingen, Germany). The AUX port was placed in such a way that there was no collision with the air conditioning ducts in the CE's top cover.

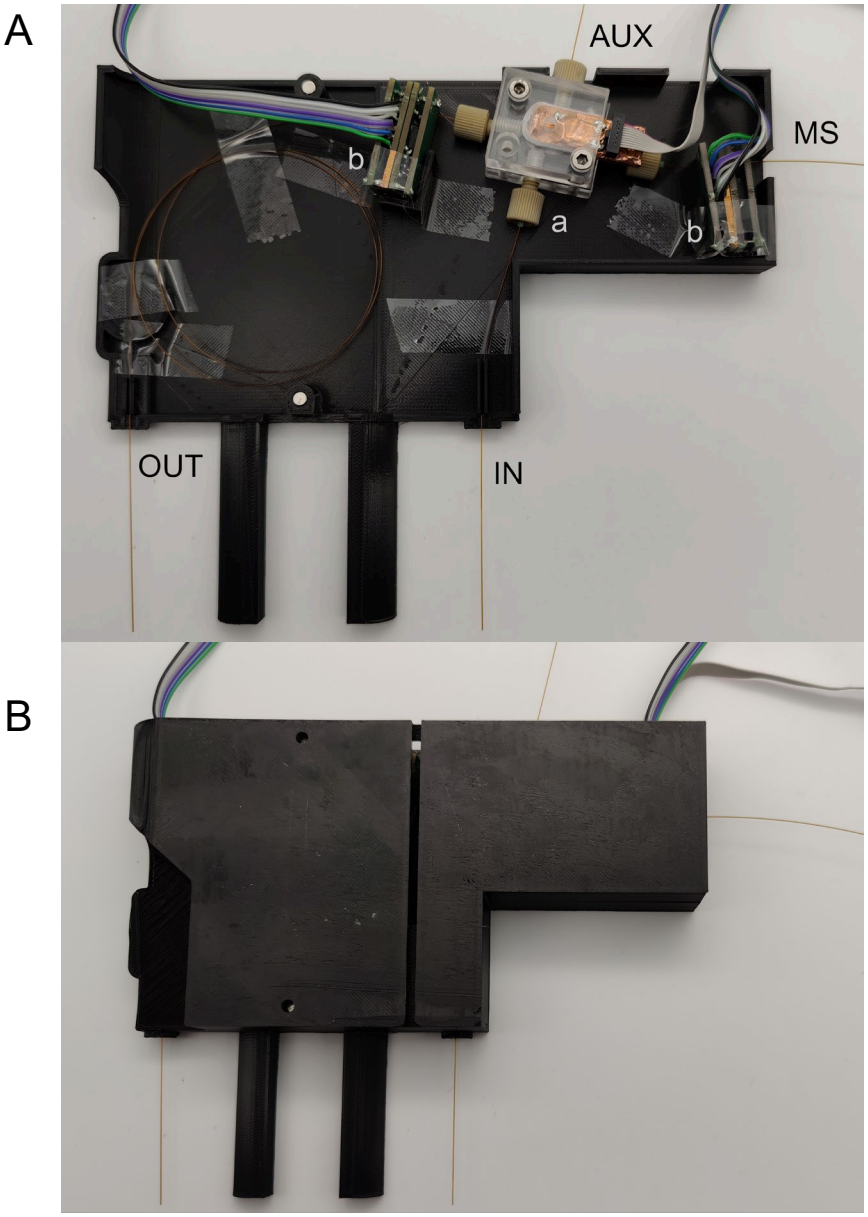


Figure S18. Photos of the opened (A) and closed (B) 3D printed cassette. On the bottom part of the cassette (A) the chip interface with on-chip $C^4D$ (a) and two on-capillary $C^4Ds$ (b) were mount. The capillaries are labeled with the ports of the setup they are connected to.

## S3.4 Software

A software to control the self-developed equipment was written in Python 3. A screenshot of the interface is depicted in Figure S19. Both manual control or the use of a timetable was possible regarding the two valves, the pressurization of the auxiliary vial and the LED strip. To synchronize the commercial software of the CE and the software to control the self-developed equipment, a trigger module presented previously [1] was used to monitor the start and end of the MS measurements. It was connected to the remote port of the CE and included a pass through to the MS.

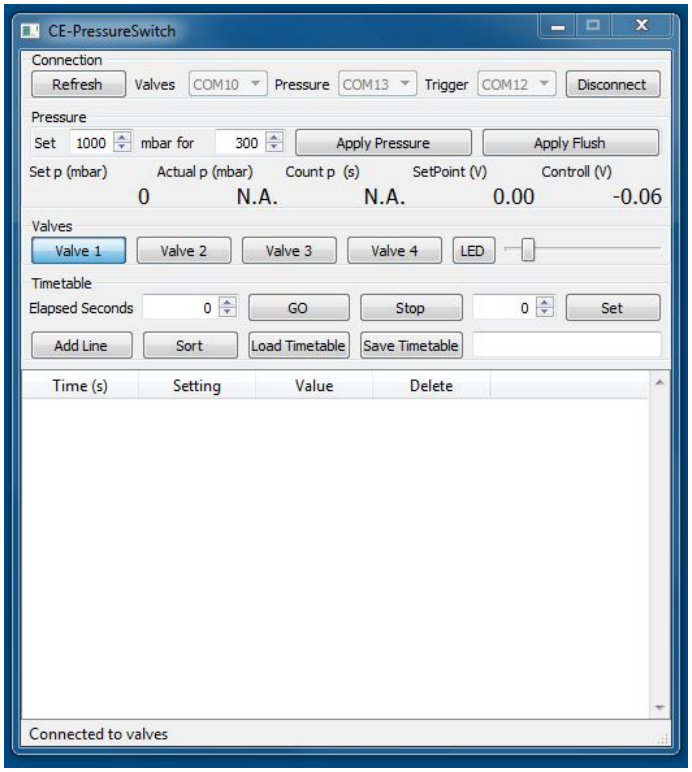


Figure S19. Screenshot of the Python software to control the pressure split device, the pressure controller, the LED strip and handle the CE's trigger signal.

## S4 Conductivity detection

The detection setup consisted of four capacitively coupled contactless conductivity detectors ($C^4D$). The $C^4D$ electronics mounted to the microfluidic chip based on the previously published CDCD [1] and allowed to detect the transition from LE to TE which is necessary to transfer reliably the ITP stack to the CE separation. The three on-capillary $C^4Ds$ based on the open$C^4Ds$ published by Francisco and do Lago [2].

### S4.1 On-chip $C^4D$

The on-chip $C^4D$ based on the previously published CDCD [1]. The only modifications were the replacement of the electrodes by spring contact pins (811-S1-006-10-016101, Preci-Dip, Delémont, Switzerland) to connect the $C^4D$ geometry in the microfluidic chip with the electronics. Due to space constraints, the connectors between the detection head and the supply unit were mounted to the opposite side of their printed circuit boards (PCB) compared to the already published design. The schemes of the top and bottom of the modified detection head's PCB are given in Figure S20. The Python software used to record the data was refined by adding the option to apply a moving average function to the raw data to smooth the real-time plot.

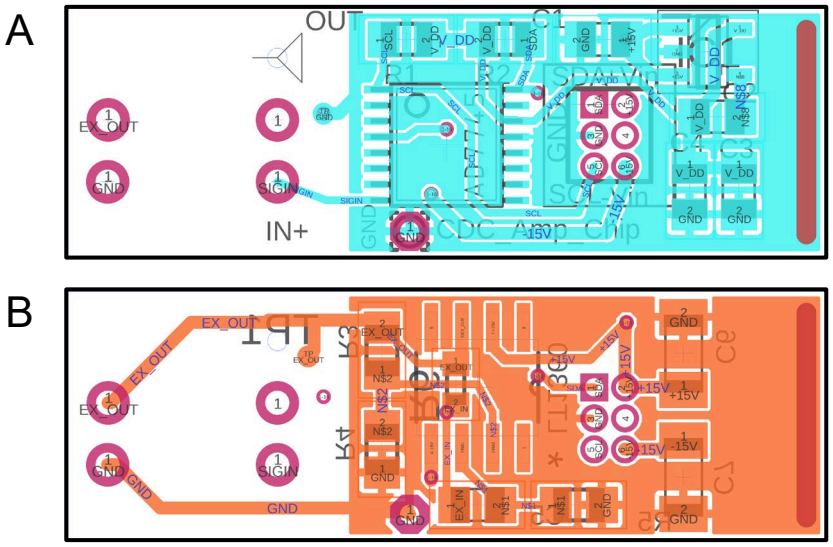


Figure S20. Scheme of the top (A) and bottom (B) of the detection head's PCB. The two dark red vertical bars on the right side indicate a plated-through slot. After removing the part on the right, the plating allowed soldering the copper shielding wrapped around to electronics to ground.

## S4.2 Modified open$C^4D$s

The on-capillary $C^4D$s were built according to Francisco and do Lago [2]. The layout of the detection head was changed to reduce its size from 21.1 × 30.5 mm² to 18.2 × 29.1 mm² while keeping its circuit and assembly. The vias used as tubular electrodes had a diameter of 0.5 mm. Around the vias, a circular area (radius: 5 mm) was kept free from the grounding plane. The PCBs used for shielding had a 1 mm hole above the electrodes and pads to solder the boards together and ensure the grounding. The supply unit, compare Figure S21, was redesigned to receive start/stop trigger signals by connecting pin 7 of the Teensy 2.0 microcontroller board (PJRC,Sherwood, OR, USA) to ground. Additionally, a DC/DC-converter (TBA 1-0519, Traco Power, Baar, Switzerland) was added to the supply unit's circuit allowing to power the $C^4D$ completely via the USB port of the microcontroller board. For some applications, the $C^4D$ was placed next to the high voltage source of the CE. Therefore, it was decided to power the setup via a power bank and send the data wirelessly via a Bluetooth HC-06 module (connected to the JP2 port) to the PC avoiding flashovers. The wireless data transmission and the changed trigger signal handling required a slightly modified software on the Teensy compared to the one provided by Francisco and do Lago [2]. A 3D printed adapter was made from polylactic acid (PLA) to avoid mechanical stress to the capillary by the open$C^4D$ place directly on top of the CE-MS interface. The slotted cylindrical part surrounded the CE-MS interface and allowed to access its sheath liquid port. The $C^4D$ electrodes were aligned to the fitting of the CE-MS interface. A technical drawing is given in Figure S22.

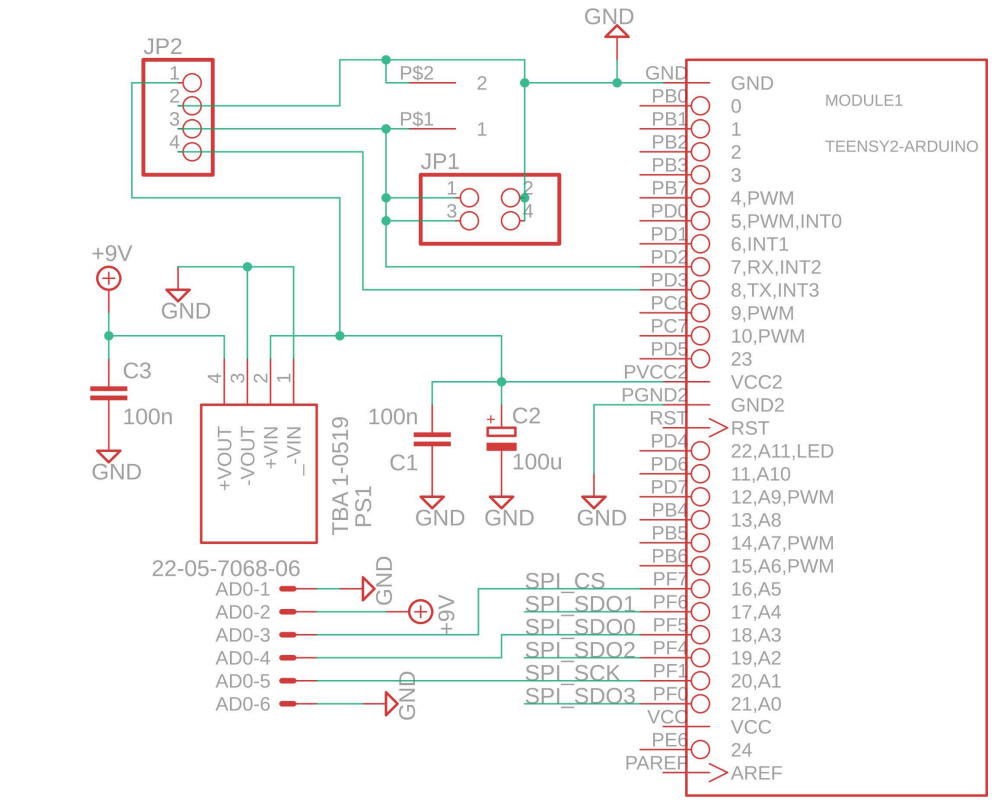


Figure S21. Schematic diagram of the supply unit's circuit of the openC$^4$D with the possibility to add a HC-06 Bluetooth module to JP2 for wireless data transmission while supplying the entire setup by the Teensy's USB port with a power bank.

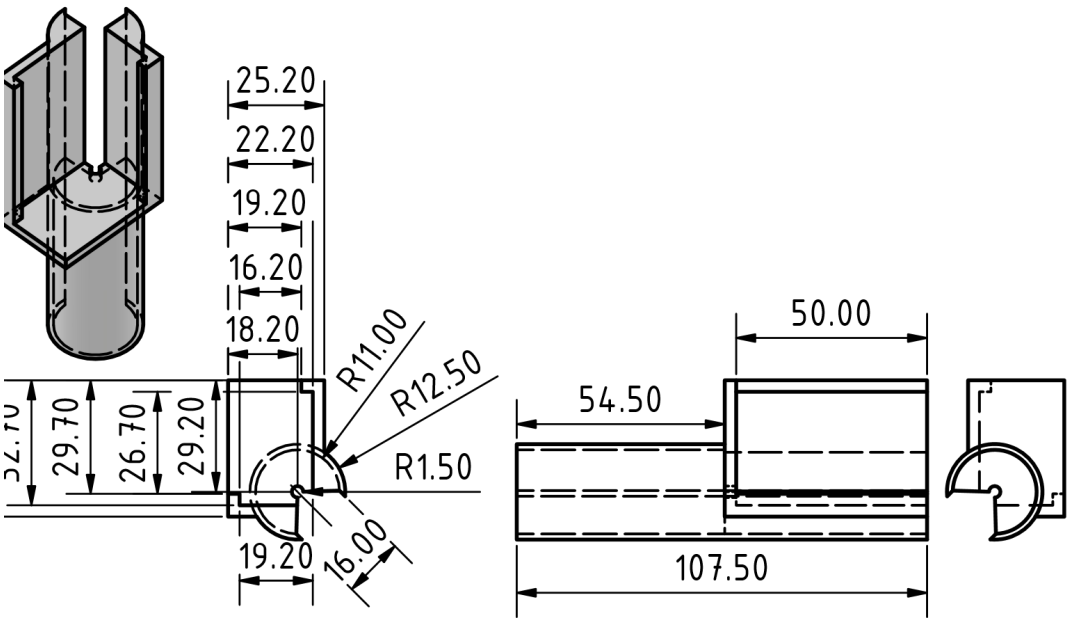


Figure S22. Technical drawing of a 3D printed adapter which enables the placement of up to two openC$^4$D heads on top of the CE-ESI-MS interface. Scale 1:2.

# S5 CE-MS electropherogram in the LOQ range

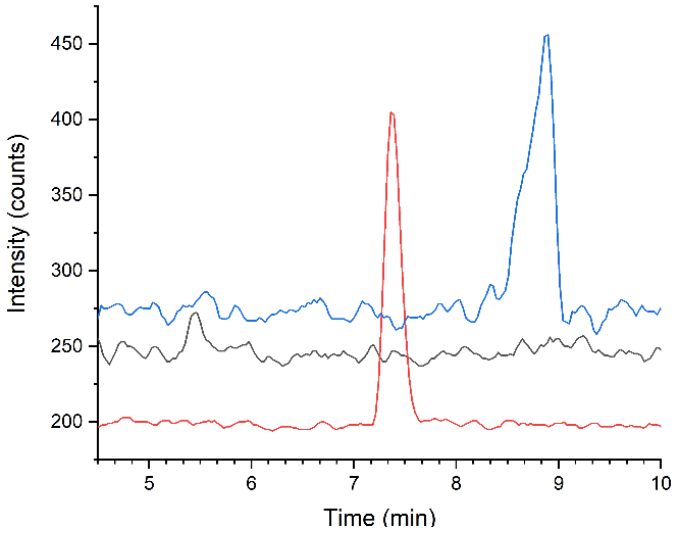


Figure S23. Electropherogram of the pseudomolecular $[M-H]^-$ ions of sarcosine (black), AMPA (red) and glyphosate (blue) (c = 5 µM, each) recorded by ESI-MS after separation by CE at +15 kV, other conditations as given for Figure 2B.

# S6 Methodological details to ITP-$C^4D$/CZE-MS

In this section some additional details for the individual steps of the ITP-$C^4D$/CZE-MS are presented.

**Preliminary remarks**

All solutions were prepared in plastic containers or vials to prevent glyphosate sorption and leaching of ionic components. The liquid levels of the vials were adjusted so that the electrodes (shorter than the capillaries) were only immersed in liquids to which voltage was applied and dipping steps were included where necessary.

**Step A) Preparation of runs**

The entire setup was flushed with LE from AUX at 1 bar for 5 min to ensured that no manual vial change at AUX was required throughout the entire method, as this end of the channel network was not connected to the CE's autosampler.

**Step B) column-coupled ITP-C4D**

Prior to the start of the ITP method, the CE's pressure regime was connected to OUT, the high voltage was connected to AUX. OUT and MS were electrically connected to ground, and the potential of IN was left floating.

The ITP method started by injecting the sample for 20 s at 100 mbar at OUT. After dipping steps, vials with LE and TE were loaded to IN and OUT, respectively. A pressure of 70 mbar was applied to OUT during the entire ITP separation which started with a delay of 0.4 min by setting the voltage to +12 kV at AUX, compare Figure 4B. Therefore, a TE plug was injected behind the sample. Anionic analytes migrating towards OUT were transported to AUX by external pressure and a high EOF. The MS' nebulizer pressure was set to 1 psig during the ITP step reducing suction effects by the ESI, while all other MS settings were set as given in Section 2.2.1 of the manuskript.

**Step D) column-coupled CZE-MS**

Prior to the start of the CZE dimension, the pressure regime and the high voltage of the CE were connected to IN. OUT and MS were connected to ground, and the potential of AUX was left floating.

The CZE separation started without a vial change by applying +15 kV to IN. No pressure support was necessary in this step, compare Figure 4D. To aid analyte transfer to the MS capillary through the suction of the ESI source, the nebulizer pressure was set to 20 psig for 0.5 min and was then reduced to 5 psig. Anions migrated towards the chip, but were transported to the MS by the high EOF.

# S7 References


[1] Graf, H. G., Rudisch, B. M., Manegold, J., Huhn, C., Advancements in capacitance-to-digital converter-based $C^4D$ technology for detection in capillary electrophoresis using amplified excitation voltages and comparison to classical and open-source $C^4Ds$. *Electrophoresis*. 2021, *42*, 1306-1316.

[2] Francisco, K. J., do Lago, C. L., A compact and high-resolution version of a capacitively coupled contactless conductivity detector. *Electrophoresis*. 2009, *30*, 3458-3464.